Design, Synthesis and Study of Functional Properties of Some Novel Metal Organic Materials Using Crystal Engineering Approach

THESIS SUBMITTED FOR THE DEGREE OF

DOCTOR OF PHILOSOPHY (SCIENCE)

JADAVPUR UNIVERSITY

2023

By

SOMEN GOSWAMI

Index no.: 185/16/Phys./25

Department of Physics, Jadavpur University

Kolkata- 700032, India

যাদবপুর বিশ্ববিদ্যালয়
কলকাতা-৭০০০৩২, ভারত

JADAVPUR UNIVERSITY
KOLKATA-700032, INDIA

FACULTY OF SCIENCE : DEPARTMENT OF PHYSICS

Dr. Sanjay Kumar
Professor
Department of Physics
e-mail: kumar_dsa@yahoo.com
sanjay.kumar@jadavpuruniversity.in

Ref No.: 16/2023
Date: 15.03.2023

CERTIFICATE FROM THE SUPERVISOR

This is to certify that the thesis entitled "**Design, Synthesis and Study of Functional Properties of Some Novel Metal Organic Materials Using Crystal Engineering Approach**" submitted by **Shri Somen Goswami** (Reference No. D-7/SC/1289/16, Index No. 185/16/Phys./25), who got his name registered on **10th November, 2016** for the award of Ph.D. (Science) degree of Jadavpur University, is absolutely based upon his own work under the supervision of **Prof. Sanjay Kumar, Department of Physics, Jadavpur University, Kolkata- 700032** and that neither this thesis nor any part of it has been submitted for either any degree/diploma or any other academic award anywhere before.

Sanjay Kumar 15.03.2023

(Signature of the Supervisor date with official seal)

Dr. SANJAY KUMAR
Professor
Department of Physics
Jadavpur University
Kolkata - 700032, India

যাদবপুর বিশ্ববিদ্যালয়
কলকাতা-৭০০০৩২, ভারত

JADAVPUR UNIVERSITY
KOLKATA-700 032, INDIA

FACULTY OF SCIENCE : DEPARTMENT OF PHYSICS

Dr. Sanjay Kumar
Professor
Department of Physics
e-mail: kumar_dsa@yahoo.com
sanjay.kumar@jadavpuruniversity.in

Ref No.: 17/2023
Date: 15.03.2023

Certificate of similarity check for plagiarism verification

This is to certify that the plagiarism checking for this thesis authored by Shri Somen Goswami has been performed using professional plagiarism prevention software 'iThenticate'. According to the report generated after plagiarism checking there is 06% similarity in this thesis, which is in category "Level 0" (minor similarities) as per 'Promotion of Academic Integrity and Prevention of Plagiarism in Higher Educational Institutions Regulations, 2018' of University Grant Commission (UGC) of India. All sentences written/rewritten by providing proper references (treated as quoted work), references (bibliography), table of content, preface, acknowledgements, generic terms used in the subject area of the present thesis, a common knowledge or coincidental terms up to 10 (Ten) consecutive words (as prescribed in the above said UGC Regulation up to 14 (fourteen) terms for such common knowledge or coincidental terms can be excluded) and own works of the candidate published in peer reviewed journals (Inorganica Chimica Acta. **2014**, 410, 111–117; Inorganica Chimica Acta. **2014**, 423, 123–132; Inorganica Chimica Acta. **2019**, 486, 352–360; Inorg. Chem. **2020**, 59,12, 8487-8497; Inorg. Chim. Acta., **2023**, 550, 121370-121379; these papers are attached in the Appendix of the thesis) are excluded from similarity checking. It is certified that the present thesis submitted by Somen Goswami is plagiarism free and he has followed standard norms of academic integrity and scientific ethics.

Sanjay Kumar 15.03.2023
(Signature of the Supervisor)

Dr. SANJAY KUMAR
Professor
Department of Physics
Jadavpur University
Kolkata - 700032, India

15.3.23
(Signature of Head, Department of Physics)

Professor and Head
Department of Physics
Jadavpur University
Kolkata – 700 032

Declaration

I, hereby, declare that the work embodied in the present thesis has been carried out by me under the supervision of Prof. Sanjay Kumar at the Department of Physics, Jadavpur University, Kolkata-700032, India. Neither this thesis nor any part thereof has been submitted for any degree whatsoever.

Somen Goswami

(SOMEN GOSWAMI)

Research Scholar
Department of Physics
Jadavpur University
Kolkata-700032, India

Date: 15.03.2023

Acknowledgements

This thesis would not have been accomplished without acknowledgement of several individuals whose relentless help, support and guidance make possible to successfully submit my Ph. D thesis.

First and foremost, I would like to express my sincere thanks and gratitude to my Ph. D supervisor Prof. Sanjay Kumar, Professor, Department of Physics, Jadavpur University. He is truly a great mentor who behaved like a teacher-in needs, philosopher-in thought and guide-in work throughout the entire course of my research work. Without his unconditional support, affection and everlasting enthusiasm, I doubt whether successful completion of this thesis work would have been possible. His immense knowledge and amazing capacity to solve any difficulty regarding research work helped me significantly during my research. His constant supervision and advice have made this thesis appear in this form. I sincerely believe that his contribution is more than just a guide to shape up each portion of my thesis. I must say, I am privileged for being his student.

Apart from my Ph. D supervisor, I sincerely acknowledge immense contribution of my friend Dr. Rajat Saha (Assistant Professor, Department of Chemistry, Kazi Nazrul University, Asansol, West Bengal) through whom I got opportunity to meet and work under same Ph. D supervisor. Moreover, his continuous guidance, inspiration, sharing insightful thoughts and unconditional help to solve any difficulty throughout my Ph. D work make me grateful to him forever.

I am delighted to extend my earnest gratefulness to my distinguished research collaborators Prof. Carlos J. Gómez García and Samia Benmansour (Departamento de Química Inorgánica. Universidad de Valencia, C/ Dr. Moliner, 50. 46100 Burjasot, Valencia Spain) for performing magnetic measurement, analysis and solving single crystal x-ray

diffraction data and thorough revisions with valuable suggestions to improve quality of manuscripts. I am also extremely grateful to all of my respected research collaborators Prof.Ian M. Steele (Department of the Geophysical Sciences, The University of Chicago, USA), prof. Manirul Islam (Department of Chemistry, University of Kalyani, West Bengal 741235, India), Dr. Indrajit Saha (Department of Chemistry, RKMRC, Narendrapur 700103, WB, India), prof.Antonio Frontera (Departament de Quiḿ ica, Universitat deles Illes Balears, 07122 Palma de Mallorca, Baleares, Spain), prof. Asok Poddar (Experimental Condensed Matter Physics Division, Saha Institute of Nuclear Physics, Kolkata 700064, India).

I am extremely grateful to Prof. Partha Pratim Ray (Professor,Department of Physics, Jadavpur University), Prof. Sukhen Das (Professor, Department of Physics, Jadavpur University), Dr. Pabitra Kumar Paul (Associate Professor, Department of Physics, Jadavpur University), Dr. Saikat Kumar Seth (Assistant Professor, Department of Physics, Jadavpur University), Prof. Saurabh Das (Professor, Department of Chemistry, Jadavpur University), Prof. Kausikisankar Pramanik (Professor, Department of Chemistry, Jadavpur University), and Dr. Debajyoti Ghoshal (Associate Professor, Department of Chemistry, Jadavpur University), for their constant help, valuable suggestion and allowing me to access their laboratory.

I express my heartfelt thanks to my junior labmate Dr. Soumen Singha for his unconditional immense support, encouragement in every need and problem throughout the time of my research to reach my intended goal. I would like to acknowledge all of to my senior and junior laboratory mates Dr. Rituparna Mondal, Dr. Sanjoy Kumar Dey, Dr. Subhrajyoti Dey, Ms. Koyel Sarkar, Mrs. Arpita Barua, Dr. Md. Monwar Hoque, Mr. Sumit Kumar Maity, Dr. Sumit Majumder and Dr. Sk. Sabyasachi for their immense support in various matters related to my Ph. D. work. I would like to thank my juniors Bhaskar Khanra, Nirmal Mondal, Soumen Byapari and Moisilee Dutta.

I sincerely acknowledge all the respected teachers from whom I got valuable teaching guidance and motivation in my school and college days. I am deeply indebted to Prof. Kumaresh Ghosh, Prof. Dulal Ghosh, Prof. Shital Kumar Chattopadhyay, Prof. Bijali Bikash Bhowmick, and Prof. Surojit Chattopadhyay (department of chemistry, University of Kalyani) for their majestic teaching and guidance in my M. Sc. classes.

I sincerely acknowledge Mr. Gour Sundar Goswami (Head master of Satyabharati Vidyapith, Barasat) for his enthusiastic support and encouragement with smileful face. I am also thankful to Dr. Utpal Mukhopadhaya, Dr. Krishnapada Das, Mr. Satrajit Talukdar, Mr. Pradip Kumar Basak, Mr. Arindam Dey, Mr. Uttam Saha and all of my other colleagues for their enormous cooperation and encouragement to continue my research work smoothly.

Thanks to my friends and well-wishers Anupam Singha Roy, Suman Mallick, Dipankar Saha, Kallol Dey, Suman Sengupta, Avipsaman Roy, Somnath Chatterjee, Md. Samim, Mr. Pradip Ghosh, Rinki, Rakhi, Kaushik, Baishakhi, Sugata etc.

I convey my deep sense of gratitude and respect to my parents who always have tried to make me a good human being providing morality and good lessons. I am ever grateful to my better half Mrs. Kheya Chakraborty and my adorable son Arnit who make my life complete and joyful with blissful love and support. I would like to express my gratitude to my elder brother Mr. Subrata Goswami, elder sister Mrs. Nandini Chakraborty, brother-in-law Mr. Barendranath Chakraborty (elder sister's husband) and mother-in-law Mrs. Bhaswati Chakraborty for their unconditional support, immense love and continuous inspiration that has given me energy and enthusiasm to complete my thesis.

Above all, I am obligated to Almighty God for granting me the wisdom and strength to undertake this research task and enabling me to its completion.

Preface

Quest for new functional materials is the driving force of contemporary research of multidiscipline. Engineering properties in a single designer architecture developing multifunctional materials for targeted applications is the current trend in modern crystal engineering. Intrinsic chemical properties of solid crystalline materials depend on nature and arrangement of their molecular components. Thus, thoughtful adequate knowledge about nature, pattern and governing factors of different intermolecular interactions and metal-ligand, metal-metal bonds etc. is very crucial to achieve predefined designer crystals having predicted functionalities for targeted applications. In this regard, crystal engineering (CE) is the indispensable means to meet the goal. According to G. R. Desiraju, crystal engineering is *"the understanding of intermolecular interactions in the context of crystal packing and the utilization of such understanding in the design of new solids with desired physical and chemical properties"*. So, the main theme of crystal engineering is to synthesis predefined designer crystals having desired functionalities by judicious selection of proper molecular or ionic building units with favorable intermolecular interactions. Following crystal engineering principles, researchers have been engaged in the design and synthesis of functional metal-organic materials (MOMs) for several decades and gained extensive attention just after the seminal work presenting a Cu(I) containing MOM by Robson in 1990.

MOMs because of their unprecedented levels of porosity, inherent modularity to fine-tuning of both structure and bulk physical properties, evolve as most efficient class of materials for potential applications in all most all scientific and technological arena such as catalysis, molecular magnetism, electronic devices, gas storage, chemical separations, sensing and many others. Various weak organizing forces incorporate exciting features in supramolecular MOMs

like high flexibility, size and shape specific porosity and reversibility in molecular association-dissociation etc. These fascinating features offer a huge scope of applications of such materials in several scientific and technological fields such as ion transportation, drug delivery, catalysis, luminescence and recognition of biological molecules etc.

A dignified number of researchers of world acclaimed research groups like Groups of G. R. Desiraju, M. Zaworotko, S. Kitagawa, H. Kitagawa, M. Fujita, P. J. Stang, C. Janiak, O. M. Yaghi, H. C. Zhou, M. P. Suh, J. J. Vittal, J. R. Long, K. Kim, A. K. Cheetham, S. R. Batten, B. Chen, X. M. Chen, G. Férey, W. Lin, S. Natarajan, M. J. Rosseinsky, N. L. Rosi, C. J. Kepert, J. T. Hupp, K. Biradha, P. K. Bhardwaj, R. Banerjee, M. Das, C. M. Reddy have contributed significantly in this field.

In this background, we are bestowing the present thesis entitled "Design, synthesis and study of functional properties of some novel metal organic materials using crystal engineering approach", that deals with the design, synthesis, characterization and functional properties of some novel metal-organic materials. The thesis consists of eight chapters.

The genesis, background and definition of the problem, scopes and objectives of the thesis work as well as brief relevant literature review have been presented in **Chapter 1**. In this chapter, crystal engineering approach in the synthesis of designer crystals like metal-organic materials specially, metal organic frameworks and supramolecular metal-organic polymers has been discussed along with a brief account on the use of bridging ligands in the synthesis of metal-organic materials.

The methodologies, experimental techniques and theoretical backgrounds have been briefly illustrated in **Chapter 2**. The basic characterization techniques adopted in the thesis like single crystal x-ray diffraction (SCXRD), powder x-ray diffraction (PXRD), elemental

(CHN) analysis, Fourier transform infrared spectroscopy (FTIR), electron spray ionization mass spectroscopy (ESI-mass spectroscopy), cyclic voltammetry(CV), UV-Vis, photoluminescence (PL) spectroscopy and computational analysis like molecular orbital analysis, excited state analysis by DFT have been described in respect to their instrument used or software and methodologies used.

Chapter 3 reports the structural, thermal, magnetic and optical properties of a novel two dimensional coordination polymer, $\{[Ni^{II}(squarate)(2,2'\text{-bipy})(H_2O)]\cdot H_2O\}_n$, [squarate = 3,4-dihydroxycyclobut-3-ene-1,2-dionate, 2,2′-bipy = 2,2′-bipyridine] exhibiting a very rare $\mu_{1,2,3}$ squarato bridging. The present study reveals that the squarato-bridged metal complexes are unique model systems to carry out the study on various types of bridging modes displayed by the ligand. This metal organic material is the second example where squarato dianion ligand shows its unusual $\mu_{1,2,3}$ bridging mode. 2D coordination sheets of the complex are packed *via* π···π interactions that result in the formation of 3D supramolecular architecture with 1D supramolecular channels which are filled with guest water molecules stabilised by H- bonding interactions. Thus, this framework can act as a metal-organic supramolecular host (MOSH). Moreover, this MOM exhibits antiferromagnetic behavior and also photo-luminescent activity. This work has already been published in Inorganica Chimica Acta (Inorg. Chim. Acta., **2014**, 410, 111–117).

In **Chapter 4,** we presented the design, synthesis, crystal and supramolecular structure of a Pr (III)-complex, $\{[Pr(1,10\ phen)_2\ (H_2O)_5]\ Cl_3(H_2O)\ (CH_3OH)\}$, incorporating a 2D water-chloride-methanolic supramolecular sheet. The coordination tendency of the Pr(III) ion and the self-assembling tendency of water-chloride and methanol stabilize the system, making strong affinity of the host towards the guest molecules. Thus, the supramolecular metal-organic polymer (SMOP) can behave as a dynamic supramolecular metal-organic host with expulsion and

absorption of water molecules upon heating and cooling. The breathing nature of the system had been established by powder X-ray diffraction method. The work reported in this chapter has been published in Inorganica Chimica Acta (Inorg. Chim. Acta., **2014**, 423, 123–132).

Chapter 5 describes the design, synthesis, crystal and supramolecular structure of a novel oxalato bridged binuclear Cu (II)-complex: $[Cu_2(oxalate)(1,10phen)_2Cl_2]$. The thermal, redox and photoluminescence behavior of the complex has been explored that indicates very good thermal stability and photoluminescence activity of the complex. The presence of coordinately unsaturated Cu-centers makes the complex active catalyst in the high valued oxidation reaction of alkenes. The complex exhibits high product selective catalytic activity towards the corresponding epoxide in the oxidation of a series of alkenes viz. styrene, cyclohexene and *cis*-cyclooctene in presence of H_2O_2 as oxidant. The detail catalytic study was done to achieve the optimized reaction condition and found that in acetonitrile medium using H_2O_2 as oxidant the complex had 100% selectivity to the corresponding epoxide in oxidation of *cis*-cyclooctene at 50 ºC. The same product selectivity for oxidation of styrene and cyclohexene was about 89 and 76% under the same reaction condition. The work reported in this chapter has been published in Inorganica Chimica Acta (Inorg. Chim. Acta., **2019**, 486, 352–360).

Chapter 6 highlights the design, synthesis and structure of a metamagnetic mononuclear Mn(III)-Schiff base complex $(H_3O)[Mn(L)(H_2O)Cl]$ and a metamagnetic trinuclear Mn_2Fe complex $\{[Mn(L)(H_2O)]_2Fe(CN)_6\}^{-2}$ (L= Schiff base ligand)from the monomeric precursor and $[Fe(CN)_6]^{4-}$ anions. This report presents a unique example of an inorganic reaction where a selective metal-ligand bond undergoes dissociation assisted by the formation of intermolecular π-π and H-bonding interactions leading to the formation of the trimeric metamagnetic complex from a monomeric metamagnetic precursor for the first time. DFT calculations unequivocally prove that

the summation of the energies of all the intermolecular interactions overpasses the energy of the selective metal-ligand bond that undergoes dissociation. Crystal and supramolecular structure of both the complexes have been reported. Detailed magnetic study implies that both the monomeric and the trimeric complexes exhibit weak antiferromagnetic coupling through intermolecular π-π and H-bonding interactions. This weak antiferromagnetic interaction can be cancelled out by the application of an external magnetic field, giving rise to a metamagnetic behaviour with a critical field of *ca*. 2.0 T 2.5 T for monomeric and the trimeric samples respectively at 2 K temperature. The work reported in this chapter has been published in Inorganic Chemistry (Inorg. Chem., **2020**, 59,12, 8487-8497).

Chapter 7 deals with the design, synthesis, magnetic properties and bio-catalytic activity of a flying bee-like double phenoxido bridged dinuclear Mn^{III}-Schiff base complex decorated with double dicyanamide (dca^-) ligands and formulated as: $[Mn_2(L)_2(dca)_2]$ (where H_2L = 2,2′ -((1E,1′E)(ethane-1,2-diylbis(azanylylidene))-bis(ethan-1-yl-ylidene)) diphenol). The complex has been synthesized by one-pot stepwise reaction of the tetradentate Schiff's base ligand H_2L with $MnCl_2$ and dca^- at 1:1:2 ratio under aerobic conditions and characterized by single crystal X-ray diffraction (SC-XRD) and other spectroscopic techniques. This complex is the first reported dimeric Mn^{III} complex of a Schiff base ligand having two terminal dca^- ligands. The present study reveals that in presence of tetradentate Schiff base ligands, the use of a 1:2 Mn: dca^- ratio leads to formation of a dimeric Mn^{III} complex in contrast to the discrete mononuclear complexes or 1D structures previously obtained for the Mn:dca^- ratio of 1:1. The magnetic study indicates that the dimeric Mn^{III} complex shows a negligible Mn^{III}–Mn^{III} interaction and a large anisotropy. The AC susceptibility measurements indicate that the complex behaves as a field-induced single-molecule magnet (SMM), with a high energy barrier of 73(4) K. Moreover, the present complex exhibits a

high solvent selective catechol-oxidase-like activity for the model substrate 3,5-DTBC in acetonitrile medium. The work reported in this chapter has been published in Inorganica Chimica Acta (Inorg. Chim. Acta. **2023,** 550, 121370-121379).

Chapter 8 is the overall concluding chapter of the work carried out for this thesis. The salient observations and inferences drawn out of these investigations are presented in a nutshell. The scope of future research for the current work has also been pointed here.

(**SOMEN GOSWAMI**)
Department of Physics
Jadavpur University
Kolkata-700032, India

Contents

List of publications

Seminar, Symposium and Conferences attended

Appendix: Reprints of the published papers related to the thesis

Chapter 1

Introduction

"Synthesis is the process of making a natural product, or some other substance, artificially, in the lab, one step at a time, from extremely simple building blocks"

… Gregory. Petsko

1.1 Background and genesis of the problem

The illuminating interrogative quote of legendary scientist Richard Feynman "*What would the properties of materials be if we could really arrange the atoms the way we want them?*" [1] has acted as a stimulus to study and understand the structure-property relationship of materials which has led to design of crystalline materials by incorporating preassigned physical and chemical properties. However, fruition of such a dream in reality is a very big challenge that can be understood from the statement of Maddox "*One of the continuing scandals in the physical sciences is that it remains in general impossible to predict the structure of even the simplest crystalline solids from a knowledge of their chemical composition*" [2]. Crystal engineering (CE) along with its strong tie with modern x-ray crystallography has successfully encountered the challenges in designing and synthesis of solid crystalline materials with desired functionalities [3-15]. G. R. Desiraju has defined crystal engineering as "*the understanding of intermolecular interactions in the context of crystal packing and the utilization of such understanding in the design of new solids with desired physical and chemical properties*" [16]. Therefore, organic and metal organic designer crystals having predicted architecture and predefined functionality can be obtained by the rational understanding of covalent bonding, noncovalent interactions, molecular assembly and recognition of events and by taking help of structural topology, imposed packing similarity attained through the study of similarity in molecular structures and molecular self-assembly [17-25]. The 'node and spacer' approach proposed by Robson is the most widely used route of designing crystals with predicted architecture [26]. In the last few decades, remarkable efforts have been devoted in developing novel solid crystalline materials encompassing desired functional properties [27-36]. The metal organic frameworks (MOFs) and supramolecular metal-organic polymers (SMOPs) belonging to the

category ‘metal organic materials (MOMs)’ have gained paramount interest due to their huge technological applications [37-46]. MOFs and SMOPs both comprise two common essential units: metal moieties and organic ligands, only difference is that in case of MOFs, 2D/3D coordination networks are formed through strong metal-ligand bonds, while SMOPs are formed using non-covalent interactions [47]. In this such background, the goal of the present work is to design and synthesis of some novel transition or lanthanide metal-based MOMs and perform in depth study of their crystal structure, catalytic activity, magnetic property, host-guest behavior and enzymatic activity as per the functional properties expected to be evolved according to their structure-property relationship. In this context, a brief discussion on the ligands used in the present study and the functional properties investigated have been embedded below.

MOMs are known from several decades and gained extensive attention just after the seminal work presenting a Cu(I) containing porous coordination polymer by Robson in 1990 [48]. MOMs because of their unprecedented levels of porosity, inherent modularity offering scope of fine-tuning of both structure and bulk physical properties, evolve as most efficient class of materials for potential applications in all most all scientific and technological arena such as catalysis, molecular magnetism, electronic devices, gas storage, chemical separations, sensing etc. [49-58]. Various weak organizing forces incorporate exciting features like high flexibility, size and shape specific porosity and reversibility in molecular association-dissociation etc. in supramolecular MOMs [59-61]. These fascinating features offer a huge scope of applications of these materials in several scientific and technological fields such as ion transportation, drug delivery, catalysis, luminescence and recognition of biological molecules etc. [62-69]. The application arena of MOMs has been rapidly expanding for the last several years. The vast scope of structural fabrication and post-synthetic modification of MOMs open new avenues of

applications like electrical conduction [70], proton conduction [71], ion transportation [72], supercapacitor batteries [73], solar cell [74], ferroelectric [75], thermoelectric [76] and field-effect transistors [77] etc.

The inherent physical and chemical properties of solid crystalline materials exclusively depend on their molecular components and the fashion in which these components are aligned or linked and interact in the crystalline state [78-80]. Thus, rational understanding about nature, pattern and governing factors of different covalent and non-covalent interactions is very crucial to manipulate the arrangement of molecular or ionic components in order to achieve predefined metal-organic architectures [81-84]. According to the CE, designer extended metal-organic architectures can be easily synthesized by taking into account compatibility of the ligand used with the coordination algorithm of the metal ions [85].

Analysis of crystal structures from topological point of view as proposed by A.F. Wells has assisted in developing the ‘‘node and spacer’’ approach of crystal engineering [86-87]. Accordingly, “crystal structures are the periodic repetition of infinite 1D/2D/3D nets formed by a series of points (nodes) of certain geometry (tetrahedral, trigonal planar etc.) that are connected to a certain number of other points” [86-87]. Robson first successfully applied the ‘node and spacer’ approach to construct the metal-organic materials [26]. In the ‘node and spacer’ approach, metal ions are considered as nodes and various organic ligands act as spacers. Different organic ‘spacer’ ligands link different metal moieties (nodes) as per their coordination algorithm and generate different structural topologies such as discrete polyhedral (0D), infinite coordination chain (1D), coordination sheet (2D) and coordination cage (3D) (Figure 1). This approach is a very attractive route of designing predefined network architectures. Several research groups have employed metal

containing subunits with programmed coordination angles to synthesize metal-organic framework and macromolecular polyhedral cages [88-92].

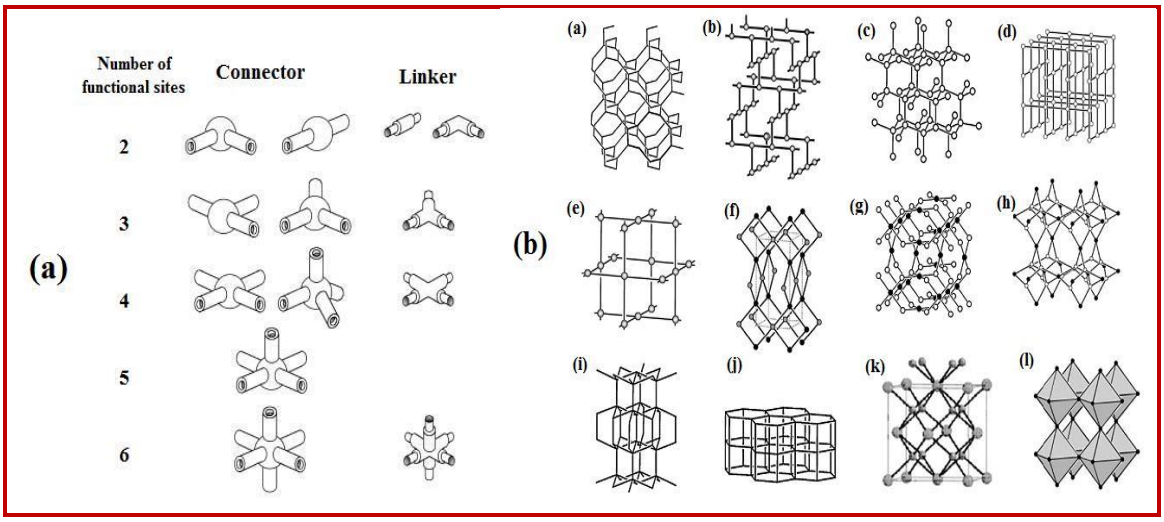

Figure 1. Different topological structures for coordination polymers that can be obtained by covalent bonding interactions (adopted with courtesy: R. Robson et.al., J. Am. Chem. Soc., 1989, 111, 15, 5962-5964, Reference no.: 26).

Bridging ligands consist of electron rich donor atoms that connect metal centers through covalent bonds in different ways and outcome is the formation of extended metal-organic frameworks or discrete metal-organic complexes with different types of nuclearities. Indeed, the supramolecular metal organic network is the upshot of assemblies of discrete metal-organic complexes through various non-covalent interactions. Thus, judicious selection of bridging ligands along with the use of proper metal ions is very crucial in the construction of every extended metal-organic network having predefined structure and functionality [93-94]. Literature survey suggests that a vast number of bridging ligands are extensively used for synthesis of metal-organic architectures of different nuclearities and dimensionalities [95-100]. A few common examples are azide, sulfate, halide, cyanate, thiocyanate, dicyanamide, oxalate, carboxylate, terepthalate, 1,3,5-benzenetricarboxylate, polycyanometallates, squarate, azobipyridine etc. Most of the bridging

ligands are capable to exhibit different bridging modes and denticities that play a decisive role in formation of the structure and functional properties of the metal-organic materials. Highly flexible structure and versatile bridging modes of dicyanamide[$N(CN)2^{-}$] ligand (Figure 2) opens scope to use dicyanamide as a building block in designing of huge varieties of molecular geometries ranging from discrete dinuclear to multinuclear and multidimensional (1D, 2D and 3D) structures [101-105]. Nature of ancillary ligands, reaction condition, metal/ dicyanamide ratio etc. are the governing factors on the bridging modes of dicyanamide ligand that determine the structural topology of synthesized materials [103,104].

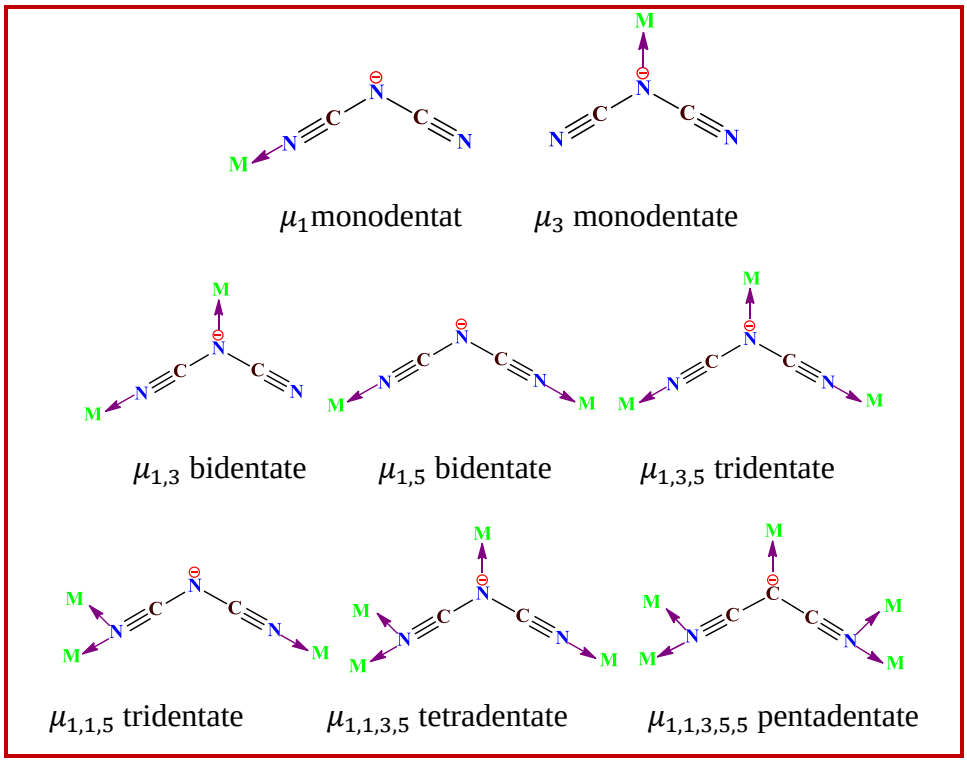

Figure 2. Various coordination and bridging modes of dicyanamide ligand.

Another interesting example of bridging ligand is squararto dianion ligand that can exhibit four different bridging modes viz *bis*- ($\mu_{1,2}$ and $\mu_{1,3}$) [106-107], *tris*- ($\mu_{1,2,3}$) [108] and *tetra-kis*- ($\mu_{1,2,3,4}$) [109] (Figure 3) and also act as bidentate chelating ligand. As per literature survey, squarate^{-2} ion adopts mono- or polymonodentate coordination modes in case of 3d transition metal

ions while bis-bidentate chelating mode are exhibited for heavy metal ions like alkaline and lanthanoid metal ions [110-111]. It has been found that the binding modes of squarate^{2-} ion can be regulated by nature of the ancillary ligands, metal ion and metal/ squarate^{2-} ratio etc. The monodentate $\mu_{1,2}$ and $\mu_{1,3}$ bridging modes are common when equimolar or excess squarate^{2-} ligand is used but in presence of excess metal ions squarate^{2-} ion adopt higher polymonodentate bridging modes ($\mu_{1,2,3}$ and $\mu_{1,2,3,4}$) [114].

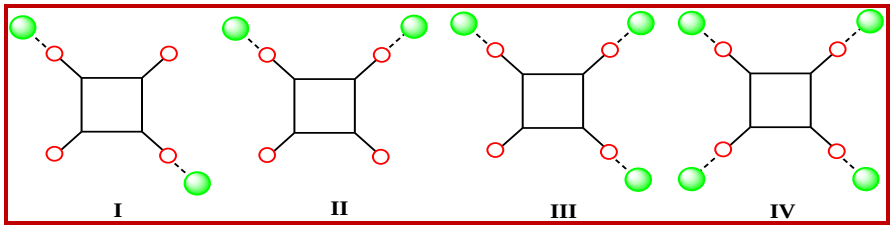

Figure 3. Various bridging modes of squarate^{2-} ligand.

Polycyanometallate anions, $[M(CN)_n]^{m-}$(n= 2–8, M= Cr, Fe, Ni, Co etc.) are considered as the most suitable linker to design metal-organic materials having both porosity and magnetic properties. Actually, strong magnetic interactions between metal centers demand short bridging structures while to incorporate porosity in frameworks requires relatively long bridging ligands [112].

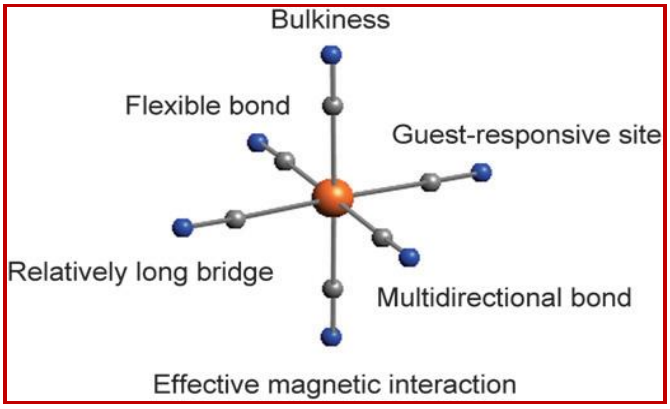

Figure 4. Important features of the polycyanometallate anion (adopted with courtesy: S. Kitagawa et.al., CrystEngComm. 2010, 12, 159–165, Reference no.: 113).

Polycyanometallate anion can fulfill both the requirements and additionally its uncoordinated cyano groups can form hydrogen bonds with guest species and make the frameworks suitable for other applications (Figure 4) [113]. Final structure and flexibility of metal-organic architectures designed by using Polycyanometallate anion depend on the metal ion ratio, auxiliary ligands and reaction condition [114-115]. Oxalate dianion ligand is capable to act as bidentate chelating ligand as well as bridging ligand with versatile binding modes. Due to its tiny size and having four oxygen donor atoms, it plays as good mediators of magnetic interaction and is also capable of forming hydrogen-bonds [116]. All these exciting features make it very appealing for designing new functional metal-organic materials of vast structural diversity ranging from zero dimensional discrete clusters to multidimensional (nD, n = 1-3) architectures [117-122]. The binding patterns of oxalate ligand to metal ions are of different fashions like syn-anti, syn-syn and anti-anti. The bridging modes, binding pattern of oxalate ligand and presence of auxiliary ligands have significant roles on structural topology as well as functionality of synthesized frameworks [116].

Approximately nine-out-of-ten chemical processes need catalysts and thus are considered as most important ingredient of industrial preparations of countless essential commodities [123]. The global catalyst market is about of 15-20 billion USD per annum making tremendous impact on the global economy [58]. The commercial value of the products achieved through industrial preparation (including refinery process) using catalyst is assessed to be closer to several trillion USD [58]. So, there is a huge commercial demand of improving efficiency of catalytic materials using new technologies and developing highly efficient new catalysts. MOMs with accessible metal sites, proactive organic linkers and tunable porosity strongly attract synthetic chemists to use them as an active catalyst or catalyst support in many organic reactions of industrial importance

[124-132]. Few worthy examples are, $[Cu_3(BTC)_2]$ MOF is an efficient heterogeneous catalyst in many organic reactions namely Michael reaction, isomerization, cyclisation etc. [133-135]. MOF-5 is a good carrier of Cu particles and Cu@MOF-5 is an active catalyst in the synthesis of methanol from synthetic gas [136]. Currently, product selective catalysis of important organic reactions is the new surge of modern organic preparations since it cut off the effort, time and money in separation of the biproducts. Catalysis of chiral and enantioselective syntheses are the important aspect of pharmaceutical industries. MOMs with shape and sizes selective porosity and the post synthesis modified MOMs may act as effective catalysts to meet this goal [137-140].

Metal-organic materials are capable of exhibiting fascinating magnetic behaviors depending upon the magnetic exchange interactions present between the constituting paramagnetic metal centers. Subsequently, another golden opportunity of such materials is their use as molecule-based magnets. The great advantage of the use of molecule-based magnets over traditional magnets is that the structure and functionality of molecule-based magnets can be programmed and tailored as desired [141]. Nowadays, low dimensional and low-density magnetic materials have gained utmost priority due to their huge applications in high-density data storage, magnetic switch, quantum computation and magnetic imaging etc. [142-149]. In this regard, single molecules, 1D chains or 2D layer structured metal-organic materials showing slow magnetic relaxation and high magnetic anisotropy are considered as high-valued materials [150-151]. It is noteworthy that covalent bonds as well as various weak intermolecular forces have a very significant role on magnetic properties of MOMs [152-153]. Modern research has emphasized on the design of multi-functional molecular magnets demonstrating unique magnetic behaviors in conjugation with other functional properties [154-155]. For example, Long et.al reported an outstanding example of Fe-based magnetic MOF: Fe_2(dobdc) (dobdc^{4-}: 2,5-dioxido-1,4-benzenedicarboxylate) [156] that

exhibit excellent performance in separation of different components of hydrocarbons (methane, ethane, ethylene, and acetylene) mixtures. The magnetic behavior of the compound is changed in different manners upon exposure of different hydrocarbons relating to their interaction capability with the framework (Figure 5). The thoughtful selection of organic ligands and metal ions is very crucial for developing molecular magnets combined with other functionalities.

MOMs due to its tunable porosity and functionalities are exclusively used to imitate the activity of important biomolecules, especially as enzymes and they are also used in biosensing/imaging, and biomedical applications [157-163].

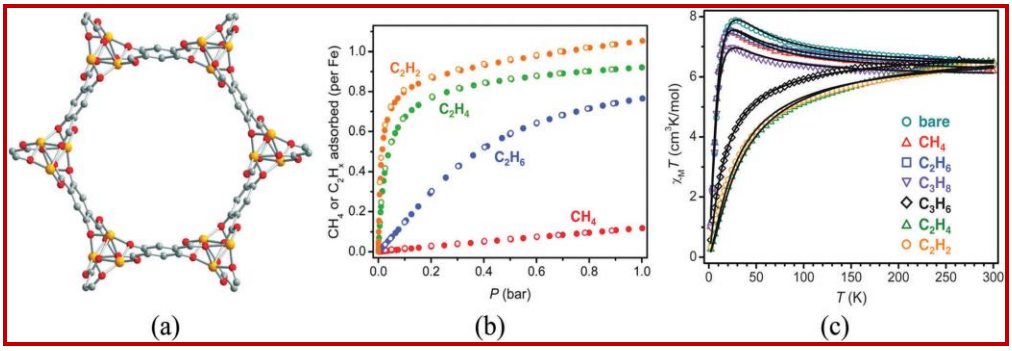

Figure 5. (a) Crystal structure of: Fe_2(dobdc), (b) gas adsorption isotherms for acetylene, ethylene, methane, ethane at 318 K in the MOF; (c) Variation in magnetic susceptibility of variable temperature of the compound in a vacuum (bare) and upon exposure of different hydrocarbons (adopted with courtesy: J. R. Long et.al., Scienc*e*, 2012, 335, 1606, Reference no.: 156).

In literature, numerous MOMs are reported that have capability to function as bio-catalyst mimicking important enzymes like catechol oxidase (CO), phenoxazinone synthase (PHS) etc. [164-166]. In recent time, many porphyrin-incorporated MOMs having enzyme mimicking and bio-sensing activities are developed [167-170]. As a representative example, a zirconium-based MOM PCN-222 was developed by Zhou's group that has an excellent peroxidase enzyme like activity [167]. Nowadays, MOMs are also used to extract toxic gases produced in living organisms.

For example, nitric oxide (NO) is found to be responsible for vasodilation causing serious toxic effects in the human body. Many MOFs of the M_2(dobdc) series are tested and found to be very efficient for adsorption and release of NO gas [171-173].

MOMS designed with lanthanide metal ions/clusters and π···electrons donor ligands exhibit excellent photoluminescence behavior. Such luminescent MOMs are very promising candidates in sensing of molecules/ions and also as light-emitting devices [174-178]. Few luminescent MOMs are reported to detect highly explosive molecules like trinitrotoluene (TNT), small hazardous organic molecules and toxic metal ions (As^{+3}, Hg^{+2}) contaminated with water samples even at very low concentration [179-181]. Mesoporous MOMs are capable for optimal uptake and delivery of drug molecules at a controlled rate due to their highly ordered porosity, framework flexibility and weak non-covalent interactions with guest drugs molecules [182-185].

In this background, the design and synthesis of new metal organic materials comprising of transition or lanthanide metal ions and the study of their structural, optical, magnetic, electrochemical, properties etc. are appear to be very much promising in the quest for of their functional application possibilities. This thesis primly focuses on (i) the design, synthesis, structural, physical and microanalytical characterization of {[Ni(squarate)(2,2′-bipy)(H_2O)]·H_2O}$_n$ (compound **I**), [Pr(1,10 phen)$_2$ (H_2O)$_5$] Cl_3(H_2O) (CH_3OH), (compound **II**), [Cu_2 (oxalate)(1,10-phen)$_2Cl_2$], (compound **III**) [Mn(L)(H_2O)Cl], (compound **IV** (H_3O)[Mn(L)(H_2O)$_2$]{[Mn(L)(H_2O)]$_2$Fe(CN)$_6$}·4H_2O (compound **V**), and [Mn_2(L)$_2$(dca)$_2$] (compound **VI**) [where, 2,2′-bipy = 2,2′-bipyridine, 1,10-phen = 1,10-phenanthroline and H_2L = Schiff's base ligand, dca= dicyanmide], (ii) modification and optimization of reaction conditions in the synthesis of the above mentioned materials using crystal engineering approach, (iii) study of magnetic property of compound **I, IV, V, VI,** product selective catalytic activity study of

compound **III**, bio-catalytic activity study of compound **VI** and host-guest activity study of compound **II**, and (iv) examining the structure-property relationship of compounds **III, IV** and **V**.

1.2 Brief literature review

The vast scope of requirement based structural modification along with several fascinating properties of MOMs expose a new horizon of applications in countless technological and industrial fields. The work embedded in the present thesis mainly deals with the functional aspects of transition and lanthanide metal ions-based MOMs in the field of catalysis, magnetic materials and host-guest study etc. In this endeavor, a brief general discussion on potential applications of transition and lanthanide metal ions-based MOMs in the above-mentioned arena has been depicted below. The detailed review of literature will be found in each chapter where the full work has been described.

1.2.1 Magnetic materials

Polymetallic systems are capable to exhibit different magnetic behaviors such as ferromagnetism, antiferromagnetism and ferrimagnetism depending upon the magnetic exchange interactions present between the paramagnetic metal centers. Transition and lanthanides metal ions are most commonly used in designing of molecule-based magnetic materials owing to their several unique properties like stable oxidation state, high spin configuration, strong spin-orbit coupling, large uniaxial anisotropy etc. [186-188] SMM and SCM are considered as the most optimist classes of low dimensional molecular magnets owing to their slow magnetic relaxation and high magnetic anisotropic nature and hence extensive effort has been paid in their design and synthesis in the last few years [189-191]. SMMs are zero-dimensional (0D) molecular systems which display slow relaxation of the magnetization and a magnetic hysteresis at a temperature lower than its blocking

temperature (T_B). Transition metal, lanthanide and mixed transition- lanthanide metal ions-based clusters are reported to exhibit SMM behaviors [192-195]. The first milestone examples of SMM is a mixed-valent Mn_{12} cluster {$[Mn_{12}O_{12}(OAc)_{16}(H_2O)_4]$,2AcOH,4$H_2O$ ($Mn_{12}OAc$)} presented by Sessoli et.al [196] and soon after several similar type of Mn_{12} cluster based SMM have been reported [197]. But all have very low blocking temperature (T_B < 10K). Till date the highest blocking temperature T_B =170K is reported for a unique tetranuclear Dy(III) cluster based SMM (Figure 6)[198].

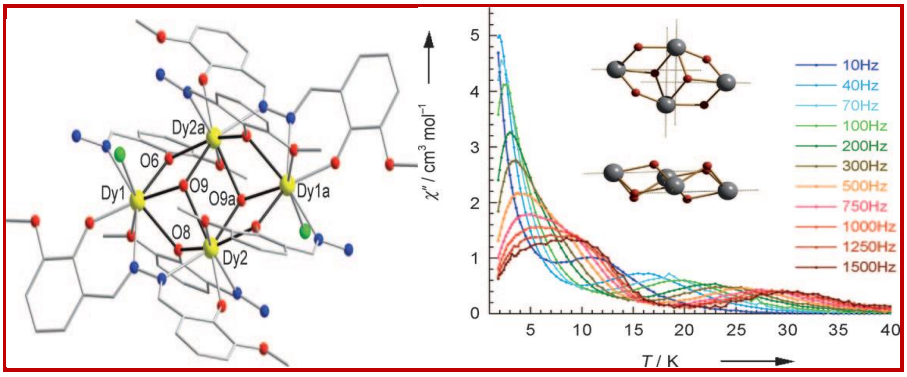

Figure 6. Crystal structure of the tetranuclear Dy(III) cluster (left), temperature variation of out-of-phase (χ") of ac susceptibility under zero dc field (right) (adopted with courtesy: M. Murugesu et.al., Angew. Chem., Int. Ed. 2009, 48, 9489, Reference no.:198).

SCM are essentially 1D or 2D systems in which the magnetic behavior arises from large uniaxial-type magnetic anisotropy associated with strong intrachain and negligible interchain magnetic interactions [199-201]. SCM have similar features as SMM but the difference is that they usually have a high blocking temperature and hence are better choice in technological applications [202]. In 2001, Caneschi et.al., reported the first example of SCM of formula {$Co(hfac)_2[NIT(C_6H_4$*p*-OMe)]} that showed magnetic hysteresis of molecular origin below 4 K [203]. Bridging ligands are very important in the design of SCM as they act as mediators for strong magnetic coupling between the spin carriers in a particular chain [204]. Several Co^{+2}, Ni^{+2}, Mn^{+3}

and Fe^{+2} based 1D or 2D polymetallic compounds have been reported till date that exhibited SCM behavior [205-208].

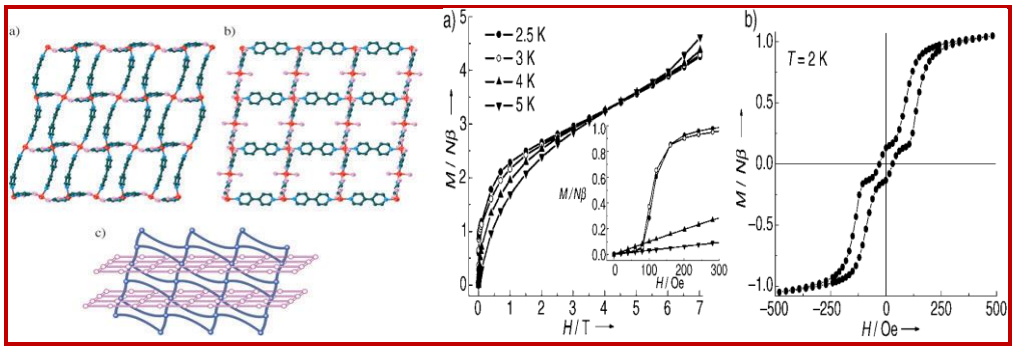

Figure 7. 2D coordination sheets (left), Plots of a) the first magnetization at 2–5 K and b) the hysteresis loop at 2 K (right) (adopted with courtesy, X-M. Chen et.al., Angew. Chem. Int. Ed. 2005, 44, 3079–3082, Reference no.: 216).

Metamagnets are a special type of magnetic materials consisting of discrete molecular or 1D or 2D magnetic motifs in which the weak antiferromagnetic interchain interactions can be overcome by a critical magnetic field at low temperature leading to ferromagnetic exchange. Metamagnetic materials have significant applications in technologies associated with magnetic switch, magnetic cooling and magnetocaloric effect [209-210]. Various transition metal ions (e.g. Co^{+2}, Ni^{+2}, Mn^{+3}, Fe^{+2} etc.) are being used to design a large number of metamagnetic materials [211-216]. For examples, Mukherjee et.al have reported a metamagnet of Ni (II) having azido bridged 1D chain structure [216] and Chen et.at reported a metamagnetic Co (II) based 2D coordination sheets (Figure 7) [216].

1.2.2 Catalysis

Transition and lanthanide metal-based MOMs with easily accessible metal sites, tunable porosity and scopes of post synthetic modification prove as effective and useful catalysts in many industrially significant organic reactions with high product selectivity. The catalytic activity of

MOMs arises due to several structural features like, i) presence of unsaturated metal centers, ii) free organic functional sites, and iii) specific functionalized porosity. Plethora of examples of MOMs comprising of transition and lanthanide metal ions as hetero- and homogeneous catalysts for important organic transformation were documented and reviewed by several groups [217-219]. Few novel examples of organic reactions catalysed by MOMs are given in the list below:

Table 2. Selected examples of MOMs-catalysed reactions

MOM materials	Substrates	Reaction type	Ref.
$Co(sal)(H_2O)(Py)_3$	Linear and cyclic olefins	Epoxidation of Olefins	220
$Cu_3(BTC)_2$	i)α-Pinene oxide, ii) Citronella iii)2-Bromopropiophenone	i)Isomerization, ii)Cyclization iii) Rearrangement	221
$[Cd(bpy)_2](NO_3)_2$	Benzaldehyde and cyanotrimethylsilane	Cyanosilylation of aldehydes	222
$[In_4(OH)_6(BDC)_3]$	1-Nitro-2methylnaphthalene, nitrobenzene + H_2	Hydrogenation	223
$[La_2(BDC)_3(H_2O)_2]H_2O$	Benzaldehyde + trimethylorthoformate	Acetalization	224
$[Ni(L\text{-}asp)bpy_{0.5}]HCl_{0.9}MeOH_{0.5}$	Cis-2,3-epoxybutane	Methanolysis of epoxides	225
$[Zn_3(m3\text{-}O)(O_2CR)_6(H_2O)_3]^{n+}$	Esters and alcohols	Transesterification	226
$[Ag_3(tpha)_2]BF_4$	Methyl-2-acetate + N-methylmaleimide	1,3-dipolar cycloaddition	227
$[Cr_3F(H_2O)_2O(BDC)_3]$	i) Benzaldehyde + ethyl cyanoacetate ii) iodobenzene + acrylic acid	i)Knoevenagel condensation ii) Heck coupling	228
$[Mn_3((Mn_4Cl)_3BTT_8(MeOH)_{10})]_2$	Aldehydes and cyanotrimethylsilane	Cyanosilylation of aldehydes	229
$Zn_4O(BDC)_3$	*tert*-Butyl chloride and toluene	Friedel-Crafts alkylation	230
$Pd(2\text{-}pymo)_2$	i) Cinnamyl alcohol and air ii) Octane/cyclododecene +H_2 iii) Aryl halides + arylboronic acids	i) Alcohol oxidation ii) Hydrogenation iii) Suzuki–Miyaura coupling	231

Post-synthetic modification (PSM) is a very interesting approach to make a MOM efficient catalyst for a particular type of reaction that sometimes yield the desired product with selectivity. For example, amine functionalized iron containing frameworks modified with cyclic anhydride act as an active catalyst in C-C bond forming reactions [232-233]. Kitagawa et.al. reported a amide functionalized 3D porous coordination polymer, $([Cd(4\text{- btapa})_2(NO_3)_2]\cdot 6H_2O\cdot 2DMF)_n$, that offer selective accommodation of guests and hence showed excellent product selective catalytic activity in Knoevenagel condensation (Figure 8)[74].Catalysis in chiral synthesis and enantioselective production of desired isomer is the important theme of pharmaceutical industries. The addition reaction of diethylzinc to 1-naphthaldehyde catalyzed by homochiral MOF,$[Cd_3L_4(NO_3)_6]\cdot 7MeOH\cdot 5H_2O$ (L = (R)-6,6-dichloro-2,2-dihydroxy-1,1-binaphthyl-4,4-bipyridine) with excess $Ti(O^iPr)_4$ in toluene yields (R)-1-(1-naphthyl)-propanol with complete conversion and 90.0% ee [234].

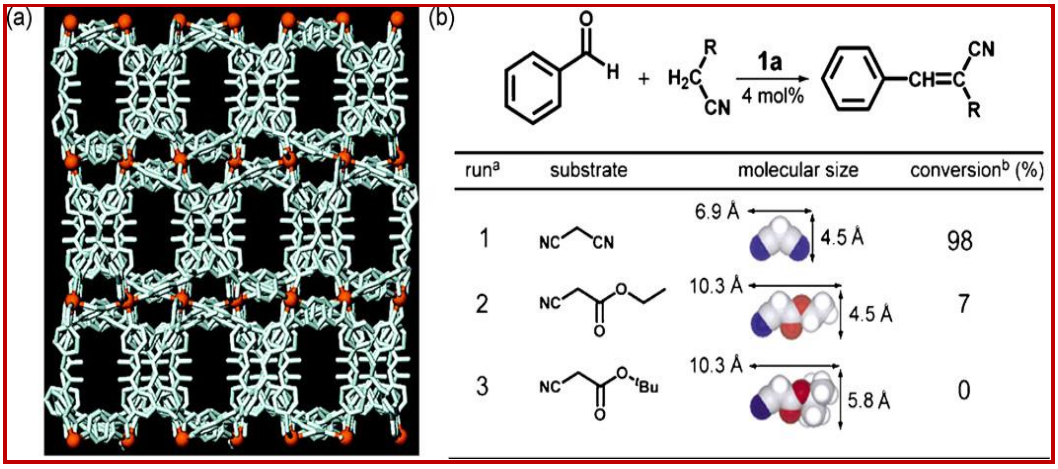

Figure 8. (a) Crystal structure to $([Cd(4\text{- btapa})_2(NO_3)_2]\cdot 6H_2O\cdot 2DMF)_n$. (b) product selective Knoevenagel condensation reaction of benzaldehyde with substrates (adopted with courtesy: S. Kitagawa et.al., J. Am. Chem. Soc. 2007, 129, 2607, Reference no.:46).

1.2.3 Host-guest activity and molecular recognition

Molecular recognition is defined as a specific supramolecular interaction between a host molecule with a matching guest molecule, which makes a host-guest complex. Generally, the host is a large molecule or aggregate of such molecules having a substantial central hole or cavity. The guest molecule may be an anion or cation or a simple small organic molecule or any solvent molecule. Molecules are capable of recognizing each other via noncovalent interactions and the process may be both static and dynamic (Figure 9) [235]. The host-guest activity of many metal organic complexes facilitate their use in various arenas like catalysis, molecular sensors, drug delivery etc. For example, supramolecular metal-ligand assemblies having M_4L_6 stoichiometry (M denote metal ions like Al^{3+}, Ti^{4+}, Fe^{3+}, Ga^{3+}, Ge^{4+}, and L = 1,5-bis(2′,3′-dihydroxybenzamido) naphthalene ligand) developed by Raymond et.al., can be utilize as catalytic host in Aza-Cope rearrangement reactions [236].

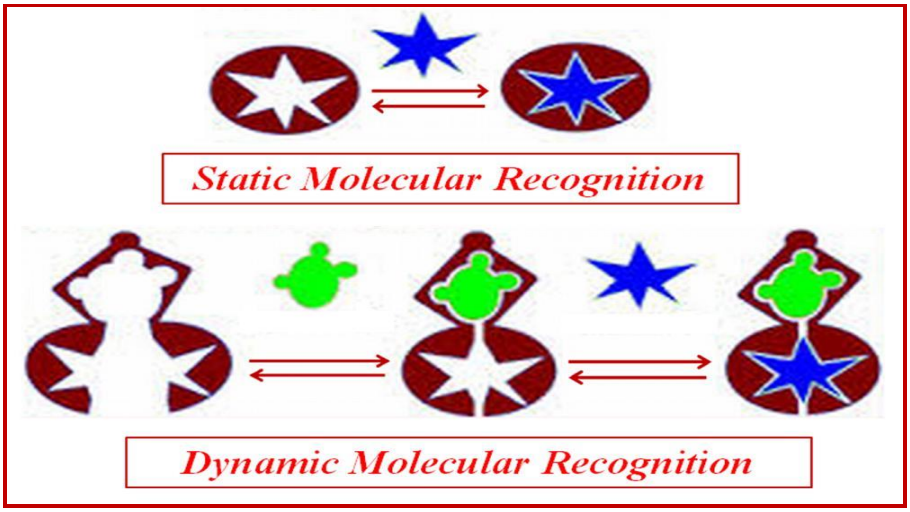

Figure 9: Static and dynamic molecular recognition phenomena (adopted with courtesy: J. M. Cram et.al., *Science*, 1974, 183, 803, Reference no.:235).

A number of lanthanide and transition metal ions-based luminescent MOMs are reported whose luminescence behavior is noticeably changed by various guest molecules present within the

materials acting as hosts [237-238]. Using this behavior, many luminescent MOMs were employed as chemical sensors to detect various guest molecules like cations, anions, solvent molecules, small organic and bio-molecules. For example, the emission maximum of Zn_2(tpce) (tpce = tetrakis(4-carboxyphenyl) ehtylene) is very sensible but different extent towards amine guests (Et_3N, ethylendiamine, NH_3 etc.) [239]. Many metal organic materials can bind guest species in reversible ways and hence can be used as potential carriers of drug molecules [240]. MOFs having composition [$M^{III}_3OX(H_2O)_2L_n$, H_2O] (where, M=Cr, X=F/OH, L= BDC or BTC and n=2) are capable to bind ibuprofen molecule through π-π interactions and hence can show controlled uptake and release of ibuprofen [241].

1.3 Objectives and scopes of the work

The objectives of the present thesis are:

(i) design and synthesis of a nickel (Ni) based bifunctional MOF using judiciously selected spacer and bridging ligands so that it exhibits metal-organic supramolecular host (MOSH) behavior along with antiferromagnetic property,

(ii) design and synthesis of a praseodymium (Pr) based flexible supramolecular metal-organic polymer (SMOP) and detail study of its dynamic MOSH behavior upon the expulsion and reabsorption of guest water molecules,

(iii) preparation of a Cu based SMOP using 1,10-phenanthroline as spacer and oxalate as bridging ligands along with exploring its product selective catalytic activity in significant organic reactions like oxidation of alkenes,

(iv) design and synthesis of Mn(III) based metamagnetic MOMs using crystal engineering approach with judicious selection of appropriate Schiff base and bridging ligands along with detail study of their magnetic properties,

(v) design and synthesis of a Mn(III) based multifunctional MOM using dicyanamide as bridging ligand and exploring its magnetic as well as model enzyme mimic activity for catechol-oxidase using 3,5-di-tert-butylcatechol (3,5-DTBC) as model substrate in different solvents,

(vi) to achieve above mentioned MOMs in solid crystalline state with good yield by rational modification of reaction techniques and tuning of various reaction parameters like temperature, solvent polarity, solvent ratio, pH, reagent ratio and reaction time etc,

(vii) analysis of crystal and supramolecular structure of the synthesized materials using SC-XRD data along with their microanalytical analysis, thermal property study and physical characterization by using FTIR, UV-Vis, ^{1}H-NMR, ESI-mass techniques, and

(viii) examining the structure-property relationship of the materials through theoretical study for three representative samples viz., compounds III, IV and V .

In this context, the scopes of the present thesis are as follows:

1. to design, synthesis, analyzing crystal structure and supramolecular structure and study of the thermal, photoluminescence and magnetic properties of an unusual μ-$_{1,2,3}$-squarato-bridged 2D coordination polymer: $\{[Ni(squarate)(2,2'\text{-bipy})(H_2O)]\cdot H_2O\}_n$ with the target to examine the possibility of utilizing it as metal-organic supramolecular host and photo-luminescent agent,

2. to synthesize the designer crystal of a dynamic metal organic supramolecular host of Pr (III)-complex, $\{[Pr(1,10\ phen)_2\ (H_2O)_5]\ Cl_3(H_2O)\ (CH_3OH)\}$, by incorporating a 2D water-chloride-methanolic supramolecular sheet and thorough investigation of its structural, thermal and optical properties for following dynamical binding character of this host with the guest solvents and chloride ions,

3. (a) to synthesize and study the structural, thermal, spectral and redox behavior of a binuclear Cu (II)-complex: $[Cu_2(oxalate)(1,10phen)_2Cl_2]$ containing hydrophilic oxalate as bridging ligand and

the hydrophobic 1,10-phen as the blocker ligand, (b) to explore the homogeneous product selective catalytic activity of the sample in the oxidation of a series of alkenes (*cis*-cyclooctene, styrene and cyclohexene) by various oxidizing agents, and (c) to examine the role of various reaction parameters to achieve optimized reaction conditions of the above said catalytic reaction,

4. (a) to synthesize the designer crystal of a metamagnetic mononuclear Mn(III)-Schiff base complex :[Mn(L)(H_2O)Cl] and a metamagnetic trinuclear Mn_2Fe complex:$\{[Mn(L)(H_2O)]_2Fe(CN)_6\}^2$ from its monomeric precursor and $[Fe(CN)_6]^{4-}$ anions, (b) to investigate its structural, thermal and magnetic behavior, and (c) to examine selective and irreversible metal-ligand bond breaking reaction occurring during the synthesis of the trinuclear Mn_2Fe complex from the monomeric [Mn(L)(H_2O)Cl] and $[Fe(CN)_6]^{4-}$ anions as precursors through experimental and theoretical study, and

5. (a) to dsign and synthesis of a dimeric Mn(III) complex having unique combination of double phenoxido bridge and terminal dicynamide ligand, (b) to analyze crystal and supramolecular structure and study of optical and magnetic properties of the sample, (c) to investigate the solvent selective catechol oxidase enzyme like activity of the sample, and d) to elucidate of structure-property relationship of the complex.

References

[1] R. Feynman, *Eng. Sci*., **1960**, 23, 5, 22.

[2] J. Maddox, *Nature*, **1988**, 335, 201.

[3] G. R. Desiraju and A. Gavezzotti, *Chem. Commun.*, **1989**, 621-623.

[4] M. C. Etter, *J. Phys. Chem.*, **1991**, 95, 4601-4610.

[5] G. R. Desiraju, *Chem. Commun.*, **1997**, 16, 1475.

[6] D. Braga, F. Grepioni and G. R. Desiraju, *Chem. Rev.*, **1998**, 98, 1375.

[7] N. N. Laxmi Madhavi, C. Bilton, J. A. K. Howard, F. H. Allen, A. Nangia and G. R. Desiraju, *New J. Chem.*, **2000**, 24, 1.

[8] B. Moulton and M. J. Zaworotko, *Chem. Rev.*, **2001**, 101, 1629.

[9] G. R. Desiraju, *Angew. Chem., Int. Ed.*, **2007**, 46, 8342.

[10] G. M. Sheldrick, *Acta Cryst. A*, **2008**, 64, 112.

[11] G. R. Desiraju, *J. Chem. Sci.*, **2010**, 122, 667.

[12] E. R. T. Tiekink, J. J. Vittal and M. J. Zaworotko, *Organic Crystal Engineering: Frontiers in Crystal Engineering*, John Wiley & Sons, Ltd, **2010**.

[13] A. Ramanan, G. R. Desiraju and J. J. Vittal, *Crystal Engineering: A Textbook*, World Scientific, **2011**.

[14] C. R. Groom, I. J. Bruno, M. P. Lightfoot and S. C. Ward, *Acta Cryst. B*, **2016**, 72, 171.

[15] A. K. Nangia and G. R. Desiraju, *Chem. Int. Ed.*, **2019**, 58, 4100.

[16] G. R. Desiraju, *Crystal Engineering: The Design of Organic Solids*, Materials Science Monographs 54, Elsevier, Amsterdam, **1989.**

[17] G. Cavallo, P. Metrangolo, R. Milani, T. Pilati, A. Priimagi, G. Resnati and G. Terraneo, *Chem. Rev.*, **2016**, 116, 2478.

[18] C.A. Hunter and J. K. M. Sanders, *J. Am. Chem. Soc.*, **2017**, 112, 5525.

[19] S. Yamada., *Chemical Reviews*, **2018**, 118, 11353.

[20] M. T. Rodgers and P. B. Armentrout, *Chemical Reviews*, **2016**, 116, 5642.

[21] Q. Li and Z. Li, *Acc. Chem. Res.*, **2020**, 53, 962.

[22] J. D. Dunitz, *Thoughts on Crystals as Supermolecules*, John Wiley & Sons, Ltd., **2007**, 1-30.

[23] J. W. Steed and J. L. Atwood, *Supramolecular Chemistry. 2 ed.*, John Wiley & Sons Ltd, Hoboken, New Jersey, **2009**.

[24] J. M. Lehn, *Supramolecular Chemistry: Concepts and Perspectives*, VCH, Weinheim, **1995.**

[25] G. R. Desiraju, *Acc. Chem. Soc.*, **1996**, 29, 441.

[26] B. F. Hoskins and R. Robson, *J. Am. Chem. Soc.*, **1989**, 111, 15, 5962–5964.

[27] J. Liu, L. Chen, H. Cui, J. Zhang, L. Zhang and C.Y. Su, *Chem. Soc. Rev.*, **2014**, 43, 6011.

[28] S. R. Batten, N. R. Champness, X. M. Chen, J. Garcia-Martinez, S. Kitagawa, L.Öhrström, M. O'Keeffe, M. P. Suh and J. Reedijk, *Cryst Eng.Comm.*, **2012**, 14, 3001.

[29] J. Perry IV, J. Perman and M. Zaworotko, *Chem. Soc. Rev.*, **2009**, 38, 1400.

[30] T. Glaser, *Chem. Commun.*, **2011**, 47, 116–130.

[31] P. D. Beer and J. Cadman, *Coord. Chem. Rev.*, **2000**, 205, 131–155.

[32] J. L. C. Rowsell and O.M. Yaghi, *Angew. Chem. Int. Ed.*, **2005**, 44, 4670.

[33] M. Dinca and J. R. Long, *Angew. Chem. Int. Ed.*, **2008**, 47, 6766.

[34] J. Goldsmith, A. G. W. Foy, M. J. Cafarella and D. J. Siegel, *Chem. Mater.*, **2013**, 25, 3373.

[35] L. Yan, C. Li and X. Chen, *Journal of Molecular Structure*, **2014**, 1058, 277.

[36] L. Yan, C. Li, J. Fu and M. Sun, *Synthesis and Reactivity in Inorganic, Metal-Organic, and Nano-Metal Chemistry*, **2014**, 44, 814.

[37] R. J. Kuppler, D. J. Timmons, Q. R. Fang, J. R. Li, T. A. Makal, M. D. Young, D. Yuan, D. Zhao, W. Zhuang and H.-C Zhou, *Coord. Chem. Rev.*, **2009**, 253, 3042–3066.

[38] P. H. Dinolfo and J. T. Hupp; *Chem. Mater.*, **2001**, 13, 3113-3125.

[39] H. Furukawa, K. E. Cordova, M- O'Keeffe, and O. M. Yaghi, *Science.*, **2013**, 341, 1230.

[40] G. Givaja, P. Amo-Ochoa, C. J. Gomez-García and F. Zamora, *Chem. Soc. Rev.*, **2012**, 41, 115−147.

[41] J.-R. Li, R. J. Kuppler and H.-C. Zhou, *Chem. Soc. Rev.*, 2009, **38**, 1477−1504.

[42] J. Lee, O. K. Farha, J. Roberts, K. A. Scheidt, S. T. Nguyen and J. T. Hupp, *Chem. Soc. Rev.*, **2009**, 38, 1450−1459.

[43] S. Goswami, L. Ma, A. B. F. Martinson, M. R. Wasielewski, O. K. Farha and J.T. Hupp; *ACS Appl. Mater. Interfaces.*, **2016**, 8, 45, 30863–30870.

[44] M. H. Alkordi, Y.L. Liu, R.W. Larsen, J.F. Eubank and M. Eddaoudi, *J. Am. Chem. Soc.*, **2008**, 130, 12639.

[45] C. Biswas, P. Mukherjee, M.G.B. Drew, C.J. Gomez-Garcia, J.M. Clemente-Juan and A. Ghosh, *Inorg. Chem.*, **2007**, 46, 10771.

[46] S. Hasegawa, S. Horike, R. Matsuda, S. Furukawa, K. Mochizuki, Y. Kinoshita and S. Kitagawa, *J. Am. Chem. Soc.*, **2007**, 129, 2607.

[47] S. R. Batten, N. R. Champness, X.M. Chen, J. Garcia-Martinez, S. Kitagawa, L. Öhrström, M. O'Keeffe, M.P. Suh, and J. Reedijk, *Pure Appl. Chem.*, **2013**, 85, 1715–1724.

[48] B. F. Hoskins and R. Robson, *J. Am. Chem. Soc.*, **1990**, 112, 1546-1554.

[49] S. K. Ghosh, *Metal-Organic Frameworks (MOFs) for Environmental Applications*, Elsevier, **2019**.

[50] S. R. Batten, B. F. Hoskins and R. Robson, *Chem.Commun.*, **1991**, 6, 445.

[51] B. Chen, C. Liang, J. Yang, D.S. Contreras, Y.L. Clancy, E.B. Lobkovsky, O.M. Yaghi and S. Dai, *Angew. Chem. Int. Ed.*, **2006**, 45, 1390.

[52] P. P. Bag, G. P. Singh, S. Singha and G. Roymahapatra, *Engineered Science*, **2021**,13, 1.

[53] N. W. Ockwig, O. Delgado-Friedrichs, M. O'Keeffe and O. M. Yaghi, *Acc. Chem. Res.*, **2005**, 38, 176.

[54] D. Tanaka, K. Nakagawa, M. Higuchi, S. Horike, Y. Kubota, L.C. Kobayashi, M. Takata and S. Kitagawa, *Angew. Chem. Int. Ed.*, **2008**, 47, 3914.

[55] R. B. Lin, S. Xiang, B. Li, Y. Cui, W. Zhou, G. Qian and B. Chen, *Isr. J. Chem.*, **2018**,

58, 949.

[56] M. Fujita, K. Umemoto, M. Yoshizawa, N. Fujita, T. Kusukawa and K. Biradha, *Chem. Commun.*, **2001**, 6, 509.

[57] Y. Li and R. T. Yang, *Langmuir*, **2007**, 23, 12937.

[58] A. U. Czaja, N. Trukhanb and U. Muller, *Chem. Soc. Rev.*, **2009**, 38, 1284–1293.

[59] S. Kitagawa, R. Kitaura and S. Noro, *Angew. Chem. Int. Ed.*, **2004**, 43, 2334 –2375.

[60] R. Kitaura, K. Seki, G. Akiyama and S. Kitagawa, *Angew. Chem. Int. Ed.*, **2003**, 42, 428-431.

[61] J. Zhang, H. Wu, T. J. Emge and J. Li, *Chem. Commun.*, **2010**, 46, 9152–9154.

[62] M. R. Jensen, K. Houben, E. Lescop, L. Blanchard, R. W. H. Ruigrok and M. Blackledge, *J. Am. Chem. Soc.*, **2008**, 130, 8055.

[63] R. E. Babine and S. L. Bender, *Chem. Rev.*, **1997**, 97, 1359

[64] R. R. French, P. Holzer, M.G. Leuenberger and W.-D.Woggon, *Angew. Chem., Int. Ed.*, 2000, **39**, 1267.

[65] M. Xu, S. Wu, F. Zeng and C. Yu, *Langmuir*, **2009**, 26, 4529.

[66] Y. Yamanoi, Y.Sakamoto, T. Kusukawa, M. Fujita, S. Sakamoto and K. Yamaguchi, *J. Am. Chem. Soc.*, **2001**, 123, 980-981.

[67] M. Plabst, L. B. McCusker and T. Bein, *J. Am. Chem. Soc.*, **2009**, 131, 18112-18118.

[68] A. C. McKinlay, R. E. Morris, P. Horcajada, G. Férey, R. Gref, P. Couvreur and C. Serre, *Angew. Chem. Int. Ed.*, **2010**, 49, 6260–6266.

[69] B. V. Harbuzaru, A. Corma, F. Rey, P. Atienzar, J. L. Jordá, H. García, D. Ananias, L. D. Carlos and J. Rocha, *Angew. Chem. Int. Ed.*, **2008**, 47, 1080–1083.

[70] A. A. Talin, A. Centrone, A. C. Ford, M. E. Foster, V. Stavila, P. Haney, R. A. Kinney, V. Szalai, F. El Gabaly, H. P. Yoon, F. Leonard and M. D. Allendorf, *Science*, **2014**, 343, 66-69.

[71] M. Yoon, K. Suh, S. Natarajan, and K. Kim, *Angew. Chem. Int. Ed.*, **2013**, 52, 2688 – 2700.

[72] S. Horike, D. Umeyama and S. Kitagawa, *Acc. Chem. Res.*, **2013**, 46, 2376.

[73] Z. Zhang, H. Yoshikawa and K. Awaga, *Chem. Mater.,* **2016**, 28,1298.

[74] K. M. Choi, H. M. Jeong, J. H. Park, Y. Zhang, J. K. Kang and O. M. Yaghi, *ACS Nano*, **2014**, 8, 7451.

[75] J. Liu, W. Zhou, J. Liu, I. Howard, G. Kilibarda, S. Schlabach, D. Coupry, M. Addicoat, S. Yoneda, Y. Tsutsui, T. Sakurai, S. Seki, Z. Wang, P. Lindemann, E. Redel, T. Heine, and C. Wöll, *Angew. Chem., Int. Ed.*, **2015**, 54, 7441.

[76] D. Di Sante, A. Stroppa, P. Jain and S. Picozzi, J. Am. Chem.Soc., 2013, 135, 18126.

[77] X. Huang, P. Sheng, Z. Tu, F. Zhang, J. Wang, H. Geng, Y. Zou, C. Di, Y. Yi, Y. Sun, W. Xu and D. Zhu, *Nat. Commun.*, **2015**, 6,7408.

[78] G. R. Desiraju; *Nature Mater*, **2002**, 1, 77.

[79] D. Braga, F. Grepioni, K. Biradha, V. R. Pedireddi and G. R. Desiraju, *J. Am. Chem. Soc*., **1995**, 117, 3156.

[80] K. Biradha, *CrystEngComm*, **2003**, 66, 374–384.

[81] L. Brammer, *Chem. Soc. Rev.*, **2004**, 33, 476 – 489.

[82] D. L. Caulder and K. N. Raymond, *Acc. Chem. Res.*, **1999**, 32, 975–982.

[83] P. J. Stang and B. Olenyuk, *Acc. Chem. Res.*, **1997**, 30, 502–518.

[84] D. Tranchemontagne, Z. Ni, M. O'Keeffe and O. Yaghi, *Angew. Chem., Int. Ed.*, **2008**, 47, 5136–5147.

[85] J. M. Lehn, *Angew. Chem. Int. Ed. Engl.*,**1990**, 29, 1304.

[86] A. F. Wells, *Three-dimensional Nets and Polyhedra*; Wiley: New York, **1977**.

[87] A. F. Wells, *Structural Inorganic Chemistry*, 5th ed.; Oxford University Press: Oxford, 1984.

[88] M. Fujita, O. Sasaki, T. Mitsuhasi, T. Fujita, J. Yazaki, K. Yamaguchi and K. Ogura, *Chem. Comm.*, **1996**, 1535.

[89] P. J. Stang and D. H. Cao, *J. Am. Chem. Soc.*, **1994**, 116, 4981.

[90] B. Olenyuk, M. D. Levin, J. A. Whiteford, J. E. Shield and P. J. Stang, *J. Am. Chem. Soc.*, **1999**, 121, 10434-10435.

[91] B. Hasenknopf, J. M. Lehn, B. O. Kneisel, G. Baum and D. Fenske, *Angew. Chem., Int. Ed. Eng.*, **1996**, 35, 1838-1840.

[92] C. S. Campos-Fernandez, R. Clerace, J. M. Koomen, D. H. Russell, K. R. Dunbar, *J. Am. Chem. Soc.*, **2001**, 123, 773-774.

[93] U. G.-Couceiro, O. Castillo, A. Luque, J. P. G.-Terán, G. Beobide and P. Román, *Eur. J. Inorg. Chem.*, **2005**, 4280–4290.

[94] B. J. Hollyday and C. A. Mirkin, *Angew. Chem. Int. Ed.*, **2001**, 40, 2022–2043.

[95] D. Sil, S. Bhowmik, F. S. T. Khan, and S. P. Rath, *Inorg. Chem.*, **2016**, 55, 3239.

[96] F. S. T. Khan, T. Guchhait, S. Sasmal and S. P. Rath, *Dalton Trans.*, **2017**, 46, 1012.

[97] L. A. Dubraja, M. Jurić, F. Torić and D. Pajić, *Dalton Trans.*, **2017**, 46, 11748.

[98] J. R. Zimmerman and A. Bettencourt-Dias, *Inorg. Chem. Commun.*, **2011**, 14, 753.

[99] E. Coronado and P. Day, *Chem. Rev.*, **2004**, 104, 5419.

[100] C. Genre, E. Jeanneau, A. Bousseksou, D. Luneau, S.A. Borshch and G.S. Matouzenko, *Chem. Eur. J.*, **2008**, 14, 697–705.

[101] S. R. Batten and K. S. Murray, *Coord. Chem. Rev.*, **2003**, 246, 103.

[102] S. S. Massoud, F. R. Louka, M. Mikuriya, H. Ishida and F. A. Mautner, *Inorg. Chem. Commun.*, **2009**, 12, 420.

[103] S. Dalai, P. S. Mukherjee, E. Zangrando, N. Ray Choudhuri, *New J. Chem.*, **2002**, 26, 1185-1189.

[104] I. Dasna, S. Golhen, L. Ouahab, N. Daro and J. P. Sutter, *New J. Chem.*, **2001**, 25, 1572-1576.

[105] M. Maiti, D.Sadhukhan, S. Thakurta, S.Roy, G. Pilet, R. J. Butcher, A. Nonat, L.J. Charbonniere and S. Mitra, *Inorg. Chem.*, **2012**, 51, 12176-12187.

[106] C. -C. Wang, C. -H. Yang, G. -H. Lee and H. -L. Tsai, *Eur. J. Inorg.Chem.* **2005**, 7, 1334.

[107] E. Escrivá, L. Soto, J. Server-Carrió, C. J. Gómez-García, G. M. Espallargas, N. Ruiz, A. Sancho, J.García-Lozano and C. R. de Arellano, *Polyhedron*, **2013**, 5, 90.

[108] R. Vicente, E. Ruiz, J. Cano, S. S. Massoud and F. A. Mautner, *Inorg. Chem.*, **2008**, 47, 4648.

[109] S. S Massoud, F. A Mautner, R. Vicente and J. S Dickens, *Inorg. Chim. Acta.*, **2008**, 361, 299.

[110] J. Carranza. J. Sletten, F. Lloret and M. Julve, *Inorg. Chim. Acta.*, **2011**, 371, 13-19.

[111] Massoud, S. S.; Mautner, F. A.; Vicente, R.; Dickens, J. S. *Inorg. Chim. Acta.*, **2008**, 361, 299.

[112] I. Castro, J. Sletten, M. L. Calatayud, M. JuIve, J. Cano, F. Lloret and A. Caneschi, *Inorg. Chem.*, **1995**, 34, 4903-4909.

[113] A. Hazra, P. Kanoo and T. K. Maji, *Chem. Commun.*, 2011, **47**, 538–540.

[114] M. Ohba, K, Yonedaa and S. Kitagawa, *Cryst.EngComm*., **2010**, 12, 159–165.

[115] M. Ohba, W. Kaneko, S. Kitagawa, T. Maeda and M. Mito, *J. Am. Chem. Soc*., **2008**, 130, 4475–4484.

[116] M. Ohba, K. Yoneda, G. Agustı´, M.C. Munoz, A.B. Gaspar, J. A. Real, M. Yamasaki, H. Ando, Y. Nakao, S. Sakaki and S. Kitagawa, *Angew. Chem. Int. Ed*., **2009**, 48, 4767–4771.

[117] W-Y. Wu, T-H. Tang, Y. Li and S. Xu, *Dalton Trans*., **2021**, 50, 485-489.

[118] J. Martínez-Lillo, T. F. Mastropietro, G. De Munno, F. Lloret, M. Julve and J. Faus, *Inorg. Chem*., **2011**, 50, 5731.

[119] M. Sadakiyo, H. Okawa, A. Shigematsu, M. Ohba, T. Yamada and H. Kitagawa, *J. Am. Chem. Soc*., **2012**, 134, 5472-5475.

[120] O. Castillo, A. Luque, P. Roma´n, F. Lloret and M. Julve, *Inorg. Chem.***2001**, 40, 5526.

[121] K. Pasinska, A. Ciupa, A. Pikul, A. Gagor, A. Pietraszko and A. Cizman, *J. Mater. Sci. C*, **2020**, 8, 6254-6263.

[122] M. J. Belousoff, B. Graham, B. Moubaraki, K. S. Murray and L. Spiccia, *Eur. J. Inorg. Chem.*, **2006**, 48, 4872.

[123] E. Coronado, J. R. Galan-Mascaros, C. J. Gomez-Garcia and V. Laukhin, *Nature*, **2000**, 408, 447– 449.

[124] National Research Council, in Catalysis Looks to the Future, (Panel on New Directions in Catalytic Science and Technology).

[125] D. Jiang, T. Mallat, F. Krumeich and A. Baiker, J. Catal., **2008**, 257, 390–395.

[126] M. J. Ingleson, J. P. Barrio, J. Bacsa, C. Dickinson, H. Park and M. J. Rosseinsky, Chem. Commun., **2008**, 1287–1289.

[127] R.Q. Zou, H. Sakurai and Q. Xu, *Angew. Chem. Int. Ed.*, **2006**, 45, 2542.

[128] J. Perles, M. Iglesias, C. Ruiz-Valero and N. Snejko, *J. Mater. Chem.*, **2004**, 14, 2683.

[129] M. H. Alkordi, Y. L. Liu, R. W. Larsen, J. F. Eubank and M. Eddaoudi, *J. Am. Chem. Soc*., **2008**, 130, 12639.

[130] F. Schröder, D. Esken, M. Cokoja, M. W. E. V. Berg, O.I. Lebedev, G. Tendeloo, B. Walaszek, G. Buntkowsky, H. H. Limbach, B. Chaudret and R.A. Fischer, *J. Am. Chem. Soc*., **2008**, 130, 6119.

[131] Y. K. Hwang, D. Y. Hong, J. S. Chang, S. H. Jhung, Y. K. Seo, J. Kim, A. Vimont, M. Daturi, C. Serre and G. Férey, *Angew. Chem. Int. Ed*., **2008**, 47, 4144.

[132] T. Sato, W. Mori, C. N. Kato, E. Yanaoka, T. Kuribayashi, R. Ohtera and Y. Shiraishi, *J. Catal*., **2005**, 232, 186.

[133] F. X. Llabre´ s i Xamena, A. Abad, A. Corma and H. Garcia, *J. Catal*., **2007**, 250, 294.

[134] L.T. Ngyen, T. T. Ngyen, K. D. Nguyen and N. T. Phan, *Appl. Catal. A*, **2012**, 44, 425.

[135] L. Alaerts, E. Seguin, H. Poelman, F. Thibault-Starzyk F, P. A. Jacobs and D. E. D Vos, *Chem. Eur. J.*, **2006**, 12, 7353–7363.

[136] S. Hermes, M.-K. Schro¨ ter, R. Schmid, L. Khodeir, M. Muhler, A. Tissler, R. W. Fischer and R. A. Fischer, *Angew. Chem.*, **2005**, 117, 6394.

[137] S. H. Cho, B. Q. Ma, S. T. Nguyen, J. T. Hupp and T. E. A. Schmitt, *Chem. Commun*., **2006**, 2563.

[138] C. D. Wu and W. B. Lin, *Angew. Chem. Int. Ed. Engl*., **2007**, 46, 1075.

[139] K. Tanaka, S. Oda and M. Shiro, *Chem. Commun*., **2008**, 820.

[140] S. Hasegawa, S. Horike, R. Matsuda, S. Furukawa, K. Mochizuki, Y. Kinoshita and S. Kitagawa, *J. Am. Chem. Soc*., **2007**, 129, 2607.

[141] A. E. Thorarinsdottir and T. D. Harris, *Chem. Rev.*, **2020**, 120, 8716–8789.

[142] M. Yamanouchi, D. Chiba, F. Matsukura and H. Ohno, *Nature*, **2004**, 428, 539–542.

[143] H. L. Sun, Z. M. Wang and S. Gao, *Coord. Chem. Rev*., **2010**, 254, 1081–1100.

[144] M. N. Leuenberger and D. Loss, *Nature*, **2001**, 410, 789–793.

[145] L. Bogani, A. Vindigni, R. Sessoli, D. Gatteschi, *J. Mater. Chem*., **2008**, 18, 4750.

[146] I. Imaz, M. Rubio-Martínez, J. An, I. Solé-Font, N. L. Rosi and D. Maspoch, *Chem. Commun.*, **2011**, 47, 7287.

[147] R. Mas-Ballest, J. Gmez-Herrero, F. Zamora, *Chem. Soc. Rev*., **2010**, 39, 4220.

[148] E. Saitoh, H. Miyajima, T. Yamaoka and G. Tatara, *Nature*, **2004**, 432, 203–206.

[149] L. Bogani and W. Wernsdorfer, *Nat. Mater.*, **2008**, 7, 179–186.

[150] X. Zhang, Z. Hao and X. Zhang, *Chem. Eur. J.*, **2011**, 17, 5588–5594.

[151] M. Gonidec, R. Biagi, V. Corradini, F. Moro, V. De Renzi, U. del Pennino, D. Summa, L. Muccioli, C. Zannoni, D. B. Amabilino and J. Veciana, *J. Am. Chem. Soc.*, **2011**, 133, 6603–6612.

[152] M. Atzori, A. Serpe, P. Deplano, J. A. Schlueter and M. L. Mercuri, *Inorg. Chem. Front.*, **2015**, 2, 108–115.

[153] M. Atzori, E. Sessini, F. Artizzu, L. Pilia, A. Serpe, C. J. GómezGarcía, C. Giménez-Saiz, P. Deplano and M. L. Mercuri, *Inorg. Chem.*, **2012**, 51, 5360–5367.

[154] D. Maspoch, D. Ruiz-Molina and J. Veciana, *Chem. Soc. Rev*.,**2007**, 36,770–818.

[155] G. M. Espallargas and E. Coronado, *Chem. Soc. Rev*., **2018**, 47, 533–557.

[156] E. D. Bloch, W. L. Queen, R. Krishna, J. M. Zadrozny, C. M. Brown and J. R. Long, *Science*, **2012**, 335, 1606.

[157] Q. Wang, Z. Yang, X. Zhang, X. Xiao, C.K. Chang and B. Xu, *Angew. Chem. Int. Ed*., **2007**, 46, 285–4289.

[158] J. Bernadou and B. Meunier, *Adv. Synth. Catal*., **2004**, 346, 171–184.

[159] J. Della Rocca and W. Lin, *Eur. J. Inorg. Chem.*, **2010**, 3725–3734.

[160] L. M. Bharadwaj, *J. Porous Mat.*, 2014, 43, 114.

[161] Q. Wang, Z. Yang, X. Zhang, X. Xiao, C.K. Chang and B. Xu, *Angew. Chem. Int. Ed.*, **2007**, 46, 4285–4289.

[162] Z. Y. Tang, Y. Wang, P. Podsiadlo, N. A. Kotov, *Adv. Mater.*, **2006**, 18, 3203–3224.

[163] I. Imaz, M. Rubio-Martínez, J. An, I. Solé-Font, N. L. Rosi and D. Maspoch, *Chem. Commun.*, **2011**, 47, 7287.

[164] K. A. D. F. Castro, F. Figueira, F. A. Almeida Paz, J. P. C. Tome, R. S. Silva, S. Nakagaki, M. P. M. S. Neves, J. A. S. Cavaleiro, and M, M. Q. Simoes, *Dalton Trans.*, **2019**, 48, 8144–8152.

[165] M. Li, J. Chen, W. Wu, Y. Fang and S. Dong, *J. Am. Chem. Soc.*, **2020**, 142, 15569–15574.

[166] S. Ganguly, P. Kar, M. Chakraborty, K. Sarkar and A. Ghosh, *New J. Chem.*, **2019**, 43, 18780–18793.

[167] D. Feng, Z.-Y. Gu, J.-R. Li, H.-L. Jiang, Z. Wei and H.-C. Zhou, *Angew. Chem. Int. Ed.*, **2012**, 51, 10307–10310.

[168] A. M. Shultz, O. K. Farha, J. T. Hupp and S. T. Nguyen, *J. Am. Chem. Soc.*, **2009**, 131, 4204–4205.

[169] Y. Chen, T. Hoang and S. Ma, *Inorg. Chem.*, **2012**, 51, 12600–12602.

[170] W. Morris, B. Volosskiy, S. Demir, F. Gándara, P.L. McGrier, H. Furukawa, D. Cascio, J. F. Stoddart and O. M. Yaghi, *Inorg. Chem.*, **2012**, 51, 6443–6445.

[171] D. A. Riccio and M. H. Schoenfisch, *Chem. Soc. Rev.*, **2012**, 41, 3731–3741.

[172] P. S. Wheatley, A. R. Butler, M. S. Crane, S. Fox, B. Xiao, A. G. Rossi, I. L. Megson and R. E. Morris, *J. Am. Chem. Soc.*, **2006**, 128, 502–509.

[173] B. E. Mann and R. Motterlini, *Chem. Commun.*, **2007**, 4197– 4208.

[174] S. Ma, X.-S. Wang, D. Yuan and H.-C. Zhou, *Angew. Chem., Int. Ed.*, **2008**, 47, 4130.

[175] B. L. Chen, L. B. Wang, Y. Q. Xiao, F. R. Fronczek, M. Xue, Y. J. Cui and G. D. Qian, *Angew. Chem. Int. Ed. Engl.*, **2009**, 48, 500.

[176] R. F. D'Vries, S. A. Garcia, N. Snejko, L. E. Bausa, E. G. Puebla, A. de Andres and M. A. Monge, *J. Mater. Chem. C*, **2013**, 1, 6316.

[177] Y. Qiu, Y. Li, G. Peng, J. Cai, L. Jin, L. Ma, H. Deng, M. Zeller and S. R. Batten, *Cryst. Growth Des.*, **2010**, 10, 1332.

[178] Y. Li, S. Zhang and D. Song, *Angew. Chem. Int. Ed.*, **2013**, 52, 710.

[179] H. Xu, F. Liu, Y. Cui, B. Chen and G. Qian, *Chem. Commun.*, **2011**, 47, 3153.

[180] Y. Cui, Y. Yue, G. Qian and B. Chen, *Chem. Rev*., **2012**, 112, 1126–1162.

[181] D. Zhao, Y. Cui, Y. Yang and G. Qian, *CrystEngComm.*, **2016**, 18, 746.

[182] Z. Ma and B. Moulton, *Coord. Chem. Rev*., **2010**, 255, 1623-1641.

[183] P. Horcajada, R. Gref, T. Baati, P. K. Allan, G. Maurin, P. Couvreur, G. Férey, R.E. Morris and C. Serre, *Chem. Rev*., **2012**, 112, 1232-1268.

[184] A. C. McKinlay, R. E. Morris, P. Horcajada, G. Férey, R. Gref, P. Couvreur, C. Serre, *Angew. Chem. Int. Ed*., **2010**, 49, 6260-6266.

[185] D. Zhao, S. Tan, D. Yuan, W. Lu, Y.H. Rezenom, H. Jiang, L.-Q. Wang and H.-C. Zhou, *Adv. Mater*., **2010**, 23, 90-93.

[186] S. Maheswaran, G. Chastanet, S. J. Teat, T. Mallah, R. Sessoli, W. Wernsdorfer and R. E. P. Winpenny, *Angew. Chem*., **2005**, 117, 5172.

[187] K. Bernot, J. Luzon, L. Bogani, M. Etienne, C. Sangregorio, M.Shanmugam, A.Caneschi, R. Sessoli and D. Gatteschi, *J. Am. Chem. Soc*., **2009**, 131, 5573.

[188] A. Watanabe, A. Yamashita, M. Nakano, T. Yamamura. and T, Kajiwara, *Chem. Eur. J*., **2011**, 17, 7428–7432.

[189] D. Gatteschi and R. Sessoli, *Angew. Chem., Int. Ed*., **2003**, 43, 268.

[190] C. Cadiou, M. Murrie, C. Paulsen, V. Villar, W. Wernsdorfer and R. E. P. Winpenny, *Chem. Commun*., **2001**, 2666–2667.

[191] D. Gatteschi and R. Sessoli, *Angew. Chem*., **2003**, 115, 278–309.

[192] J. J. Sokol, A. G. Hee and J. R. Long, *J. Am. Chem. Soc*., **2002**, 124, 7656.

[193] R. Sessoli and A. K. Powell, *Coord. Chem. Rev.*, **2009**, 253, 2328–2341.

[194] T. Kajiwara, M. Nakano, K. Takahashi, S. Takaishi and M. Yamashita, *Chem. Eur. J*. **2011**, 17, 196.

[195] P. H. Lin, T. J. Burchell, L. Ungur, L. F. Chibotaru, W. Wernsdorfer, and M. Muruges, *Angew. Chem*., **2009**, 121, 9653–9656.

[196] R. Sessoli, D. Gatteschi, A. Caneschi and M. A. Novak, *Nature*, **1993**, 365, 141–143.

[197] M. Murrie, *Chem. Soc. Rev*., **2010**, 39, 1986–1995.

[198] P. Lin, T. J. Burchell, L. Ungur, L. F. Chibotaru, W. Wernsdorfer and M. Murugesu, *Angew. Chem., Int. Ed*., **2009**, 48, 9489.

[199] R. Clerac, H. Miyasaka, M. Yamashita, C. Coulon, *J. Am. Chem. Soc*., **2002**, 124, 12837–12844.

[200] S. Dhers, H. L. C. Feltham, S. Brooker, *Coord. Chem. Rev*., **2015**, 296, 24–44.

[201] E. Heintze, F. E. Hallak, C. Claub, A. Rettori, M. G. Pini, F. Totti, M. Dressel, L. Bogani, *Nat. Mater*., **2013**, 12, 202–206.

[202] L. Bogani, A. Vindigni, R. Sessolia and D. Gatteschi, J. Mater. Chem., **2008**, 18, 4750–4758.

[203] A. Caneschi, D. Gatteschi, N. Lalioti, C. Sangregorio, R. Sessoli, G. Venturi, A. Vindigni, A. Rettori, M. G. Pini and M. A. Novak, Angew. Chem., Int. Ed., **2001**, 40, 1760.

[204] H. L. Sun, Z. M. Wang and S. Gao, *Coord. Chem. Rev*., **2010**, 254, 1081–1100.

[205] X. J. Li, X. Y. Wang, S. Gao and R. Cao, *Inorg. Chem*., **2006**, 45, 1508.

[206] X. T. Liu, X. Y. Wang, W. X. Zhang, P. Cui and S. Gao, *Adv. Mater*., **2006**, 18, 2852.

[207] K. Bernot, J. Luzon, R. Sessoli, A. Vindigni, J. Thion, S. Richeter, D. Leclercq, J. Larionova and A. Lee, *J. Am. Chem. Soc*., **2008**, 130, 1619.

[208] T. Kajiwara, M. Nakano, Y. Kaneko, S. Takaishi, T. Ito, M. Yamashita, A. Igashira-Kamiyama, H. Nojiri, Y. Ono and N. Kojima, *J. Am. Chem. Soc*., **2005**, 127, 10150.

[209] K. G. Sandeman, *Scr. Mater*. **2012**, 67, 566–571.

[210] M. P. Annaorazov, K. A. Asatryan, G. Myalikgulyev, S. A. Nikitin, A. M. Tishin and A. L. Tyurin, *Cryogenics*. **1992**, 32, 867–872.

[211] S. Naiya, S. Biswas, M. G. B. Drew, C. J. Gomez-García and A. Ghosh, *Inorg. Chem*. **2012**, 51, 5332–5341.

[212] T. D. Keene, I. Zimmermann, A. Neels, O. Sereda, J. Hauser, M. Bonin, M. B. Hursthouse, D. J. Price and S. Decurtins, *Dalton Trans*., **2010**, 39, 4937–4950.

[213] Y. L. Zhou, M. C. Wu, M. H. Zeng, and H. Liang, *Inorg. Chem*., **2009**, 48, 10146–10150.

[214] J. Boeckmann, M. Wriedt and C. Nather, *Chem. Eur. J*., **2012**, 18, 5284–5289.

[215] P. S. Mukherjee, S. Dalai, E. Zangrando, F. Lloretc and N. R Chaudhuri, *Chem. Commun*. **2001**, 1444–1445.

[216] M. H. Zeng, W. X. Zhang, X. Z. Sun and X. M. Chen, *Angew. Chem. Int. Ed*., **2005**, 44, 3079–3082.

[217] S. Kitagawa, R. Kitaura and S. Noro, *Angew. Chem. Int. Ed.*, **2004**, 43, 2334.

[218] J. Gascon, A. Corma, F. Kapteijn and F. X. Llabrés, *ACS Catal.*, **2014**, 4, 361.

[219] A. H. Chugtai, N. Ahmad, H. A. Younus, A. Laypkov and F. Verpoort, *Chem Soc. Rev.*, **2015**, 44, 6804.

[220] A. Pramanik, S. Abbina and G. Das, *Polyhedron*, **2007**, 26, 5225.

[221] L. Alaerts, E. Se´ guin, H. Poelman, F. Thibault-Starzyk, P. A. Jacobs and D. E. De Vos, Chem. Eur. J., **2006**, 12, 7353.

[222] M. Fujita, Y. J. Kwon, S. Washizu and K. Ogura, *J. Am. Chem. Soc.*, **1994**, 116, 1151.

[223] B. Gomez-Lor, E. Guiterrez-Puebla, M. Iglesias, M. A. Monge, C. Ruiz-Valero and N. Snejko, *Inorg. Chem*., **2002**, 41, 2429.

[224] F. X. Llabre´, S. I. Xamena, A. Abad, A. Corma and H. Garcia, *J. Catal*., **2007**, 250, 294.

[225] M. Ingleson, J. Perez Barrio, J. Bacsa, C. Dickinson, H. Park and M. Rosseinsky, *Chem. Commun*., **2008**, 1287.

[226] J. S. Seo, D. Whang, H. Lee, S. I. Jun, J. Oh, Y. J. Jeon and K. Kim, *Nature*, **2000**, 404, 982–986.

[227] X. Jing, C. He, D. Dong, L. Yang and C. Duan, *Angew. Chem. Int. Ed.*, **2012**, 51,10127.

[228] Y. K. Hwang, D.-Y. Hong, J.-S. Chang, S. H. Jhung, Y.-K. Seo, J. Kim, A. Vimont, M. Daturi, C. Serre and G. Fe´rey, *Angew.Chem., Int. Ed*., **2008**, 47, 4144–4148.

[229] S. Horike, M. Dinca, K. Tamaki and J. Long, *J. Am. Chem. Soc*., **2008**, 130, 5854.

[230] U. Ravon, M. E. Domine, C. Gaudillere, A. Desmartin-Chomel and D. Farrusseng, *New J. Chem*., **2008**, 32, 937–940.

[231] F. X. Llabre´, S. I. Xamena, A. Abad, A. Corma and H. Garcia, *J. Catal*., **2007**, 250, 294–298.

[232] Z. Wang, K. K. Tanabe and S. M.Cohen, *Inorg. Chem*., 2009, 48, 296.

[233] Y. K. Hwang, D. Y. Hong, J. S. Chang, S. H. Jhung, Y. K. Seo, J. Kim, A. Vimont, M. Daturi, C. Serre and G. Férey, *Angew. Chem. Int. Ed. Engl*., **2008**, 47, 4144.

[234] C. D. Wu and W. B. Lin, *Angew. Chem. Int. Ed. Engl*., **2007**, 46, 1075.

[235] D. J. Cram and J. M. Cram, *Science*, **1974**, 183, 803.

[236] D. Fiedler, H. van Halbeek, R. G. Bergman and K. N. Raymond, *J. Am. Chem. Soc*., **2006**, 128, 10240.

[237] S. Khatua, S. Goswami, S. Biswas, K. Tomar, H.S. Jean and S. Konar, *Chem. Mater.*, **2015**, 27, 5349.

[238] Y. Q. Huang, A. de Andres, B. Gomez-Lor, E. Gutiérrez-Puebla, M. Iglesias, M. A Monge, D. M. Proserpio and N. Snejko, *Cryst. Growth Des.*, **2008**, 8, 378.

[239] N. B. Shustova, B. D. McCarthy and M. Dincă, *J. Am. Chem. Soc.*, **2011**, 133, 20126.

[240] Y. Q. Huang, B. Ding, H. B. Song, B. Zhao, P. Ren, P. Cheng, H. G. Wang, D. Z. Liao and S. P. Yan, *Chem. Commun.*, **2006**, 4906.

[241] P. Horcajada, C. Serre, M. Vallet-Regí, M. Sebban, F. Taulelle and G. Férey, *Angew. Chem. Int. Ed.*, **2006**, 45, 5974–5978.

Chapter 2

Experimental techniques and methodology

2.1 Synthesis techniques

Synthesis of desired metal organic materials is a very crucial part of experiment and it requires employment of proper reaction conditions and synthesis techniques. The prerequisite ligands, molecular building blocks were synthesized and purified. The desired MOMs were synthesized in pure and solid crystalline form either single step or by multistep reaction processes. The prerequisite ligands, molecular building blocks were synthesized following previously reported methods and purified either by simple work up or by crystallization techniques whichever is appropriate. All the reactions were carried out in the solution phase only. The reaction techniques adopted to synthesis the desired sample are: i) simple stirring at room temperature, ii) reflux at ambient temperature, iii) layer diffusion of reaction mixture with buffer solution, iv) solvothermal etc. All the desired MOMs were purified in solid crystalline form by crystallization following the techniques: a) slow evaporation of the solvent, b) diffusion of another solvent having low polarity and boiling point, c) slow layer diffusion. Good quality single crystals were achieved after a few days/weeks which were then separated by filtration and dried over vacuum. Suitable single crystals for SCXRD study were collected or kept in the mother solution until their structure determination. The proper reaction conditions were employed by tuning of various governing factors such as temperature, solvent polarity, pH, reagent ratio, reaction time and also various reaction techniques like reflux, hydrothermal, mixing-stirring at room temperature, layer diffusion etc. The detail of synthesis techniques has been discussed in the experimental section of each chapter of this thesis.

2.2. Experimental sample characterization techniques

The synthesized sample/materials were immediately undertaken for structure determination by single crystal x-ray diffraction. The microanalytical, spectroscopic, thermal and

other characterizations of the samples were performed thoroughly and then used for functional property studies.

(i) Single Crystal X-ray Diffraction Study

The single crystal X-ray diffraction (SCXRD) is the most useful method to analyze crystal structures of crystalline materials. In SCXRD, a beam of X-rays strikes on a single crystal and the obtained scattered beams are directed in different ways. These beams make a diffraction pattern of spots when they fall on the detector. Intensities and angles of these scattered beams are recorded as the crystal is rotated gradually. A 3D electron density map, known as Fourier map of electrons within the crystal system can be produced from the angles and intensities of these scattered X-ray beams.

According to the theory of Fourier transform ρ(x, y, z), the electron density, (i.e. image of the molecule under investigation) is the Fourier transform of the structure factor F_{hkl}. Therefore,

$$\rho(x, y, z) = \frac{1}{V} \sum_h \sum_k \sum_l F(h, k, l)\, e^{-2\pi i(hx + ky + lz)}$$

The crystal and molecular structure of the complexes can be determined if sufficient number of F(h, k, l) could have been determined experimentally. But, it is the intensity of the diffracted X-ray maxima [I(h, k, l)] that are measured experimentally. From these data only the magnitude /*F*(*h, k, l*)/ can be derived and the phases of the complex quantity $F(h, k, l)$ are lost. We can't compute ρ(x, y, z) directly from experimental data. This is a well-known phase problem in X-ray crystallography. We solve the phases problem using Patterson and Direct methods implemented in different software suites described in subsequent sections [1-8]. Bruker SMART diffractometer fitted with a graphite

mono-chromator and Mo-Kα (λ=0.71073 Ǻ) radiation were used to mount the most suitable single crystal of the complexes to record the diffraction data. The details of the methods were discussed in individual chapters.

(ii) Powder X-ray Diffraction Study (PXRD)

PXRD data collection has been recorded at ambient temperature (20 °C) on a Bruker D8 Advance diffractometer operating in the reflection mode using Cu-Kα radiation having wavelength 1.5418 Å with the generator setting maintained at 40 kV, 40 mA. In general, the PXRD patterns were collected within the 2θ range of 20°-90° (step size 0.02°) at scan speed 6 s/step. The PXRD pattern of the sample was indexed by DICVOL06 [9] and TREOR90 [10] of Fullprof.2 k [11] package. Shape of the peaks had been evaluated by pseudo-Voigt functions. The background was fitted by the shifted Chebyshev function of the first kind with 20 points regularly distributed over the entire 2θ range. Initially, the values of atomic coordinate and site occupancy were provided in accordance with the JCPDS card number for corresponding NPs. In the beginning, the lattice parameters, profile parameters and background were refined. After few cycles of refinement, the atomic coordinates and isotropic thermal parameters were refined. Finally, the preferred orientation correction had been applied by using a generalized spherical harmonic model.

The SCXRD and powder-crystal diffraction patterns contain the same basic information; only difference is in PXRD the three-dimensional diffraction data are compressed into one dimension that results in significant overlap of peaks in the powder diffraction pattern (Figure 1). Such peak overlap conceals information of the intensities of individual diffraction maxima, and makes for difficulties in solving crystal structures directly from PXRD data. Structures obtained through this method are frequently claimed of less precise and lower accuracy compared to single

crystal structures. However, PXRD data provides significant information in case of difficulties in crystal growth, twinning, or where extreme experimental conditions are required.

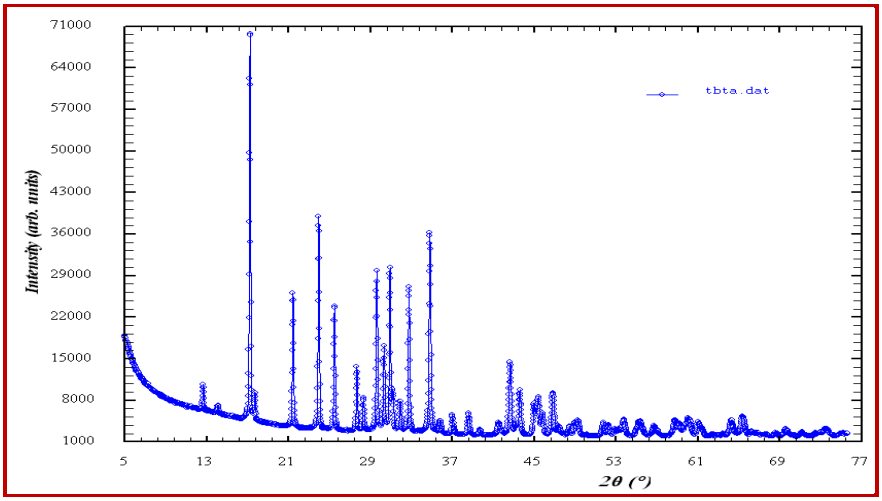

Figure 1. Powder X-ray diffraction pattern.

(iii)Microanalysis of Chemical Composition

Elemental analyses (C,H,N) were done using a Perkin Elmer 240C elemental analyzer. This is used to corroborate the experimentally found percentage of C, H, N of the sample with structural information obtained from x-ray diffraction.

(iv) Fourier-transform infrared spectroscopic (FTIR) study

Fourier transform infrared spectroscopy was carried out on the Nicolet Impact 410 spectrometer between 400 and 4000 cm-1, using the KBr pellet method. FTIR analysis is a technique where the study involves the interaction between electromagnetic field and matter in the infrared (IR) region. The material absorbs the IR frequency when it interacts with the molecule. The fundamental theory is that the elements of different bonds absorb light at different frequencies. Thus, the FTIR analysis recorded the range of wavelengths in the IR that are absorbed by a material. The spectrum is plotted as transmittance values corresponding to the wave numbers.

The IR stretching frequencies are very useful to identify functional groups present in the sample, binding and bridging modes of ligands, metal-ligand bonds and also sometimes supramolecular interactions like H-bonding. FTIR analysis can be useful to recognize unknown materials, surface contamination on a material, additives within polymers etc.

(v)Thermal Analysis

Thermogravimetric analyses have been performed to determine thermal stability and composition of the sample. It is also very useful for phase changes and structural transformation studies. Thermal analysis has been done on a Mettler Toledo TGA-DTA 85 thermal analyzer under a flow of N2 (30 $mlmin^{-1}$). In this analysis sample is heated in a uniform rate of increase of temperature in an inert atmosphere (N_2 gas is supplied uniformly). The successive weight loss is plotted against rising of temperature. The % of weight loss in each step provides information about expulsion of fragmented moieties.

(vi) UV-Visible and Photoluminescence study

The optical properties of the samples were investigated by UV-vis and Photoluminescence spectral study both in solid state and solution. UV-vis of the samples were recorded by PerkinElmer UV-vis spectrometer (Lambda 35) and JASCO V-630 equipped with a solid-state measurement attachment, respectively. Photoluminescence spectra were collected on a Shimadzu RF-5301PC spectrofluorometer. In the UV-vis spectroscopy, the electromagnetic waves (visible light or ultraviolet light) interact with the matter. As soon as the sample absorbs a beam of monochromatic light, the energy content of the atoms or molecules in the sample increases. The absorption of visible light or ultraviolet light by different chemical compounds of the sample can produce a distinct spectrum [12].

In the Photoluminescence method, the light that is focused onto the sample, is absorbed by the sample and the excess energy of the light transfers into the sample in a photo-excitation process. In the process, electrons within a material can move into permissible excited states by absorbing photons at particular wavelength. When an atom or molecule makes a transition from ground state to excited state, the system undergoes a non-radiative process. On the other hand, when this transition takes place from excited state to ground or equilibrium state, the excess energy is released by emitting the light (luminescence) and it is called radiative process. In the case of photo-excitation, this luminescence is called photoluminescence. These techniques are extremely important to investigate optical properties of the samples and also provide information about solution phase structure of the samples.

(vii) Cyclic-voltametric study

In electrochemical analysis, cyclic voltammetry (CV) is an important and powerful tool that is used to investigate the oxidation and reduction process of molecular species. Figure 2 presents a sample of Cyclic voltammogram (CV) curve [where, E_{pa} = anodic peak potential (oxidation), i_{pa} = anodic current E_{pc} = cathodic peak potential (reduction), i_{pc} = cathodic current].

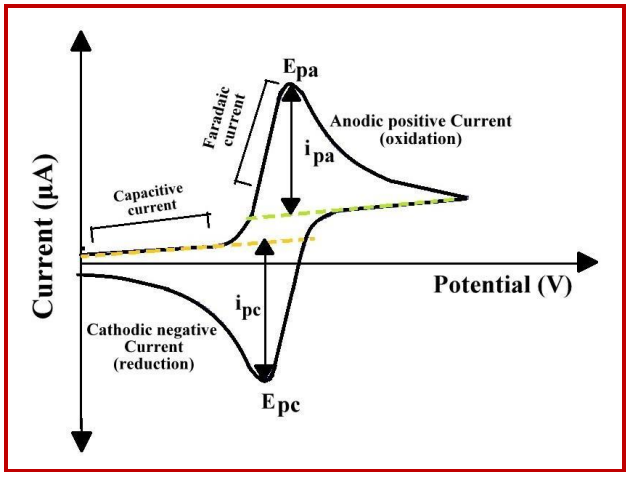

Figure 2. Cyclic voltammogram (CV) curve

The cyclic voltametric measurement of our samples was done using Epsilon Basi-C3 Cell instrument at a scan rate of 100 mV s^{-1} within potential range of 0-1.80 V with 1.0×10^{-3} M of complexes in acetonitrile solution deoxygenated by bubbling argon gas. Further, 0.1 M tetrabutylammonium perchlorate (TBAP) was taken as a supporting electrolyte. The working electrode was a glassy-carbon disk (0.32 cm^2) which was washed with absolute acetone and dichloromethane, polished with alumina solution

(viii)Variable Temperature Magnetic Study

Variable temperature (2–300K) magnetization data were recorded using a Quantum Design MPMS-XL-7 SQUID magnetometer. by using of tabulated Pascal's constants, the experimental susceptibility data had been revised for underlying diamagnetism [13].

(ix) Mass spectrometric study

The mass spectra (EIS-MS positive) of the samples were recorded with the help of Qtof Micro YA263 mass spectrometer to identify the structure of the samples and fragment species by determining their mass in solution phase.

2.3 Computational methodologies

2.3.1 Computational analysis on ground state molecular geometry

Ground state molecular geometries of the compounds were used to calculate the optimized geometry, electronic properties or frontier molecular orbitals (FMOs) and to simulate the absorption spectra or the excitations. To probe the noncovalent interactions within the components in a crystal, binding energy, MESP and NCI plot were computed from

the energies of optimized dimer geometries and the optimized monomeric coformers.

2.3.2. Geometry optimization, MO calculation and excitations calculation

The Gaussian 09 program was utilized to perform all the calculations [23] employing the DFT method using Becke's three parameter hybrid functional [14] and Lee–Yang–Parr's gradient corrected correlation functional [15] (B3LYP) along with 6-311++G(d,p) basis set. The ground state (S_0) geometries were completely optimized in gaseous phase and water medium using the default criteria of the respective program (very tight criteria in some cases). Grimme's third formulation of empirical correction for dispersion with Becke-Johnson damping [16] (GD3BJ) was applied in order to include the weak intermolecular interactions. To better reflect the solvation effect on the samples, aqueous cavity in the solvent reaction field (SCRF) was included at conductor-like polarizable continuum (CPCM) level. Frequencies were calculated by using the optimized geometries. To compute the UV-Vis transition of the samples, a single point calculation was carried out using the time dependent density functional method (TDDFT) starting with the ground state geometry optimized in both gaseous phase and water media using the same functionals and basis set. The excitation energies of the compounds in water medium were simulated by the conductor-like polarizable continuum model (CPCM model) using the non-equilibrium approach, which has been designed for the study of the absorption procedure. The singlet–singlet transitions have only been considered for deconvolution of UV-Vis transitions. Orbital analysis has been performed using GaussView and the MO composition analysis was carried out with Gausssum program [17]. The excited state computational results are interpreted using natural transition orbital (NTO) analysis based on the calculated transition density matrices [18-21]. Analyzing the geometrical parameters, the changes in the bond lengths are confirmed to be within the appreciable limit of 0.02 Å with respect to their crystal structure except for the

hydrogen bonding units of their molecular fragments which deviates abruptly that might be the consequence of absence of packing environment or the solution polarizability effect.

All the experiments and methodologies used in the present thesis is concisely depicted in the follow-chart (Figure 3). The detailed synthesis procedures of all samples, ligands and methodologies used to accomplish characterization and study of functional properties of the newly synthesized materials have been described in corresponding chapter.

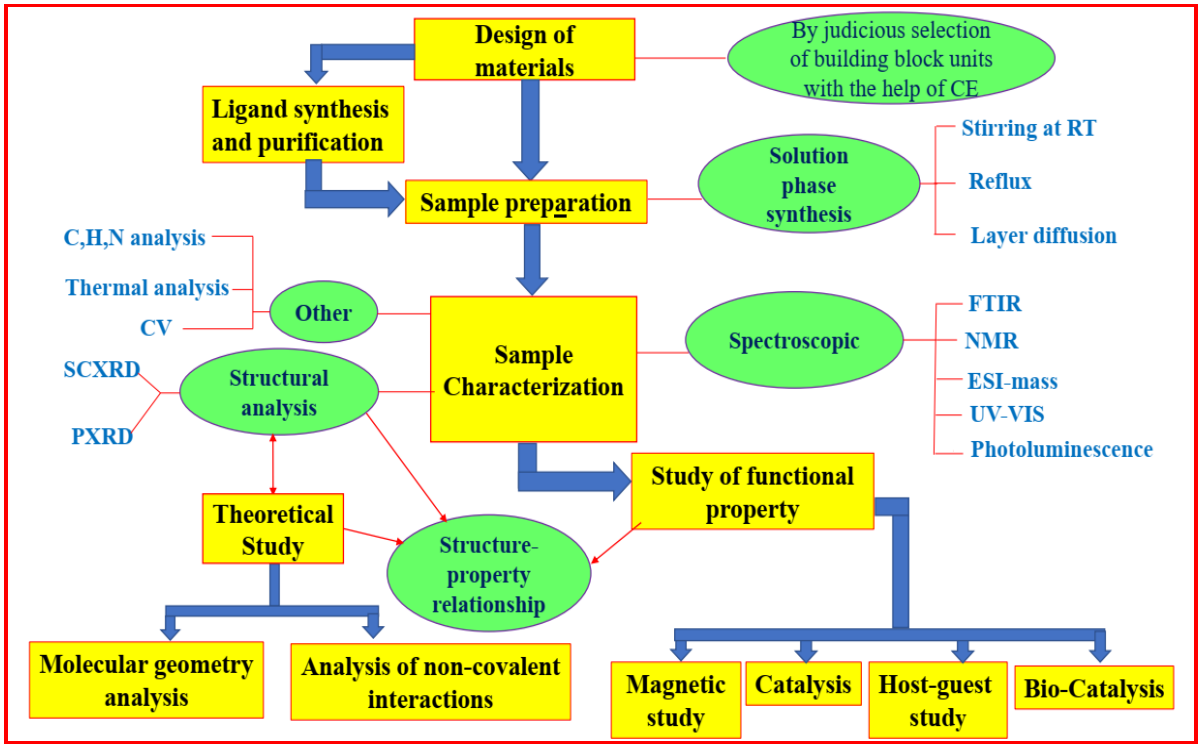

Figure 3. Flow Chart depicting experiments and methodology of the work.

References

[1] G. M. Sheldrick, *SHELXS 97*, Program for Structure Solution, University of Göttingen, Germany, **1997**.

[2] G. M. Sheldrick, *SHELXL 97*, Program for Crystal Structure Refinement, University of Göttingen, Germany, **1997**.

[3] A. L. Spek, Single-crystal structure validation with the program PLATON. *J. Appl. Crystallogr.* **2003**, 36, 7–13.

[4] L. J. Farrugia, ORTEP-3 for Windows - a version of ORTEP-III with a Graphical User Interface (GUI). *J. Appl. Crystallogr.* **1997**, 30, 565.

[5] L. J. Farrugia, WinGX suite for small-molecule single-crystal crystallography. *J. Appl. Crystallogr*. **1999**, 32, 837–838.

[6] Bruker. APEX2 (Version 2008.1-0). Bruker AXS Inc., Madison, Wisconsin, USA, **2008**.

[7] Bruker (2001b). SAINT-V6.28A. Data Reduction Software, **2001**.

[8] G. M. Sheldrick, *SADABS*. Program for Empirical Absorption Correction. University of Göttingen, Germany, **1996**.

[9] A. Boultif and D. Louer, *J. Appl. Crystallogr.*, **2004**, 37, 724.

[10] P. E. Werner, L. Eriksson and M. Westdahl, *J. Appl. Crystallogr.*, **1985**, 18, 367.

[11] J. Rodríguez-Carvajal, Recent Developments of the Program FULLPROF, Commission on Powder Diffraction (IUCr) Newslett, **2001**, 26, 12.

[12] A. D. Skoog, J. F. Holler and R. S. Crouch, *Principles of Instrumental Analysis* (6th ed.) (Belmont, CA: Thomson Brooks/Cole. pp. 169–173, **2007**).

[13] G. A. Bain and J. F. Berry, Diamagnetic corrections and Pascal's constants. *J. Chem. Educ.*, **2008**, 85, 532–536.

[14] A. D. Becke, *J. Chem. Phys.*, **1993**, 98, 5648.

[15] A. T. Lee, W. T. Yang and R. G. Parr, *Phys. Rev. B.*, **1988**, 37, 785.

[16] S. Grimme, S. Ehrlich and S. L. Goerigk, *J. Comput. Chem.*, **2011**, 32, 1456.

[17] N. M. O'Boyle, A. L. Tenderholt and K. M. Langner, *J. Comp. Chem.*, **2008**, 29, 839.

[18] S. Roy, S. Pramanik, T. Ghorui and K. Pramanik, *RSC Adv.*, **2015**, 5, 22544.

[19] L. E. Roy, G. Scalmani, R. Kobayashi and E. R. Batista, *Dalton Trans.*, **2009**, 0, 6719.

[20] U. Das, T. Ghorui, B. Adhikari, S. Roy, S. Pramanik and K. Pramanik, *Dalton Trans.*, **2015**, 44, 8625.

[21] S. Chopra, *RSC Adv.*, **2016**, 6, 20565.

Chapter 3

An unusual μ-$_{1,2,3}$-squarato-bridged two-dimensional coordination polymer: crystal structure, thermal, photoluminescence and magnetic studies

3.1 Introduction

In the recent past, the rational design and synthesis of coordination polymers have received paramount attention not only due to their aesthetical beautiful architectures and topologies but also for their several potential functional properties such as gas and solvent adsorption, catalysis, magnetism, ferroelectricity, nonlinear optical activity, optical sensing etc [1-15]. The structural topology of coordination polymers might be tuned by thoughtful choice of the metal ions, the ligands and their stereo-electronic preference of binding and also tuning of various parameters affecting reaction conditions. Moreover, several weak interactions such as directional hydrogen bonds, π···π interactions etc. may also play an important role in determining the resultant architecture [16-18].

The ordered arrangement of paramagnetic metal centers within such coordination networks allows us to design and synthesize novel magnetic materials such as ferromagnetic, ferrimagnetic, antiferromagnetic, canted-antiferromagnetic and spin glass systems [19-30]. It is well established that the propagation of magnetic exchange interaction within coordination polymers is greatly influenced by the nature of binding sites of ligands attached with metal centers and obviously on the coordination mode of the bridging ligands [31-32]. The oxygen donor-based ligands such as carboxylates have widely used to design several types of magnetic materials. Besides, the multi oxygen donor ligands like rhodizonate, croconate and squarate are highly attractive for designing the metal clusters and coordination polymers [33-36]. These ligands have multi-oxygen donor sites around a planar-aromatic motif and thus they can exhibit different binding aptitudes with metal ions.

Here, we have used squaric acid as the bridging ligand. Due to its good donor ability offered by its four oxygen atoms, presence of extensive delocalized π-electrons, highly symmetrical, cyclic

shape and the stable aromatic character, it has been attracted to several research groups. And, thus in the last few years, a large number of discrete poly-nuclear and coordination polymers with diverse structural motifs have been synthesized using Squaric acid [37–46]. The different bridging modes exhibited by the squarate (Scheme 1) are: bridging *bis*- (μ-$_{1,2}$ and μ-$_{1,3}$), *tris*- (μ-$_{1,2,3}$) and *tetra-kis*-monodentate (μ-$_{1,2,3,4}$) that leads to the formation of bridged metal complexes with different extents of nuclearity and dimensionality. It is noteworthy that the binding modes of squarate anion in the metal complexes are mainly governed by the structure and geometry of the blocking ligands coordinated to the central metal ions as well as the reaction conditions.

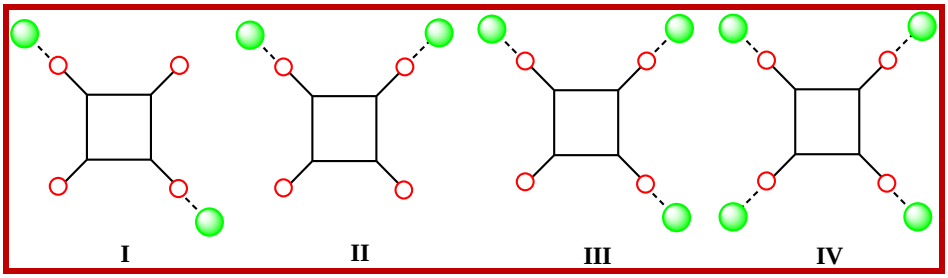

Scheme 1. Different bridging mode of squarato dianion.

According to literature surveys, the μ-$_{1,2}$ and μ-$_{1,3}$ bridging modes are most common [37-43], only in a few cases μ-$_{1,2,3,4}$ bridging modes have been found [31, 44-45]. The sole example of μ-$_{1,2,3}$ bridging pattern of squarate-dianion in a tri-nuclear Cu(II) complex has been reported by Vicente et al. [46]. In this endeavor, we are going to report a new 2D coordination polymer formed by using an unusual μ-$_{1,2,3}$ bridging mode of squarate-dianion with Ni(II) and the blocking 2,2′-bipyridyl ligand. The structural analysis reveals that the blocking 2,2′-bipyridyl moieties are hanging in the interlamellar space between 2D coordination sheets. The thermal and photoluminescence properties of the complex have been studied. The variable temperature magnetic measurements indicate that the complex is antiferromagnetic in nature.

3.2 Experimental Section:

3.2.1 Materials and methods

The Nickel (II) nitrate, hexahydrate; 2,2′-bipyridine; 3,4-dihydroxy-3-cyclobutene-1,2-dione (squaric acid) and sodium carbonate were purchased from Merck chemical company. All other chemicals were AR grade and used without further purification. A Perkin-Elmer 240C elemental analyzer was used for the elemental analysis (C, H, N). The thermal analysis was done with the help of Mettler Toledo TGA-DTA 85 thermal analyzer with a flow of N_2 gas (30 $mlmin^{-1}$). The sample was heated at a rate of 5 °C min^{-1} with inert alumina as a reference. Using the KBr pellet method, a Nicolet Impact 410 spectrometer was employed to record the infrared (IR) spectra of the sample within the frequency range of 400 to 4000 cm^{-1}. The photoluminescence spectra of the sample had been recorded using a Shimadzu RF-5301PC spectrophotometer. The magnetization measurements were carried out using a superconducting quantum interference device vibrating sample magnetometer (Quantum Design SVSM, USA) over a wide temperature range of 3-300 K. The experimental susceptibility data had been revised for basic diamagnetism using tabulated Pascal's constants.

3.2.2 Synthesis of the Complex

In 10 ml of distilled water, 0.5 mmol squaric acid (0.05703 g) was dissolved and neutralized by aqueous solution of sodium carbonate to adjust the pH at 8.0. The Nickel (II) nitrate, hexahydrate (0.2908 g, 1.0 mmol) was dissolved in 5 ml distilled water and added to the previous solution. The resultant mixture was stirred at room temperature for 15 min. Then, 10 ml methanolic solution of 2,2′-bipyridine (0.156 g, 1.0 mmol) was added with the previous solution and stirred for another 1 h. The whole mixture was then refluxed for 2 h at 90 °C. It was then cooled down to room

temperature, the blue precipitate was filtered off and light blue colored filtrate was kept in undisturbed condition. After a few days, the good quality greenish blue block shaped crystals were collected and dried in vacuum for single crystal x-ray diffraction analysis. Yield 72%. Anal. calc. for $C_{14}H_{11}N_2NiO_6$**:** C 46.2%, H 2.5%, N 7.7%. Found: C 46.5%, H 2.4%, and N 7.5%. Selected IR bands (KBr pellet, cm^{-1}): *ν* (O-H) stretching 3445 (m); *ν* (CO) 1506 (m), 1524 (s), 1483 (s) and 1445 (w).

3.2.3 Crystallographic data collection and refinement

Suitable single crystal of the complex was mounted on a Bruker SMART diffractometer equipped with a graphite monochromator and Mo-K_α (λ = 0.71073 Å) radiation. The structure was solved by Patterson method using SHELXS-97. The subsequent difference Fourier synthesis and least square refinement revealed the positions of the non-hydrogen atoms. The non-hydrogen atoms were refined with independent anisotropic displacement parameters. The hydrogen atoms were placed in idealized positions and their displacement parameters were fixed to be 1.2 times larger than those of the attached non-hydrogen atoms. The successful convergence was indicated by the maximum shift/error of 0.001 for the last cycle of the least squares refinement. All calculations have been carried out using SHELXS-97 [47], SHELXL-97 [48], PLATON-99 [49], ORTEP-32 [50] and WinGX system Ver-1.64 [51].

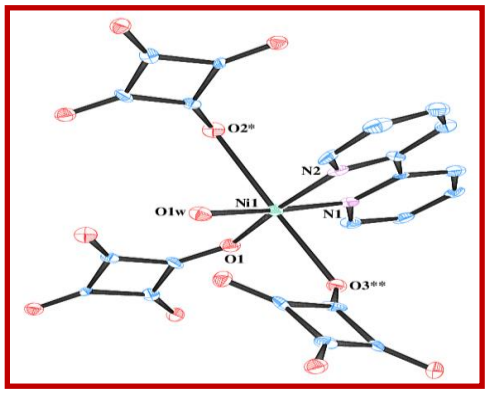

Figure 1. ORTEP diagram of the complex.

The data collection and the structure refinement parameters and the crystallographic data for the complex are given in Table 1. Some selected bond lengths, bond angles and non-covalent interaction parameters are presented in Table 2.

Table 1: Crystallographic data and refinement parameters of complex.

Crystal Data	
Formula	$C_{14}H_9N_2NiO_5$, H_2O
Formula Weight	362.97
Crystal System	Orthorhombic
Space group	P_{bca} (No. 61)
a (Å)	12.774(5)
b (Å)	16.818(6)
c (Å)	12.140(5)
V ($Å^3$)	2608.1(17)
Z	8
D(calc) (g/cm^3)	1.833
μ(Mo Kα)(mm)	1.525
F(000)	1464
Crystal Size (mm)	0.08 x 0.08 x 0.40
Data Collection	
T (K)	100
λ [Å]	Mo Kα 0.71073
θ Min-Max [°]	2.4- 25.3
Dataset	-15:12; -19:20 ; -14:13
Total	12353
Uniq data	2363
R_{int}	0.194
Observed data [I > 2.0 sigma(I)]	1088
Refinement	
Parameters refined	209
R	0.0726
wR2	0.1516
S	0.80
Min. and Max. Resd. Dens. [$e/Å^3$]	-0.75, 1.40

w = 1/[s2(Fo2) + (0.0949P)2] where P = (Fo2 + 2Fc2)/3.

Table 2: Selected bond distances (Å) and bond angles (°) of the complex

Ni1-O1	1.905(6)	Ni1-N2	1.968(7)
Ni1-O1W	1.925(5)	Ni1-O3*	2.460(6)
Ni1-N1	1.959(7	Ni1-O2**	2.555(6)
O1-Ni1-O1W	95.3(2)	O1W-Ni1-N1	175.1(3)
O1-Ni1-N1	89.4(3)	O1W-Ni1-N2	95.1(3)
O1-Ni1-N2	169.6(3)	O1W -Ni1-O3*	94.9(2)
O1-Ni1-O3*	94.7(2)	O1W-Ni1 -O2**	79.8(2)
O1-Ni1-O2**	92.7(2)	O3*-Ni1-N1	86.1(2)
O2**-Ni1-N2	89.3(2)	O2**-Ni1-N1	98.6(2)
O2**-Ni-O3*	171.23(19)	O3**-Ni1-N2	84.2(2)
N1-Ni1-N2	80.2(3)		

*** = 3/2-x, -y, 1/2+z; ** = 1-x, -y, -z**

3.3 Result and Discussion

3.3.1 Crystal structure description of the complex

The single crystal X-ray diffraction (SC-XRD) analysis reveals that the complex crystallizes in an orthorhombic P_{bca} space group where the Ni(II) is in distorted octahedral geometry. The asymmetric unit one 2,2′-bipyridine, one squarate anion, comprises one Ni (II) ion, one coordinated water molecule and one guest water molecule, (Figure 1). coordination. N1 and N2 atoms of one 2,2′-bipyridine ligand, one oxygen atom (O1) of bridging squarate and O2W form the basal plane, and two oxygen atoms (O2 and O3) of two different squarate ions are at the *trans* axial coordination sites. Thus, the oxygen atoms of three symmetry related squarato-anions occupy facial positions in the coordination sphere. The distortion from perfect octahedral geometry is reflected in *cisoid* [79.8(2)–98.6(2)°] and *transoid* [169.6(3)–175.1(3)°] angles. Ni-N bond

distances are within the range of 1.959(6)–1.968(7) Å and Ni-O bond distances are within the range of 1.905(6)–2.555(6) Å while Ni-O1W bond distance is 1.925(5) Å.

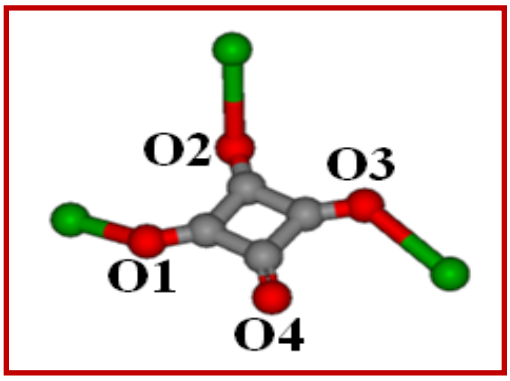

Figure 2. μ-1,2,3-bridging pattern of squarate-dianion in the complex.

The squaric acid contains a four membered ring having one oxygen atom connected to each carbon atom. It can bind with metal ions by using these four oxygen atoms. It is a well established fact that the squarate anion shows versatile bridging mode [31, 37– 46]. Here, the squarate anion binds with three different metal ions in μ-$_{1,2,3}$ mode using its three oxygen donor centers O1, O2 and O3 while the other oxygen atom O4 remains inert towards coordination with metal ions (Figure 2). The squarate anion binds two metal centers Ni1 and Ni1* through O1 and O3 oxygen atoms in a *trans* bridging mode leading to formation of 1D coordination chain (Figure 3) which is further connected by O2 oxygen atom of another squarate anion which consequently binds with other two metal ions and this gives rise to a 2D coordination sheet structure within the crystallographic ***ac***-plane (Figure 4).

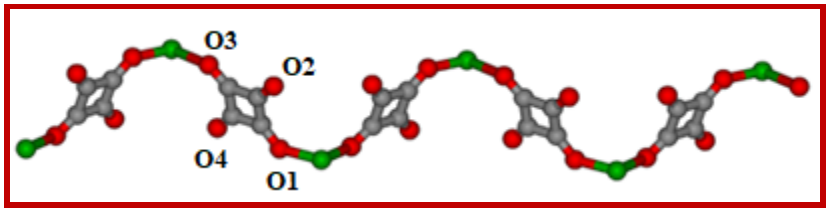

Figure 3. *trans*-binding mode of squarate-dianion ligand forms 1D coordination chain with metal centers.

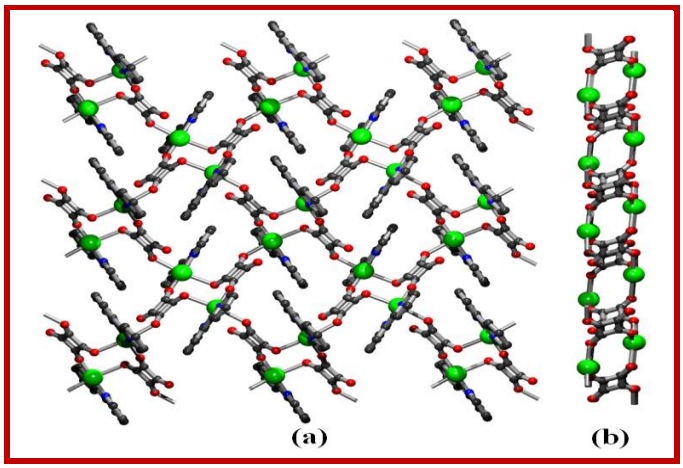

Figure 4. (a) 2D coordination sheet of the complex within the ***ac***-plane; **(b)** view along ***b***-axis (coordinated 2,2′-bipyridyl moieties are omitted for clarity).

The 2D coordination sheets are packed in parallel along crystallographic ***b***-axis. The coordinated 2,2′-bipyridyl units are pendant within the interlamellar spaces. Such 2D sheets are packed along crystallographic ***b***-axis by recognizing each other to inter-digitated 2D + 2D structure *via* π···π stacking interactions. The pyridyl rings of pendant 2, 2′-bipyridyl moieties of a 2D sheet interact with other pyridyl rings of neighboring 2D coordination sheets and by virtue of this the formation of 3D supramolecular structure takes place (Figure 5).

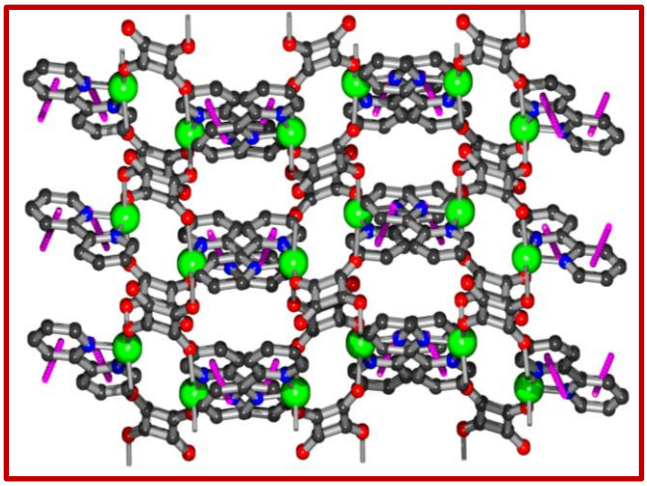

Figure 5. 3D supramolecular structure formed by π···π interactions (magenta).

The distance between their centroids is 3.861(5) Å and the dihedral angle is 8.5(4)° (Symmetry: x, 1/2-y, -1/2+z). In the course of formation of 3D supramolecular structure, 1D supramolecular channels are created along crystallographic ***c***-axis (Figure 6). The guest water molecules persist within such supramolecular channels. The hanging π-rings from the 2D coordination sheets create hydrophobicity between the 2D sheets while in contrast the uncoordinated O4 oxygen atom of squarate anion (directed toward the interlamellar spaces) creates hydrophilicity within such channels.

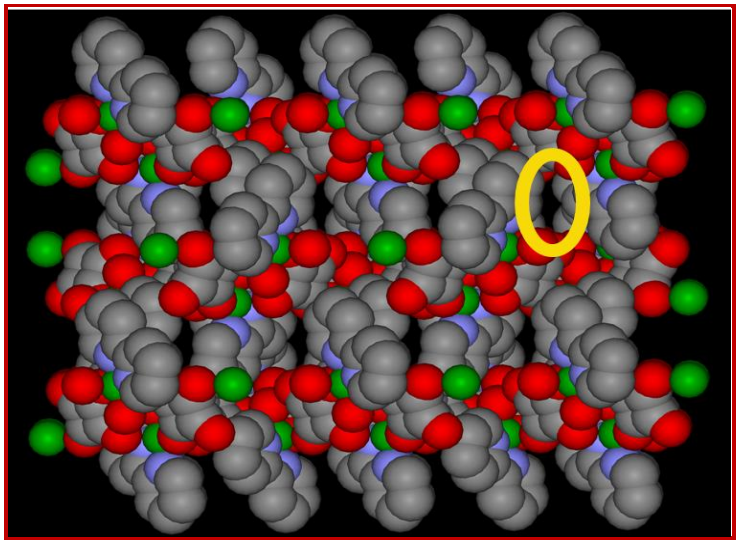

Figure 6. During formation of 3D supramolecular structure 1D supramolecular channel is formed along crystallographic ***c***-axis.

The overall 3D structure behaves as a metal-organic supramolecular host (MOSH) and the uncoordinated water molecules act as guests. The guest water molecules also act as a bridge between the 2D coordination sheets through O2W-H1W2···O4 and O2W-H2W2···O3 hydrogen bonding interactions which give further stability to the three-dimensional (3D) supramolecular structure (Figure 7). All hydrogen bonding interactions have been summarized in Table 3.

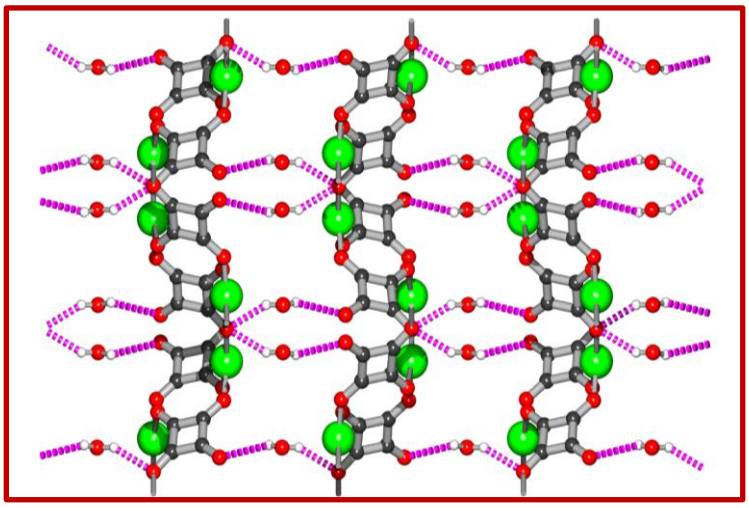

Figure 7. 2D coordination sheets are connected by water mediated hydrogen bonding to form 3D supramolecular structure.

Table 3: Hydrogen bond dimensions of the complex

D–H···A	D-H/(Å)	H···A/(Å)	D···A/(Å)	<D–H···A	Symmetry
O1W-H1W1···O4	0.87	2.04	2.553(8)	117	3/2-x,-y,1/2+z
O1W-H2W1···O2	0.90	1.78	2.657(8)	164	
O2W-H1W2··· O4	0.85	2.50	2.892(7)	109	-1/2+x,1/2-y,-z
O2W-H2W2···O3	0.85	2.08	2.819(7	144	1-x,-y,-z
C1-H1···O1	0.95	2.30	2.818(10)	114	
C1-H1···O2W	0.95	2.36	3.146(11)	140	1/2+x,1/2-y,-z
C8-H8···O2W	0.95	2.25	3.203(11)	175	x,1/2-y,1/2+z
C10-H10···O1W	0.95	2.51	3.044(11)	116	

3.3.2 Thermal analysis

The thermal (TG–DTA) studies of coordination and supramolecular polymers are important to analyze their thermal stability and to verify the stability of the guest species within the host. The thermal study confirms that the complex undergoes decomposition in 3 steps. The TG curve of the

complex has shown that mass loss starts at 50 ºC (Figure 8). A mass loss occured within the temperature range 50-85 ºC that corresponds to the loss of guest water molecules. In the next step, the coordinated water molecules are released in the temperature range of 125-150 °C. The anhydrous compound is stable up to 275 °C and it decomposes at ~350 ºC.

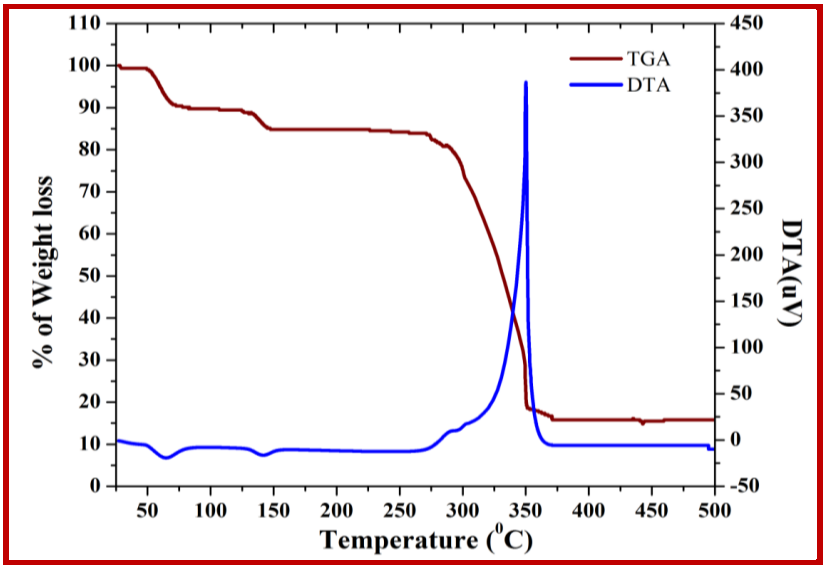

Figure 8. TG-DTA plot of the complex.

The DTA plot also supports the dehydration pattern of the complex (Figure 8). Two small and broad endothermic peaks at 65º and 140ºC have been observed in the DTA curve of the complex. These endothermic peaks in the DTA curve correspond to the removal of the guest water and the coordinated water molecules, respectively. The endothermic peak (at 140 ºC) is also indicating the conversion from the crystalline to the anhydrous state of the complex. The large exothermic peak at 350°C corresponds to decomposition of the complex.

3.3.3 Magnetic study of the complex

The variable temperature magnetic studies have been performed in the temperature range 3-300 K. The χ_m*vs*T and χ_mT*vs*T plots of the complex are shown in Figure 9. The value of χ_m at 300 K is

0.0037 $cm^3 mol^{-1}$, and on cooling χ_m value increases very slowly and reaches to 0.025 cm^3mol^{-1} at 40 K. Afterward, it increases sharply to the maximum value of 0.118 cm^3mol^{-1} at 3 K. The susceptibility data were fitted to the Curie–Weiss law to find out the nature of magnetic interaction present in the complex. The Curie and Weiss constants are 1.11 $cm^3mol^{-1}K$ and θ = -5.496 K respectively (Figure 10). The Weiss constant with negative magnitude indicates the presence of antiferromagnetic interaction between Ni (II) ions. The $\chi_m T$ value is 1.12 $cm^3mol^{-1}K$ at room-temperature which is slightly lower than that expected ($\chi_m T$ at 300 K = 1.32 $cm^3 mol^{-1}K$) for an isolated Ni(II) ion having two uncoupled spins, S = 1. The $\chi_m T$ value decreases monotonically with the decrease of temperature. Upon cooling $\chi_m T$ value decreases slowly up to 40 K and then it decreases very sharply with further lowering temperature and attains a value of 0.59 $cm^3mol^{-1}K$ at 3K. Such a behavior is typical of antiferromagnetic interaction. The isothermal magnetization (M) *vs* field (H) shows no hysteresis loop at 3K (vide Inset of Figure 10) indicating antiferromagnetic exchange interactions between Ni(II) centers. It may therefore be concluded that Ni(II) centers are coupled by antiferromagnetic interaction.

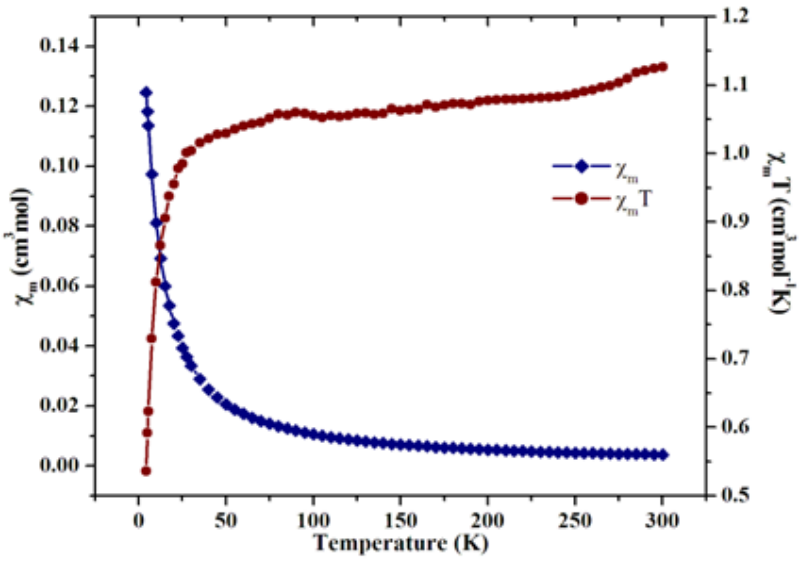

Figure 9. Both χ_m*vs*T and χ_mT*vs*T plots of the complex.

In order to correlate the magnetic behavior of the complex with the bridging mode of squarate anion, we have taken into account the magnetic behavior of some previously reported squarato-bridged metal complexes. The detailed literature survey reveals that most of the squarato-bridged transition metal (II) complexes exhibit antiferromagnetic behavior irrespective of nature of binding mode of the squarate ligand, presence of other blocking ligand and dimensionality of the resultant complex.

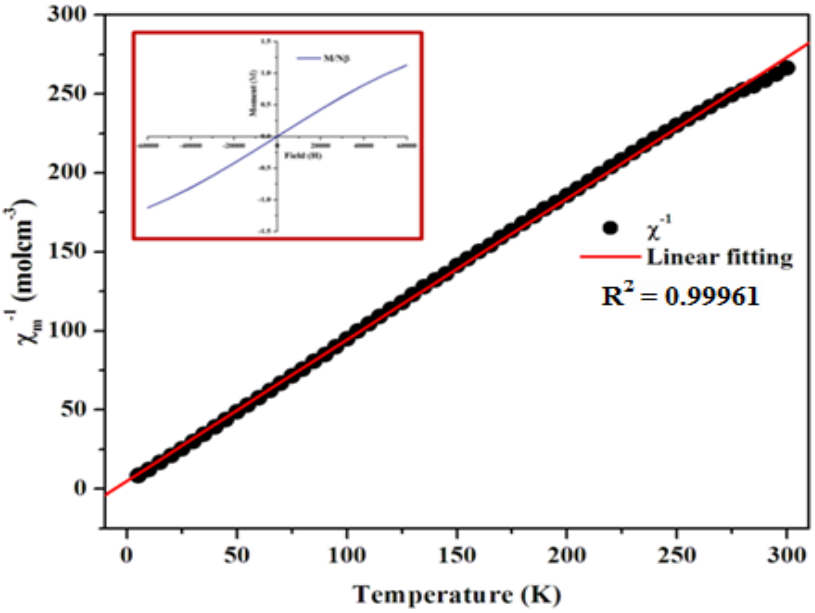

Figure 10. The χ^{-1}*vs*T plot for the complex (Inset: M *vs* H plot).

Massoud et al. have reported μ-1,2 squarato-bridged complex $[Ni_2(TPA)_2(\mu\text{-}_{1,2}\text{-}C_4O_4)(H_2O)_2](ClO_4)_2$ {TPA=tris(2-pyridylmethyl)amine} that show antiferromagnetic interactions between Ni(II) ions [37]. Xanthopoulos et al. have reported a Cu (II) containing μ-1,2squarato bridged complex $[Cu_2(SalNEt_2)_2(H_2O)(C_4O_4)]H_2O$ {$SalNEt_2$=N-(2-(diethylamino)ethyl)salicylideneaminate}in which antiferromagnetic coupling between the two Cu(II) ions has also been observed [41]. behaviour [12, 23, 38-43]. The one and the only reported

μ-$_{1,2,3}$-squarato bridged complex [Cu_3-(pmap)3(μ-$_{1,2,3}$-C_4O_4)](ClO_4)$_4$·2H_2O] {pmap = bis-[2-(2-pyridyl)ethyl]-(2-pyridyl)methylamine} also exhibits antiferrromagnetic coupling between its three Cu(II) centers [46]. Castro et al. have reported μ-$_{1,2,3,4}$-squarato bridged tetranuclear compound [Cu_4(tren)$_4$(μ-$_{1,2,3,4}$-C_4O_4)](ClO_4)$_6$ complex that displays antiferromagnetic coupling between metal centers [31]. Their result has been corroborated by different groups for other μ-$_{1,2,3,4}$-squarato bridged metal complexes [44,45]. After literature survey, it can be said that the extent of antiferromagnetic interaction depends upon the bridging fashion of the squarate ligand and obviously the metal ions present in the complexes. In contrast, Cangussu et. al. have reported a bi-nuclear squarato bridged [Cu_2(bpcam)$_2$(μ$_{1,3}$-C_4O_4)(H_2O)$_4$]·10H_2O {where bpcam = bis(2-pyrimidylcarbonil)amidate} complex that shows weak ferromagnetic interaction due to accidental orthogonality in the complex [37]. Such weak to very weak ferromagnetic interaction has also been reported for some other squarato bridged metal complexes having μ-$_{1,2}$, μ-$_{1,3}$, μ-$_{1,2,3,4}$ types bridging fashions [13, 24, 37, 52]. The complex under present investigation is a μ-$_{1,2,3}$–squarato bridged compound where a squarato dianion simultaneously binds three different Ni(II) ions and also exhibits antiferromagnetic behaviour following the general trend for squarato bridged metal complexes.

3.3.4 Photoluminescence study

The emission spectra of the complex have been carried out in solid state at room temperature. The luminescent behavior of the complex corresponds to a ligand–centered (LC) fluorescence. The complex has shown emission maxima at 424 nm and 487 nm upon excitation at 300 nm (Figure 11). This can be attributed to the π-π* transition in the squarate and 2,2′-bipyridine ligands. The small peak around 531 nm is possibly caused by extended π-conjugation within the ligand system.

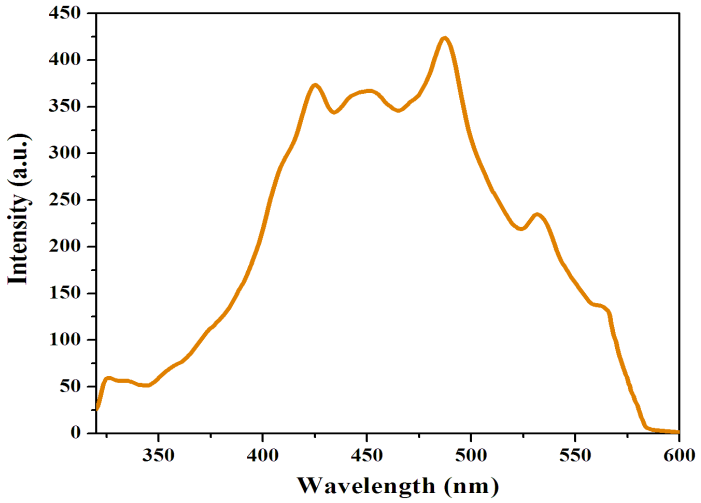

Figure 11. Photoluminescence spectra of the complex.

3.4 Conclusion

In conclusion, we have successfully synthesized a novel squarato-bridged 2D coordination polymer $\{[Ni(squarate)(2,2'\text{-bipy})(H_2O)]\cdot H_2O\}_n$ where the squarato di-aninon exhibits a very rare μ-$_{1,2,3}$ bridging aptitude. These 2D coordination sheets are packed *via* $\pi\cdots\pi$ interactions leading to the formation of 3D supramolecular structure with 1D supramolecular channels. These 1D channels are filled with guest water molecules which get stability through hydrogen bonding interactions. The structural study shows the presence of an unusual rare $\mu_{1,2,3}$ bridging mode of squarato aninon in the complex and the magnetic measurements have revealed that the complex is antiferromagnetic in nature. This is in agreement with the magnetic property of the sole previous example of μ-$_{1,2,3}$-squarato-bridged compound. Due to the presence of π-electrons the complex becomes fluorescence active. By providing the second example of μ-$_{1,2,3}$ bridging pattern of squarato-dianion we have established that the squarate ligand exhibits versatile bridging modes due to strong donor ability of its oxygen atoms.

Taking into account the present and large number of previous works it may be concluded that the squarato-bridged metal complexes provide the unique opportunity to study the wide variety

of bridging modes exhibited by the ligand and to investigate the influence of different bridging modes on magnetic property of such systems. Finally, we have presented a new 2D coordination polymer formed by utilizing unusual μ-$_{1,2,3}$ bridging pattern of squarato-dianion that exhibits multiple functionalities: (a) acts as metal-organic supramolecular host, (b) exhibits antiferromagnetic behavior and (c) photo-luminescent activity.

References

[1] K. Maruoka, N. Murase and H. Yamamoto, *J. Org. Chem*., **1993**, 58, 2938.

[2] C. Chen and K. S. Suslick, *Coord. Chem. Rev*., **1993**, 128, 293.

[3] D. Gatteschi, A. Caneschi, R. Sessoli and A. Cornia, *Chem. Soc. Rev*., **1996**, 25, 101.

[4] D. Gatteschi, *Adv. Mater*., **1994**, 6, 635.

[5] C. Cadiou, R. A. Coxell, A. Graham, A. Harrison, M. Helliwell, S. Parsons and R. E. P. Winpenny, *Chem. Commun*., **2002**, 10, 1106. (And references therein).

[6] D. J. Price, S. R. Batten, B. Moubaraki and K. S. Murray, *Chem. Commun*., **2002**, 7, 762.

[7] M. Eshel, A. Bino, I. Felner, D. C. Johnston, M. Luban and L. L. Miller, *Inorg. Chem*., **2000**, 39, 1376. (And references therein).

[8] L. K. Thompson, *Coord. Chem. Rev*., **2005**, 249, 2549.

[9] O. Kahn, *Molecular Magnetism*, VCH, New York, **1993**.

[10] D. Gatteschi and R. Sessoli, *Angew. Chem., Int. Ed*., **2003**, 42, 268.

[11] I. Castro, M. L. Calatayud, J. Sletten, F. Lloret and M. Julve, *Inorg. Chim. Acta*., **1999**, 287, 173.

[12] D. S. Cangussu, H. O.tumpf, H. Adams, J. H. Thomas, F. Lloret and M. Julve, *Inorg. Chim. Acta*., **2005**, 358, 2292.

[13] Y. Akhriff, J. Server-Carrió, A. Sancho, J. Garcia-Lozano, E. J.;Escrivá and L. Soto, *Inorg. Chem*., **2001**, 40, 6832.

[14] S. Konar, P. S. Mukherjee, E. Zangrando, F. Lloret and N. R. Chaudhuri, *Angew. Chem., Int. Ed*., **2002**, 41, 1561.

[15] S. Dalai, P. S. Mukherjee, E. Zangrando, F. Lloret and N. R. Chaudhuri, *J. Chem. Soc., Dalton Trans*., **2002**, 25, 822.

[16] I. L. Karle, D. Ranganathan and V. Haridas, *J. Am. Chem. Soc*., **1996**, 118, 7128.

[17] B. D. Alleyne, L. A. Hall, H. A. Hosein, H. Jaggernauth, A. J. P. White and D. J. J. Williams, *J. Chem. Soc., Dalton Trans*., **1998**, 22, 3845.

[18] S. Lopez and S. W. Keller, *Inorg. Chem*., **1999**, 38, 1883.

[19] P. S. Mukherjee, S. Konar, E. Zangrando, T. Mallah, J. Ribas and N. R. Chaudhuri, *Inorg. Chem*., **2003**, 42, 2695.

[20] J. M. Rueff, J. F. Nierengarten, P. Gilliot, A. Demessence, O. Cregut, M. Drillon and P. Rabu, *Chem. Mater*., **2004**, 16, 2933.

[21] J. D. Martin, R. F. Hess and P. D. Boyle, *Inorg. Chem*., **2004**, 43, 3242.

[22] P. Chaudhuri, K. Oder, K. Wieghardt, S. Gehring, W. Haase, B. Nuber and J. Weiss, *J. Am. Chem. Soc*., **1988**, 110, 3657.

[23] X. Solans, M. Aguilló, A. Gleizes, J. Faus, M. Julve and M. Verdaguer, *Inorg. Chem*., **1990**, 29, 775.

[24] H. -A. Hosein, H. Jaggernauth, B. D. Alleyne, L. A. Hall, A. J. P. White and D. J. Williams, *Inorg. Chem*., **1999**, 38, 3716.

[25] H. Tamaki, Z. J. Zhong, N. Matsumoto, S. Kida, M. Koikawa, N. Achiwa, Y. Hashimoto and H. Okawa, *J. Am. Chem. Soc*., **1992**, 114, 6974.

[26] E. Coronado, J. R. G. Mascaros and C. M. Gastaldo, *J. Mater. Chem*., **2006**, 16, 2685. [27] E. Coronado, J. R. G. Mascaros and C. M. Gastaldo, *CrystEngComm*., **2009**, 11, 2143.

[28] E. Coronado, J. R. G. Mascaros and C. M. Gastaldo, *J. Am. Chem. Soc*., **2008**, 130, 14987.

[29] Y. C. Ou, J. Wang, J. D. Leng, Z. J. Lin and M. L. Tong, *Dalton Trans*., **2011**, 40, 3592.

[30] R. Saha and S. Kumar, *CrystEngComm*., **2012**, 14, 4980.

[31] I. Castro, J. Sletten, M. L. Calatayud, M. Julve, J. Cano, F. Lloret and A. Caneschi, *Inorg. Chem*., **1995**, 34, 4903.

[32] M. Viertelhaus, H. Henke, C. E. Anson and A. K. Powell, *Eur. J. Inorg. Chem*., **2003**, 12, 2283.

[33] D. Braga, G. Cojazzi, L. Maini and F. Grepioni, *New J. Chem*., **2001**, 25, 1221.

[34] D. Deguenon, G. Bernardinelli, J. P. Tuchagues and P. Castan, *Inorg. Chem*., **1990**, 29, 3031.

[35] C. C. Wang, C. H. Yang and G. H. Lee, *Inorg. Chem*., **2002**, 41, 1015.

[36] L. Soto, N. Ruiz, H. Núñez, J. Server-Carrió, E. Escrivà, A. Sancho and J. Gracía-Lozano, *Inorg. Chim. Acta*., **2006**, 359, 3221.

[37] S. S. Massoud, F.A. Mautner, R. Vicente and F.R. Louka, *Eur. J. Inorg. Chem.*, **2008**, 23, 3709.

[38] C. C. Wang, C. H. Yang, G. H. Lee and H. L. Tsai, *Eur. J. Inorg.Chem.*, **2005**, 7, 1334.

[39] R. Kirchmaier, E. Altin, A. Lentz and Z. Kristallogr. *New Cryst. Struct.*, **2003**, 218, 541.

[40] I. Castro, M. L. Calatayud, J. Sletten, F. Lloret and M. Julve, *J.Chem. Soc., Dalton Trans*., **1997**, 5, 811.

[41] C. E. Xanthopoulos, M. P. Sigalas, G. A. Katsoulos, C. A. Tsipis, C. C. Hajikostas, A. Terzis and M. Mentzafos, *Inorg. Chem.*, **1993**, 32, 3743.

[42] J. A. C.van Ooijen, J.Reedijk and A. L. Spek, Inorg. Chem., **1979**, 18, 1184.

[43] E. Escrivá, L. Soto, J. Server-Carrió, C. J. Gómez-García, G. M. Espallargas, N. Ruiz, A. Sancho, J.García-Lozano and C. R. de Arellano, *Polyhedron*, **2013**, 56, 90.

[44] F. Dumestre, B. Soula, A. M. Galibert, P.-L. Fabre, G. Bernardinelli, B. Donnadieu and P. Castan, *J. Chem. Soc., Dalton Trans*., **1998**, 24, 4113.

[45] S. S Massoud, F. A Mautner, R. Vicente and J. S Dickens, *Inorg. Chim. Acta*., **2008**, 361, 299.

[46] R. Vicente, E. Ruiz, J. Cano, S. S. Massoud and F. A. Mautner, *Inorg. Chem.*, **2008**, 47, 4648.

[47] G. M. Sheldrick, *SHELXS 97*, Program for Structure Solution, University of Gottingen, Germany, **1997**.

[48] G.M. Sheldrick, *SHELXL 97*, University of Gottingen, Germany, Program for Crystal Structure Refinement, **1997**.

[49] A. L. Spek, *J. Appl. Crystallogr*., **2003**, 36, 7.

[50] L. J. Farrugia, *J. Appl. Crystallogr*., **1997**, 30, 565.

[51] L. J. Farrugia, J. Appl. Crystallogr., **1999**, 32, 837.

[52] P. S. Mukherjee, S. Konar, E. Zangrando, C. Diaz, J. Ribas and N. R. Chaudhuri, *J. Chem. Soc., Dalton Trans.*, **2002**, 18, 3471.

Chapter 4

A dynamic metal-organic supramolecular host based on weak π-stacking interactions incorporating 2D water-chloride-methanolic supramolecular sheet

4.1. Introduction

The design and fabrication of new polymeric compounds having desired potential applications needs self-assembly of discrete molecular units via covalent or non-covalent interactions like H-bonding, π-π interactions, ion- π interaction etc. [1-6]. During self-assembly the discrete metal-organic moieties connect themselves through cooperative non-covalent interactions and this leads to formation of metal-organic supramolecular host (MOSH) [7-12]. The guest molecules get stability in the MOSHs through supramolecular interactions. The MOSHs can very efficiently release and absorb guest molecules in a controlled manner [13-14]. Depending on the design strategy, the MOSHs are classified in two broad categories, viz., charged MOSH and uncharged MOSH. The uncharged MOSHs are capable of accommodating neutral guest species like simple water clusters [15-19], whereas the cationic MOSHs can easily accommodate anionic guest species like chloride-hydrates [20-24]. Since the ion transportation is a very important phenomenon in various chemical and biological processes in the living systems [25-29], several novel strategies have been adopted for recognition and transportation of ions in the self-assembled complexes [30-31]. The self-assembly is one of the unique approaches for construction of ion channels in cationic MOFs. The cationic metal-organic complex formation can be realized without using any anionic donor ligands.

Studies on water clusters in metal-organic host complexes have attracted a great deal of attention during recent times [32-36]. On the other hand, hybrid clusters of water and other small organic molecules or ions formed by hydrogen bonding interaction have drawn relatively less attention. In particular, there are very few reports on experimental identification and analysis of discrete water-chloride clusters (the hydrogen-bonded assemblies of water on crystallization and chloride counter ions in crystalline materials) [19-24]. The hydration phenomenon of chloride ion

has canonical importance in the field of biochemistry [37] and supramolecular chemistry. Moreover, drug molecules are generally organic molecules and they dissolve in organic solvents like methanol, ethanol etc. For efficient delivery of the anionic drug molecules a better understanding of the mode of interaction of the anions with organic solvents and water is a prerequisite. More than 70% of enzymes, substrates and cofactors are anions. Thus, more theoretical and experimental investigations on hybrid water-chloride clusters with other organic molecules are very essential.

In this context, we have reported previously the formation of a 2D water sheet, a helical-water chain and water-chloride tape in chiral supramolecular complexes and supramolecular hosts [38,39]. As a continuing effort, in this report, we have shown that a water-chloride-methanol 2D supramolecular network can be created within the hydrophobic interlayer cavities of a dynamic MOSH. A simple strategy that can be adopted for possible isolation of a hybrid water-chloride system is to use a neutral ligand in synthesizing Pr (III)-based cationic complexes. In this effort, we have successfully synthesized a metal-organic complex $[Pr(1,10\text{-phen})_2(H_2O)_5]Cl_3(H_2O)(CH_3OH)$, which includes water, chloride and methanol as guest molecules using 1,10-phenanthroline ligand. It is expected that the chelating nature of 1,10-phenanthroline along with its inherent π-stacking capability would integrate the discrete metal moieties at least in one direction. The x-ray crystal structure analysis has revealed that the complex assembles into a 2D supramolecular architecture via π···π interactions. The complex behaves like a dynamic metal-organic supramolecular host (MOSH). Three chloride ions, one guest water molecule and one guest methanol molecule along with five coordinated water molecules form a unique water-chloride-methanol hybrid 2D hydrogen bonded network and is stabilized within the hydrophobic interlayer cavities. The most important property of the present MOSH is its breathing nature –

when the host is heated up it expels the guest molecules and during cooling the species absorbs the water molecules from the atmosphere. The dynamic breathing metal-organic frameworks (MOFs) are easy to design but a dynamic supramolecular host like the present one is rarely observed as it requires involvement of weak forces. The present work shows how weak π···π stacking forces can be employed in designing host-guest frameworks and may work as effective examples in designing new dynamic MOSHs.

4.2. Experimental

4.2.1. General

The ingredients praseodymium (III) chloride, hepta-hydrate and 1,10-phenanthroline were purchased from Merck Chemical Company and all other chemicals used were AR grade. The elemental analysis (C, H and N) was carried out using a Perkin-Elmer 240C elemental analyzer. The IR spectrum was recorded between 400 and 4000 cm^{-1} using a Nicolet Impact 410 spectrometer employing the KBr pellet method. The thermal analysis was done with a Mettler Toledo TGA-DTA 85 thermal analyzer under a flow of N_2 (30 ml min^{-1}). The sample was heated at a rate of 10 ºC min^{-1} with inert alumina as a reference. The photoluminescence spectra were collected on a Shimadzu RF-5301PC Spectrophotometer. The Powder X-ray diffraction (PXRD) patterns were recorded by using Cu-K_α radiation (Bruker D8; 40 kV, 40 mA).

4.2.2. Synthesis of complex 1 {$[Pr(1,10\text{-}phen)_2(H_2O)_5]Cl_3(H_2O)(CH_3OH)$}

To a methanolic solution of 1,10-phenanthroline (0.90 g, 0.005 mol), 5 ml aqueous solution of $PrCl_3 \cdot 7H_2O$ (0.93 g, 0.0025 mol) was added drop wise. The resulting solution was then filtered off and was kept in open air. After 10 days, the light greenish yellow coloured single crystals suitable for single crystal x-ray (SCXRD) study appeared and they were collected by filtration. Yield: 1.40 g (75% based on Pr). Anal. Calcd. (%) for $C_{25}H_{32}PrN_4O_7Cl_3$: C, 40.15; H, 4.31; N, 7.49. Found

(%): C, 40.02; H, 4.39; N, 7.36. IR (KBr, cm^{-1}): 3332br, 2298vw, 1627s, 1593s, 1574s, 1518s, 1421m, 1343s, 1299m, 1102m, 1091w, 863m, 846s, 772s, 722w, 635w. λ_{max} (in MeOH) 260 nm, 324 nm (shoulder).

4.2.3 Crystallographic data collection and refinement

The suitable single crystal of the complex was mounted on a Bruker SMART diffractometer equipped with a graphite monochromator and Mo-K_α (λ = 0.71073 Å) radiation and the data was collected at room temperature. The structure was solved by Patterson method using the SHELXS97 program. The hydrogen atoms were placed in idealized positions and their displacement parameters were fixed to be 1.2 times larger than those of the attached non-hydrogen atoms. The position of non-hydrogen atoms was refined with independent anisotropic displacement parameters. The subsequent difference Fourier synthesis and least-square refinement revealed the positions of the non-hydrogen atoms. The successful convergence was indicated by the maximum shift/error of 0.001 for the last cycle of the least square refinement. All calculations were carried out using SHELXS 97[40], SHELXL 97[41], PLATON 99[42], ORTEP-32[43] and WinGX system Ver-1.64[44]. The data collection, structure refinement parameters and crystallographic data of the complex 1 are provided in Table 1.

4.3 Results and discussion

4.3.1 Crystal structure of complex 1{$[Pr(1,10\text{-phen})_2(H_2O)_5]Cl_3(H_2O)(CH_3OH)$}

The analysis of SCXRD data has revealed that complex 1 is a neutral mononuclear compound in which the Pr^{3+} ion is coordinated to two different 1,10-phen ligands and five water molecules as shown in Figure1. Each asymmetric unit contains one metal-organic moiety, three chloride anions, one guest methanol molecule and one guest water molecule. In the present case Pr(III) shows nine coordination modes. The four nitrogen atoms (N1, N2, N3 and N4) of two different 1,10-phen

ligands and five water molecules (O1W, O2W, O3W, O4W and O5W) fulfill the nine coordination of Pr(III) through formation of a paddle-wheel shaped molecular structure.

Table 1: Crystallographic data and refinement parameters of the complex 1

Crystal Data	
Formula	$C_{24}H_{26}N_4O_5Pr$, CH_4O, H_2O, 3Cl
Formula Weight	747.81
Crystal System	Triclinic
Space group	P-1
a [Å]	8.872(3)
b [Å]	9.192(3)
c [Å]	18.920(6)
α [°]	88.790(5)
β [°]	84.689(5)
γ [°]	69.159(5)
V [$Å^3$]	1435.7(8)
Z	2
D(calc) [g/cm^3]	1.730
μ(MoKα) [/mm]	2.027
F(000)	752
Data Collection	
Temperature (K)	100
Radiation [Angstrom]	MoKα 0.71073
Theta Min-Max [Deg]	1.1, 28.4
Dataset	-11: 11 ; -12: 12 ; -25: 24
Tot.	16947
Uniq. Data	6698
R(int)	0.015
Observed data [I > 2.0	6510
Refinement	
Nref, Npar	6698; 361
R	0.0276
wR2	0.0717
S	1.06
Max. and Av. Shift/Error	0.00, 0.00
Min. and Max. Resd. Dens.	-0.91, 1.51

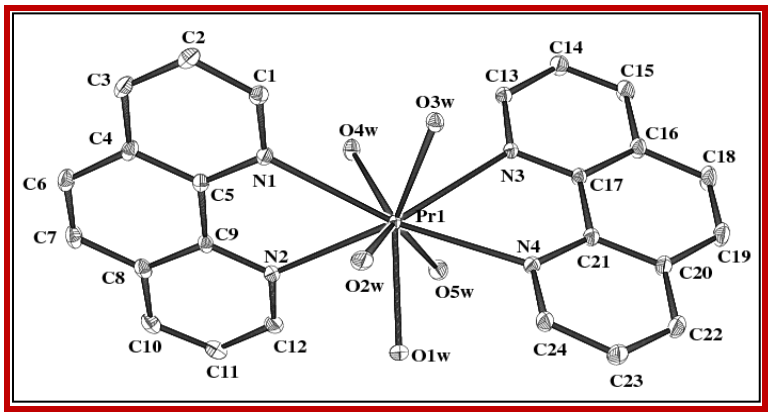

Figure 1. The ORTEP diagram of the complex 1

Some selected coordination bond lengths and bond angles are listed in Table 2 and 3, respectively. The two 1,10-phen moieties are nearly at the *trans* position to each other. The Pr-N bond lengths lie between 2.662(2)-2.723(2) Å which are well within the range of other reported Pr(III)-phen complexes [45-48]. The lanthanide ions have high affinity to hard donor centers and ligands with oxygen or hybrid oxygen–nitrogen atoms are the best fit for this purpose [49]. The $Pr–O_{water}$ distances are in the range between 2.448(2)-2.487(2) Å (average 2.477 Å), which are comparable with those observed in other Pr^{3+} ion complexes with analogous ligands [48]. It is noteworthy that the monomeric units are further connected by supramolecular hydrogen bonding and π··· interactions with the guest molecules to form a 3D supramolecular structure.

Table 2: Selected bond lengths (Å) of the complex 1

Bonds	Bond distance	Bonds	Bond distance
Pr1-O1W	2.4826(19)	Pr1-O2W	2.484(2)
Pr1-O3W	2.487(2)	Pr1-O4W	2.448(2)
Pr1-O5W	2.481(3)	Pr1-N1	2.709(2)
Pr1-N2	2.662(2)	Pr1-N3	2.723(2)
Pr1-N4	2.677(2)		

Table 3: Selected bond angles (°) of the complex 1

O1W-Pr1-O2W	70.13(8)	O5W-Pr1-N3	69.76(6)
O1W-Pr1-O3W	132.85(7)	O5W-Pr1-N4	78.94(6)
O1W-Pr1-O4W	131.25(7)	N1-Pr1-N2	61.66(6)
O1W-Pr1-O5W	70.69(8)	N1-Pr1-N3	121.07(5)
O1W-Pr1-N1	117.99(6)	N1-Pr1-N4	148.66(6)
O1W-Pr1-N2	71.28(6)	N2-Pr1-N3	139.58(6)
O1W-Pr1-N3	120.93(6)	N2-Pr1-N4	139.99(5)
O1W-Pr1-N4	69.50(6)	N3-Pr1-N4	61.26(5)
O2W-Pr1-O3W	72.48(6)	O2W-Pr1-O4W	140.55(6)
O2W-Pr1-O5W	140.40(6)	O2W-Pr1-N1	73.26(6)
O2W-Pr1-N2	91.74(6)	O2W-Pr1-N3	128.55(6)
O2W-Pr1-N4	82.37(6)	O3W-Pr1-O4W	95.90(6)
O3W-Pr1-O5W	135.36(6)	O3W-Pr1-N1	76.02(6)
O3W-Pr1-N2	137.58(6)	O3W-Pr1-N3	65.66(6)
O3W-Pr1-N4	78.07(6)	O4W-Pr1-O5W	73.53(6)
O4W-Pr1-N1	67.32(6)	O4W-Pr1-N2	71.39(6)
O4W-Pr1-N3	73.85(6)	O4W-Pr1-N4	133.18(6)
O5W-Pr1-N1	132.31(6)	O5W-Pr1-N2	81.04(6)

4.3.2 Supramolecular structure

In the present system, the monomeric metal-organic units are connected by supramolecular π-interactions to from 2D supramolecular sheets and between two 2D supramolecular sheets one guest methanol molecule, one guest water molecule and three charge neutralized chloride ions are accumulated by self-assembly. The pyridyl ring [Cg1] of the 1,10-phen ligand in one metal-organic unit bridges the phenyl ring [Cg5] of a symmetry [2-x, -y, 1-z] related metal-organic unit. Again, the pyridyl ring [Cg4] of the same 1,10-phen unit interacts with another phenyl ring [Cg6] of the

same symmetry [2-x, -y, -z] related unit. In this manner, the monomeric units are interlinked along the crystallographic ***c***-axis to form 1D supramolecular chains as shown in Figure 2. The 2D supramolecular sheets are formed by the further connection of 1D supramolecular chains by π···π interactions within the *ac*-plane, (Figure 3). The pyridyl ring [Cg2] of one 1,10-phen unit connects the self-complementary pyridyl ring [Cg2] of a symmetry related [1-x, -y, 1-z] nearby unit.

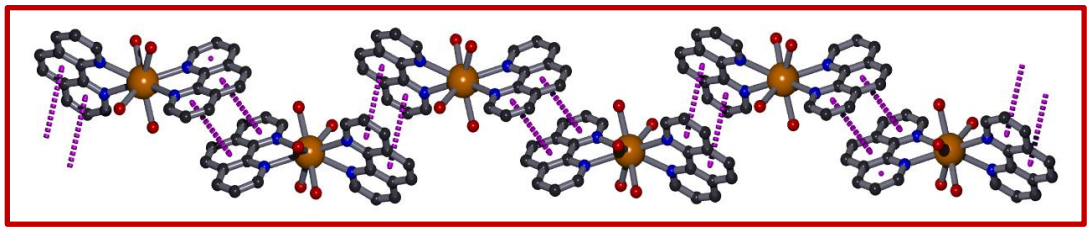

Figure 2. 1D supramolecular chain is formed along crystallographic ***c***-axis by π•••π interactions (Pr = Orange, C = Grey, N = Blue, O = Red).

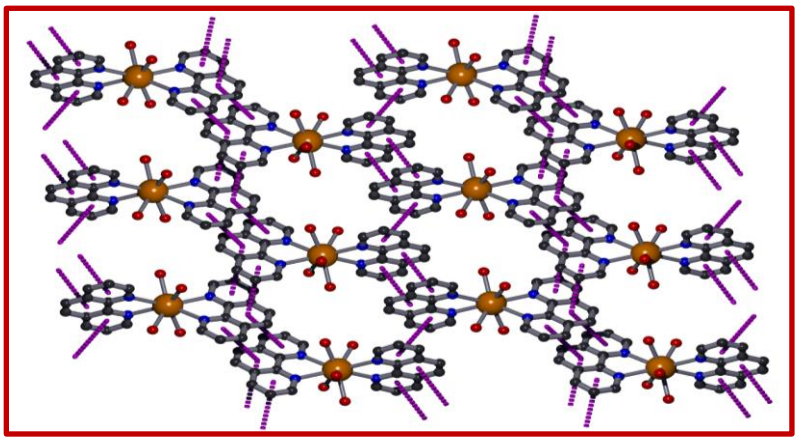

Figure 3. 1D chains are further connected by π•••π interactions to form 2D supramolecular sheets within *ac*-plane

All the π···π interaction parameters are summarized in Table 4. The 2D supramolecular sheets are packed along the ***b***-axis to form metal-organic supramolecular hosts (Figure 4) bearing hydrophobic pockets lined up by the 1,10-phen ligands.

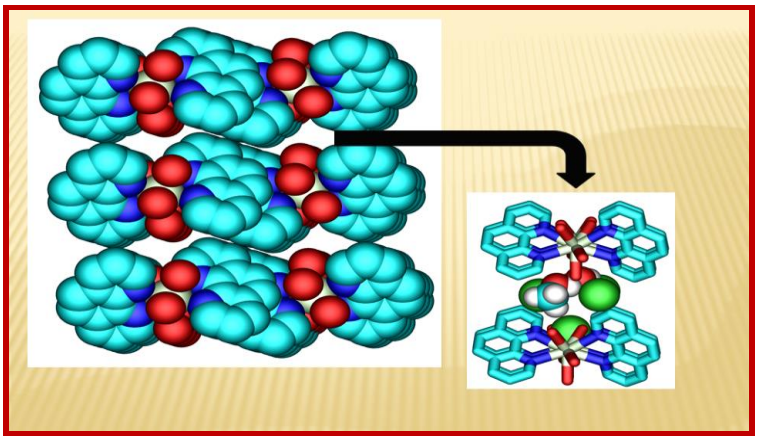

Figure 4. Supramolecular hosts are filled up by guest molecules

These hydrophobic pockets are filled up by one water molecule, one methanol molecule and three counter chloride ions. All these guest molecules interact with the metal-organic moieties through hydrogen bonding interactions. Among the guest species, only Cl1 is connected with the framework by hydrogen bonding interactions as shown in Figure 5. Two chloride ions, one water molecule and one methanol molecule form a $[Cl_2(H_2O)(MeOH)]$ cluster by hydrogen bonding interactions as shown in Figure 6.

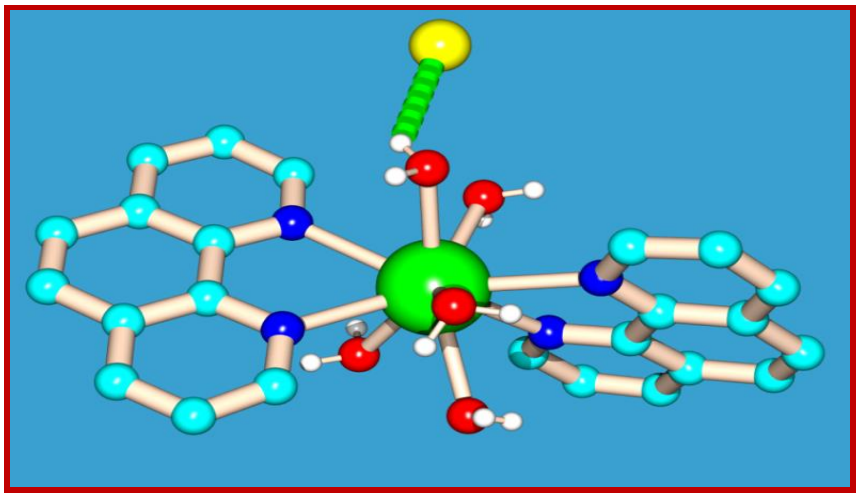

Figure 5. Cl1 atom is bound to metal-organic moiety by hydrogen bonding interactions.

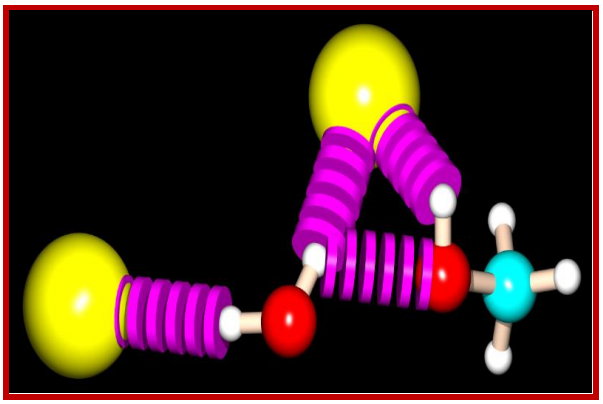

Figure 6. [$Cl_2(H_2O)(MeOH)$] cluster formed by hydrogen bonding interactions.

The hydrogen bonding interactions between the coordinated water molecules and the guest species have formed a 2D supramolecular network in the crystallographic *ab*-plane (Figure 7 & Figure 8). Cl1 is bound to H2W2 of O2W water molecule and the other hydrogen atom H1W2 is connected with methanolic oxygen atom O1. O1 is also connected with H2W1 of O1W water molecule. Methanolic hydrogen atom H1O1 is attached with Cl3.

Table 4: π··· interactions in the complex 1.

$Cg_i \cdots Cg_j$	Cgi···Cgj	α/(°)	Cgi perpendicular	Symmetry
Cg1···Cg5	3.715(2)	1.07(13)	3.4051(11)	2-x, -y, 1-z
Cg2···Cg2	4.136(2)	0	3.5163(11)	1-x, -y, 1-z
Cg2···Cg5	3.919(2)	1.95(13)	3.5368(11)	1-x, -y, 1-z
Cg4···Cg4	3.703(2)	0	3.5580(11)	2-x, -y, -z
Cg4···Cg6	3.883(2)	3.68(14)	3.5809(12)	2-x, -y, -z
Cg5···Cg1	3.715(2)	1.07(13)	3.3901(11)	2-x, -y, 1-z
Cg5···Cg2	3.919(2)	1.95(13)	3.4800(11)	1-x, -y, 1-z
Cg5···Cg5	3.918(2)	0	3.3807(11)	2-x, -y, 1-z
Cg6···Cg4	3.883(2)	3.68(14)	3.4788(12)	2-x, -y, -z
Cg6···Cg6	3.850(2)	0	3.4849(13)	1-x, -y, -z

*Cg1: N1--> C1 --> C2 --> C3 --> C4--> C5 -->; Cg2: N2 --> C9 --> C8 --> C10 -->C11 -->C12 -->; Cg4: N4-->C21--> C20-->C22-->C23 --> C24-->; Cg5: C4--> C5-->C9 -->C8-->C7-->C6-->; Cg6: C16-->C17-->C21-->C20-->C19-->C18-->

The other hydrogen atom H1W1 is bound to atom Cl2 and Cl2 binds the H2W5 of O5W water molecule. Another hydrogen atom H1W5 is bound to Cl1. This Cl1 is also connected with the H1W4 of O4W water molecule. Second hydrogen atom H2W4 of O4W binds the Cl3 atom which is consequently bound to H1W6 of O6W. The other hydrogen atom H2W6 of O6W has formed a bond with Cl2 while Cl2 is bound to H2W3 of O3W water molecule and H1W3 of O3W is connected with Cl1, which is bound to H2W2. All these together build up a supramolecular 2D sheet of $\{(H_2O)_6\text{-}(CH_3OH)\text{-}Cl_3\}_n$. The hydrogen bonding association of the guest with the host leads to the formation of a 3D supramolecular assembly of the host-guest framework (Figure 9). All the H-bonding interactions are summarized in Table 5.

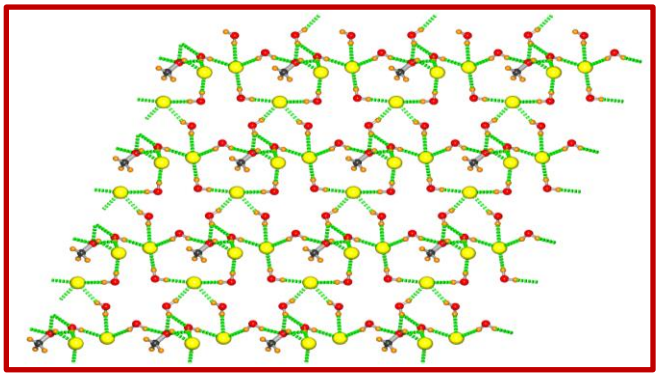

Figure 7. 2D supramolecular sheet in crystallographic ***ab***-plane formed by hydrogen bonding (green) interactions (C = Cyan, O = Red, H = White, Cl = Yellow).

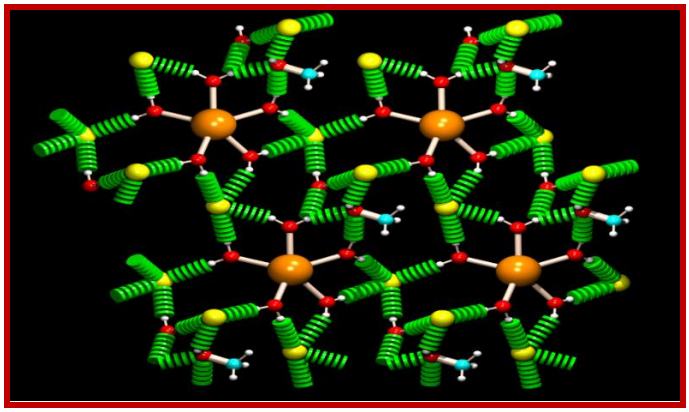

Figure 8. 2D supramolecular water-chloride-methanol sheet containing metal ions (Pr^{3+}) at the center of five coordinated water molecules (C=cyan, H=white, Pr=Orange, Cl=yellow, O=Red).

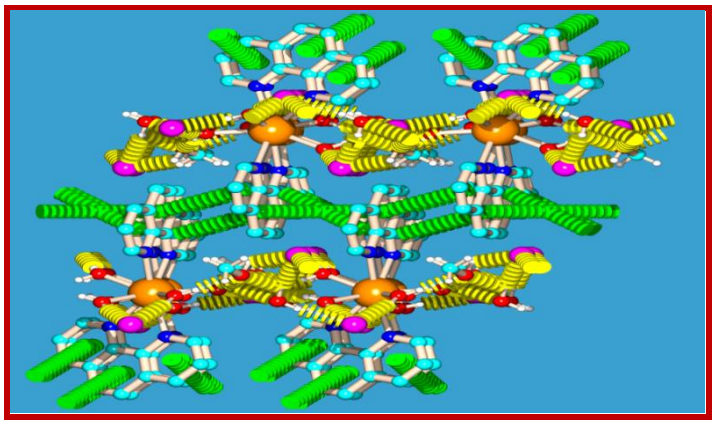

Figure 9. 1D chains along ***c***-axis are connected by hydrogen bonding interactions (yellow) through $[Cl_2(H_2O)(MeOH)]$ cluster to form 3D supramolecular structure.

Table 5: Hydrogen bond dimensions of the complex 1.

D-H···A	D-H/Å	H···A/Å	D···A/Å	<D-	Symmetry
O1W-H1W1···Cl2	0.87	2.27	3.110(3)	163	x, -1+y, z
O1W-H2W1···O1	0.88	1.91	2.758(5)	163	1+x, -1+y, z
O2W-H1W2···O1	0.85	1.95	2.769(5)	162	1+x, -1+y, z
O2W-H1W2···O6W	0.85	2.17	2.711(4)	121	1+x, -1+y, z
O2W-H2W2···Cl1	0.86	2.24	3.077(2)	164	1+x, y, z
O3W-H1W3···Cl1	0.88	2.21	3.092(2)	180	1+x, y, z
O3W-H2W3···Cl2	0.87	2.25	3.122(2)	179	.
O4W-H1W4···Cl1	0.89	2.21	3.098(2)	179	.
O4W-H2W4···Cl3	0.88	2.07	2.949(2)	179	.
O5W-H1W5···Cl1	0.82	2.43	3.156(3)	149	.
O5W-H2W5···Cl2	0.82	2.46	3.276(2)	169	x, -1+y, z
O1-H1O1···Cl3	0.86	1.98	2.444(5)	113	.
O6W-H1W6···Cl3	0.87	2.22	3.087(3)	172	.
O6W-H1W6···O1	0.87	1.84	2.336(6)	114	.
O6W-H2W6···Cl2	0.86	2.32	3.176(4)	173	.
C1-H1···O3W	0.95	2.44	3.130(3)	129	.
C11-H11···Cl3	0.95	2.74	3.524(3)	140	x, -1+y, z
C13-H13···O4W	0.95	2.50	3.087(3)	120	.
C19-H19···Cl1	0.95	2.80	3.744(3)	176	1-x, -y, -z
C24-H24···O1W	0.95	2.56	2.955(3)	106	.
C25-H25B···Cl3	1.00	2.48	2.934(6)	107	.
C25-H25C···Cl1	0.96	2.42	3.237(4)	143	.

4.3.3 Thermal analysis

We have studied the thermal stability of the complex (Figure 10). The thermogravimetric analysis displays a weight loss of 12.43% (calculated 13.91%) in the temperature range 40–117 °C that corresponds to the removal of one lattice water molecule, one methanol molecule and three coordinated water molecules. A further weight loss of 3.96% occurs between 117-257 °C consistent with the loss of two coordinated water molecules (calculated 4.82%). The observed weight losses are a little bit lower than the theoretical values. The slight discrepancy is due to weight loss occurring even at lower than 40°C, illustrating the dynamic nature of the water molecules in the solid state.

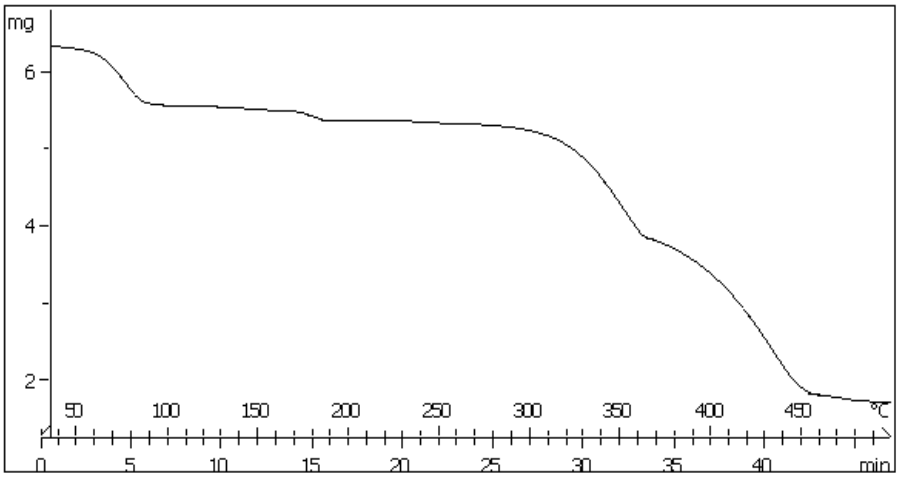

Figure 10. The thermal plot of the complex 1.

4.3.4 Study on dynamic nature of the host-guest binding-removal and reintroduction of guests

The rigid metal–organic coordination polymers have gained significant attention owing to their huge potential applications in catalysis, adsorption and ion exchange [50-52]. However, the flexible metal-organic frameworks are more efficient for these applications [53-56], as flexible frameworks are very sensitive to the presence of guests and undergo structural changes depending

upon the number and nature of the guest molecules [57-60]. The thermal study of complex 1 has revealed that within 117 ºC one guest water molecule, one methanol molecule and three coordinated water molecules escape from the complex. Therefore, to study the nature of the framework after evacuation of the guest water, guest methanol and coordinated water molecules we have heated complex 1 at 117 ºC for 3 hours and subsequently recorded the PXRD data of the heat-treated sample. The PXRD analysis indicates that this heat-treated sample is crystalline in nature. So, even after the removal of the coordinated and guest water and methanol molecules the host retains its crystallinity. Due to heating, the peak at 9.37º (1^{st} peak) disappears while a new peak appears at 13.56º. Moreover, the intensity of the peak at 10.27º decreases. As the 1^{st} peak appears at a higher angle compared to that of the parent complex (complex 1) so it can be inferred that upon thermal treatment shrinking occurs i.e., the supramolecular sheets come closer to each other after heating. The PXRD pattern of this new complex matches well with the simulated XRD pattern of $[Pr(phen)_2Cl_3,H_2O]$ (Figure 11) [61]. It may therefore be inferred that the structure of the sample obtained by heating complex 1 at 117 ºC is similar to that of $[Pr(phen)_2Cl_3,OH_2]$. Thus, upon removal of guest molecules and coordinated water molecules (partly) by heating, the supramolecular complex undergoes structural changes that leads to the formation of a new complex having the crystal structure similar to that of $[Pr(phen)_2Cl_3,H_2O]$.

The crystalline nature of the partially evacuated complex inspired us to study the flexibility of the complex upon heat treatment. So, this partially evacuated complex was kept in open air. After 14 days, a light green crystalline solid (complex 1a) was collected and the PXRD pattern of complex 1a was recorded. The PXRD pattern shows that the peak at 9.37º reappears which indicates that the heated complex absorbs water from air and water molecules enter between the 2D supramolecular metal-organic sheets and this in turn has expanded the channels between the

sheets. There are some notable dissimilarities between the PXRD patterns of complex 1, complex 1a and the partially dehydrated complex. For complex 1a the intensity of the peak at 10.27º has diminished and the highest peak has been found at 11.27º. Thus, it can be concluded that due to soaking of water a new phase has been generated. All the PXRD patterns are presented in Figure 11. The results of PXRD study on complex 1, complex 1a and the partially dehydrated complex have clearly revealed that the MOSH under investigation exhibits 'shrinking and expanding ability'upon evacuation and reintroduction of guest molecules.

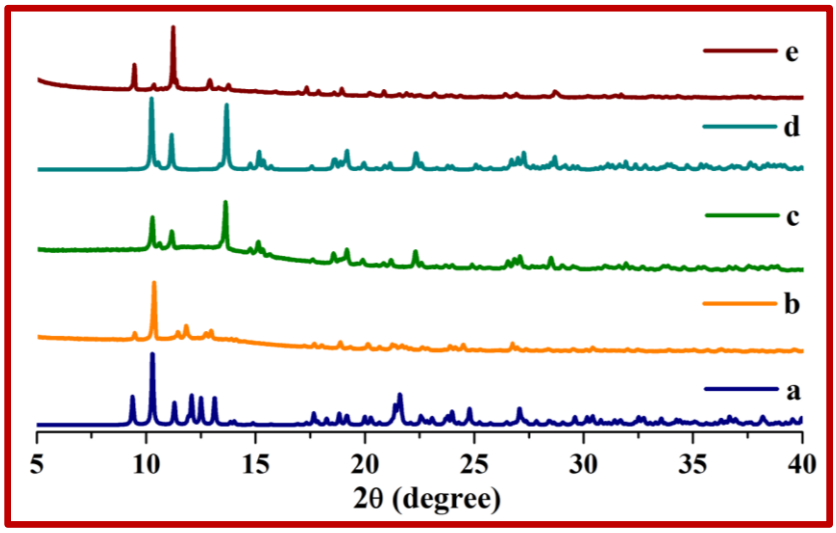

Figure 11. PXRD patterns of the complexes: (a) simulated pattern of complex; (b) PXRD pattern of the as synthesized material; (c) PXRD pattern of the specimen obtained after removal of guest molecules; (d) simulated pattern of compound reported by M. Khorasani-Motlagh et.al.; (e) PXRD pattern of the compound after re-absorption of water.

We have examined the thermal behavior of complex 1a (Figure 12). According to Figure 10 and Figure 12 thermal behavior of complex 1 and 1a is different up to 250 ºC but it is nearly similar above 250 ºC. This difference is due to the fact that complex 1 contains methanol and water as guests along with the coordinated water molecules while complex 1a does not have any methanol molecule. The similarity of thermogravimetric curves of complex 1 and 1a indicates that

the main structural pattern of the MOSH remains more or less same upon evacuation and reintroduction of guest molecules.

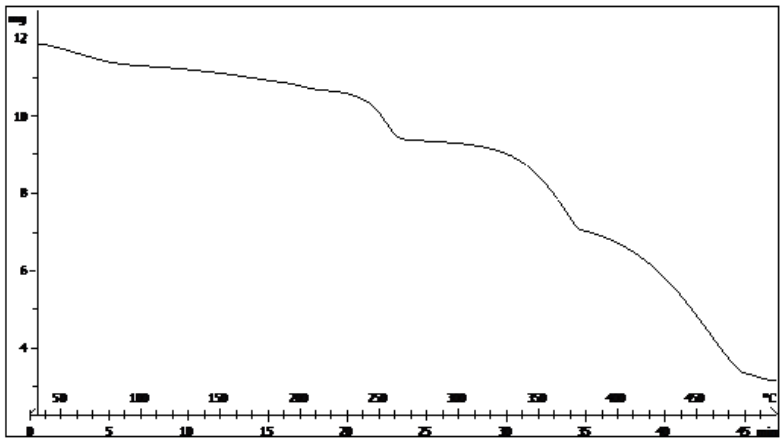

Figure 12. Thermal plot of complex 1a.

4.3.5 Temperature and heating time dependent PXRD Studies

In order to investigate the mechanism of structural transformation, we have heated complex 1 at different temperatures and for different time duration at a fixed temperature and we have recorded PXRD patterns of the samples obtained after heating (Figures 13 and 14). We have heated the sample at 75, 100 and 120 ºC for 1 hr in each case and recorded the PXRD pattern of these heated products. The changes occurred in the PXRD patterns are shown in Figure 13. The PXRD analysis reveals that upon heating at 75 ºC the 1st peak shifts toward higher angle (at 9.67º from 9.43º) and a new sharp peak appears at 13.50º along with the changes in other peaks. The PXRD pattern obtained after heating complex 1 at 120 ºC is distinctly different from all previous phases. We have recorded the PXRD pattern of the sample after heating it at 120 ºC for 40 min, 80 min and 120 min. No significant change has been observed in these PXRD patterns (Figure 14**)**. It may therefore be concluded that with the increase in heating temperature the structural transformation proceeds in stepwise manner through gradual removal of guest molecules. Moreover, upon heating at 120 ºC for a certain time the guest water molecule, methanol molecule and three coordinated

water molecules get released from the host framework and so a new phase has been produced and no further change occurs.

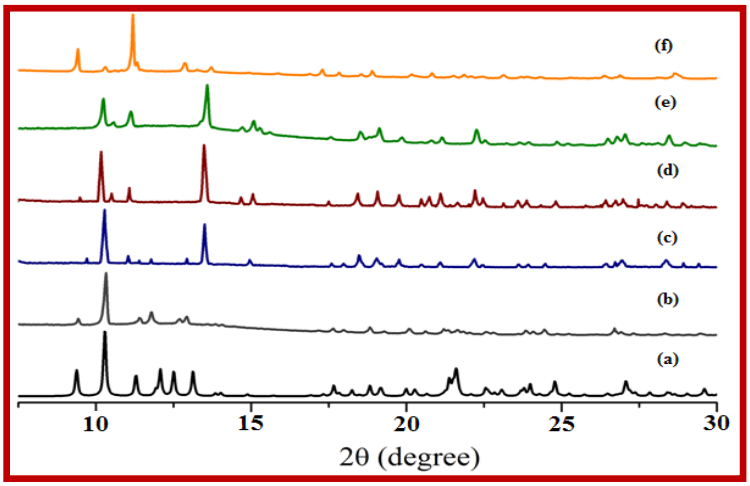

Figure 13: PXRD patterns (a) black: simulated pattern, (b) deep gray: as synthesized pattern, (c) royal: after heating at 75 ºC, (d) wine: after heating at 100 ºC, (e) orchid: after heating at 120 ºC, (f) orange: after rehydration.

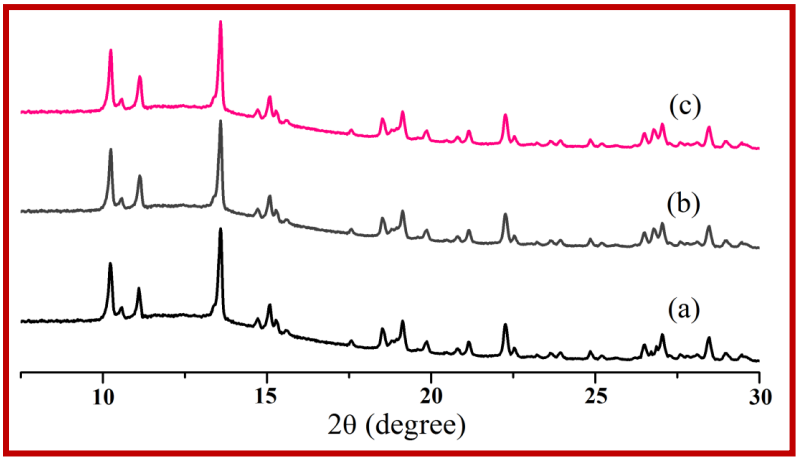

Figure 14. PXRD patterns (a) black: after heating for 40 min, (b) deep gray: after heating for 80 min, (c) pink: after heating for 120 min at 120 ºC.

4.3.6. Photoluminescence study

For praseodymium (III), there are three possible emitting f-states, e.g., $^3P_0$, $^1D_2$ and $^1G_4$. However, in solution transitions take place from two excited states ($^3P_0$ and $^1D_2$) [62], and from three excited states ($^3P_0$, $^1D_2$ and $^1G_4$) in solids [63-65]. Moreover, Pr^{3+} also emits efficient ultraviolet 5d-4f-

luminescence [80-83] and this transition is used for the fluorometric determination of Pr^{3+} in solutions [65-67].

The emission spectra of complex 1 in solid state are depicted in Figure 15. It is showed of four emission peaks: an intense peak due to $^3P_0 \rightarrow {}^3H_4$ transition appears at 484 nm, the weak $^3P_0 \rightarrow {}^3H_5$ transition peaks appear at around 505nm, a complex band system appears in range of 558-670 nm which include the $^1D_2 \rightarrow {}^3H_4$ transition (572 nm), $^3P_0 \rightarrow {}^3H_6$ (592 nm) and $^3P_0 \rightarrow {}^3F_2$ (672 nm) transitions, and the weak peak for $^3P_0 \rightarrow {}^3F_{3,4}$ emission at around 719 nm. The π-π^* transition of 1,10-phen appears in the wavelength region of 340–420 nm with a broad band around 384 nm, which can be attributed to the phosphorescence of 1,10-phen [68]. The appearance of such a phosphorescence band at room temperature is a very rare case and it indicates the presence of stable triplet state in 1,10-phen.

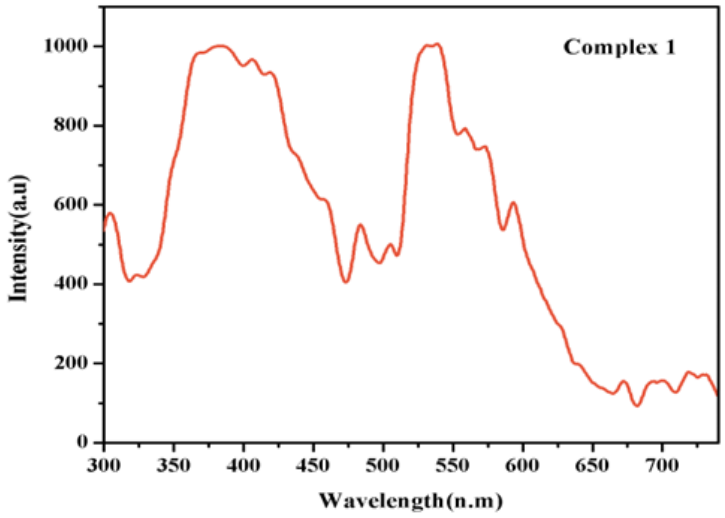

Figure 15. Photoluminescence spectra of the complex 1.

The emission spectrum of complex 1a (Figure 16) is quite similar to that of complex 1. It shows an intense $^3P_0 \rightarrow {}^3H_4$ transition at 486 nm, a very weak peak at 500 nm for $^3P_0 \rightarrow {}^3H_5$ transition. A set of peaks with small intensity are also observed within the wavelengths range of

567-670 nm that includes the $^1D_2 \rightarrow {}^3H_4$ transition (567 nm), $^3P_0 \rightarrow {}^3H_6$ transition (594 nm) and $^3P_0 \rightarrow {}^3F_2$ (668 nm) transition. The π-π* transition of 1,10-phen appears in the wavelength region of 330–415 nm with a broad band around 385 nm, which can be assigned to the phosphorescence of 1,10-phenanthroline. Thus, the photoluminescence property of complex 1 and 1a is similar in nature.

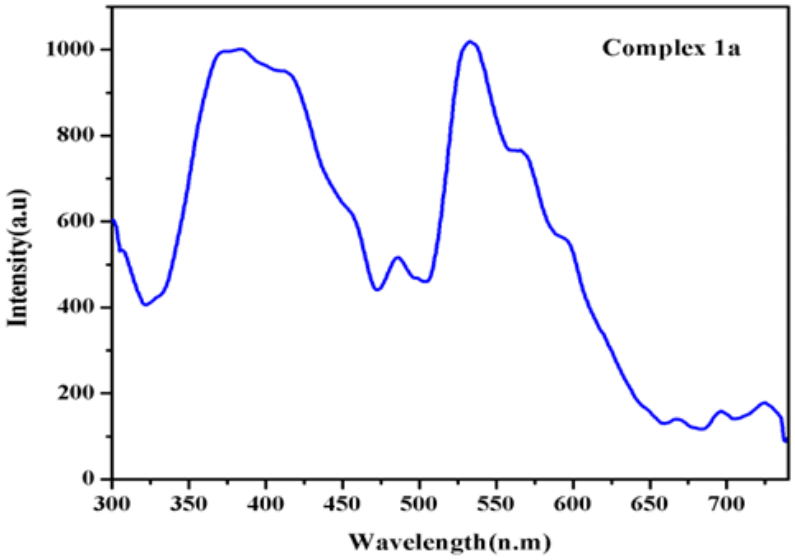

Figure 16. Photoluminescence spectra of complex 1a.

4.3.7 Theoretical study

We performed an *ab initio* geometrical optimization of the H-atom positions at the MP2 level of DFT theory with the 6-31**G(d,p) basis set by freezing the positions of the heavy oxygen atoms for a quantitative understanding of the stability of the water-chloride-methanol cluster. All calculations have been implemented with the GAUSSIAN-03 package [69]. We have performed the calculation with one motif made of six water-one methanol-three chloride, $[(H_2O)_6\text{-}(CH_3OH)\text{-}Cl_3]_n^{3-}$ (Figure 17) as it is the basic repeating unit of the whole water–chloride-methanolic sheet. We consider the stabilization energy of the cluster association having *n* number of water molecules ($E_{n\text{-mer}}$) to be equal to $E_{n\text{-mer}}$ - (nE_{monomer}) and a similar approach has been adopted for chloride ion

and methanol molecule. The monomeric energy was calculated by optimizing a single H_2O molecule, methanol molecules and chloride ion at the same level of the theory.

Table 6: MP2 optimized coordinates of Water-Chloride-Methanol Cluster.

Atom	X	Y	Z
Cl	0.000000	0.000000	0.000000
Cl	0.000000	0.000000	4.790300
Cl	4.908650	0.000000	-1.067567
O	-1.777013	-0.492141	2.488733
H	-1.272554	-0.355537	1.770198
H	-1.248166	-0.349620	3.180442
O	-2.880876	-1.282195	-0.131061
H	-2.316511	-0.688270	-0.198843
H	-3.325427	-1.553869	-0.768548
O	2.095533	0.879590	-2.097141
H	1.502809	0.632180	-1.498664
H	2.879301	0.635822	-1.803043
O	2.043466	-2.240235	4.212969
H	1.529468	-1.549978	4.352830
H	1.578920	-2.959502	4.327755
O	4.387017	0.086101	1.997369
H	4.342674	0.049008	1.133701
H	3.571419	0.049353	2.314898
O	4.410427	-0.989169	4.640174
H	3.617378	-0.761061	4.444437
H	4.436926	-1.427020	5.378963
O	2.080126	-0.013873	3.506147
H	1.876618	0.343005	4.260081
C	1.741797	0.859306	2.590359
H	2.284056	1.597503	2.627226
H	0.799011	1.165570	2.755834
H	1.619334	0.416453	1.752358

The basis set superposition error (BSSE) was taken into account following the counterpoise method in the calculation of stabilization energy. The corrected stabilization energy of the $[(H_2O)_6$-(CH_3OH)-$Cl_3]_n^{3-}$ was found to be -1949.427Kcal mol^{-1} for the complex 1. The MP2 optimized coordinates of water–chloride-methanol cluster for the complex 1 is given in Table 6.

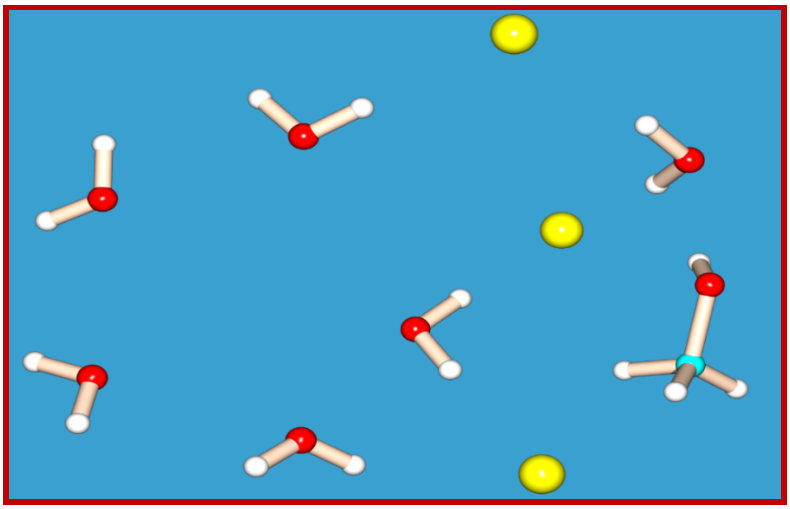

Figure 17. $[(H_2O)_6$-(CH_3OH)-$Cl_3]_n^{3-}$ building motif of the 2D supramolecular sheet used for MP2 optimization.

4.4 Conclusion

In this work, we have shown that hybrid water chloride system can be incorporated in a Pr (III)-based complex synthesized by using a neutral ligand 1,10-phenanthroline. The cationic complex $[Pr(phen)_2(H_2O)_5]^{3+}$ has been stabilized by the counter chloride anions. The 2D sheets are formed within the *ac*-plane by using the π···π interactions between 1D supramolecular chains formed by connecting the monomeric units. These 2D sheets are further packed by π···π interactions to form the MOSH having hydrophobic pockets in which guest water, chloride and methanol are stabilized through weak interactions. The hydrogen bonding interactions among coordinated water along with the guests form a unique 2D supramolecular water-chloride-methanol sheet. The guest responsive hydrophobic pockets between 2D supramolecular sheets are flexible in nature. The

MOSH can shrink and readjust itself with the retention of crystallinity upon the expulsion and introduction of guest species. It also regains its original shape upon reabsorption of guest species. The present system thus behaves like a dynamic supramolecular metal-organic host which can breathe upon heating and cooling with simultaneous aquation. This dynamic nature is due to the strong affinity of the host towards the guest molecules. The coordination tendency of the Pr(III) ion and the self-assembling tendency of water-chloride and methanol stabilize the system and these are responsible for the affinity of the host towards the guest molecules. The unique hydrogen bonded network of water-chloride and methanol molecules obtained in the present crystalline host will enhance our knowledge on the water-anion assembly and further work may help to understand how water-chloride and methanol may behave in biological processes like chloride ion transportation. In summary, the present crystal structure is a very interesting example of dynamic supramolecular metal-organic host and will act as a guide in the design of further metal-organic host systems – where metal coordination tendency towards water molecules and anion-water self-assembling tendency can be utilized.

References

[1] J. M. Lehn, *Supramolecular Chemistry*, VCH, Weinheim, **1995**.

[2] J. M. Lehn, *Angew. Chem. Int. Ed. Engl*., **1990**, 29, 1304.

[3] J. W. Ko, K. S. Min and M. P. Suh, *Inorg. Chem*., **2002**, 41, 2151.

[4] T. K. Maji, P. S. Mukherjee, G. Mostafa, E. Zangrando and N. Ray Chaudhuri, *Chem. Commun*., **2001**, 48, 1368.

[5] L. Carlucci, G. Ciani, M. Moret, D. M. Proserpio and S. Rizzato, *Angew. Chem. Int. Ed*., **2001**, 39, 1506.

[6] S. Biswas, G. Mostafa, Ian M. Steele, S. Sarkar and K. Dey, *Polyhedron*, **2009**, 28, 1010.

[7] S. Kitagawa, R. Kitaura, and S. Noro, *Angew. Chem. Int. Ed*., **2004**, 43, 2334.

[8] G. Ferey, C. Mellot-Draznieks, C. Serre, F. Millange, J. Dutour, S. Surble and I. Margiolaki, *Science*, **2005**, 309, 2040.

[9] M. Dincă and J. R. Long, *J. Am. Chem. Soc*., **2007**, 129, 11172.

[10] C. D. Wu, A. Hu, L. Zhang and W. Lin, *J. Am. Chem. Soc*., **2005**, 127, 8940.

[11] S. Horike, M. Dinc, K. Tamaki and J. R. Long, *J. Am. Chem. Soc*., **2008**, 130, 5854.

[12] S. Hasegawa, S. Horike, R. Matsuda, S. Furukawa, K. Mochizuki, Y. Kinoshita and S. Kitagawa, *J. Am. Chem. Soc*., **2007**, 129, 2607.

[13] H. Q. Hao, W. T. Liu, W. Tan, Z. Lin and M. L. Tong, *Cryst. Growth Des*., **2009**, 1, 1459.

[14] K. Nagayoshi, Md. K. Kabir, H. Tobita, K. Honda, M. Kawahara, M. Katada, K. Adachi, H. Nishikawa, I. Ikemoto, H. Kumagai, Y. Hosokoshi, K. Inoue, S. Kitagawa and S. Kawata, *J. Am. Chem. Soc*., **2003**, 125, 221.

[15] M. Ding, J. Wu, Y. Liu and K. Lu, *Inorg. Chem*., **2009**, 48, 7457.

[16] A. L. Gillon, N. Feeder, R. J. Davey and R. Storey, *Cryst. Growth Des*., **2003**, 3, 663.

[17] C. Janiak and T. G. Scharmann, *J. Am. Chem. Soc*., **2002**, 124, 14010.

[18] S. Pal, N. B. Sankaran and A. Samanta, *Angew. Chem., Int. Ed*., **2003**, 42, 1741.

[19] M. T. Ng, T. C. Deivaraj, W. T. Klooster, G. J. McIntyre and J. J. Vittal, *Chem. Euro. J*, **2004**, 10, 5853.

[20] A. K. Ghosh, D. Ghoshal, J. Ribas, G. Mostafa and N. R. Chowdhury, *Cryst. Growth Des*., **2006**, 6, 36.

[21] R. R. Fernandes, A. M. Kirillov, C. M. F´atima, G. da Silva, Z. Ma, J. A. L. da Silva, J. J. R. F. da Silva and A. J. L. Pombeiro, *Cryst. Growth Des*., **2008**, 8, 782.

[22] P. S. Lakshminarayanan, E. Suresh and P. Ghosh, *Angew. Chem.Int. Ed*., **2006**, 45, 3807.

[23] R. Custelcean and M. G. Gorbunova, *J. Am. Chem. Soc*., **2005**, 127, 16362.

[24] M. C. Das, S. K. Ghosh, S. Sen and P. K. Bharadwaj, *CrystEnggComm*., **2010**, 12, 2967.

[25] M. C. Koch, K. Steinmeyer, C. Lorenz, K. Ricker, F. Wolf, M. Otto, B. Zoll, F. L. Horn, K. H. Grzeschik and T. J. Jentsch, *Science*, **1992**, 257, 797.

[26] K. Wichmann, B. Antonioli, T. Söhnel, M. Wenzel, K. Gloe, K. Gloe, J. R. Price, L. F. Lindoy, A. J. Blake and M. Schröder, *Coord. Chem. Rev*., **2006**, 250, 2987.

[27] S. Chakrabarti, M. F. L. Parker, C.W. Morgan, C. E. Schafmeister and D. H. Waldeck, *J. Am. Chem. Soc*., **2009**, 131, 2044.

[28] J. L. Sessler, P. A. Gale and W. S. Cho, *Anion Receptor Chemistry*, The Royal Society of Chemistry, **2006**.

[29] E. C. Constable, G. Zhang, C. E. Housecroft, M. Neuburger and S. Schaffner, *CrystEngComm*., **2009**, 11, 1014.

[30] P. D. Beer and A. P. Gale, *Angew. Chem., Int. Ed*., **2001**, 40, 486.

[31] E. A. Meyer, R. K. Castellano and F. Diederich, *Angew. Chem., Int. Ed*., **2003**, 42, 1210.

[32] L. Infantes, J. Chisholm and S. Motherwell, *CrystEngComm*., **2003**, 5, 480.

[33] I. Ravikumar, P. S. Lakshminarayanan, E. Suresh and P. Ghosh, *Cryst. Growth Des*., **2006**, 6, 2630.

[34] P. Ren, B. Ding, W. Shi, Y. Wang, T. B. Lu and P. Cheng, *Inorg. Chim. Acta*., **2006**, 359, 3824.

[35] Z. G. Li, J. W. Xu, H. Q. Via and N. H. Hu, *Inorg. Chem. Commun*., **2006**, 9, 969.

[36] P. S. Lakshminarayanan, D. K. Kumar and P. Ghosh, *Inorg. Chem*., **2005**, 44, 7540.

[37] J. M. Berg, J. L. Tymoczko and L. Stryer, Biochemistry, *Fifth Edition*.

[38] R. Saha, S. Biswas and G. Mostafa, *CrystEngComm*., **2011**, 13, 1018.

[39] R. Saha, S. Biswas, I. M. Steele, K. Dey and G. Mostafa, *Dalton Trans*., **2011**, 40, 3166.

[40] G. M. Sheldrick, *SHELXS 97*, Program for Structure Solution, University of Göttingen, Germany, **1997**.

[41] G. M. Sheldrick, *SHELXL 97*, Program for Crystal Structure Refinement, University of Göttingen, Germany, **1997**.

[42] A. L. Spek, *PLATON*, Molecular Geometry Program, *J. Appl. Crystallogr*., **2003**, 36, 7.

[43] L. J. Farrugia, *J. Appl. Crystallogr*., **1997**, 30, 565.

[44] L. J. Farrugia, *J. Appl. Crystallogr*., **1999**, 32, 837.

[45] Y. H. Wana, L. P. Zhanga and L. P. Jina, *J. Mol. Struct*., **2003**, 658, 253.

[46] L. Huang and L. P. Zhang, *J. Mol. Struct*., **2004**, 692, 249.

[47] L. Huanga, L. P. Zhanga and L. P. Jin, J. Mol. Struct., **2004**, 692, 169.

[48] M. Khorasani-Motlagh, M. Noroozifar, S. Niromand, S. Khajeh and B. O. Patrick, *Inorg. Chim. Acta*., **2009**, 362, 3785.

[49] Y. Li, F. P. Liang, C. F. Jiang, X. L. Li and Z. L. Chen, *Inorg. Chim. Acta*., **2008**, 361, 219.

[50] O. M. Yaghi, M. O'Keeffe, N. W. Ockwig, H. K. Chae, M. Eddaoudi and J. Kim, *Nature,* **2003**, 423, 705.

[51] M. J. Rosseinsky, *Microporous Mesoporous Mater*., **2004**, 73, 15.

[52] S. Kitagawa, R. Kitaura and S. I. Noro, *Angew. Chem., Int. Ed*., **2004**, 43, 2334.

[53] S. Kitagawa, R. Kitaura and S. I. Noro, *Angew. Chem., Int. Ed*., **2004**, 116, 2388.

[54] S. Kitagawa and R. Matsuda, *Coord. Chem. Rev*., **2007**, 251, 2490.

[55] G. S. Papaefstathiou and L. R. MacGillivray, *Coord. Chem. Rev*., **2003**, 246, 169.

[56]D. N. Dybtsev H. Chun and K. Kim, *Angew. Chem., Int. Ed*., **2004**, 116, 5143.

[57] R. J. Robson, *Chem. Soc. Dalton Trans*., **2000**, 3735.

[58] B. Moulton and M. J. Zaworotko, *Chem. Rev*., **2001**, 101, 1629.

[59] C. N. R. Rao, S. Natarajan and R. Vaidhyanaathan, *Angew. Chem., Int. Ed*., **2004**, 116, 1490.

[60] M. Dincă, A. F. Yu and J. R. Long, *J. Am. Chem. Soc*., **2006**, 128, 8904.

[61] M. K. Motlagh, M. Noroozifar, S. Niromand, S. Khajeh and B. O. Patrick, *Inorganica Chimica Acta*., **2009**, 362, 3785.

[62] E. B. Sveshnikova and N. T. Timofeev, *Opt. Spektroskopiya*., **1980**, 48, 503.

[63] H. Dornauf and J. Heber, *J. Lumin*., **1979**, 20, 271.

[64] V. P. Dotsenko, N. P. Efryushina and I. V. Berezovskaya, *Opt. Spektroskopiya*., **1995**, 79, 105.

[65] W. Strek, J. Legendziewicz, E. Lukowiak, K. Maruszewski, J. Sokolnicki, A. A. Boiko and M. Borzechowska, *Spectrochim. Acta A*., **1998**, 54, 2215.

[66] A.G. Svetashev and M. P. Tsvirko, *Zh. Prikl. Spektrosk*., **1995**, 62, 249.

[67] V. T. Mishchenko, D. V. Demeshko and V. A. Perfilev, *J. Anal. Chem*., **1993**, 48, 1268.

[68] M. Hasegawa, A. Ishii and S. Kishi, *J. Photochem. Photobiol. A*., **2006**, 178, 220.

[69] M. J. Frisch, G. W. Trucks, H. B. Schlegel, G. E. Scuseria, M. A. Robb, J. R. Cheeseman, J. A. Jr. Montgomery, T. Vreven, K. N. Kudin, J. C. Burant, J. M. Millam, S. S. Iyengar, J. Tomasi, V. Barone, B. Mennucci, M. Cossi, G. Scalmani, N. Rega, G. A. Petersson, H. Nakatsuji, M. Hada, M. Ehara, K. Toyota, R. Fukuda, J. Hasegawa, M. Ishida, T. Nakajima, Y. Honda, O. Kitao, H. Nakai, M. Klene, X. Li, J. E. Knox, H. P. Hratchian, J. B. Cross, C. Adamo, J. Jaramillo, R. Gomperts, R. E. Stratmann, O. Yazyev, A. J. Austin, R. Cammi, C. Pomelli, J. W. Ochterski, P. Y. Ayala, K. Morokuma, G. A. Voth, P. Salvador, J. J. Dannenberg, V. G. Zakrzewski, S.

Dapprich, A. D. Daniels, M. C. Strain, O. Farkas, D. K. Malick, A. D. Rabuck, K. Raghavachari, J. B. Foresman, J. V. Ortiz, Q. Cui, A. G. Baboul, S. Clifford, J. Cioslowski, B. B. Stefanov, G. Liu, A. Liashenko, P. Piskorz, I. Komaromi, R. L. Martin, D. J. Fox, T. Keith, M. A. Al-Laham, C. Y. Peng, A. Nanayakkara, M. Challacombe, P. M. W. Gill, B. Johnson, W. Chen, M. W. Wong, C. Gonzalez and J. A. Pople, *Gaussian 03, Revision C.02*, Gaussian, Inc., Wallingford, CT, **2004**.

Chapter 5

A bi-nuclear Cu(II)-complex for selective epoxidation of alkenes: crystal structure, thermal, photoluminescence and cyclic voltammetry

5.1 Introduction

In the family of multinuclear metal complex, the di-, tri- and polynuclear Cu(II) complexes have drawn special attention for few decades due to their structural diversity, distorted coordination geometry, simple electronic configuration as well as their application in the field of magnetism, catalysis, biochemistry, medicine and sensing [1-17]. Plethora of examples of multinuclear metal complexes is available in the literature [1-25]. It is noteworthy that judicious selection of the metal ions, bridging and also terminal ligands is indispensable for rational design of multinuclear metal complexes with specific physicochemical properties [26-28]. Bridging ligands with potentially active oxygen or nitrogen donor atom such as phenoxo [1-4, 10], azido [5], oxo/alkoxo [6, 7, 21, 22], sulfato [11], dicyanamide [12], hydroxo [1, 10, 16, 20], oxalato [14, 23-25, 29-38], carboxylate [4, 39-44] etc., have been widely used to synthesize multinuclear homo- and hetero-metallic Cu(II) complexes. Again, oxalato dianion is a very attractive bridging ligand for synthesizing a diverse type of homo- and hetero- metallic Cu(II) complexes with interesting physical and chemical properties (magnetic, optical and catalytic) [23-25, 36-38]. In this context, we have used the oxalate ligand in combination with 1,10-phenanthroline to synthesize a Cu(II) complex to explore the possible catalytic activity.

Synthesis of inorganic-organic hybrid catalysts for the selective production of organic compounds is of paramount importance in the field of synthetic and industrial chemistry [45]. In literature, numerous transition metal based complexes are reported with their several important catalytic activities based on several organic transformations and product selectivity. In this context, Cu(II) complexes have emerged as potential candidates for synthesis of organic molecules because of their very good catalytic activity in catechol oxidation, sulfoxidation, alkene oxidation, epoxidation, condensation, atom transfer radical addition, olefin aziridination etc. under both

homogeneous and heterogeneous conditions [45-48]. The catalytic efficiency and product selectivity of these complexes can also be tuned effectively by varying the ligand environment around the metal center and reaction conditions [49-52].

Various oxygen containing value-added products like alcohols, aldehydes, ketones, and epoxides can be developed through oxidation of olefins, which is an extremely important and useful reaction in both chemical and pharmaceutical industries [45,53-55]. Epoxide is considered as the most important product of olefin oxidation reaction because of their widespread applications in the production of epoxy resins, paints, perfumes, surfactants, pharmaceuticals and polymers. Further, epoxides act as a mediator in many organic syntheses and epoxidation of olefins is the key step in several organic synthesis and biological processes [56-65]. The traditional procedure for epoxidation of olefins using conventional oxidizing agents like H_2O_2, peracids, atmospheric O_2 suffers from very low conversion percentage and also lead to the formation of undesirable side products, which are sometimes very difficult to separate. Thus, finding the catalytic materials capable of producing epoxide by the oxidation of olefins with high selectivity is of immense importance from synthetic as well as industrial viewpoints. In this context, transition metal-based coordination complexes have emerged as a viable alternative to environmentally hazardous reagents abundantly used in both homogeneous and heterogeneous catalysis.

Under this background, herein we report the synthesis, characterization and selective catalytic activity of a binuclear Cu(II) complex $[Cu_2(oxalate)(1,10\text{-phen})_2Cl_2]$ synthesized by using hydrophilic oxalate ligand to bridge the metal centers and the hydrophobic 1,10-phen as the blocking ligand to prevent the formation of infinite architecture. This Cu-based binuclear complex shows selective catalytic behavior with very good yield for the oxidation of alkenes to their

corresponding epoxides e.g., 100% selectivity with 70% conversion for epoxidation of *cis*-cyclooctene.

5.2 Experimental

5.2.1. Materials and methods

The copper (II) chloride dihydrate (99 %), oxalic acid (99.9 %) and 1,10-phenanthroline (99.9 %) were bought from Sigma Aldrich and used as received without any further purification. Sodium carbonate (99 %) and all other chemicals (AR grade) were got from Merck India and used as received. A Perkin- Elmer 240C elemental analyzer was employed to carry out Elemental analysis (C, H, N). The thermal analysis was performed using a Mettler Toledo TGA-DTA 85 thermal analyzer under a flow of N_2 (30 ml min^{-1}). The sample was heated at a rate of 10 °C min^{-1} using inert alumina as a reference. IR study was done on the Nicolet Impact 410 spectrometer between 400 and 4000 cm^{-1}, using the KBr pellet method. A Perkin Elmer Lambda 365 UV-vis spectrophotometer was used to record the UV-vis absorption spectrum of the sample. Photoluminescence spectrum of the sample was recorded by the Shimadzu RF-5301PC spectrophotometer. The cyclic voltametric measurement on the sample was carried out using Epsilon Basi-C3 Cell instrument at a scan rate of 100 mV s^{-1} within potential range of 0-1.80 V with 1.0×10^{-3} M of complexes in acetonitrile solution deoxygenated by bubbling argon gas. Further, 0.1 M tetrabutylammonium perchlorate (TBAP) was taken as a supporting electrolyte. The working electrode was a glassy-carbon disk (0.32 cm^2) which was washed with absolute acetone and dichloromethane, polished with alumina solution and positively dried in air before individual electrochemical run. The Ag/AgCl was used as the reference electrode and Pt was used in the counter electrode. All experiments were done at standard electrochemical cells at 25 °C. The EIS-MS was recorded with the help of Qtof Micro YA263 mass spectrometer. The powder X-ray

diffraction (PXRD) pattern was collected at room temperature (22 °C) on Bruker D8 Advance Diffractometer using CuKα radiation having wavelength 1.5418 Å. The generator voltage and current were set at 40 kV and 40 mA, respectively. The PXRD data was collected within the 2θ range of 5˚- 60˚ with a scan speed of 1 s/ step and step size of 0.02°.

5.2.2 Synthesis of the Complex

At first, 0.5 mmol oxalic acid (0.04501 g) was dissolved in 10 ml distilled water and neutralized by aqueous solution of sodium carbonate to adjust the pH at 8.0 and 1.0 mmol of 1,10-phenanthroline (0.1802 g) was dissolved in 10 ml methanol separately. These two solutions were mixed together and stirred for 15 min at room temperature. Then the $CuCl_2 \cdot 2H_2O$ (0.1704 g, 1.0 mmol) was dissolved in 5 ml distilled water and added to the previous solution. The resultant mixture was stirred at room temperature for 30 min. The whole mixture was then refluxed for 1 hour at 80°C. It was then allowed to cool down to room temperature and kept in undisturbed condition for 2 hours. A very small amount of precipitate formation was observed. Afterwards, the precipitate was filtered off and green colored filtrate was kept in undisturbed condition. After a few (2-3) days, the block shaped green colored crystals suitable for single crystal x-ray structural study were obtained and these were separated and dried. Yield 79%. Anal. Calc. for $C_{26}H_{16}Cl_2Cu_2N_4O_4$: C, 48.2; H, 2.5; N, 8.6. Found: C, 48.5; H, 2.4; and N, 8.5%. Selected IR bands (KBr pellet, cm^{-1}): *ν* (O-H) stretching 3445 (m); *ν* (CO) 1506 (m), 1524 (s), 1483 (s), 1445 (w).

5.2.3 Crystallographic data collection and refinement

Suitable single crystal of the complex was mounted on a Bruker SMART diffractometer equipped with a graphite monochromator and Mo-Kα (λ = 0.71073 Å) radiation. The structure was solved by Patterson method using SHELXS-97 program. Subsequent difference Fourier synthesis and

least square refinement revealed the positions of the non-hydrogen atoms. Non-hydrogen atoms were refined using independent anisotropic displacement parameters.

Table 1: Crystallographic data and refinement parameters of the complex

Formula	$C_{26}H_{16}Cl_2Cu_2N_4O_4$
Formula weight	646.43
Crystal System	Monoclinic
Space group	P21/n (No. 14)
a (Å)	8.631(5)
b (Å)	11.927(7)
c (Å)	11.779(7)
β (º)	100.223(9)
V (Å^3)	1193.3(12)
Z	2
D(calc) (g/cm^3)	1.799
μ(Mo Kα)(mm)	2.050
F(000)	648
Crystal Size (mm)	0.12 × 0.12 × 0.48
T (K)	100
λ [Å]	Mo Kα 0.71073
Theta Min-Max [°]	2.4- 25.3
Dataset	-10: 10 ; -14: 14 ; -14: 14
Total, Unique data	10723, 2140
R_{int}	0.093
Observed data	1392
Nref, Npar	2140, 172
R	0.0517
wR2	0.1092
S	0.94
Max. and Av. Shift/Error	0.00, 0.00
Min. and Max. Resd. Dens.	-0.52, 0.53

w = 1/[s2(Fo2) + (0.0949P)2] where P = (Fo2 + 2Fc2)/3

Hydrogen atoms were placed in idealized positions and their displacement parameters were fixed to be 1.2 times larger than those of the attached non-hydrogen atoms. Successful convergence was indicated by the maximum shift/error of 0.001 for the last cycle of the least squares refinement.

Analysis of single crystal X-ray data were carried out using SHELXS-97 [66], SHELXL-97 [67], PLATON-99 [68], ORTEP-32 [69] and WinGX system Ver-1.64 [70]. Data collection, structural refinement parameters and crystallographic data of the complex are provided in Table 1. Some selected bond lengths, bond angles and weak interaction parameters are summarized in Table 2.

Table 2: Some selected bond lengths (Å) and bond angles (º) of the complex.

Cu1-Cl1	2.287(2)	Cu1-O1	2.215(4)
Cu1-O2	1.999(4)	Cu1-N1	2.019(5)
Cu1-N2	2.050(5)	Cl1-Cu1-O1	110.69(10)
Cl1-Cu1-O2	94.40(11)	Cl1-Cu1-N1	96.36(14)
Cl1-Cu1-N2	142.72(14)	O1-Cu1-O2	80.75(14)
O1-Cu1-N1	90.42(16)	O1-Cu1-N2	106.56(16)
O2-Cu1-N1	167.98(17)	O2-Cu1-N2	92.78(17)
N1-Cu1-N2	81.87(19)		

5.2.4 Computational Methodology

All theoretical calculations were performed with the Gaussian 09W software package [71] employing the analytical gradient methods of DFT with Becke's three parameters (B3) exchange functional [72] and the Lee-Yang-Parr (LYP) nonlocal correlation functional (symbolized as B3LYP) [73]. For C, H, N, O and Cl atoms the 6-311++G (d,p) basis set was used while for the Cu atom LanL2DZ basis set was adopted. The ground state (S_0) geometries were fully optimized using the default criteria of the respective program in both the gaseous phase and solution phase with acetonitrile as solvent. Frequencies were calculated on the optimized geometries and the character of the stationary point was evaluated by doing a normal mode analysis, where all the vibrational frequencies have been found to be positive, which confirms that the optimized structure

is at one of the minima of the potential energy surface. Orbital analysis has been performed using GaussView and the MO composition analysis was carried out with Gausssum program [74].

5.2.5 Catalytic reaction methodology

The catalytic reactions were done in a glass batch reactor as per the following procedure. 5 mmol of substrate, 2 mg catalysts (i.e., 0.062% of mole of the substrate) and 5 ml solvent and were first mixed. The mixture was then equilibrated to the desired temperature in an oil bath. After addition of 30% hydrogen peroxide (10 mmol), the reaction mixture was stirred continuously. The reactions were performed in open air. Varian 3400 gas chromatograph equiped with a 30 m CP-SIL8CB capillary column and a flame ionization detector were employed to quantify the reaction products were (GC data) and identified by Trace DSQ II GCMS equipped with a 60 m TR-50MS capillary column. The oxidation products have been identified by comparing their retention times with those of available pure samples.

5.3 Results and Discussion

5.3.1. Molecular and supramolecular structure of the complex

Single crystal X-ray diffraction (SCXRD) analysis revealed that the complex crystallizes in achiral $P2_1/n$ space group. The asymmetric unit contains one Cu^{2+} ion, one coordinated Cl^- ion, one phenanthroline ligand and half of oxalate moiety. The ORTEP diagram is presented in Figure 1. The metal center exhibits five coordinated distorted square pyramidal geometry with τ value of 0.42 [75]. Two nitrogen atoms (N1 and N2) of phenanthroline ligand, one oxygen atom (O2) of the oxalate ligand and the chloride ion (Cl1) constitute the basal plane while the other oxygen atom (O1) of the oxalate occupies the axial positions. Here, the oxalate ligand acts as a bridge between two metal centers, on the other hand, the hydrophobic 1,10-phen acting as blocking ligand prevents the formation of an infinite chain and in consequence the binuclear-complex formation takes place.

The oxalate acts as both bridging ligand as well as chelating ligand. Using two oxygen atoms of two different carboxylato groups, oxalate binds one metal center in *syn-syn* fashion as a chelating ligand and using two oxygen atoms of the same carboxylato groups, it bridges between two metal centers in *anti-anti* binding mode. Wang et al., have reported a similar structure with $P2_1/c$ space group and distorted trigonal bipyramidal geometry while our complex crystallizes in $P2_1/n$ space group and its Cu(II) centers show square pyramidal coordination geometry [76]. Further, the structural parameters and packing behavior of the present complex is different from those reported earlier. The molecular structure of this compound is similar to $[(bpy)_2Cu_2(C_2O_4)Cl_2]\cdot H_2O$ where the complex has a guest water molecule while the complex under investigation is devoid of any water molecule [77]. It has been reported that in $[(bpy)_2Cu_2(C_2O_4)Cl_2]\cdot H_2O$, Cu atom exhibits square pyramidal coordination where two nitrogen atoms of one 2,2´-bypyridyl and two syn oxygen atoms of oxalate moiety constitute the basal plane while chloride ion occupies the apical position. Here, the oxalate ion acts as bridging ligand and 2,2´-bypyridyl serves as blocking ligand. Although for both complexes, Cu atom exhibits square pyramidal coordination, there are distinct differences in constitution of the basal plane, apical position and bridging mode.

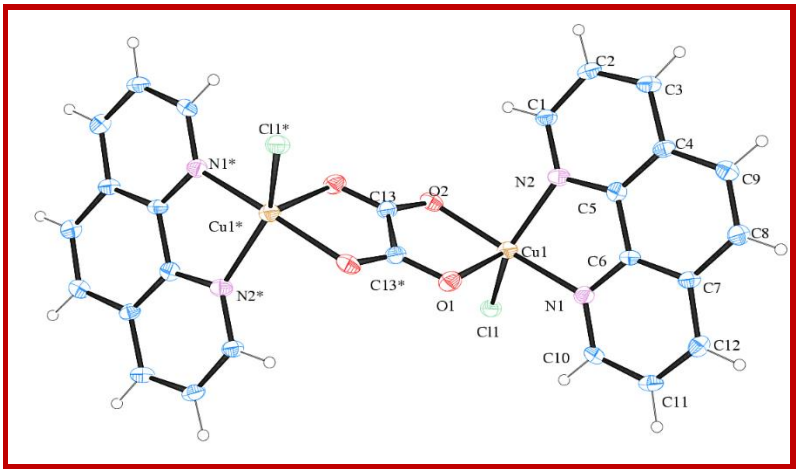

Figure 1. ORTEP diagram of the complex

The Cu-N bond distances are in the range of 2.019 - 2.050 Å, Cu-O bond distances are in the range of 1.999 - 2.215 Å and Cu-Cl bond distance is ~ 2.287 Å. All other coordinated bond distances and bond angles are provided in Table 2. The supramolecular C-H···Cl (C1-H1···Cl1) and C-H···O (C8-H8···O1) hydrogen bonding interactions connect each molecular unit to form 3D supramolecular structures (Figure 2 and Figure 3). π···π interactions among the aromatic rings of phenanthroline moieties also facilitate the 3D supramolecular structure formation, as shown in Figure 2 and Figure 3. All the hydrogen bonding and π···π interactions are summarized in Table 2 and 3, respectively.

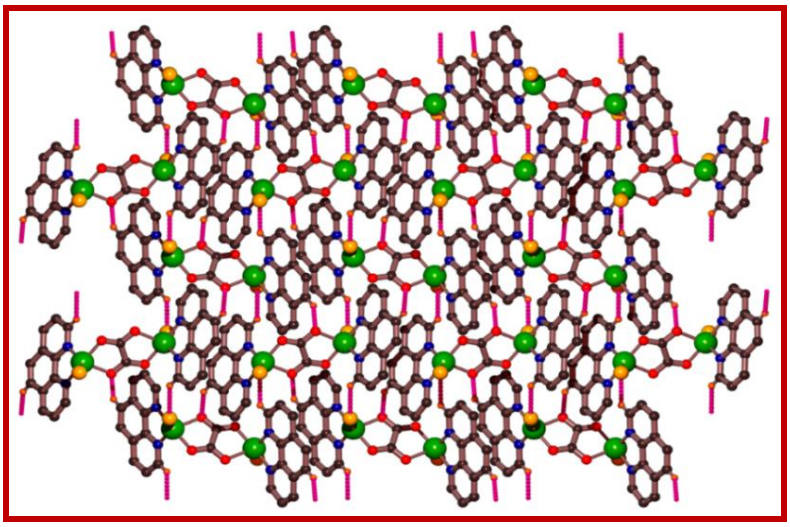

Figure 2. 3D supramolecular structure of the complex formed by C-H···Cl and C-H···O hydrogen bonding interactions.

Table 2: Hydrogen bond dimensions of the complex.

D-H···A	D-H	H···A (Å)	D···A (Å)	<D-H···A (º)	Symmetry
C5-H5···O2	0.95	2.60	3.460(7)	151	-1/2+x,1/2-y,1/2+z
C10-H10···Cl2	0.95	2.81	3.629(6)	145	1/2-x,1/2+y,3/2-z

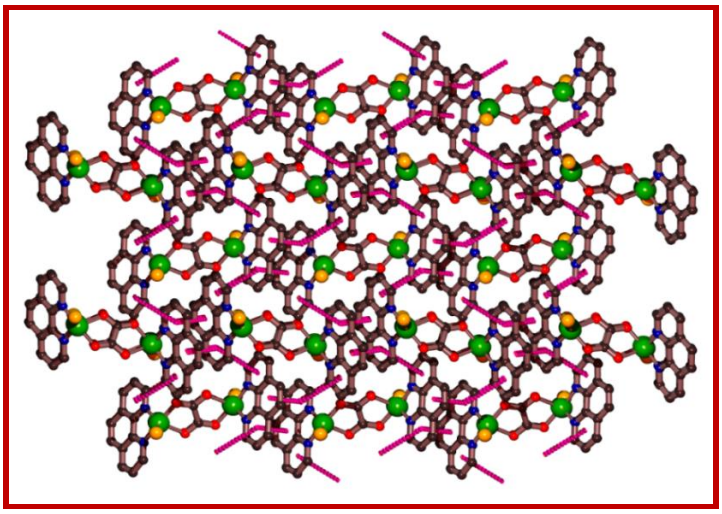

Figure 3. 3D supramolecular structure is formed by π···π interactions among the phenanthroline rings.

Table 3: π··· interactions of the complex

Cgi···Cgj	Cgi···Cgj distance/(Å)	Dihedral angle between Planes I and J [α (°)]	Symmetry
Cg2···Cg5	3.712(4)	3.3(2)	-x,1-y,2-z
Cg2···Cg6	3.853(4)	2.5(2)	-x,1-y,2-z
Cg4···Cg5	3.973(4)	17.0(3)	-1/2-x,-1/2+y,3/2-z
Cg4···Cg5	3.819(4)	4.5(3)	-x,1-y,2-z
Cg5···Cg2	3.712(4)	3.3(2)	-x,1-y,2-z
Cg5···Cg4	3.973(4)	17.0(3)	-1/2-x,1/2+y,3/2-z
Cg5···Cg4	3.819(4)	4.5(3)	-x,1-y,2-z
Cg4···Cg5	3.973(4)	17.0(3)	-1/2-x,-1/2+y,3/2-z
Cg4···Cg5	3.819(4)	4.5(3)	-x,1-y,2-z
Cg1···Cg5	4.267(4)	71.3(2)	x,y,z
Cg2···Cg2	4.539(4)	0	-x,1-y,2-z
Cg3···Cg5	4.267(4)	71.3(2)	-x,1-y,1-z
Cg5···Cg5	4.208(4)	0	-x,1-y,2-z
Cg5···Cg6	3.552(4)	0.8(3)	-x,1-y,2-z
Cg6···Cg2	3.853(4)	2.5(2)	-x,1-y,2-z
Cg6···Cg5	3.552(4)	0.8(3)	-x,1-y,2-z
Cg6···Cg6	4.405(4)	0	-x,1-y,2-z

5.3.2 PXRD and Thermal investigation

The phase purity of the bulk sample was examined by PXRD study. The PXRD pattern of the complex matches well with the X-ray diffraction pattern simulated from the SC-XRD data (Figure 4).

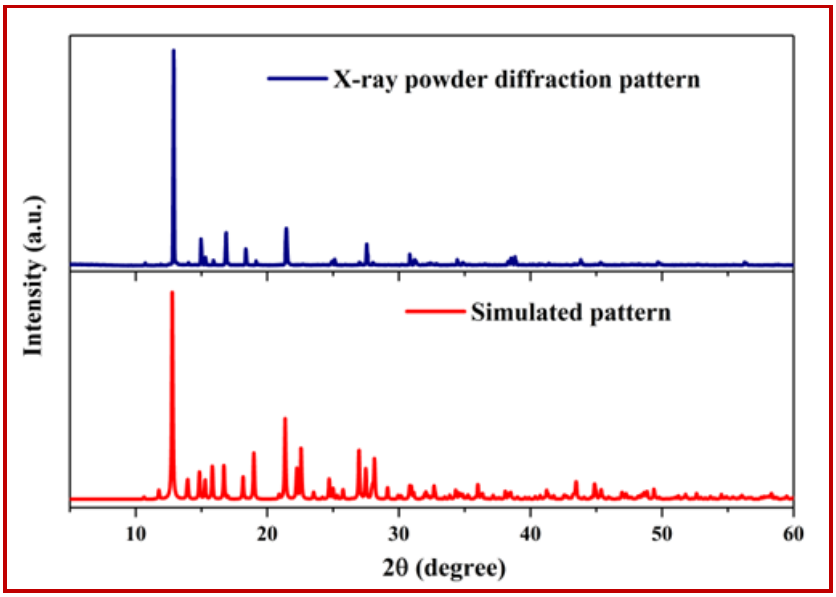

Figure 4. Powder X-ray diffraction pattern of the complex along with and simulated pattern obtained from SCXRD data

Thermogravimetric analysis (TGA) for coordination and supramolecular polymers are very important to analyze their thermal stability. The TGA curve of the sample (Figure 5) reveals that it is stable up to 230°C. A very few amounts of weight loss (<1%) below 100°C can be attributed to the loss of absorbed moisture. The complex gradually decomposes in stepwise fashion within the temperature range of 230 and 900 °C due to the successive loss of coordinated moieties such as Cl^- ions, bridging oxalate ligand and phenanthroline (theo: 78%, exp: 91%). The final black residue after decomposition of the complex is probably the anhydrous copper oxide.

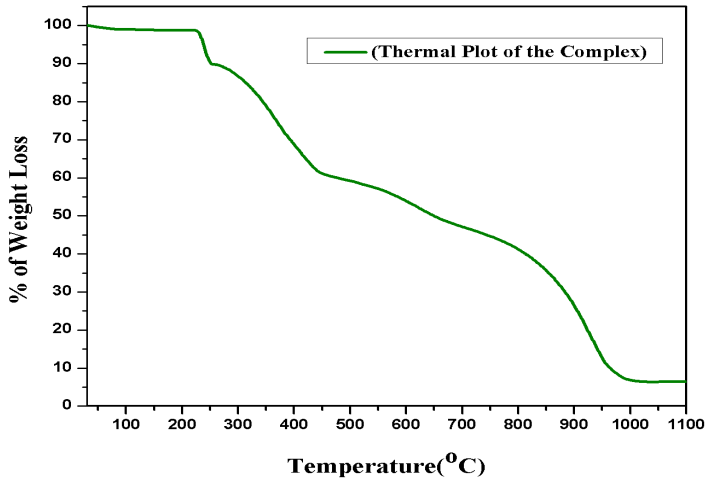

Figure 5. Thermal plot of the complex

5.3.3 Cyclic voltametric investigation

The cyclic voltammogram of the complex in acetonitrile is reversible in nature with $E_{1/2}$ ~ 27 mV and ΔE_p = 206 mV. The $E_{1/2}$ ~ 27 mV corresponds to one electron transfer process in the $Cu^{II/I}$ redox couple. It is already reported that strongly electronically coupled systems can display surprisingly high ΔE_p value in cyclic voltametric study [78]. Hence, the large ΔE_p value implies that, in the present complex, two redox active copper centers are strongly electronically coupled to each other by the bridging oxalate dianion ligand**.** The reversibility of the redox process suggests that the basic geometry around the copper center remains intact during the redox event (Figure 6).

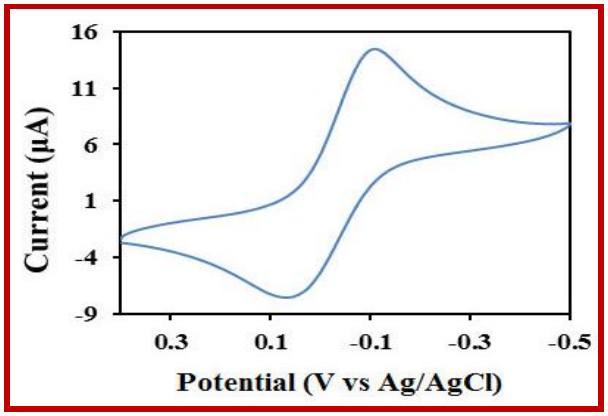

Figure 6. CV plot of the complex

5.3.4 Spectral studies

The electronic spectra of the complex were recorded at 300 K in acetonitrile medium. The UV-Vis spectra (Figure 7) exhibit a peak at 270 nm (molar extinction coefficient (ε):39800$M^{-1}cm^{-1}$) that can be attributed to the π-π* transition within the 1,10-phenanthroline ligands. The absorption peak at 344 nm (ε: 7950 $M^{-1}cm^{-1}$) is due to the charge transfer from 1,10-phenanthroline ligand to Cu(II) metal ion. The absorption spectra also shows a broad band around 720 nm (ε: 3060 $M^{-1}cm^{-1}$) which can be assigned to the *d-d* transition.

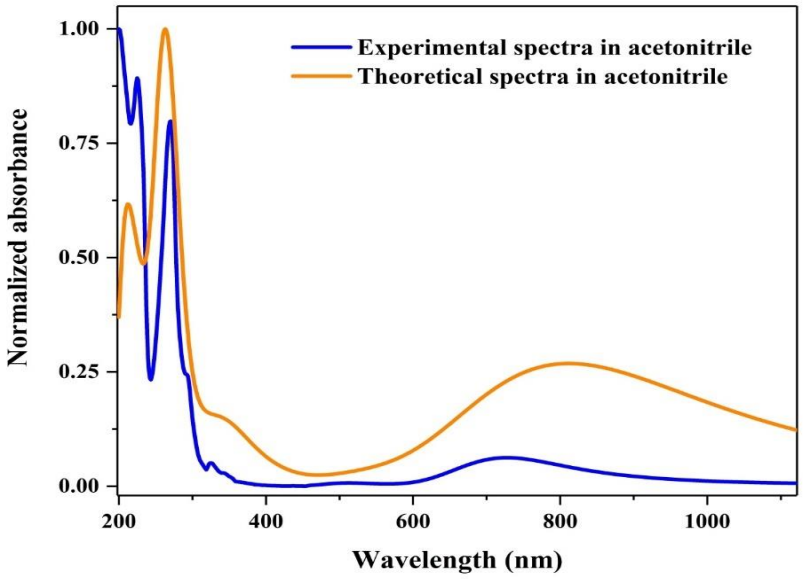

Figure 7. UV-Vis spectra of the complex in acetonitrile medium

The emission spectra of the complex have been studied in solid state at 300 K. The complex shows emission maxima at 451 and 480 nm upon excitation at 340 nm (Figure 8) and this can be attributed to the π-π* transition in the aromatic π-rings of 1,10-phenanthroline ligands. The small peak around 522 nm is possibly caused by extended π-conjugation within the ligand system. The luminescent behavior of the complex corresponds to a ligand-centered (LC) fluorescence.

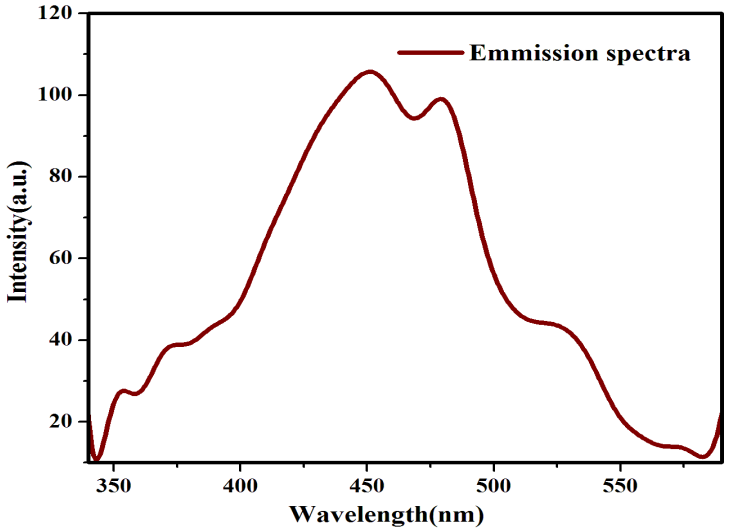

Figure 8. Photoluminescence spectra of the complex in solid state.

The emission spectra of the complex have been studied in acetonitrile medium. Upon exciting at 344 nm, the emission spectra show maxima at 405 nm and 430 nm (Figure 9) due to the π-π* transition in the aromatic π-rings of 1,10-phenanthroline ligands. Hence, in the solution phase a blue shift of the peaks is observed but the emission spectra of the complex are almost similar in nature in both solid state and solution phase. Thus, it may be inferred that the basic structure of the complex remains unchanged in solvent phase.

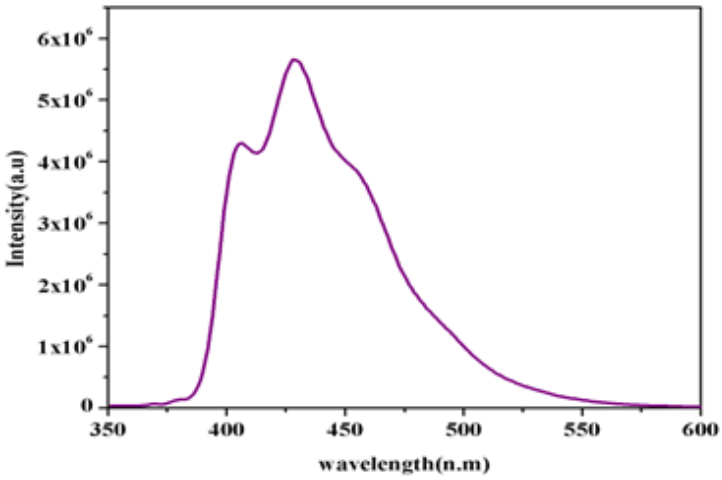

Figure 9. Photoluminescence spectrum of the complex in acetonitrile medium

5.3.5 Study of ground state structure and molecular orbitals

We have optimized the molecular structures of the complex at electronic ground state (S_0) in both gaseous state and in acetonitrile solvent. The geometry optimized structures of the complex computed both in the gaseous and in solution phases are presented in Figure 10.

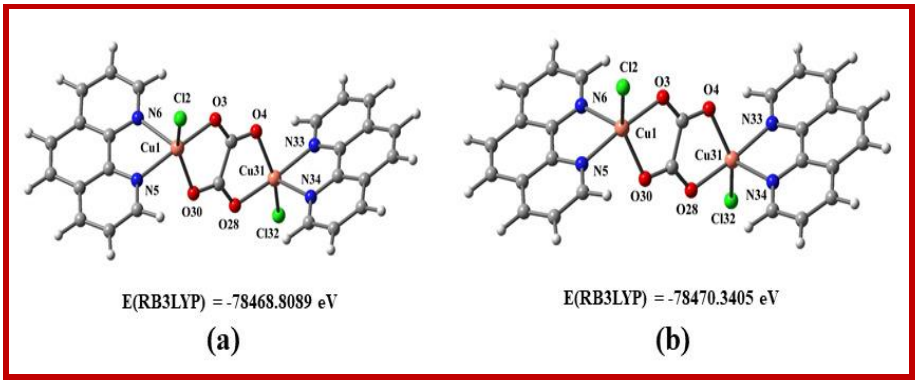

Figure 10. Ground state optimized geometries and coordination environment of the complex in (a) gaseous phase and (b) solution state with acetonitrile as solvent.

Some selected optimized geometrical parameters (bond lengths and bond angles) of the complex are summarized in Tables 4 and 5. In the optimized structures, both the Cu(II) centers of the complex show five coordinated distorted square pyramidal geometry. In the optimized structures, two oxygen atoms of two different carboxylate groups of oxalate ligand along with one Cl atom and one of the two N atoms of phenanthroline ligand constitute the basal plane whereas the remaining N atom of phenanthroline ligand occupies the axial position. On the other hand, in the crystalline molecular structure of the complex two N atoms of phenanthroline ligand, one oxygen atom of the oxalate ligand together with one Cl atom form the basal plane and another oxygen atom of a different carboxylate group of the oxalate ligand is in the apical position. Although the calculated structure and the crystal structure are geometrically same in nature (square pyramidal), the dissimilarity in position of atoms within the metallic coordination environment

and different degree of distortion among them leads to apparent mismatch between the bond angles and bond lengths of these molecular structures.

Table 4: Some selected calculated bond distances of the complex.

Bond distances (Å)					
Bond	**Gas phase**	**In acetonitrile**	**Bond**	**Gas phase**	**In acetonitrile**
Cu1-Cl2	2.2975	2.3668	Cu31-O28	2.0277	2.0189
Cu1-N5	2.0632	2.0241	Cu31-O4	2.0824	2.1198
Cu1-N6	2.2993	2.2441	Cu31-Cl32	2.2887	2.3667
Cu1-O30	2.0894	2.1199	Cu31-N33	2.0595	2.0242
Cu1-O3	2.0320	2.0190	Cu31-N34	2.3209	2.2443

Table 5: Selected calculated bond angles for the complex

Bond angles (°)					
Bond angle	**Gas phase**	**In acetonitrile**	**Bond angle**	**Gas phase**	**In acetonitrile**
Cl2-Cu1-O30	146.9696	145.2403	Cl32-Cu31-O4	152.9230	145.3056
Cl2-Cu1-N6	109.5029	111.7906	O4-Cu31-N34	94.1315	102.9483
N6-Cu1-O30	103.3660	102.9679	N33-Cu31-Cl32	93.2414	94.9743
N5-Cu1-Cl2	93.4563	94.9940	O28-Cu31-Cl32	96.8047	92.9660
O3-Cu1-Cl2	97.3419	92.9607	N33-Cu31-O4	89.7659	91.6670
N5-Cu1-N6	77.0682	79.1260	O28-Cu31-O4	81.6359	81.0416
O3-Cu1-N6	97.2088	99.0903	N33-Cu31-N34	76.8491	79.1233
N5-Cu1-O30	90.6772	91.6631	N34-Cu31-O28	98.4334	99.1072
O3-Cu1-O30	81.4302	80.0391	N34-Cu31-Cl32	112.7623	111.7449

Some selected frontier orbitals of the complex optimized in both the gaseous and solution phases are shown in Figure 11. The HOMO–LUMO energy differences are 1.03 eV and 1.02 eV for the structures optimized in gaseous phase and in solution phase, respectively. For MO

composition analysis the contributions from five fragments viz., Cu, phen1, phen2, Cl and oxalato have been considered. The energies of the orbital and each fragment contribution from in terms of atomic orbital contribution to the frontier molecular orbital (MO) are listed in Table 3. For the HOMOs and LUMOs of the complex in both gaseous and solution phase, the degree of contribution coming from the p-orbitals of the C atoms in phenanthroline moieties, *d*-orbital of Cu atom, Cl and oxalato is significantly different.

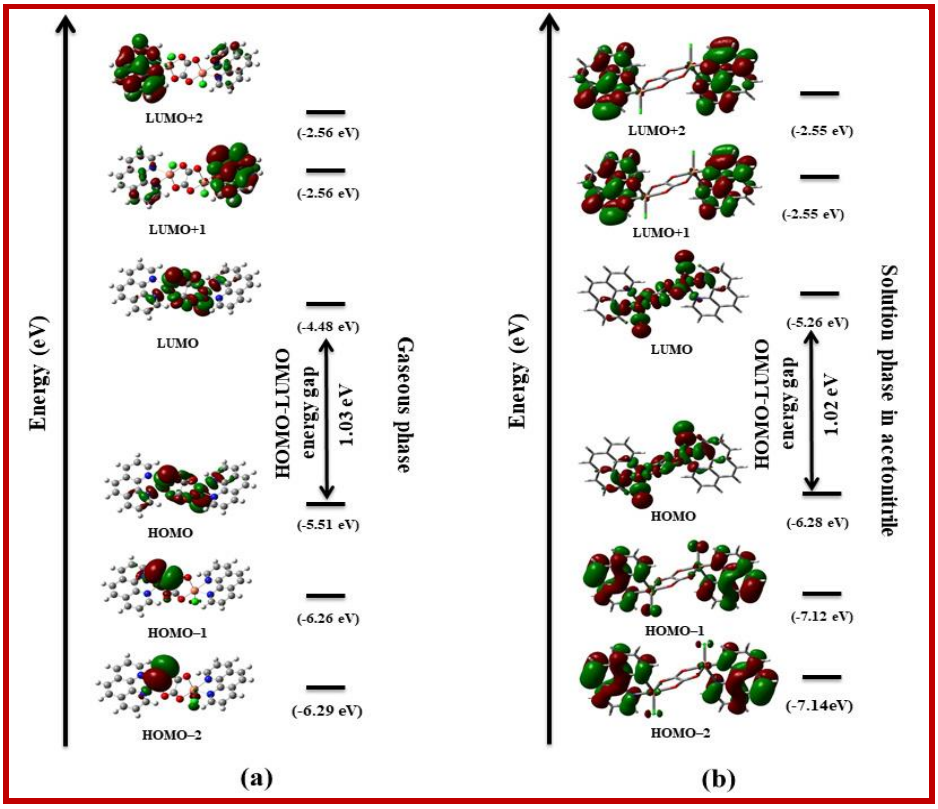

Figure 11. Schematic diagram showing the selective frontier molecular orbitals for the complex in (a) gas phase and (b) solution state with acetonitrile as solvent.

5.3.6 Catalytic activity

The complex contains five coordinated - coordinatively unsaturated Cu-centers and thus the complex was been used for the Lewis acidic catalysis reaction under homogeneous conditions. Catalytic activity of the complex was assessed by studying the oxidation reaction of alkenes. In

this study, *cis*-cyclooctene was selected as the model substrate to optimize the catalytic oxidation reaction conditions using H_2O_2 as oxidant. The catalytic oxidation of *cis*-cyclooctene produces the corresponding epoxide as the sole product in acetonitrile solvent with H_2O_2 at 50 °C (Scheme 1). The same experiment was performed without using H_2O_2 as oxidant keeping all the reaction parameters unchanged. The outcomes of the control experiments indicate that the presence of both the catalyst and oxidant are essential for the oxidation reaction. The oxidation of *cis*-cyclooctene in the absence of H_2O_2 does not occur and also in absence of the catalyst, trace amount of desired product was formed. Again, the same experiment was done in presence of $CuCl_2$ using H_2O_2 as oxidant in both methanol and acetonitrile medium. These experiments result very low conversion rate of *cis*-cyclooctene to the product suggesting very mild catalytic activity of $CuCl_2$ in the epoxidation reaction. Effects of solvent, oxidant, the ratio of oxidant/substrate and the temperature were also studied to find the most suitable reaction conditions to achieve the maximum conversion of *cis*-cyclooctene.

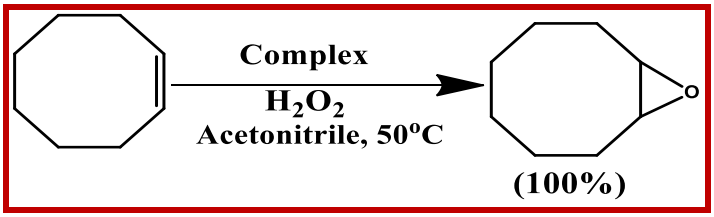

Scheme 1: Catalytic oxidation of *cis*-cyclooctene

In order to study the solvent effect, catalytic oxidation reactions were carried out in methanol, ethanol, acetonitrile, chloroform and dichloromethane solvent and it was found that the highest conversion, 70% after 3 h, was obtained in acetonitrile at 50 °C. The catalytic activity of the complex decreased in the order: acetonitrile > methanol > ethanol > chloroform ~ dichloromethane (Figure 12). In summary, the reactivity of the catalyst in other solvents was much lower than in acetonitrile. The efficiency of various oxidants, namely *tert*-BuOOH, H_2O_2, NaOCl

and O_2 (1 atm) was studied in the same homogeneous catalytic oxidation reaction of *cis*-cyclooctene keeping all other conditions unchanged. The experimental outcomes revealed that H_2O_2 is the most efficient oxidant with complex as catalyst (Table 6).

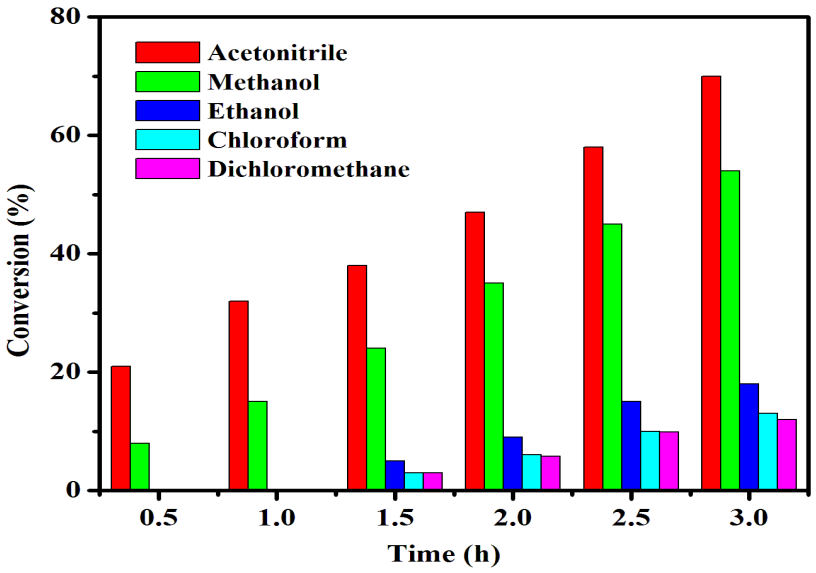

Figure 12. Influence of solvent in the catalytic epoxidation of *cis*-cyclooctene by the complex. Reaction condition - catalyst: 2 mg, *cis*-cyclooctene: 5 mmol, H_2O_2:10 mmol, temperature: 50 ºC, solvent: 5 ml.

The effect of temperature on the performance of the catalyst was also investigated. The same reaction has been carried out at three different temperatures *viz*., 40 ºC, 50 ºC and 60 ºC with the fixed amount of *cis*-cyclooctene (5 mmol), H_2O_2 (10 mmol) and the complex (2 mg) in 5 ml acetonitrile (Table 4, entries: 3, 6 and 7) keeping the reaction conditions same as earlier. A maximum of 70% conversion was achieved at 50 ºC while at 40 ºC, the conversion was low. On the other hand, at 60 ºC the initial conversion of *cis*-cyclooctene was higher than at 50 ºC but when the reaction continued the conversion of *cis*-cyclooctene became almost the same. Therefore, 50 ºC is marked as the optimum temperature and hence catalytic oxidation reactions of all other alkenes were performed at 50 ºC. The molar ratio of *cis*-cyclooctene to H_2O_2 was also varied (Table 4**,** entries: 3, 8 and 9) keeping all other experimental conditions the same to examine the effect of

the molar ratio of the parent compound on the conversion process. The conversion of *cis*-cyclooctene was increased from 38% to 70% on increasing the *cis*-cyclooctene: H_2O_2 ratio from 1:1 to 1:2. On further increasing this ratio to 1:3, the conversion was barely affected. Hence, it can be inferred that 1:2 ratio of *cis*-cyclooctene to H_2O_2 is sufficient for significant conversion of *cis*-cyclooctene. A blank experiment (Table 4, entry: 10) was also carried out in absence of the complex with H_2O_2 under the same experimental conditions which resulted in very low conversion of *cis*-cyclooctene that confirmed the high efficiency of the complex as a catalyst. All these optimized reaction conditions were applied to the complex-catalyzed oxidation reactions of other alkenes.

Table 6: Epoxidation of *cis*-cyclooctene using different oxidants with the complex as catalyst.

Entry	Oxidant	Temperature (°C)	Conversion (%)[b]
1	-	50	-
2	NaOCl	50	34
3	H_2O_2	50	70
4	*tert*-BuOOH	50	56
5	O_2 (1 atmosphere)	50	12
6	H_2O_2	50	45
7	H_2O_2	60	72
8[c]	H_2O_2	50	38
9[d]	H_2O_2	50	74
10[e]	H_2O_2	50	6

Reaction conditions: catalyst (2 mg), *cis*-cyclooctene (5 mmol), oxidant (10 mmol), acetonitrile (5 mL), time (3 h). [b] Determined by GC. [c]5mmol H_2O_2. [d]15mmol H_2O_2. [e]Without the complex.

It is noteworthy that the complex-catalyzed oxidation reaction of *cis*-cyclooctene with H_2O_2 yields the corresponding epoxide with 100% product selectivity in acetonitrile medium (Table 7). The product was identified by GC spectroscopic study (Figure 13). Under the same reaction condition, styrene gives styrene oxide with 89% product selectivity (67 % conversion) along with a trace amount of benzaldehyde. In case of cyclohexene, product selectivity to the corresponding epoxide is about 76% with conversion % of 82. A little amount of allylic oxidation products (2-cyclohexene-1-ol and 2-cyclohexene-1-one) were also formed as side products in this case. All these experimental results are summarized in Table 7.

Table 7: Oxidation[a] of various alkenes by the complex using H_2O_2 in acetonitrile

Entry	Substrate	Conversion (%)[b]	Product	Selectivity (%)[b]	TOF[c]
1	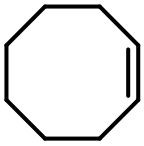	70	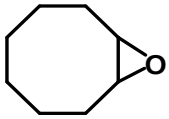	100	376.4
2	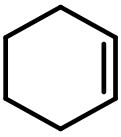	82	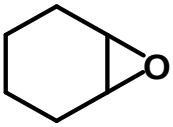	76	440.8
3	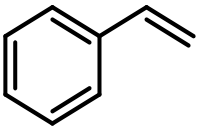	67	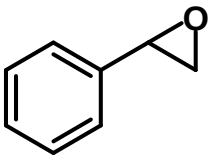	89	360.2

[a]Reaction conditions: catalyst (2 mg), alkenes (5 mmol), H_2O_2 (10 mmol), temperature 50ºC), acetonitrile (5 mL), time (3 h). [b]Determined by GC. [c]TOF: turnover frequency = (moles of substrate converted per mole of metal complex per hour.

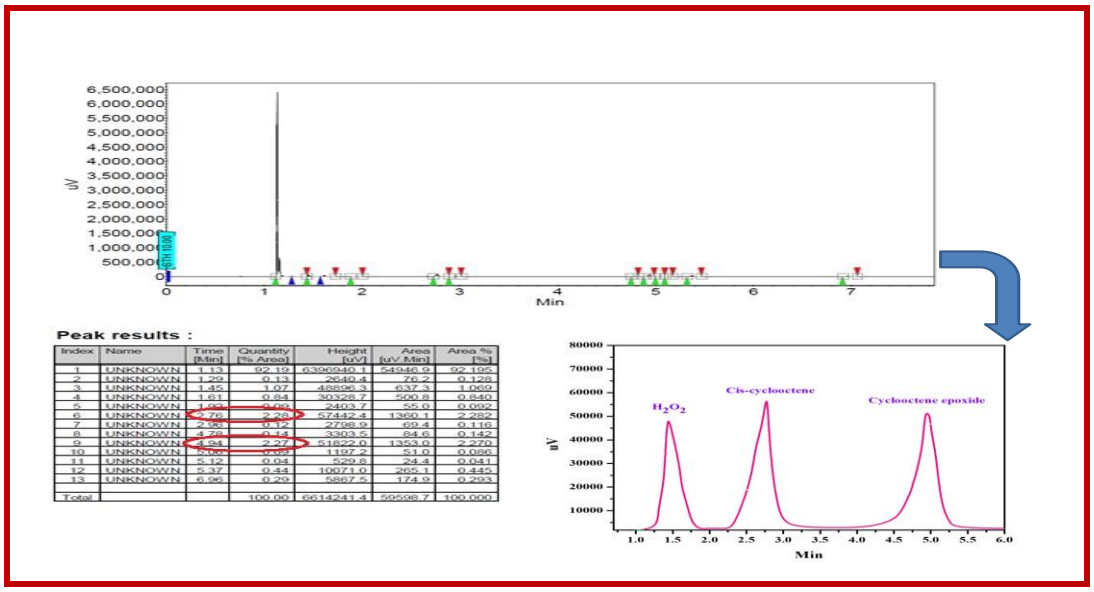

Figure 13. Gas chromatogram of *cis*-cyclooctene oxidation catalyzed by complex using H_2O_2 as oxidant.

Definite identification of the active species involved in homogeneous catalysis is very difficult. In literature, it has been reported that in the reaction of a copper complex with H_2O_2, Cu(II) binds the peroxo- group and forms a Cu–hydroperoxo or Cu–peroxo pre-catalyst species that can act as a mediator to enable the oxo functionality of the organic substrates to produce the corresponding oxidized products [79-80]. In order to identify the active species, we have recorded the UV-Vis spectra of the complex in presence of excess H_2O_2 in acetonitrile medium (Figure 14). The UV-Vis spectra show an intense peak at around 430 nm with a shoulder in the range of 445–470 nm. This may be due to the existence of Cu–hydroperoxo or Cu–peroxo species [81-82]. In order to get an idea about the number of copper atom(s) present in the complex in solution state, we have recorded the ESI mass spectrum of the complex in acetonitrile medium. The mass spectrum of the complex shows m/z peaks at 611.5356, and 575.9754 (Figure 15). These peaks are observed due to the fragments of the complex after expulsion of one and two Cl atom(s), respectively. The fragments consisting of three peaks for isotopic distribution of two Cu atoms has

been observed in the mass spectrum at lower m/z values. Hence, from the mass spectrum it can be inferred that two copper atoms bridged through oxalate ligands are present in the solution state and the complex exists as a binuclear species in acetonitrile medium. Further, from the photoluminescence study of the complex it has been found that the basic binuclear structure of the complex in solid state and solution phase is nearly identical. Thus, the result of mass spectroscopy study corroborates the outcome of the photoluminescence study. In case of homogeneous catalysis, recovery of the catalyst for reuse is a very difficult task as the catalyst does not remain in its original form after the reaction. We have recovered the residue obtained after completion of the catalytic cycle. However, the FTIR spectra and PXRD pattern of this recovered material does not match with those of the original complex.

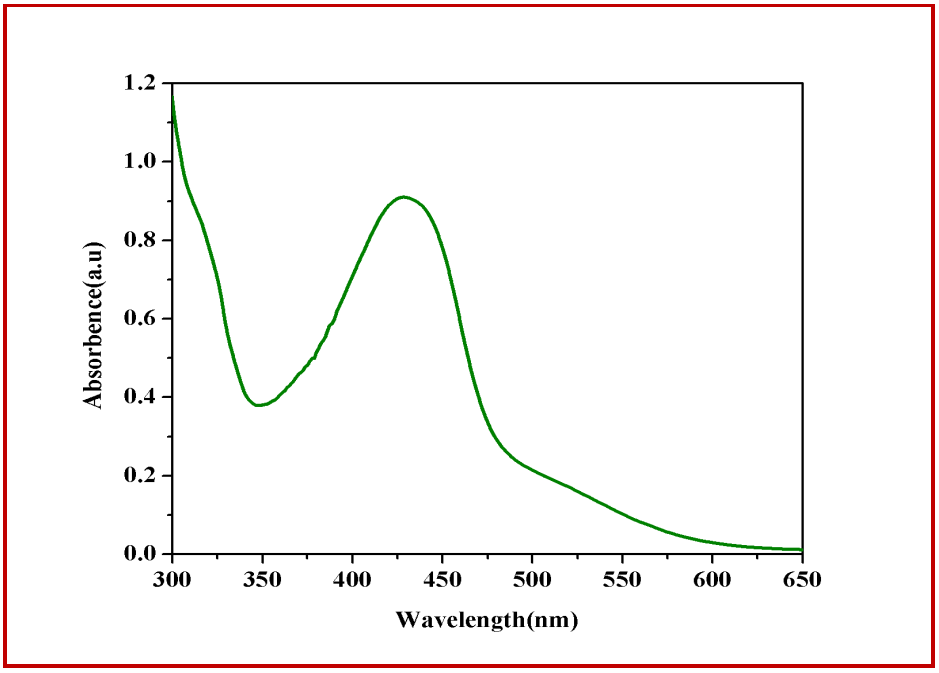

Figure 14. UV-vis spectrum of the complex in presence of H_2O_2 in acetonitrile at room temperature.

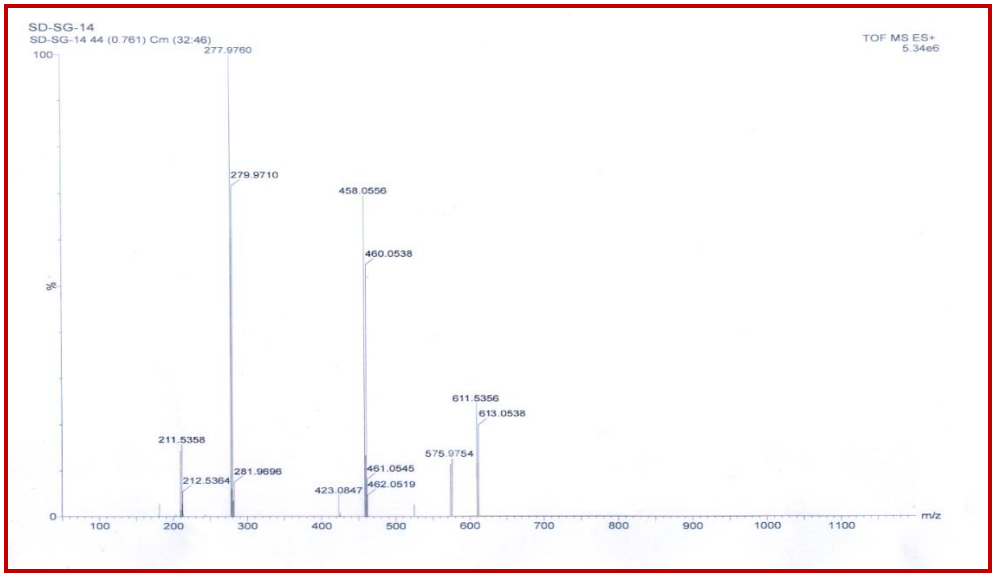

Figure 15. ESI-Mass spectrum of the complex in acetonitrile medium

5.4 Conclusion

In summary the binuclear Cu(II) complex, $[Cu_2(oxalate)(1,10\text{-phen})_2Cl_2]$ (where 1,10-phen = 1,10-phenanthroline), designed by using hydrophilic oxalate as bridging ligand and the hydrophobic 1,10-phen as the blocking ligand exhibits very good thermal stability and photoluminescence activity along with selective catalytic activity for epoxidation of alkenes in presence of H_2O_2. Structural analysis has revealed that binuclear metallic units of the complex are packed by supramolecular hydrogen bonding and π···π interactions and forms a 3D supramolecular architecture. The cyclic voltametric study suggests that both the copper centers are strongly coupled to each other through the oxalato-bridge**.** Owing to the presence of π-electrons in auxiliary ligands (1,10-phenenthroline), the complex shows strong fluorescence.

The presence of coordinately unsaturated Cu-centers inspired us to examine the catalytic activity of the complex toward oxidation of alkenes. By optimizing the oxidation reactions of alkenes using this binuclear Cu(II) complex, it has been established that in all cases the maximum catalytic efficiency can be achieved at 50 °C in presence of H_2O_2 as oxidant with acetonitrile

solvent. Interestingly, the complex shows 100% selectivity for the oxidation of *cis*-cyclooctene to the corresponding epoxide in presence of H_2O_2 as oxidant at 50 ºC with 70% conversion in acetonitrile. The complex also exhibits product selectivity and percentage conversion of 89 % and 67 %, respectively, for styrene and 76 % and 82 % for cyclohexene under the same reaction condition. Our future research goal is to design novel homogeneous and heterogeneous catalysts for industrial application.

References

[1] F. Gennarini, R. David, I. López, Y. Le Mest, M. Réglier, C. Belle, A.Thibon-Pourret, H. Jamet and N. Le Poul, *Inorg. Chem*., **2017**, 56, 7707.

[2] S. K. Barman, T. Mondal, D. Koley, F. Lloretc and R. Mukherjee, *Dalton Trans*., **2017**, 46, 4038.

[3] D. Venegas-Yazigi, D. Aravenab, E. Spodine, E. Ruizd and S. Alvarez, *Coord. Chem. Rev*., **2010**, 254, 2086.

[4] S. Sarkar, A. Mondal, D. Chopra, J. Ribas and K.K. Rajak, *Eur. J. Inorg. Chem*., **2006**, 3510.

[5] M. G. Sommer, Y. Rechkemmer, L. Suntrup, S. Hohloch, M. van der Meer, J. van Slageren and B. Sarkar, *Dalton Trans*. **2016**, 45, 17770.

[6] S. Sagar, S. Sengupta, A. J. Mota, S. K. Chattopadhyay, A. E. Ferao, E. Riviere, W. Lewisf and S. Naskar, *Dalton Trans*., **2017**, 46, 1249.

[7] R. Golbedaghi, S. Azimi, A. Molaei, M. Hatami and B. Notash, *J. Mol. Struct*., **2017**, 1146, 309.

[8] R. Vafazadeh, R. Esteghamat-Panah, A.C. Willis and A.F. Hill, *Polyhedron*, **2012**, 48, 51.

[9] A. Parween, S. Naskar, A. J. Mota, A. E. Ferao, S. K. Chattopadhyay, E. Rivière, W. Lewis and S. Naskar, *New J. Chem*., **2017**, 41, 11750.

[10] R. Sanyal, P. Kundu, E. Rychagova, G. Zhigulin, S. Ketkov, B. Ghosh, S. K. Chattopadhyay, E. Zangrando and D. Das, *New J. Chem*., **2016**, 40, 6623.

[11] R. Vafazadeh, B. Khaledi, A.C. Willis and M. Namazian, *Polyhedron*, **2011**, 30, 1815.

[12] B. Vangdal, J. Carranza, F. Lloret, M. Julve and J. Sletten, *J. Chem. Soc., Dalton Trans*., **2002**, 566.

[13] A. Bhattacharjee, S. Halder, K. Ghosh, C. Rizzoli and P. Roy, *New J. Chem*., **2017**, 41, 5696.

[14] M. J. Belousoff, B. Graham, B. Moubaraki, K. S. Murray and L.Spiccia, *Eur. J. Inorg. Chem*., **2006**, 4872.

[15] K. Dhara, P. Roy, J. Ratha, M. Manassero and P. Banerjee, *Polyhedron*, **2007**, 26, 4509.

[16] P. Adak, B. Ghosh, A. Bauz´a, A. Frontera, A. J. Blake, M. Corbella, C. Das Mukhopadhyay and S. K. Chattopadhyay, *RSC Adv*., **2016**, 6, 86851.

[17] K. Dhara, S. Karan, J. Ratha, P. Roy, G. Chandra, M. Manassero, B. Mallik and P. Banerjee, *Chem. Asian J*., **2007**, 2, 1091.

[18] A. Ray, G.M. Rosair, R. Kadam and S. Mitra, Polyhedron, **2009**, 28, 796.

[19] J. Yuan,W.-B. Shi and H.-Z. Kou, *Transit Metal Chem*., **2015**, 40, 807.

[20] D. Sil, S. Bhowmik, F. S. T. Khan and S. P. Rath, *Inorg. Chem*., **2016**, 55, 3239.

[21] F. S. T. Khan, T. Guchhait, S. Sasmal and S. P. Rath, *Dalton Trans*., **2017**, 46, 1012.

[22] D. Mondal and M. C. Majee, *Inorg. Chim. Acta*., **2017**, 465, 70.

[23] J. M. Lillo, T. F. Mastropietro, G. De Munno, F. Lloret, M. Julve and J. Faus, *Inorg. Chem*., **2011**, 50, 5731.

[24] I. Gryca, J. Palion-Gazda, B. Machura, M. Penkala, F. Lloret and M. Julve, *Eur. J. Inorg. Chem*., **2016**, 5418.

[25] L. A. Dubraja, M. Jurić, F. Torić and D. Pajić, *Dalton Trans*., **2017**, 46, 11748.

[26] B. J. Hollyday and C. A. Mirkin, *Angew. Chem. Int. Ed*., **2001**, 40, 2022.

[27] C. N. R. Rao, S. Natarajan and R. Vaidhyanathan, *Angew. Chem. Int. Ed*., **2004**, 43, 1466.

[28] S. T. Zheng and G.Y. Yang, *Chem. Soc. Rev*., **2012**, 41, 7623

[29] U. G. Couceiro, O. Castillo, A. Luque, J. P. G. Terán, G. Beobide and P. Román, *Eur. J. Inorg. Chem.*, **2005**, 4280.

[30] S. Anbu and M. Kandaswamy, *Polyhedron*, **2011**, 30, 123.

[31] I. Banerjee, J. Marek, R. Herchel and M. Ali, *Polyhedron*, **2010**, 29, 1201.

[32] J. Hagiwara, Y. Shimazaki and G. Saito, *Inorg. Chim. Acta*., **2010**, 363, 3178.

[33] P. Roy, M. Nandi, M. Manassero, M. Ricc´o, M. Mazzani, A. Bhaumik and P. Banerjee, *Dalton Trans*., **2009**, 9543.

[34] J. R. Zimmerman and A. Bettencourt-Dias, *Inorg. Chem. Commun*., **2011**, 14, 753.

[35] R. Pedrido, M.J. Romero, M. R. Bermejo, M. Martinez-Calvo, A.M. Gonzalez- Noyab and G. Zaragoza, *Dalton Trans*., **2009**, 8329.

[36] M. Verdaguer, *Polyhedron*, **2001**, 20, 1115–1128.

[37] E. Coronado and P. Day, *Chem. Rev*., **2004**, 104, 5419.

[38] M. K. Saha, D. K. Dey, B. Samanta, A. J. Edwards, W.Clegg and S. Mitra, *Dalton Trans*., **2003**, 0, 488.

[39] R. N. Patel, D. K. Patel, K. K. Shukla and Y. Singh, *J. Coord. Chem*., **2013**, 66, 4131.

[40] R Baggio, M. T. Garland, J. Manzur, O. Peña, M. Perec and E. Spodine, A. Vega, *Inorg. Chim. Acta*., **1999**, 286, 74.

[41] E. Colacio, J. M. D. Vera, M. Ghazi, R. Kivekäs, M. Klinga and J. M. Moreno, *Eur. J. Inorg. Chem*., **1999**, 441.

[42] E. Colacio, M. Ghazi, R. Kiveka and J. M. Moreno, *Inorg. Chem*., **2000**, 39, 2882.

[43] V. Tangoulis, D. Panagoulis, C. P. Raptopoulou and C. Dendrinou-Samara, *Dalton Trans*., **2008**, 0, 1752.

[44] M. H. Sadhua, C. Mathoniereb, Y. P. Patilc and S. B. Kumar, *Polyhedron*, **2017**, 122, 210.

[45] J. E. Backvall (Ed.), *Modern Oxidation Methods*, Weinheim, Germany, Wiley-VCH, **2004**.

[46] S. Halder, A. Mukherjee, K.Ghosh, S. Dey, M. Nandi and P. Roy, *J. Mol. Struct*., **2015**, 01, 1.

[47] R. Saha, B. Joarder, A. Singha Roy, Sk. M. Islam and S. Kumar, *Chem. Eur. J*., **2013**, 19, 16607.

[48] K.C. Gupta and A. K. Sutar, *Coord. Chem. Rev*., **2008**, 252, 1420.

[49] I.T. Horvath, *Green Chem*., **2008**, 10, 1024.

[50] M.C. Pirrung, *Chem. Eur. J*., **2006**, 12, 1312.

[51] N. Shapiro and A. Vigalok, *Angew. Chem. Int. Ed*., **2008**, 47, 2849.

[52] M. Meunier, *Chem. Rev*., **1992**, 92, 1411.

[53] B. Fredrich and W. Gerhartz, *Ullmann's encyclopedia of industrial chemistry*, Weinheim, New York, vol A3. p 470.

[54] Q. H. Xia, H. Q. Ge, C. P. Ye, Z. M. Liu, K and X. Su, Chem. Rev., **2005**, 105, 1603.

[55] A. K. Yudin, *Aziridines and Epoxides in Organic Synthesis*, Wiley-VCH: Weinheim, **2006**.

[56] A. J. Wu, J. E. Penner-Hahn and V. L. Pecoraro, *Chem. Rev*., **2004**, 104, 903.

[57] B. S. Lane and K. Burgess, *Chem. Rev*., **2003**, 103, 2457.

[58] R. Noyori, M. Aoki and K. Sato, *Chem. Commun*., **2003**, 1977.

[59] T. Katsuki, *Chem. Soc. Rev*., **2004**, 33, 437.

[60] T. Punniyamurthy, S. Velusamy and J. Iqbal, *Chem. Rev*., **2005**, 105, 2329.

[61] H. C. Kolb, M. S. Van Nieuwenhze and K. B. Sharpless, *Chem. Rev*., **1994**, 94, 2483.

[62] D. W. Nelson, A. Gypser, P.T. Ho, H. C. Kolb, T. Kondo, H. L. Kwong, D. V. McGrath, A. E. Rubin, P. O. Norrby, K. P. Gable and K. B. Sharpless, *J. Am. Chem. Soc*., **1997**, 119, 1840.

[63] T. Katsuki and K. B. Sharpless, *J. Am. Chem.Soc*., **1980**, 102, 5974.

[64] K. Sato, M. Aoki, M. Ogawa, T. Hashimoto and R. Noyori, *J. Org. Chem*., **1996**, 61, 8310.

[65] W. A. Herrmann, R. W. Fischer and D. W. Marz, *Angew. Chem., Int. Ed. Engl*., **1991**, 30, 1638.

[66] G. M. Sheldrick, *SHELXS 97*, Program for Structure Solution, University of Gottingen, Germany, **1997**.

[67] G. M. Sheldrick, *SHELXL 97*, University of Gottingen, Germany, Program for Crystal Structure Refinement, **1997**.

[68] A. L. Spek, *J. Appl. Crystallogr*., **2003**, 36, 7.

[69] L. J. Farrugia, *J. Appl. Crystallogr*., **1997**, 30, 565.

[70] L. J. Farrugia, *J. Appl. Crystallogr*., **1999**, 32, 837.

[71] Gaussian 09, Revision A.02, M. J. Frisch, G. W. Trucks, H. B. Schlegel, G. E. Scuseria, M. A. Robb, J. R. Cheeseman, G. Scalmani, V. Barone, G. A. Petersson, H. Nakatsuji, X. Li, M. Caricato, A. V. Marenich, J. Bloino, B. G. Janesko, R. Gomperts, B. Mennucci, H. P. Hratchian, J. V. Ortiz, A. F. Izmaylov, J. L. Sonnenberg, D. Williams-Young, F. Ding, F. Lipparini, F. Egidi, J. Goings, B. Peng, A. Petrone, T. Henderson, D. Ranasinghe, V. G. Zakrzewski, J. Gao, N. Rega, G. Zheng, W. Liang, M. Hada, M. Ehara, K. Toyota, R. Fukuda, J. Hasegawa, M. Ishida, T. Nakajima, Y. Honda, O. Kitao, H. Nakai, T. Vreven, K. Throssell, J. A. Montgomery, Jr., J. E. Peralta, F. Ogliaro, M. J. Bearpark, J. J. Heyd, E. N. Brothers, K. N. Kudin, V. N. Staroverov, T. A. Keith, R. Kobayashi, J. Normand, K. Raghavachari, A. P. Rendell, J. C. Burant, S. S. Iyengar, J. Tomasi, M. Cossi, J. M. Millam, M. Klene, C. Adamo, R. Cammi, J. W. Ochterski, R. L. Martin, K. Morokuma, O. Farkas, J. B. Foresman, and D. J. Fox, *Gaussian*, Inc., Wallingford CT, **2016**.

[72] A. D. Becke, *J. Chem. Phys*., **1993**, 98, 5648.

[73] C. T. Lee, W. T. Yang and R. G. Parr, *Phys. Rev. B*, **1988**, 37, 785.

[74] M. O'Boyle, A. L. Tenderholt and K. M. Langner. *J. Comp. Chem*., **2008**, 29, 839.

[75] A. W. Addison, T. N. Rao, J. Reedijk, J. van Rijn and G. C. Verschoor, *J. Chem. Soc. Dalton Trans*., **1984**, 1349.

[76] M. Wang, B. Hu, X. T. Deng and C. G. Wang, *Acta Cryst. E*, **2003**, 63, 710.

[77] S. K. Chattopadhyay, S. Seth and T. C. W. Mak, *J. Coord. Chem*., **2002**, 55, 259.

[78] H. Dong, C. J. White, B. Zhang, C. Krebs, and N. Lehnert. *J. Am. Chem. Soc*., **2018**. 140, 13429.

[79] T. Osako, S. Nagatomo, Y. Tachi, T. Kitagawa and S. Itoh, *Angew. Chem. Int., Ed. Eng*., **2002**, 41, 4325.

[80] S. T. Prigge, B. A. Eipper, R. E. Mains, and L. M. Amzel, *Science*, **2004**, 304, 864.

[81] P. Roy, K. Dhara, M. Manassero and P. Banerjee, *Inorg. Chem. Commun*., **2008**, 4, 265.

[82] J. Reim, R. Werner, W. Haase and B. Krebs, *Chem.Eur. J.*, **1998**, 4, 289.

Chapter 6

Selective metal-ligand bond breaking driven by weak intermolecular interactions: from metamagnetic Mn(III)-monomer to hexacyanoferrate(II)-bridged metamagnetic Mn_2Fe-trimer

6.1 Introduction

Selective bond making-bond breaking is the finest art of chemistry and has tremendous significance in molecular and supramolecular chemistry [1-4]. After prolonged research over centuries, chemists have gained mastery over covalent and metal-ligand coordination bond breaking-bond making processes whereas control over the supramolecular interactions is still a daunting task. Several catalytic processes [5-9] are well-known for the selective bond activation, bond breaking and bond making in organic chemistry. In coordination chemistry, the so-called *trans* effect, [10-11] the HSAB principle [12-13] etc. can successfully explain the selective metal-ligand bond breaking-bond making. In supramolecular chemistry, molecular recognition and aggregation constitute the base of selectivity and determine the final compound and structure [14-18]. Supramolecular interactions are much weaker than covalent/coordinate bonds and therefore a minor chemical or physical perturbation may cause a severe change on the weak interaction network of the system. Here, we present a case study where weak interactions drive a metal-ligand coordination bond dissociation during the formation of a hexacyanoferrate(II)-bridged Mn_2Fe trimer from Mn(III)-monomeric precursor.

In molecular magnetism, metamagnets [19-22] are a special type of magnetic materials in which two magnetic motifs (which may be a molecule, a 1D chain or a 2D layer) interact antiferromagnetically (AF) through weak inter-motif (molecule or chain or layer) interactions and the application of a DC field above a certain critical field (H_C) can alter this weak AF coupling into a ferromagnetic (FM) one at low temperature (T_N) [23-24]. Such co-existence of AF and FM in a material is difficult to predict and consequently highly challenging to design but may have significant applications in technologies associated with magnetic cooling [25] and magnetocaloric effect [26]. This magnetic field induced first order transition from AF to FM is critically dependent

on the weak inter-motif interactions. Mukherjee et.al. [22], have reported that the metamagnetism arises due to weak C-H···N H-bonding interactions between azido bridged 1D coordination chains of Ni^{II}-Schiff base complex. Chen et.al. [27], have reported the metamagnetic behavior of 2-fold interpenetrated 2D coordination layers where weak hydrogen bonding and dipolar interactions between adjacent layers are responsible for such metamagnetic transition. Ghosh et.al. [28], reported metamagnetism due to weak interchain C-H···N H-bonding between neighboring coordination chains formed by Mn(III)-tridentate Schiff base units connected with azide ligands in its *end-on* (μ-1,1´) coordination mode. So, to design a metamagnetic material, we need to control the weak intermolecular interactions, although, due to the difficulty of this control, most of the reported molecular metamagnets are basically serendipitous. With this background, we have designed a strategy to prepare molecular metamagnets through controlled breaking of metal-ligand bonds helped by the cumulative functions of large number of weak interactions.

In last few years, high spin Mn(III)-Schiff base complexes have been used as structural building units to design several types of magnetic materials like single chain magnets [29-30] (SCMs), single molecule magnets [31-32] (SMMs), ferromagnets [33-34], antiferromagnets [35-36] etc. thanks to several unique properties of the Mn(III) ions: i) stable oxidation state, ii) high spin configuration (S = 2), iii) easily substitutable axial sites and iv) unusual uniaxial anisotropy (D) arising from Jahn-Teller elongation in octahedral geometry.

In this context, we have synthesized a Mn(III) complex with a N_2O_2 donor based Schiff base ligand and studied its structure and magnetic properties. X-ray structural study reveals Mn(III)-monomeric units with axial water and chloride ligands, that are further assembled by H-bonds and π-π interactions to form a supramolecular dimer with a very small intra-dimer antiferromagnetic coupling and a metamagnetic behaviour with a critical field of *ca*. 2.0 T at 2 K.

The hard acid-soft base interaction makes the coordinated chlorides highly labile and the reaction of complex **1** with $K_4[Fe(CN)_6]$ replaces the chlorides from the coordination sphere of two adjacent monomeric Mn(III) units to yield a *trans* cyanide bridged Mn_2Fe trimer (complex **2**) that co-crystallizes in a 1:1 ratio with a Mn(III) monomer closely related to complex **1**. Structural analysis reveals the preservation of weak intermolecular H-bonds and π-π interactions during the transformation of the monomer into the trimer as well as the metamagnetic behaviour. These Mn_2Fe trimers are assembled by H-bonds and π-π interactions giving rise to supramolecular chains that also present a metamagnetic transition with a critical field of *ca*. 2.5 T at 2 K.

6.2 Experimental section

6.2.1Materials and methods

$MnCl_2{\cdot}4H_2O$ (99 %), 2-hydroxy-5-methoxybenzaldehyde (99.5 %), ethylenediamine (99.5 %) and $K_4[Fe(CN)_6]$ (99 %) have been purchased from Sigma Aldrich and utilized without further purification. Triethylamine and all other chemicals (AR grade) were got from Merck India and used as received. A Perkin-Elmer 240C elemental analyser were used to record the C, H, N elemental analysis. The FT-IR spectral study was done by a Nicolet Impact 410 spectrometer within the range of 400-4000 cm^{-1} using KBr pellets.

6.2.2 Synthesis of the Ligand (H_2L)

The Schiff's base ligand (H_2L=2,2'-((1*E*,1'*E*)-(ethane-1,2diylbis(azaneylylidene))bis (methaneylylidene))bis(4-methoxyphenol)) was synthesized (Scheme 1) by refluxing 2-hydroxy-5-methoxybenzaldehyde (10 mmol, 1.525 g) with ethylenediamine (5 mmol, 300 mg) in a 2:1 ratio in methanol (20 mL) at 90ºC for 1 h. After that, the reaction mixture was cooled down and filtered to separate out the yellow-coloured crystalline solid product, washed with diethyl ether, dried in air. Yield: ~90%.

6.2.3.1 Synthesis of [(L)Mn(H_2O)Cl] (1)

The Schiff base ligand H_2L (165 mg, 0.5 mmol) was dissolved in 20 mL of boiling methanol and the pH of the methanolic solution was adjusted to 9 by Et_3N. An aqueous solution (5 mL) of $MnCl_2 \cdot 4H_2O$ (100 mg, 0.5 mmol) was added to the previous solution and the mixed solution was refluxed for 2 h. The reaction mixture was cooled, filtered off and the light yellowish-brown filtrate was kept undisturbed for crystallisation. Brown needle like crystals reasonable for single crystal X-ray analyses were collected after 2 weeks. Yield: ~86 %. Anal. Calc. for $C_{18}H_{20}ClMnN_2O_5$: C, 49.7; H, 4.6; N, 6.4 %. Found: C, 49.8; H, 4.5; and N, 6.5 %. Selected IR bands (cm^{-1}): ν (C=N) 1605(s); ν (O-H) 3385(broad).

6.2.3.2 Synthesis of $(H_3O)[Mn(L)(H_2O)_2]\{[Mn(L)(H_2O)]_2Fe(CN)_6\} \cdot 4H_2O$ (2)

The co-crystal of this hexacyanoferrate(II)-bridged trimeric complex was synthesized by a layering technique using the monomeric complex **1** and a $K_4[Fe(CN)_6]$ solution in a 1:1 ratio with a water-methanol buffer solution. Complex **1** (110 mg, 0.25 mmol) was dissolved in 30 mL of a 9:1 methanol-water mixture. A second solution was prepared by dissolving $K_4[Fe(CN)_6]$ (108 mg, 0.25 mmol) in 25 mL of distilled water. These two solutions were layered in eight different tubes using a 1:1 water-methanol buffer and kept undisturbed for crystallization. Deep brown needle shaped crystals suitable for X-ray diffraction analysis were collected after one month, then washed with hexane and dried. Yield 79 %. Anal. Calc. for $C_{60}H_{73}FeMn_3N_{12}O_{21}$: C, 47.4; H, 4.8; N, 11.1 %. Found: C, 47.5; H, 4.7; and N, 11.1 %. Selected IR bands (KBr pellet, cm^{-1}): ν (C≡N) stretching 2123, 2105(s); ν (C≡N) 1608(s); ν (O-H) 3410(broad).

6.2.4 Magnetic measurements

Magnetic measurements on compound 1 and 2 (with masses of 33.446 and 4.406 mg, respectively) were performed using a Quantum Design MPMS-XL-7 SQUID magnetometer in the temperature

range 2-300 K in presence of an external magnetic field of 0.1 T (and in the temperature range 2-10 K with different applied fields in the range 0.1-3.0 T). The isothermal magnetizations were measured at 2 K with magnetic fields of up to 7 T on the same samples. The susceptibility data were corrected for the sample holders as previously measured using the same conditions and for the diamagnetic contributions of the compounds as deduced by using Pascal's constant tables [37].

6.2.5 Theoretical methods

All DFT calculations included in this manuscript have been done using the Gaussian-16 program [38] at the PBE1PBE-D3/def2-TZVP level of theory and using the crystallographic coordinates. The formation energies of the assemblies have been evaluated by calculating the difference between the overall energy of the assembly and the sum of the monomers that constitute the assembly, which have been maintained frozen. The Atoms-in-Molecules (AIM) [39] analysis was carried out at the same level of theory. The AIM properties were calculated by using the AIMAll program [40].

6.2.6 Crystallographic data collection and refinement

Single crystals of complexes **1** and **2** were mounted on a Bruker SMART CCD diffractometer equipped with a graphite monochromator and MoKα (λ = 0.71073 Å) radiation. The structures were solved by the Patterson method and followed by successive Fourier and difference Fourier synthesis. Full matrix least squares refinements were performed on F^2 using SHELXL-97 with anisotropic displacement parameters for all non-hydrogen atoms. The hydrogen atoms were refined isotropically, and their locations were determined from a different Fourier map. All calculations were carried out using SHELXL 97, [41] SHELXS 97, [42] PLATON 99, [43] ORTEP 32, [44] and WinGX system v1.64 [45]. All the crystallographic data and refinement

parameters of both complexes are presented in Table 1. Complex 2 contains disordered guest water molecules.

Table 1. Crystallographic data collection and refinement parameters of compounds **1** and **2**

	Compound **1**	Compound **2**
Formula	$C_{18}H_{20}ClMnN_2O_5$	$C_{60}H_{73}FeMn_3N_{12}O_{21}$
Formula weight	434.75	1518.97
Crystal system	Orthorhombic	Triclinic
Space group	P_{bca}	P-1
a (Å)	11.826(6)	14.0832(14)
b (Å)	12.872(7)	15.0504(15)
c (Å)	22.919(12)	17.0031(18)
α (º)	90	108.703(3)
β (º)	90	101.649(3)
γ (º)	90	90.023(4)
V(Å^3)	3489(3)	3335.1(6)
Z	8	2
ρ_{calc} (g/cm^3)	1.655	1.513
μ (Mo Kα) (mm)	0.945	0.850
F(000)	1792	1572
Crystal size (mm^3)	0.08x0.12x0.16	0.12x0.16x0.20
T (K)	100	152
$\theta_{min-max}$ (°)	1.8, 25.3	2.5, 27.2
Total data	28731	34615
Unique Data	3156	14564
R_{int}	0.177	0.126
Observed data [I >	1625	7216
N_{ref}	3156	14564
N_{par}	244	878
R	0.0581	0.0963
wR_2	0.1195	0.2874
S	0.80	1.01

$^aR_1 = \sum||F_o|-|F_c||/\sum|F_o|$; $^bwR_2$ $(F_o^2) = [\sum[w(F_o^2-F_c^2)^2/\sum wF_o^4]^{½}$;
^{c}GooF $= [\sum[w(F_o^2-F_c^2)^2/(N_{obs}-N_{params})]^{½}$

6.3 Result and discussion

6.3.1 Synthesis

The tetradentate Schiff base ligand (H_2L) was synthesized by the combination of ethylene diamine with 2-hydroxy-5-methoxybenzaldehyde in a 2:1 ratio (Scheme **1**). Combination of the synthesized ligand with $MnCl_2$ leads to the aerial oxidation of Mn(II) to Mn(III) with formation of the neutral complex **1**, that, besides the ligand L^{2-}, contains one Cl^- and one water molecule at the axial sites (Scheme **1**). When complex **1** is reacted with $[Fe(CN)_6]^{4-}$, the cyanide groups replace the coordinated chloride ions of two neighbouring Mn(III)-monomers, connecting them through a Mn-NC-Fe-CN-Mn bridge (Scheme 1).

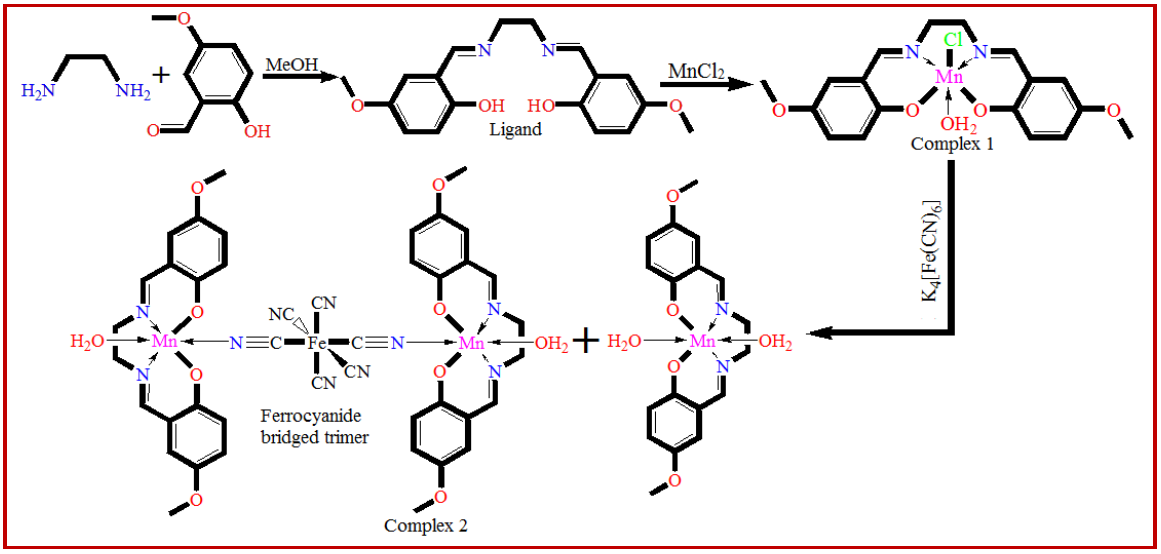

Scheme 1. The complete synthetic scheme of the ligand (H_2L) and complex **1** and **2.**

6.3.2 Structure of complex [Mn(L)(H$_2$O)Cl] (1)

The mononuclear complex **1** crystallizes in the orthorhombic centro-symmetric space group P_{bca}. The asymmetric unit contains one mononuclear unit which contains one Mn(III) ion, one deprotonated ligand L^{2-}, one coordinated Cl^- and one coordinated water molecule (Figure 1). Selected coordination bond distances and angles are given in Table 2.

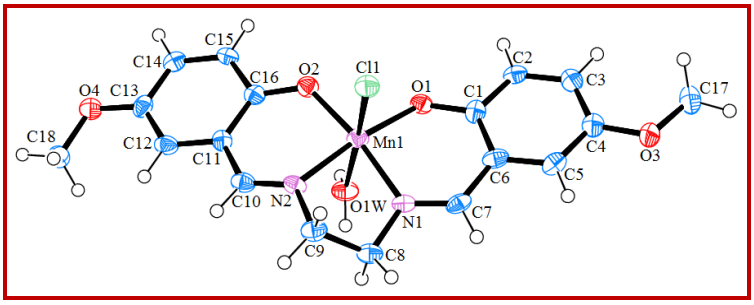

Figure 1. ORTEP diagram of complex **1** with 30 % ellipsoid probability.

The metal centre shows a distorted octahedral geometry. As observed in other N_2O_2 donor Schiff base metal complexes, the four equatorial positions are occupied by the four donor atoms (N1, N2, O1 and O2) of the Schiff base while the *trans*-axial sites are occupied by one chloride ion (Cl1) and one water molecule (O1W). The Mn-O and Mn-N bond lengths of the Schiff base donor atoms are in the normal range: Mn1-O1 = 1.881(4) Å, Mn1-O2 = 1.863(4) Å, Mn1-N1 = 1.979(4) Å and Mn1-N2 = 1.973(4) Å, whereas the axial bond lengths are comparatively longer: Mn1-Cl1 = 2.554(2) Å and Mn1-O1W = 2.287(3) Å. These distances reflect the expected Jahn-Teller elongation along the axial bonds. The Mn centre is displaced towards the Cl1 atom ~ 0.073 Å from the mean plane formed by the donor atoms (O1-N1-N2-O2) of the Schiff base ligand.

Table 2: Some selected bond lengths (Å) and angles (°) in complex **1**

Atoms	**Length**	**Atoms**	**Length**
Mn1-Cl1	2.554(2)	Mn1-O2	1.863(4)
Mn1-O1	1.881(4)	Mn1-N1	1.979(4)
Mn1-O1W	2.287(3)	Mn1-N2	1.973(4)
Atoms	**Angle**	**Atoms**	**Angle**
O1-Mn1-O2	94.46(16)	Cl1-Mn1-N1	88.99(12)
O1-Mn1-N2	172.56(16)	Cl1-Mn1-N2	88.12(12)
O1W-Mn1-N1	87.12(15)	O1-Mn1-O1W	91.28(12)
O2-Mn1-N1	171.60(17)	O1-Mn1-N1	91.91(17)
N1-Mn1-N2	81.37(17)	O1W-Mn1-O2	87.26(15)
Cl1-Mn1-O1	94.98(10)	O1W-Mn1-N2	85.25(15)
Cl1-Mn1-O1W	172.74(10)	O2-Mn1-N2	91.94(17)
Cl1-Mn1-O2	95.90(13)		

Supramolecular structural analysis reveals that two neighbouring mononuclear units are connected in an antiparallel fashion by π-π interactions to form a supramolecular dimer which is further stabilized by a double O1W-H1W1···O1 hydrogen bonding interaction (Figure 2).

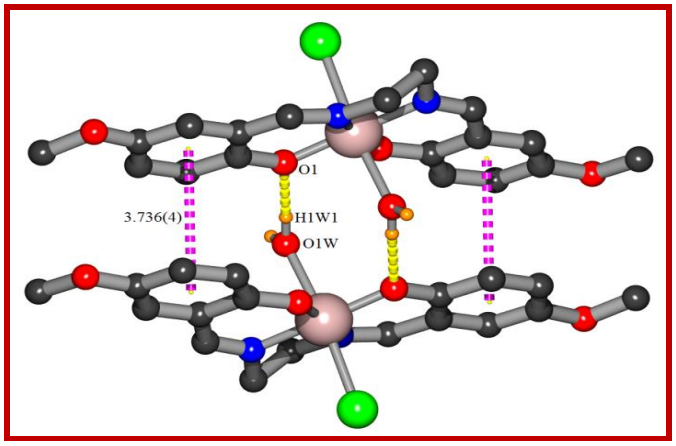

Figure 2. Supramolecular dimer formation with π-π and O1W-H1W1···O1 hydrogen bonding interactions in complex **1.**

These dimers are bridged by O1W-H2W1···Cl1 hydrogen bonding interactions to form supramolecular layers parallel to the crystallographic *ab*-plane (Figure 3). These supramolecular layers are further bridged by C8-H8A···Cl1 and C15-H15···Cl1 H-bonding interactions to build a 3D supramolecular structure (Figure 4). The hydrogen bonding and π-π interaction parameters are summarized in Tables 3 and 4.

Table 3: H-bonding dimensions present in complex **1**

D-H···A	D-H/(Å)	H···A/(Å)	D···A/(Å)	<D-H···A/(°)	Symmetry
O1W –H1W1···O1	0.85	1.99	2.830(5)	170	-x, 1-y, 2-z
O1W -H2W1···Cl1	0.85	2.54	3.175(4)	132	1/2-x, 1/2+y, z
C8 -H8A···Cl1	0.99	2.83	3.465(5)	123	1/2+x, 1/2-y, 2-z
C15 -H15···Cl1	0.95	2.81	3.756(5)	171	-1/2+x, 1/2-y, 2-z
C17 -H17B···O4	0.98	2.47	3.410(7)	161	-x, 1-y, 2-z
C18 -H18A···Cl1	0.98	2.76	3.535(5)	136	x, 1/2-y, -1/2+z

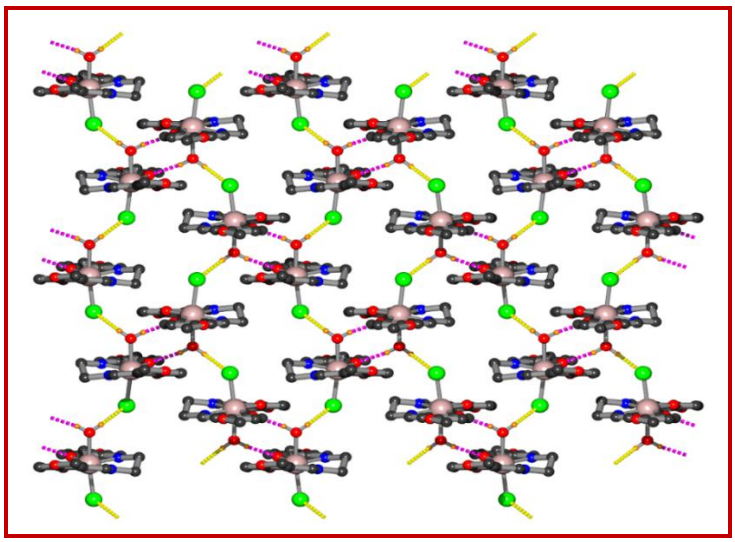

Figure 3. 2D supramolecular sheets are formed by O1W-H1W1···O1 (magenta) and O1W-H2W1···Cl1 (yellow) hydrogen bonding interactions in complex **1**.

Table 4: π···π interaction parameters in complex **1**

Ri···Rj	Centroid separation Cg–Cg/(Å)	Dihedral angle (i,j)/(°)	Perp. distance between ring i to ring j/(Å)	Symmetry
R1···R2	3.736(4)	4.6(2)	3.351(2)	-x, 1-y, 2-z
R2···R1	3.736(4)	4.6(2)	3.319(2)	-x, 1-y, 2-z

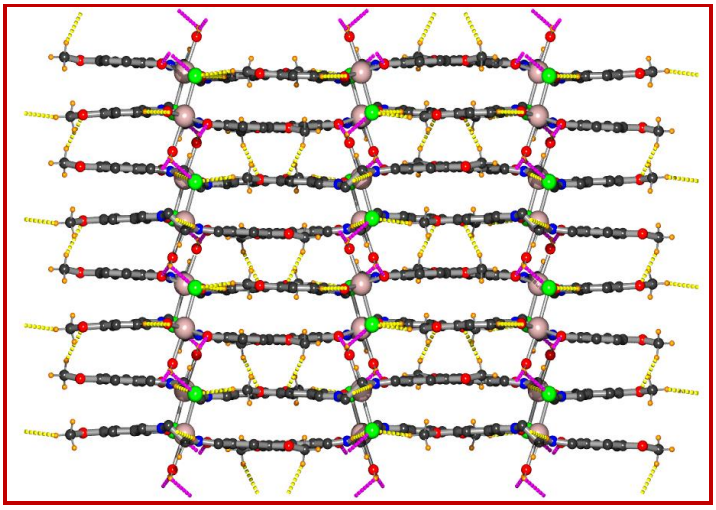

Figure 4. 3D supramolecular structure formed by O1W-H1W1···O1 (magenta) and C-H···Cl and C-H···O (yellow) hydrogen bonding interactions in complex **1**.

6.3.3 Crystal structure of $(H_3O)[Mn(L)(H_2O)_2]\{[Mn(L)(H_2O)]_2Fe(CN)_6\}\cdot 4H_2O$ (2)

The single crystal X-ray (SCXRD) analysis has established that this compound crystallizes in the centrosymmetric triclinic *P*-1 space group. It is a 1:1 co-crystal of a Mn_2Fe trimer and a Mn(III) monomer. The asymmetric unit contains one monomeric unit, two halves trimeric units, one oxonium cation and four disordered guest water molecules (Figure 5). The trimeric unit is dianionic and its charge is balanced by the monocationic monomer and one oxonium ion. Note that the presence of the oxonium cation is not only established by charge balance requirements but also by the X-ray crystal data that shows three H atoms around the O5W atom with the expected trigonal pyramidal geometry with similar H-O-H bond angles of 104.4º, 104.6º and 105.1º. The crystallographic data is presented in Table 1 and some selected coordination bond lengths and angles are summarized in Table 5. The co-crystal contains two different trimeric units. Each trimeric unit is formed by two Mn(III)-Schiff base complexes connected through two *trans* cyanide groups of the hexacyanoferrate(II) unit that acts as a linear bridge -replacing the chloride groups in the original monomeric complex **1**. Interestingly, the water molecule remains coordinated with the Mn(III) ions, precluding the formation of an alternating cyanide bridged Mn(III)-Fe(II) chain. In each trimer the asymmetric unit contains a full Mn(III)-Schiff base complex moiety and half $[Fe(CN)_6]^{4-}$ unit. In both trimers the Mn(III)-ions show a distorted octahedral geometry where the four equatorial positions are fulfilled by the four donor sites of the Schiff base ligands and the axial positions are occupied by a water molecule and N atom of the CN group of the bridging $[Fe(CN)_6]^{4-}$ bridging unit (Figure 3). In both trimers the bond lengths from the N_2O_2 Schiff base donor atoms to the metal centres are quite similar: Mn1-O1 = 1.862(5) Å, Mn1-O2 = 1.889(5) Å, Mn1-N1 = 1.981(6) Å and Mn1-N2 = 1.985(6) Å for trimer 1 and Mn2-O5 = 1.872(5) Å, Mn2-O6 = 1.902(5) Å, Mn2-N6 = 1.977(6) Å and Mn2-N7 = 1.997(6) Å, for trimer 2. In both trimers the two axial

bond lengths are longer than the equatorial ones: Mn1-O1W = 2.290(5) Å and Mn1-N3 = 2.316(6) Å in trimer 1 and Mn2-O2W = 2.294(5) Å and Mn2-N8 = 2.2478(6) Å in trimer 2, indicating the presence of a Jahn-Teller elongation in both trimers, as observed in complex **1** (see above). The trimers are not linear since the Mn-N≡C bond angles are 143.38° and 145.01° in trimers 1 and 2, respectively.

Table 5: Some selected bond lengths (Å) and angles (°) in complex **2**

Atoms	**Length**	**Atom**	**Length**
Fe1-C19	1.913(8)	Fe2-C42	1.913(9)
Fe1-C20	1.949(8)	Fe2-C40	1.944(8)
Fe1-C21	1.926(7)	Fe2-C41	1.958(8)
Mn1-O1	1.873(5)	Mn2-O2W	2.285(5)
Mn1-O1W	2.294(5)	Mn2-O6	1.863(5)
Mn1-O2	1.900(5)	Mn2-N6	1.984(6)
Mn1-N1	1.981(6)	Mn2-O5	1.889(5)
Mn1-N2	1.998(6)	Mn2-N8	2.318(6)
Mn1-N3	2.245(6)	Mn2-N7	1.983(6)
Mn3-O10	1.894(6)	Mn3-O9	1.874(5)
Mn3-N11	1.989(6)	Mn3-N12	1.985(6)
Mn3-O4W	2.216(5)	Mn3-O3W	2.304(6)
Atoms	**Angle**	**Atoms**	**Angle**
C19-Fe1-C20	94.1(3)	O1-Mn1-O2	93.3(2)
C19-Fe1-C21	89.4(3)	O1-Mn1-O1W	89.43(19)
C19-Fe1-C19*	180.00	O1-Mn1-N1	92.1(2)
C19-Fe1-C20*	85.9(3)	O1-Mn1-N2	173.3(2)
C19-Fe1-C21*	90.7(3)	O1-Mn1-N3	94.1(2)
C40-Fe2-C41	90.4(3)	H1W1-O1W-H2W1	108.00
C40-Fe2-C42	89.0(3)	N6-Mn2-N8	84.3(2)
C40-Fe2-C40**	180.00	N6 -Mn2-N7	82.4(2)
N2-Mn1-N3	89.5(2)	N1-Mn1-N3	88.7(2)

(* = 1-x, 1-y, 1-z, ** = -x, 2-y, 1-z)

In the monomeric unit, the metal ion (Mn3) also shows a distorted octahedral geometry, as in complex **1**. The Schiff base occupies the four equatorial coordination sites using its four donor sites (O9, O10, N11 and N12). The corresponding bond lengths are similar to those observed in compound **1** and in both trimers in compound **2**: Mn3-O9 = 1.874(5) Å, Mn3-N12 = 1.984(6) Å, Mn3-O10 = 1.894(6) Å and Mn3-N11 = 1.988(6) Å. In contrast to complex **1**, the two axial sites are occupied by two water molecules (O3W and O4W). As expected, the axial Mn-O bond lengths: Mn3-O3W = 2.299(6) Å and Mn3-O4W = 2.215(5) Å are longer than the equatorial ones, showing, once more, the existence of a Jahn-Teller elongation in the Mn(III)-monomeric unit. The Mn3 centre is displaced towards the O4W molecule by ~ 0.043 Å from the mean equatorial plane.

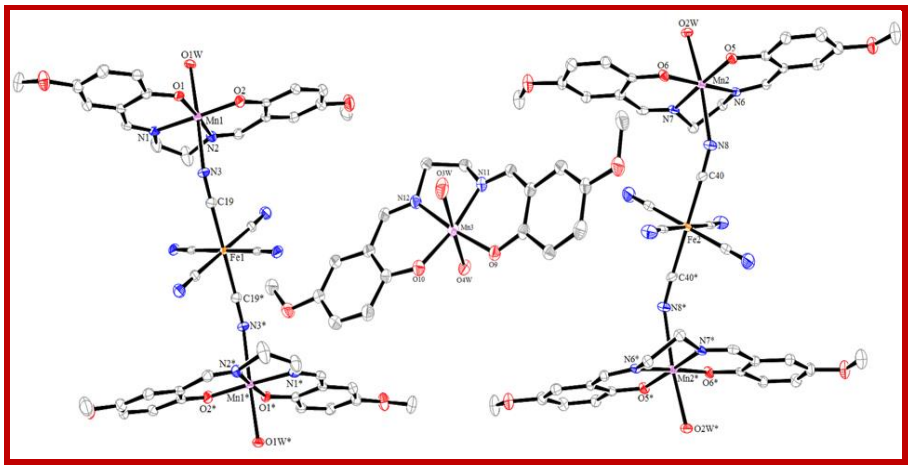

Figure 5. ORTEP diagram in **2** showing two complete trimers and a monomer with atom labelling. The solvent molecules, oxonium cation and hydrogen atoms are omitted for clarity. Ellipsoids drawn at 15% probability.

Supramolecular structural analysis reveals that each trimeric unit is connected by hydrogen bonding interactions implying the coordinated water molecules and by π-π interactions to form supramolecular chains straight way to the crystallographic *b*-axis. Each independent trimer forms a different type of supramolecular chain (Figure 6). These two different chains are arranged

parallel and are connected by O2W-H1W2···N4 and O1W-H1W1···N10 hydrogen bonding interactions to form a supramolecular layer in the *ab*-plane.

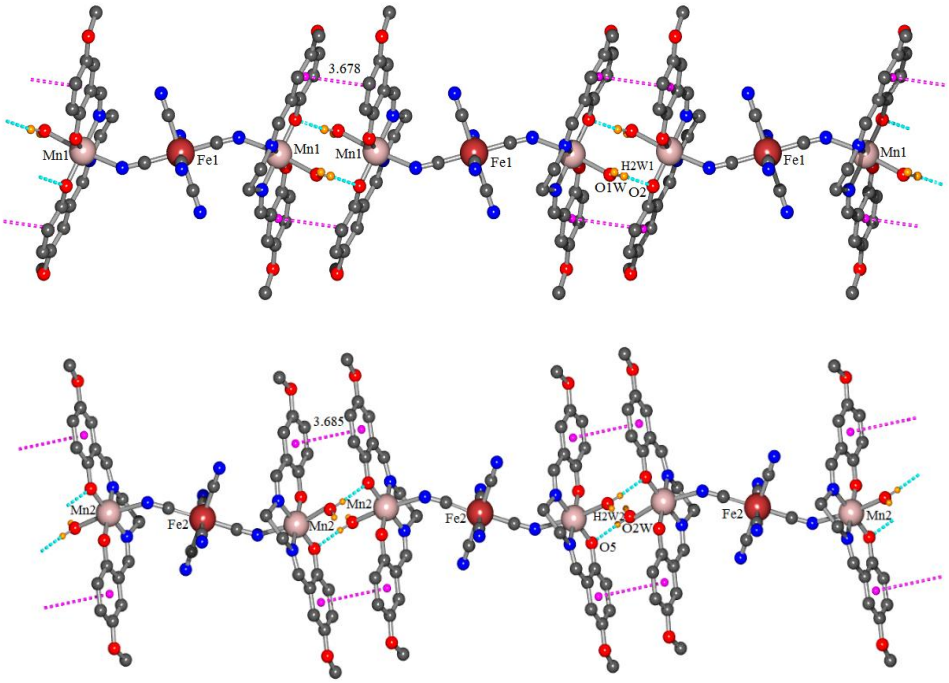

Figure 6. View of the chains of trimers Mn1-Fe1-Mn1 (top) and Mn2-Fe2-Mn2 (bottom) showing the centroids of the aromatic rings of the ligands (as pink spheres) and the shortest C_g-C_g distances (as pink dotted lines). H-bonds are indicated as light blue dotted lines.

The cations (the monomeric Mn(III) complex and the oxonium ions) and the disordered solvent molecules are located in the interlayer space. These molecules and ions are connected with the anionic supramolecular layers by means of hydrogen bonding interactions. All these supramolecular interactions are summarized in Tables 6 and 7.

Table 6: π···π interaction parameters in complex **2**

$R_i \cdots R_j$*	R_i-R_j centroid distance (Å)	R_i-R_j dihedral angle (°)	R_i-R_j distance (Å)	Symmetry
$R_1 \cdots R_2$	3.682(5)	10.1(4)	3.403(3)	1-x, 2-y, 1-z
$R_2 \cdots R_1$	3.684(5)	10.1(4)	3.503(3)	1-x, 2-y, 1-z
$R_3 \cdots R_4$	3.678(4)	7.7(4)	3.390(3)	-x, 1-y, 1-z
$R_4 \cdots R_3$	3.679(4)	7.7(4)	3.514(3)	-x, 1-y, 1-z

Table 7: Hydrogen bond dimensions in complex **2**

D-H···A	D-H/(Å)	H···A/(Å)	D···A/(Å)	<D-H···A/(°)	Symmetry
O1W-H1W1···N10	0.85	1.93	2.762(7)	168	1+x, y, z
O1W-H2W1···O2	0.85	2.01	2.847(7)	168	1-x, 2-y, 1-z
O2W-H1W2···N4	0.85	2.03	2.823(7)	155	
O2W-H2W2···O5	0.85	1.92	2.767(7)	174	-x, 1-y, 1-z
O3W-H2W3···N13	0.85	2.13	2.741(15)	129	
O4W-H1W4···N5	0.85	2.12	2.717(8)	127	
O4W-H2W4···O7	0.85	2.05	2.898(8)	176	1-x, 1-y, 1-z
O5W-H1W5···O2	0.78	2.21	2.982(8)	169	1-x, 1-y, 1-z
O5W-H3W5···O6W	0.78	2.16	2.814(11)	142	
O6W-H2W6···O3W	0.82	2.37	2.848(10)	118	1-x, 1-y, 1-z
O7W-H1W7···N10	0.78	2.08	2.836(12)	164	1+x, y, z
C2-H2···N10	0.95	2.47	3.367(11)	157	-x, 2-y, 1-z
C9-H9B···O6	0.99	2.58	3.551(10)	166	1+x, y, z
C14-H14···N13	0.95	2.45	3.230(16)	139	1-x, 2-y, 2-z
C29-H29B···N4	0.99	2.59	3.361(9)	134	
C30-H30A···O5W	0.99	2.50	3.280(10)	135	1-x, 1-y, 1-z
C33-H33···O11	0.95	2.48	3.321(10)	147	1-x, 2-y, 2-z
C59-H59B···O4	0.98	2.50	3.482(11)	175	

6.3.4 Theoretical DFT study of non-covalent interactions

We have performed DFT calculations at the PBE1PBE-D3/def2-TZVP level of theory (see theoretical methods for details) to perceive the behavior of compounds **1** and **2** cited above and the facile replacement of the chloride ligand by the hexacyanoferrate(II) unit. First, we have compared the H-bonded dimerization energy of the supramolecular dimer shown in Figure 2 to the dissociation energy of the Mn(III)-Cl coordination bond. The interaction energy of the dimer of compound **1** along with the QTAIM distribution of bond critical points and bond paths are given in Figure 5. It can be observed that the dimerization energy is very large (ΔE_1 = -30.1 kcal/mol)

due to the cooperative formation of several O···H and C–H···O H-bonds and π-π interactions, which are characterized by the corresponding bond critical points (CPs) and bond paths interconnecting the interacting atoms. In order to measure the contribution of the H-bonds we have used the AIM energy densities at the bond CPs. This methodology has successfully worked for us and others to analyze several types of non-covalent interactions [46-48]. The dissociation energy of each H-bonding contact can be estimated according to the approach proposed by Espinosa *et al.*[49] and Vener *et al*. [50] which developed energy descriptors specifically for H-bonds. Figure 5 also shows the dissociation energy (in kcal/mol) obtained for each H-bond using both indicators, i.e. the potential energy density V(r) and the Lagrangian kinetic energy G(r). The energies are indicated in Figure 7 and they evidence that the contribution of both O-H···O H-bonds is approximately 10.4 kcal/mol and that of the C-H···O bonds involving the methoxide groups are significantly smaller (i.e. 3.6 kcal/mol), using the G(r) descriptor.

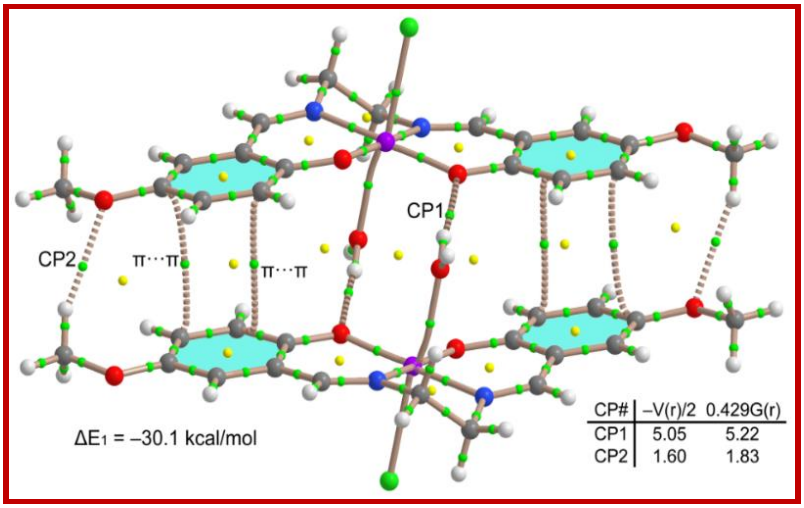

Figure 7. AIM distribution of bond and ring critical points (green and yellow spheres, respectively) and bond paths obtained for the self-assembled dimer of compound **1**. The dissociation energies of the H-bonds using the V(r) and G(r) values at the bond CP are indicated in (kcal/mol) at the down-right corner and the formation energy of the assembly (ΔE_1) is also given nearby the assembly.

Therefore, the contribution of the π-stacking and other long range van der Waals interactions is very significant (approximately 16 kcal/mol). The dissociation energy of the Mn(III)-Cl coordination bond computed for **1** in MeOH at the same level of theory is -29.3 kcal/mol, slightly weaker than the dimerization energy.

We have also evaluated the reaction energy of the transformation depicted in Scheme 2 in order to rationalize the transformation of compound **1** into **2** upon addition of hexacyanoferrate(II). Agreeably, the energy formation of **2** from **1** is strongly favoured (ΔEr = –19.7 kcal/mol) using methanol as solvent in the calculation. It should be mentioned that this reaction energy does not compensate for the energy of the H-bonded dimer formation of **1** observed in the solid state (ΔE_1, see Figure 7). However, this matter is not important because the same combination of interactions is also found in the solid state of compound **2**, as detailed in the supramolecular polymers shown in Figure 8. We have performed the QTAIM analysis of a dimeric model of the polymer that is shown in Figure 8, and exactly the same distribution of critical points and bond paths is obtained. It is also worthy to comment that the O-H···O H-bonds in **2** are even stronger than those in compound **1**.

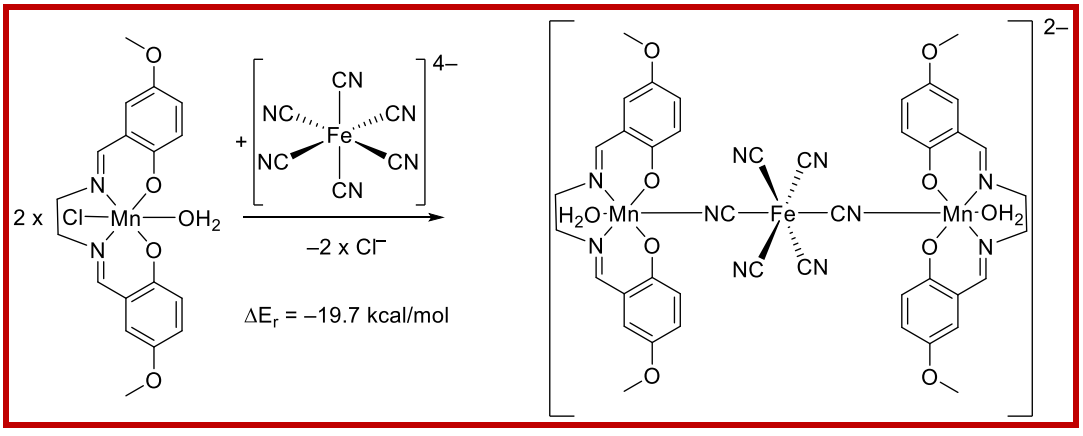

Scheme 2: Transformation from 1 to 2 is energetically favourbale in methanol medium.

Taken together, the results from the theoretical DFT study of complexes **1** and **2** revealed that the ligand exchange of Cl^- by $[Fe(CN)_6]^{4-}$ is energetically favored and preferred over the water substitution since the Mn–Cl coordination bond is weaker than the strength of the weak interactions involved in the formation of the dimer/polymers (H-bonds and π-π interactions).

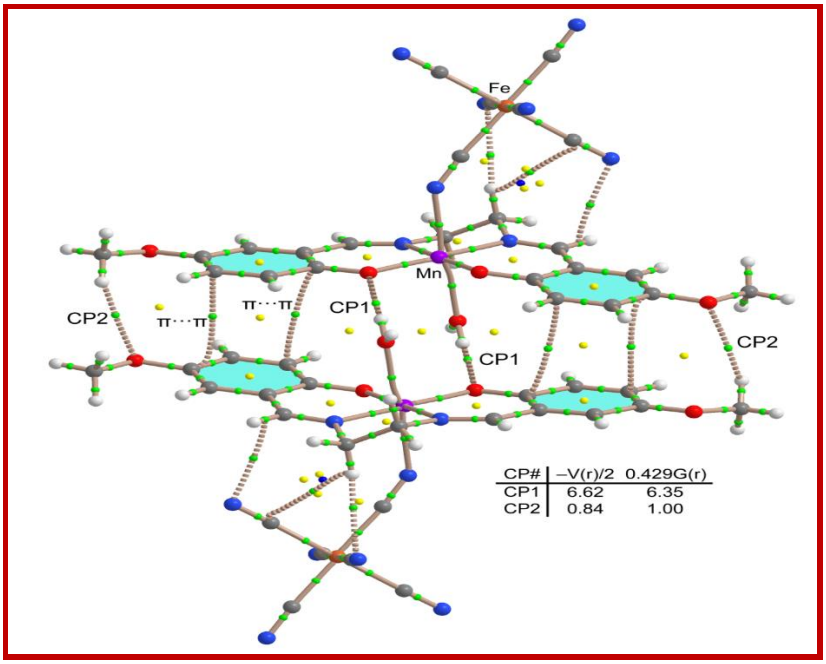

Figure 8. AIM distribution of bond and ring critical points (green and yellow spheres, respectively) and bond paths obtained for a model dimer of compound **2**. The dissociation energies of the H-bonds using the V(r) and G(r) values at the bond CP are indicated in (kcal/mol) at the down-right corner.

6.3.5 Magnetic properties of compound 1

The $\chi_m T$ value per Mn(III) ion for compound **1** shows at room temperature a value of *ca*. 3.0 cm^3 K mol^{-1}, close to the expected value for an isolated Mn(III) ion with a ground spin state S = 2 and a g value close to 2. When the sample is cooled, $\chi_m T$ remains constant down to *ca*. 20 K and shows a sharp decrease at lower temperatures to reach a value of *ca*. 0.8 cm^3 K mol^{-1} at 2 K (Figure 7) which suggests the presence of a weak antiferromagnetic interaction in **1** and/or the presence of a

zero field splitting in the Mn(III) ions. Since the structure of this compound indicates the presence of quasi-isolated Mn(III) monomers, we have fit the magnetic properties to a simple model considering an isolated S = 2 ion with a zero field splitting (ZFS) to account for the sharp decrease in $\chi_m T$ at low temperatures using the program PHI [51]. This model reproduces very satisfactorily the magnetic properties of complex **1** in the whole temperature range with g = 1.958 and |D| = 0.69 cm^{-1} with a residual of 0.0679 (dotted line in Figure 9).

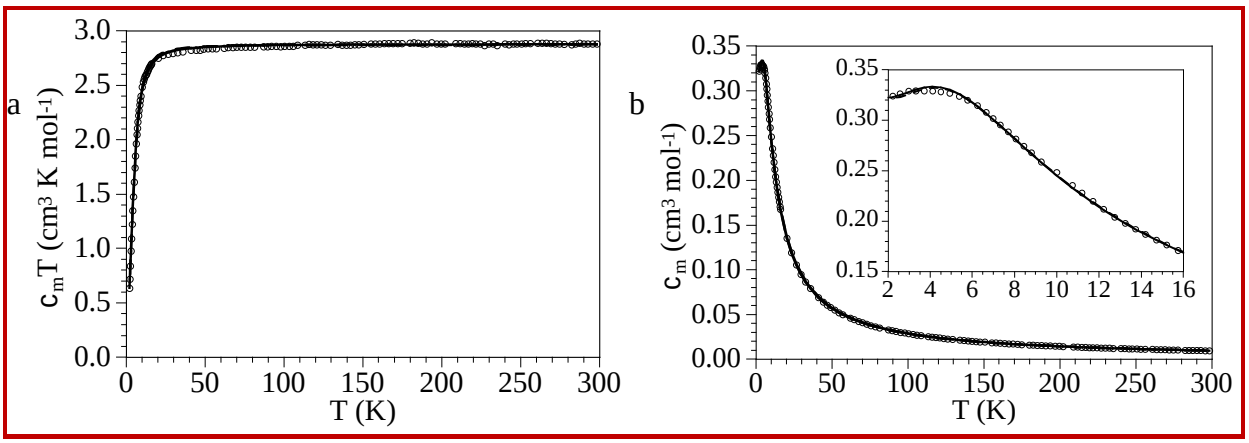

Figure 9. (a) $\chi_m T$ vs T plot and (b) χ_m vs T plot for compound **1**. Solid and dotted lines present the best fit to the models (see text).

This magnetic fitting to a monomer with a ZFS produces very satisfactory result and we have also considered the possible presence of a weak intermolecular interaction through the π-π and H-bonding interactions. The appearance of a maximum in the χ_m *vs*. T plot (Figure 7b) at very low temperature confirmed such weak intermolecular coupling. Thus, if we include the presence of a weak intermolecular coupling with the mean field approximation (zJ) we can replicate even better the magnetic properties of compound **1** with g = 1.959, zJ = -0.03 cm^{-1} and |D| = 1.23 cm^{-1} with a residual of 0.0158 (solid line in Figure 7). In a similar way, the interaction between the Mn(III) centres is weak and antiferromagnetic, since usually π···π interactions give rise to weak

couplings [52-57]. On the other side, the D value found for the isolated Mn(III) center is quite low and is in the typical range observed (-3.8 to +3.1 cm^{-1}) for mononuclear Mn(III) ions [58].

A further confirmation of the presence of a very weak antiferromagnetic intermolecular interaction is provided by the isothermal magnetization at 2 K of compound **1** (Figure 10a). This measurement shows a sigmoidal shape with a maximum slope at *ca*. 2.0 T, as can be found in the derivative of the M *vs*. H (Figure 10b) which suggests that **1** is a metamagnet with a critical field of *ca*. 2.0 T at 2 K (i.e., the weak antiferromagnetic coupling is cancelled out by applying a high magnetic field, above *ca*. 2.0 T, giving rise to a ferromagnetic coupling). Therefore, we can confirm that there is a very weak antiferromagnetic intermolecular interaction when the applied magnetic field is below *ca*. 2.0 T.

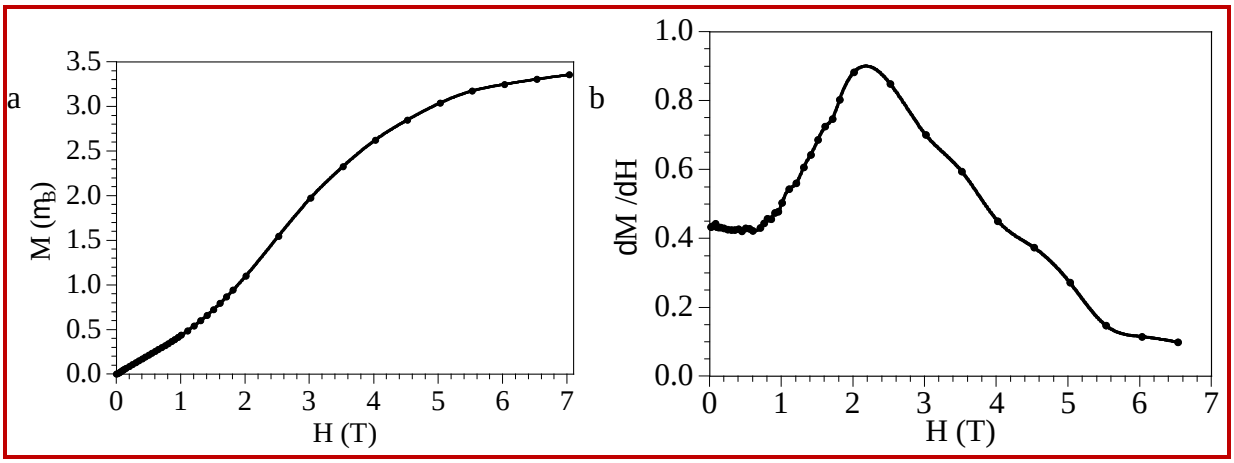

Figure 10. (a) Isothermal magnetization at 2 K for compound **1**. (b) Derivative of the magnetization as a function of the magnetic field showing a broad maximum at *ca*. 2.0 T.

A further confirmation of this metamagnetic behaviour is represented by the thermal variation of χ_m for different applied fields (Figure 11). As can be seen, χ_m shows a maximum at very low temperatures when the applied field is below *ca*. 2.0 T and the maximum disappears for fields above 2.0 T, in concurrence with the isothermal magnetization measurements.

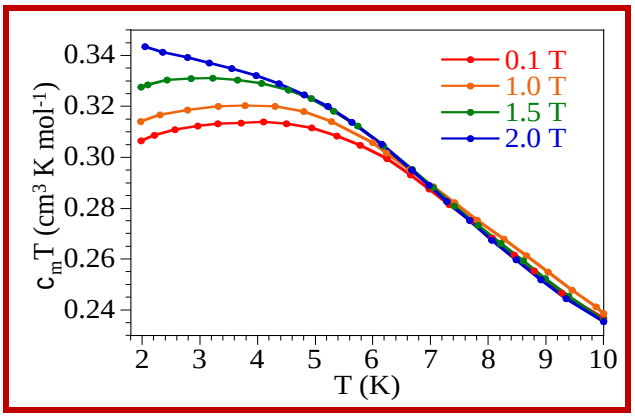

Figure 11. Thermal variation of χ_m for compound **1** in the low temperature region with different applied fields.

6.3.6 Magnetic properties of complex 2

The room temperature value of χ_mT per formula unit (i.e., three Mn(III) ions and a Fe(II) ion) is *ca*. 9.0 cm^3 K mol^{-1} (Figure 12a). This value is close to the expected one for three S = 2 Mn(III) with g = 2 and indicates that the Fe(II) ion is a diamagnetic low spin Fe(II) ion (as expected for a Fe(II) coordinated to six strong field CN ligands). When the temperature is lowered, χ_mT stays the same up to ca. 25 K and underneath this temperature it shows a progressive decrease to *ca*. 1.1 cm^3 K mol^{-1} at 2 K (inset in Figure 12a). This behaviour suggests the presence of a weak antiferromagnetic interaction in compound **2** and/or the presence of a zero field splitting in the Mn(III) ions. As observed in compound **1**, the thermal variation of χ_m shows a maximum at *ca*. 6 K(Figure 12b) suggesting that there is also a very weak antiferromagnetic coupling in compound **2**.

A critical observation at the structure of compound **2** indicates that the Mn(III) monomeric units are well isolated but each Mn_2Fe trimer presents two short inter-trimer $\pi\cdots\pi$ interactions and two H-bonds with its two neighbouring trimers to generate a regular chain of trimers (Figure 4). Nevertheless, since the Fe(II) ions are diamagnetic, the chains can be considered from the magnetic

point of view as isolated Mn(III)-Mn(III) dimers. Note that since the two C_g-C_g distances and the H-bonding parameters are very similar in both chains (see Tables S5 and S6), we can consider that the Mn(III)-Mn(III) coupling is the same in both chains.

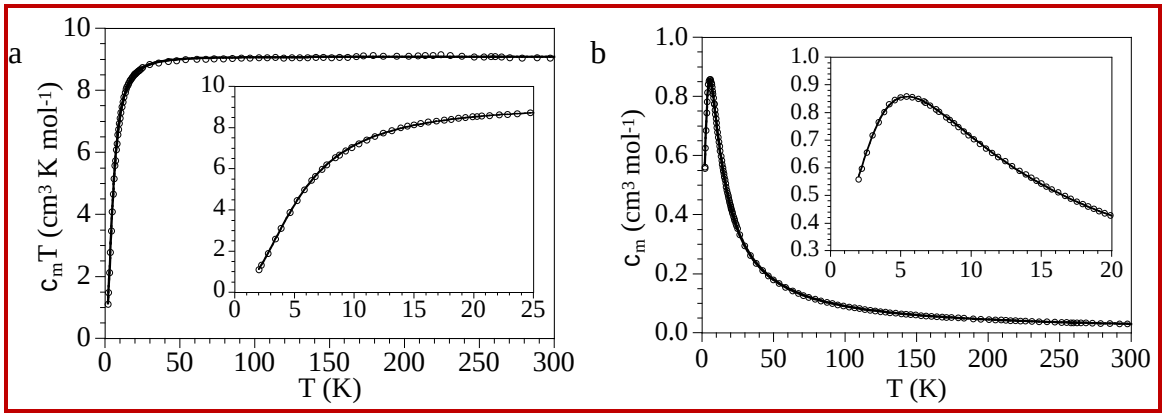

Figure 12. Thermal variation of χ_mT (a) and χ_m (b) for compound **2**.

Accordingly, we have fit the magnetic properties to a model of an isolated S = 2 ion with a ZFS plus a S = 2 dimer with a weak antiferromagnetic coupling (J) and a ZFS utilizing the program PHI.[43] In order to decrease the quantity of adjustable parameters we have assumed that both Mn(III) dimers (Mn1-Mn1 and Mn2-Mn2) have the same coupling constant (J) and that all the Mn(III) ions have the same g and D values. This model satisfactorily reconstructs the magnetic properties of compound **2** in the entire temperature range with g = 2.009, |D| = 1.21 cm^{-1} and J = -0.42 cm^{-1} with a residual of 0.1355 (solid lines in Figure 10; the exchange hamiltonian is written as $H = -JS_1S_2$). As observed for compound **1**, the magnetic interaction between the Mn(III) centres is weak and antiferromagnetic, as expected for $\pi\cdots\pi$ interactions.[44-49] Again the D value found is low and is within the typical range observed (-3.8 to +3.1 cm^{-1}) for Mn(III) ions.[50]

An additional confirmation of the presence of an antiferromagnetic interaction in compound **2** is also given by the isothermal magnetization at 2 K (Figure 13a). This plot shows a sigmoidal

shape with a maximum slope at *ca*. 2.5 T as deduced from the maximum of the derivative (Figure 13b), suggesting that compound **2** also behaves as a metamagnet.

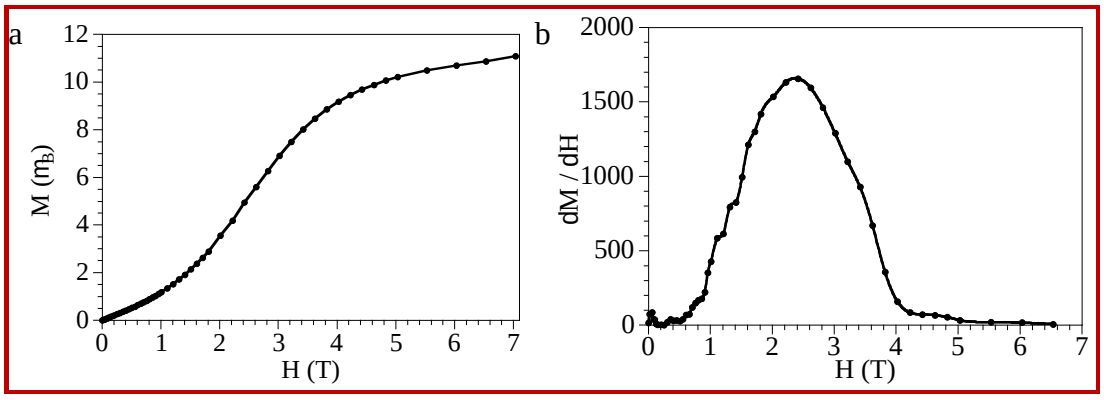

Figure 13. (a) Isothermal magnetization at 2 K for compound **2**. (b) Derivative of the M as a function of H showing a broad maximum at *ca*. 2.5 T.

To confirm this metamagnetic behaviour we have also measured the magnetic susceptibility with different applied fields in the low temperature region (Figure 14). These measurements show the presence of a maximum in χ_m at low temperatures (around 6 K) that shifts to lower temperatures as the applied field increases and finally disappears for fields above 2.5 T, confirming that compound **2** is a metamagnet with a critical field of *ca*. 2.5 T.

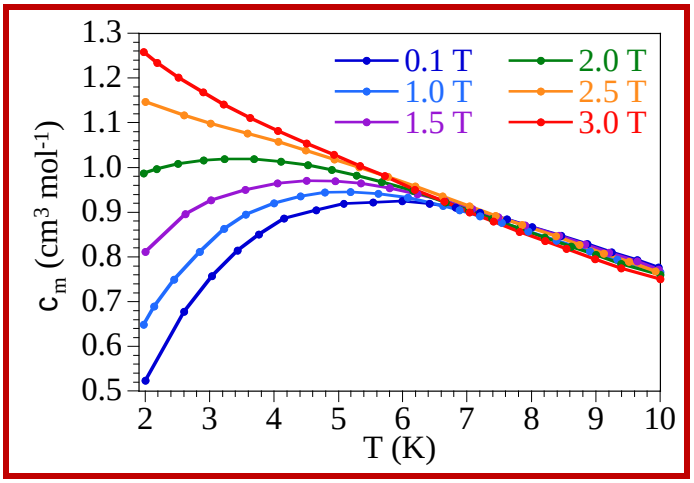

Figure 14. Thermal variation of χ_m for compound **2** in the low temperature region with different applied fields.

6.4 Conclusions

In this work, we have reported a unique example of an inorganic reaction where a metal-ligand bond undergoes dissociation assisted by the formation of intermolecular π-π and H-bonding interactions. DFT calculations at the PBE1PBE/def2-TZVP level confirm that the summation of the energies of all these intermolecular interactions overpasses the metal-ligand one. This fact has allowed us to prepare a trimeric molecular metamagnet from a monomeric metamagnetic precursor for the first time.

Thus, we present the formation of a novel Schiff base ligand (H_2L) and the use of this ligand to prepare a Mn(III) monomer that shows a very weak antiferromagnetic coupling through intermolecular π-π and H-bonding interactions. This weak antiferromagnetic interaction can be cancelled out by the application of an external magnetic field, giving rise to a metamagnetic behaviour with a critical field of ca. 2.0 T at 2 K. Combination of this Mn(III) monomer with $[Fe(CN)_6]^{4-}$ generates a Mn_2Fe trimer where the diamagnetic $[Fe(CN)_6]^{4-}$ complex acts as a linear connector between two monomeric Mn(III) complexes. These anionic trimers crystallize with a cationic Mn(III) monomer (closely related to the precursor monomer) in a 1:1 co-crystal to form compound **2**. The trimers are further assembled by π-π and H-bonding interactions to build 1D supramolecular chains. Compound **2** also behaves as a metamagnet with a slightly higher critical field of *ca*. 2.5 T at 2 K. The magnetic behaviour of both compounds has been reproduced with a simple model of a S = 2 monomer with a ZFS and a very weak intermolecular interaction (for **1**) and a S = 2 monomer with ZFS plus an antiferromagnetically coupled S = 2 dimer with a ZFS (for **2**). Finally, we hope that such a study will help to analyse several biological processes like oxygen transport by haemoglobin and myoglobin, different metallo-enzymatic catalysis etc.

References

[1] J. T. Nicholas, *PNAS* ,**2002**, 99, 4805-4809.

[2] G. R. Desiraju, *Nature*, **2001**, 412, 397-400.

[3] M. L. Merlau, M. D. P. Mejia, S. T. Nguyen and J. T. Hupp, *Angew. Chem. Int. Ed.*, **2001**, 40, 4239-4242.

[4] D. H. Leung, D. Fiedler, R. G. Bergman and K. N. Raymond, *Angew. Chem. Int. Ed.*, **2004**, 43, 963-966.

[5] C. H. Jun, *Chem. Soc. Rev.*, **2004,** 33, 610-618.

[6] L. Annamalai, Y. Liu and P. Deshlahra, *ACS Catal.*, **2019**, 9, 10324-10338.

[7] N. Della Ca', M. E. M. Fontana and M. Catellani, *Acc. Chem. Res.*, **2016**, 49, 1389-1400.

[8] K. An and G. A. Somorjai, G. A. *ChemCatChem.* **2012**, 4, 1512-1524.

[9] I**.** Lee, F. Delbecq, R. Morales, M. A. Albiter and F. Zaera, *Nature Materials*, **2009**, 8, 132-138.

[10] B. Pinter, V. V. Speybroeckb, M. Waroquierb, P. Geerling and F. D. Proft, *Phys. Chem. Chem. Phys.*, **2013,** 15, 17354-17365.

[11] J. L. Shaw, C. R. Dockery, S. E. Lewis, L. Harris and R. Bettis, *J. Chem. Educ.* **2009**, 86, 1416-1418.

[12] R. G. Pearson, *J. Chem. Educ.* **1968**, 45, 643-648.

[13] C. Cárdenas and P. W. Ayers, *Phys. Chem. Chem. Phys.* **2013**, 15, 13959-13968.

[14] G. Yu, K. Jie and F. Huang, *Chem. Rev.*, **2015**, 115, 7240-7303.

[15] T. Haino, *Polymer Journal.*, **2013**, 45, 363–383.

[16] Li. Chunju, *Chem. Commun.* **2014**, 50, 12420-12433.

[17] B**.** Roy, T. Noguchi, Y. Tsuchiya, D. Yoshihara, T. Yamamoto and S. Shinkai, *J. Mater. Chem. C*, **2015**, *3*, 2310-2318.

[18] D. Fiedler, D. H. Leung, R. G. Bergman and K. N. Raymond, *Chem. Res.* **2005**, 38, 349-358.

[19] X. M. Zhang, Y. Q. Wang, K. Wan, E. Q. Gao and C. M. Liu, *Chem. Commun*. **2011**, 47, 1815-1817.

[20] P. S. Mukherjee, S. Dalai, E. Zangrando, F. Lloretc and N. R. Chaudhuri, *Chem. Commun*. **2001**, 1444-1445.

[21] Y. L. Zhou, M. C. Wu, M. H. Zeng and H. Liang, *Inorg. Chem*. **2009**, 48, 10146-10150.

[22] J. Boeckmann, M. Wriedt and C. Nather, *Chem. Eur. J.* **2012**, 18, 5284-5289.

[23] W. W. Sun, Y. C. Tian, X. H. Jing, Y. Q. Wang and E. Q. Gao, *Chem. Commun*. **2009**, 31, 4741-4743.

[24] N. Motokawa, S. Matsunaga, S. Takaishi, H. Miyasaka, M. Yamashita and K. R. Dunbar, *J. Am. Chem. Soc*. **2010**, 132, 11943-11951.

[25] K. G. Sandeman, *Scr. Mater*. **2012**, 67, 566-571.

[26] M. P. Annaorazov, K. A. Asatryan, G. Myalikgulyev, S. A. Nikitin, A. M. Tishin and A. L. Tyurin, *Cryogenics*. **1992**, 32, 867-872.

[27] M. H. Zeng, W. X. Zhang, X. Z. Sun and X. M. Chen, *Angew. Chem. Int. Ed*. **2005**, 44, 3079–3082.

[28] S. Naiya, S. Biswas, M. G. B.Drew, C. J. Gomez-García and A. Ghosh, *Inorg. Chem*. **2012**, 51, 5332-5341.

[29] H. Miyasaka, R. Cle´rac, K. Mizushima, K. I. Sugiura, M. Yamashita, W. Wernsdorfer, and C. Coulon, *Inorg. Chem*. **2003**, 42, 8203-8213.

[30] R. Clérac, H. Miyasaka, M. Yamashita and C. Coulon, *J. Am. Chem. Soc.* **2002**, 124, 12837-12844.

[31] H. Miyasaka, R. Clerac, W. Wernsdorfer, L. Lecren, C. Bonhomme, K. Sugiura and M. Yamashita, *Angew. Chem. Int. Ed.* **2004**, 43, 2801-2805.

[32] Z. Lü, M. Yuan, F. Pan, S. Gao, D. Zhang and D. Zhu, *Inorg. Chem.* **2006**, 45, 3538-3548.

[33] S. S. Tandon, L. K. Thompson, M. E. Manuel and J. N. Bridson, *Inorg. Chem*. **1994**, 33, 5555-5570.

[34] S. Naiya, M. G. B. Drew, C. Diaz, J. Ribas and A. Ghosh, *Eur. J. Inorg. Chem.* **2011**, 32, 4993-4999.

[35] T. T. Wang, S. S. Bao, J. Huang, Y. Z. Li and L. M. Zheng, *Dalton Trans.*, **2013**, 42, 1842-1847.

[36] M. Yuan, S. Gao, H. L. Sun and G. Su, *Inorg. Chem.* **2004**, 43, 8221-8223.

[37] G. A. Bain and J. F. Berry, *J. Chem. Educ.* **2008**, 85, 532-536.

[38] Gaussian 09, Revision A.02, M. J. Frisch, G. W. Trucks, H. B. Schlegel, G. E. Scuseria, M. A. Robb, J. R. Cheeseman, G. Scalmani, V. Barone, G. A. Petersson, H. Nakatsuji, X. Li, M. Caricato, A. V. Marenich, J. Bloino, B. G. Janesko, R. Gomperts, B. Mennucci, H. P. Hratchian, J. V. Ortiz, A. F. Izmaylov, J. L. Sonnenberg, D. Williams-Young, F. Ding, F. Lipparini, F. Egidi, J. Goings, B. Peng, A. Petrone, T. Henderson, D. Ranasinghe, V. G. Zakrzewski, J. Gao, N. Rega,

G. Zheng, W. Liang, M. Hada, M. Ehara, K. Toyota, R. Fukuda, J. Hasegawa, M. Ishida, T. Nakajima, Y. Honda, O. Kitao, H. Nakai, T. Vreven, K. Throssell, J. A. Montgomery, Jr., J. E. Peralta, F. Ogliaro, M. J. Bearpark, J. J. Heyd, E. N. Brothers, K. N. Kudin, V. N. Staroverov, T. A. Keith, R. Kobayashi, J. Normand, K. Raghavachari, A. P. Rendell, J. C. Burant, S. S. Iyengar, J. Tomasi, M. Cossi, J. M. Millam, M. Klene, C. Adamo, R. Cammi, J. W. Ochterski, R. L. Martin, K. Morokuma, O. Farkas, J. B. Foresman, and D. J. Fox, *Gaussian*, Inc., Wallingford CT, **2016**.

[39], R. F. W. Bader, *J. Phys. Chem. A.* **1998**, 102, 7314-7323.

[40] T. A. Keith, AIMAll (Version 13.05.06), TK Gristmill Software, Overland Park, KS, **2013**.

[41] G. M. Sheldrick, *SHELXS 97*, Program for Structure Solution, University of Gottingen, Germany, **1997**.

[42] G.M. Sheldrick, *SHELXL 97*, University of Gottingen, Germany, Program for Crystal Structure Refinement, **1997**.

[43] A. L. Spek, *J. Appl. Crystallogr.* **2003**, 36, 7-13.

[44] L. J. Farrugia, *J. Appl. Crystallogr.* **1997**, 30, 565.

[45] L. J. Farrugia, *J. Appl. Crystallogr.* **1999**, 32, 837-838.

[46] M. J. Białek, J. K. Zaręba, J. Janczak and J. Zoń, *Cryst. Growth Des*. **2013**, 13, 4039-4050.

[47] Mahmoudi, G.; Zaręba, J. K.; Gurbanov, A. V.; Bauzá, A.; Zubkov, F. I.; Kubicki, M.; Stilinović, V.; Kinzhybalo, V.; Frontera, A. *Eur. J. Inorg. Chem*. **2017**, *40*, 4763-4772.

[48] A. García-Raso, A. Terrón, A. López-Zafra, A. García-Viada, A. Barta, A. Frontera, J. Lorenzo, S. Rodríguez-Calado, E. M. Vázquez-López and J. J. Fiol, *New J. Chem*. **2019**, 43, 9680-9688.

[49] E. Espinosa, E. Molins and C. Lecomte, *Chem. Phys. Lett*. **1998**, 285, 170-173.

[50] M. V. Vener, A. N. Egorova, A. V. Churakov, V. G. Tsirelson, *J. Comput. Chem.* **2012**, 33, 2303-2309.

[51] N. F. Chilton, R. P. Anderson, L. D. Turner, A. Soncini, K. S. Murray, *J. Comput. Chem.* **2013**, 34, 1164-1175.

[52] A. Wojciechowska, J. Janczak, W. Zierkiewicz, P. Rytlewski, T. Rojek, M. Duczmal, *Mater. Chem. Phys.* **2019**, 228, 272-284.

[53] Y. Chi, J. Shi, H. Li, W. Wei, E. Cottrill, N. Pan, H. Chen, Y. Liang, L. Yu, Y. Zhang and C. Hou, **2013**, 42, 15559-15569.

[54] H. Li, S. Zhang, L. Xie, L. Yu and J. Shi, *J. Coord. Chem.* **2011**, 64, 1456-1468.

[55] Y. Chi, W. Wei, J. Shi, Y. Zhang and S. Liu, *J. Coord. Chem.* **2012**, 65, 2379-2390.

[56] M. Sutradhar, L. M. Carrella and E. Rentschler, *Polyhedron* **2012**, 38, 297-303.

[57] Y. Chi, L. Yu, J. Shi, Y. Zhang, T. Hu, G. Zhang, W. Shi and P. Cheng, *Dalton Trans.* **2011**, 40, 1453-1462.

[58] R. Boca, *Coord. Chem. Rev*. **2004**, 248, 757-815.

Chapter 7

Double dicyanamide decorated double phenoxide bridged Mn (III) dimer with single-molecule magnetic behaviour and bio-catalytic activity

7.1. Introduction

Among the transition metal ions, multinuclear manganese complexes have gained remarkable attention due to their potential applications in molecular magnetism [1-4] as well as their rich biochemistry [5-7] and versatile catalytic activities [8-10]. Large variety of ligands containing oxygen or nitrogen donor atoms like Schiff's bases, oxalato, carboxylato, azido, phenoxido/oxido, sulfato, dicyanamido, etc. are widely used to design and synthesize Mn-based complexes of different nuclearities and dimensionalities [11-17]. Moreover, high spin Mn^{III} -Schiff base complexes are extensively used as the basic building blocks for designing metal clusters due to their unique properties [18-21].

Due to its versatile coordination and bridging modes, quasi π-conjugated dicyanamide (dca^-) is one of the most widely employed bridging ligand in designing multinuclear and multidimensional metal complexes (Scheme 1). The nuclearity and architecture of dicyanamido bridged metal complexes exclusively depend upon the binding and bridging modes adopted by the dca^- ligand and metal:dca^- ratios [22-25]. From the literature survey, it is evident that, in presence of tetradentate Schiff base ligands, the use of dca^- at 1:1 Mn:dca^- ratio results in either different types of $\mu_{1,5}$-dca^- bridged 1D coordination polymers [26-29] or in discrete Mn^{III} complexes having terminal dca^- ligands [30]. In the present report, we have successfully synthesized a dimeric Mn^{III} complex $[Mn_2(L)_2(dca)_2]$ (**1**), having double terminal dca^- ligands, by taking Mn and dca^- in 1:2 ratio for the first time.

The double phenoxido bridged Mn^{III} -Schiff base dimeric complexes show both ferro- or antiferromagnetic couplings with large uniaxial anisotropy that may lead to single-molecule magnet behaviour (with and without an applied DC field) [31-37]. Miyasaka et al. have performed

a detailed investigation in order to find the origin of the magnetic properties of such dimers [38]. They have shown that the magnetic coupling depends on the Mn-O (bridging) bond distance. In most cases, when the Mn-O bond distance is within the range 2.40 - 2.70 Å, the dimers show ferromagnetic interactions, whereas below this range they show antiferromagnetic couplings and above 2.80 Å the magnetic interaction is almost negligible.

Catechol-oxidase is an important plant enzyme that catalyses the oxidation of a range of *o*-diphenols (catechols) and produces corresponding quinones having a significant role in disease resistance of higher plants [39]. Manganese ions are omnipresent in a large variety of naturally occurring redox enzymes because of their lower redox potentials [40-42]. In photosystem-II of plants and cyanobacteria a tetra-manganese cluster acts as an active site in catalytic oxidation of water to O_2 [43]. Therefore, Mn-based complexes are widely used to mimic the catechol-oxidase activity in presence of model substrates in order to examine the mechanism and factors of the enzyme catalysed oxidation of catechols [44-47].

In this context, herein we report synthesis, crystal structure, spectral behaviour, magnetic property and catalytic response of a dinuclear Mn^{III}-complex with a Schiff's base and dca^- ligands in 1:2 Mn:dca^- ratio. The dimeric Mn^{III} complex, with structural formula $[Mn_2(L)_2(dca)_2]$ (**1**) (H_2L = 2,2'-((1E,1'E) -(ethane-1,2-diylbis(azanylylidene))-bis(ethan-1-ylylidene)) diphenol) shows a rare assembly of double phenoxido bridges along with double terminal dca^- ligands. The magnetic properties of the complex reveal very weak antiferromagnetic interactions in it and, more interestingly, a field-induced single-molecule magnet behaviour thanks to the large magnetic anisotropy of the Mn^{III} ions. Complex **1** also exhibits solvent selective enzyme catechol oxidase-

like activity for the oxidation of the model substrate 3,5-di-tert-butylcatechol (3,5-DTBC) in presence of aerial oxygen.

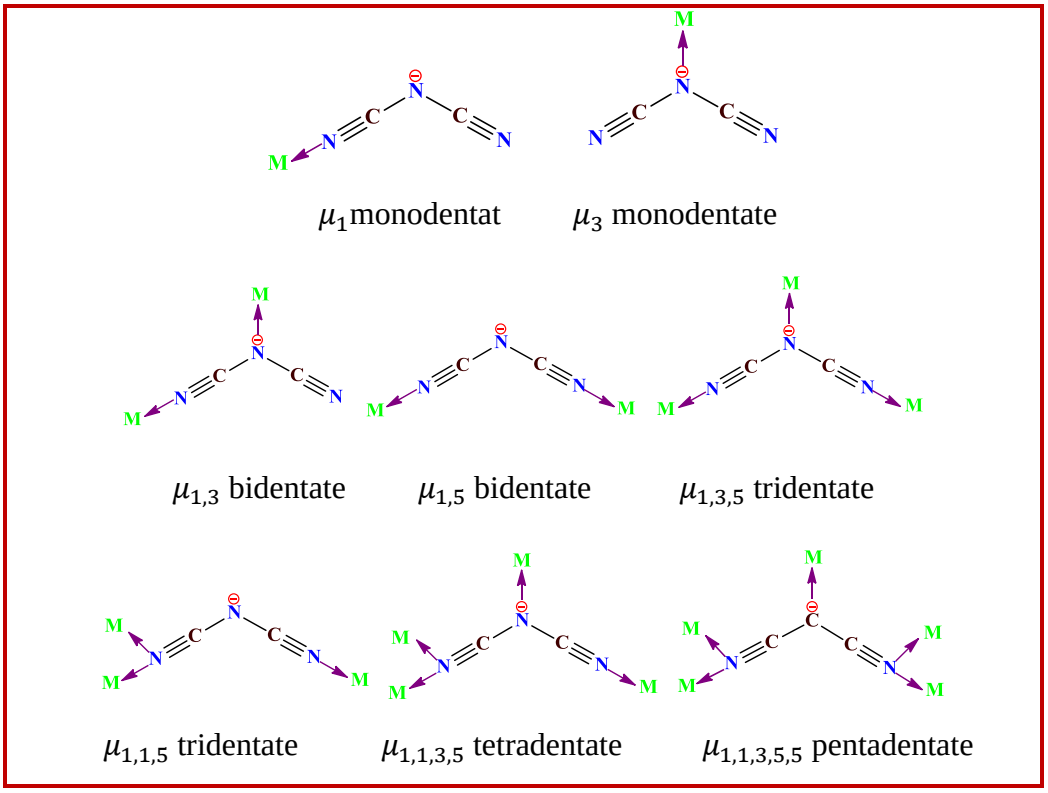

Scheme 1: Different coordination and bridging modes of the dicyanamide ligand

7.2. Experimental

7.2.1 Materials and methods

$MnCl_2 \cdot 4H_2O$ (99.9 %), 2-hydroxyacetophenone (98 %), sodium dicyanamide (96 %) and ethylenediamine (99.5 %) were obtained from Sigma Aldrich and used as received. Triethylamine and all other chemicals (AR grade) were obtained from Merck India and used as received. Elemental analysis (C, H, N) was performed by using a Perkin-Elmer 240C elemental analyser. A Nicolet Impact 410 spectrometer was used to record the FT-IR spectrum in the 400-4000 cm^{-1} range. Electronic absorption spectra were recorded in 10^{-4} (M) acetonitrile solutions using a Hitachi U-3501 spectrophotometer.

The cyclic voltametric measurement on complex **1** was carried out using Autolab/PGSTAT204 electrochemical workstation (Model Number: AUT204.S: 204 Potentiostat Galvanostat Module FRA32M.MAC204.S) at a scan rate of 50 mVs^{-1} within the potential range +1.50 to -1.50 V by taking 1.0×10^{-3} (M) of complex in acetonitrile solution deoxygenated by bubbling nitrogen gas. Further, 0.1 (M) tetrabutylammonium bromate (TBAB) was used as a supporting electrolyte. The working electrode was a glassy-carbon disk (0.32 cm^2) which was washed with absolute acetone and dichloromethane, polished with alumina solution and air-dried before each electrochemical run. The Ag/AgCl and platinum wire were used as reference and counter electrodes, respectively. The experiments were performed in standard electrochemical cells at 25 °C.

7.2.2 Synthesis of the Schiff base ligand (H_2L)

The Schiff base ligand (H_2L = 2,2'-((1E,1'E)-(ethane-1,2 diylbis(azanylylidene))-bis(ethan-1-yl-1-ylidene))diphenol) was synthesized by following a standard procedure.[2] 2-hydroxyacetophenone (272 mg) was refluxed with ethylenediamine (60 mg) at a 2:1 ratio in methanol (25 mL) during 1.5 h. The yellow crystalline solid that precipitated upon cooling the solution was collected by filtration, washed with diethyl ether, dried and used directly for the preparation of the complex. Yield: 264 mg (89 %). Anal. Calc. (%) for $C_{18}H_{20}N_2O_2$ (M = 296.3 g/mol): C, 72.9; H, 6.7; N, 9.4. Found: C, 72.8; H, 6.8; N, 9.0. Selected FT-IR bands (KBr pellet, cm^{-1}): ν(C=N) = 1654(s), ν(C-$O_{Phenolic}$) = 1260(s) and ν(O-H) = 3405(b).

7.2.3 Synthesis of $[Mn_2(L)_2(dca)_2]$ (1)

The Schiff base ligand H_2L has been synthesised by following standard procedure [48], detail of which has been provided in ESI file. The Schiff base ligand H_2L (297 mg, 1.0 mmol) was dissolved in 25 mL of a 1:1 methanol-acetonitrile mixture under boiling. The pH of the reaction

mixture was adjusted to 9 by dropwise addition of Et_3N. The $MnCl_2 \cdot 4H_2O$ (250 mg, 1.25 mmol) was dissolved in 5 mL of methanol by stirring and then added to the previous solution. The resulting solution was refluxed ~ 90 ºC for 2 hours. The reaction mixture was cooled to room temperature and sodium dicyanamide (224 mg, 2.5 mmol), dissolved in 2 mL of distilled water, was added to the previous reaction mixture and stirred for another 1.5 hours. The resulting light brown precipitate was filtered off and the deep brown filtrate was kept in undisturbed condition for crystallisation at room temperature. Brown block-shaped single crystals suitable for single crystal X-ray diffraction were obtained after two weeks. The crystals were filtered and air-dried. Yield: 1.323 g (74 %). Anal. Calc. (%) for $C_{40}H_{36}Mn_2N_{10}O_4$ (M = 830.67 g/mol): C, 57.78; H, 4.33 and N, 16.85 %. Found: C, 57.8; H, 4.3 and N, 16.9 %. Phase purity was confirmed by the X-ray powder diffractogram that shows a good agreement with the simulated one from the single crystal X-ray structure (Figure 1).

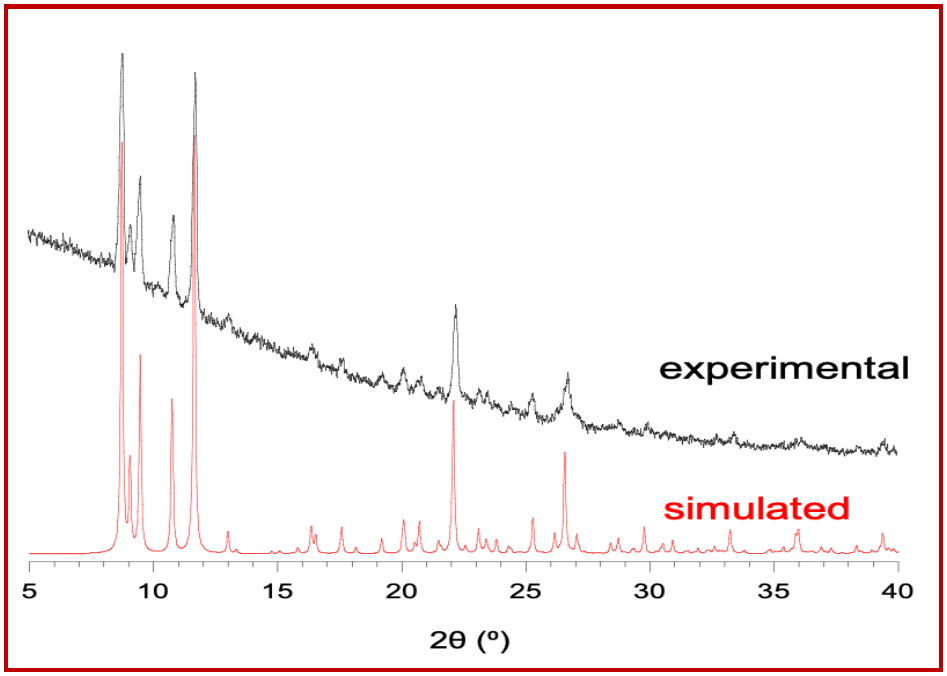

Figure 1. Experimental and simulated X-ray powder diffractograms for compound **1**

7.2.4 Magnetic measurements

Variable temperature magnetic susceptibility measurements were carried out in the temperature range 2-300 K with an applied magnetic field of 0.1 T (1000 Oe) on a polycrystalline sample with a mass of 13.598 mg using a Quantum Design MPMS-XL-7 SQUID magnetometer. The AC susceptibility measurements were performed on the same sample at 2.0 K with different applied dc fields (in the range 0-4300 Oe) with a field of 8 Oe oscillating in the range 10-10000 Hz using a Quantum Design PPMS equipment. From the plot of the relaxation time *vs*. the dc field (Fig. S6, ESI file), we determined an optimum dc field of 0.2 T (2000 Oe). Accordingly, we performed the frequency sweep from 10 to 10000 Hz at different temperatures in the range 2 - 4 K with an applied dc field of 0.2 T. The susceptibility data were corrected for the sample holder previously measured using the same conditions and for the diamagnetic contribution of the sample as deduced by using Pascal´s constant tables [49].

7.2.5 Crystallographic data collection and refinement

Bruker SMART diffractometer equipped with a graphite monochromator and Mo-K_α (λ = 0.71073 Å) radiation were employed to collect the single crystal X-ray crystallographic data of compound **1**. Unit cell parameters were determined by using the APEX2 [50] program. The SAINT [50] program was used for data reduction and correction or absorption was made using the SADABS [50] program. The structure was solved by the Patterson method using the SHELXL-2014[51] program embedded in WINGX software package [52]. Subsequent difference Fourier synthesis and least-square refinement revealed the positions of the non-hydrogen atoms. Non-hydrogen atoms were refined with independent anisotropic displacement parameters. Hydrogen atoms were put in idealized positions and their displacement parameters were fixed to be 1.2 times larger than those of the attached non-hydrogen atoms. These results have been embedded in the

CIF file. All Figures were drawn by using PLATON, ORTEP and Crystal Maker software [53,54]. Data collection and structure refinement parameter and crystallographic data for the complex are given in Table 1.

Table 1. Crystallographic data and refinement parameters of the complex **1**

Crystal data	
Formula	$C_{40}H_{36}Mn_2N_{10}O_4$
Formula weight	830.67
Crystal system	Triclinic
Space group	*P*-1 (#2)
a (Å)	8.6221(15)
b (Å)	10.8616(19)
c (Å)	11.741(2)
α (º)	64.798(5)
β (º)	73.308(6)
γ (º)	88.199(6)
V(Å^3)	947.7(3)
Z	1
ρ_{calc} (g/cm^3)	1.455
μ (Mo Kα) (mm)	0.723
F(000)	428
Crystal size (mm^3)	0.20 x 0.16 x 0.12
T (K)	293
$\theta_{min-max}$ (°)	2.0-27.2
Total data	27641
Unique Data	4178
R_{int}	0.0667
Observed data [I > 2σ(I)]	3004
N_{par}	265
R	0.0790
wR_2[a]	0.2167
G.O.F	1.052
Largest Peak/hole [e/Å^3]	0.710/-0.989

7.3. Result and Discussion

7.3.1 Synthesis

The N_2O_2-donor based tetradentate Schiff base ligand (H_2L) has been synthesized by the condensation through refluxing the mixture of 2-hydroxyacetophenone and ethylenediamine in a 2:1 ratio in methanol (Scheme 2). The synthesis of the dimeric Mn^{III} complex has been performed in a simple one-pot reaction by refluxing the ligand (H_2L) with $MnCl_2 \cdot 4H_2O$ at pH = 9 in a 1:1 mixture of methanol-acetonitrile, followed by the addition of an aqueous solution of sodium dicyanamide at room temperature (Scheme 2). It is noteworthy that this reaction is performed in open air at pH = 9, as a result the Mn^{II} ions are easily oxidized to Mn^{III} by atmospheric O_2 during the initial reaction with H_2L.

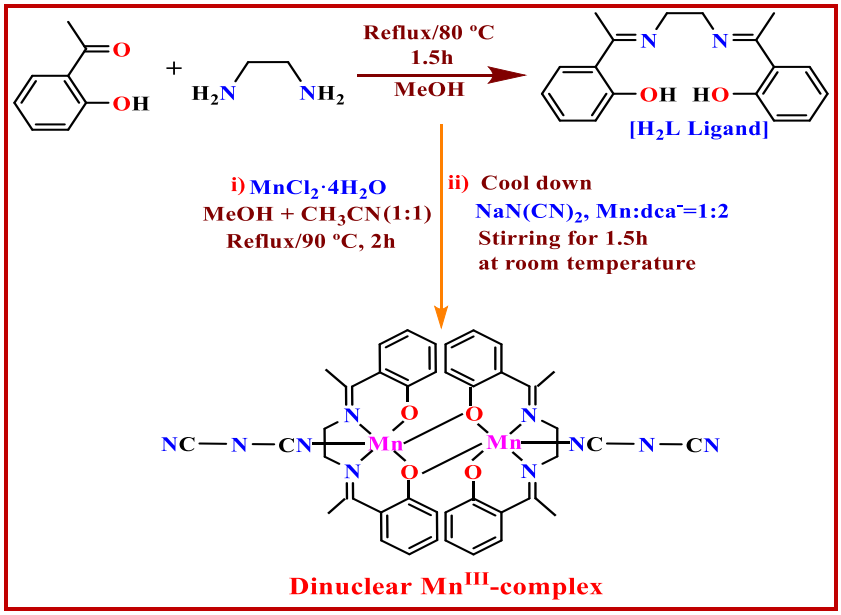

Scheme 2. Synthesis of the H_2L ligand and of the dimeric Mn^{III} complex **1**.

7.3.2 Molecular and supramolecular structure of Complex 1

The single crystal X-ray diffraction analysis reveals that complex **1** crystallizes in the triclinic *P*-1 space group and is a centrosymmetric dimeric neutral metal complex. The asymmetric

unit contains one Mn^{III} ion, one L^{2-} ligand and one dca^{-} ligand (Figure 2). Two such neighbouring asymmetric units are connected by double phenoxido bridges through O1 atoms to form the centrosymmetric dimer $[Mn_2(L)_2(dca)_2]$ (Figure 2). The Mn ions present an elongated octahedral geometry with the four equatorial positions occupied by two imine N donor atoms (N1 and N2) of the Schiff base ligand and two oxygen atoms (O1 and O2) of the deprotonated hydroxyl groups of the ligand. One of the axial coordination sites is occupied by a nitrogen atom (N5) of the dicyanamide ligand whereas the other is occupied by the O1 atom of the neighboring Mn-Schiff base moiety. The two equatorial Mn-O bonds (Mn1-O2 = 1.853(3) Å and Mn1-O1 = 1.914(3) Å) are shorter in length than the Mn-N ones (Mn1-N1 = 1.989(4) Å and Mn1-N2 = 2.002(4) Å). All these equatorial bond distances are shorter than the axial ones: Mn1-O1* = 2.388(3) Å and Mn1-N5 = 2.199(5) Å, as expected for a Mn^{III} ion with Jahn-Teller distortion. All the *cisoid* and *transoid* angles are in the range of 78.88(12) - 96.53(15)º and 166.02(15) - 176.41(13)º, respectively. All the bond lengths and angles around the Mn center are listed in Table 2 and are similar to those found in other similar Mn^{III} dimers with phenoxido bridges and Schiff base ligands [55-57].

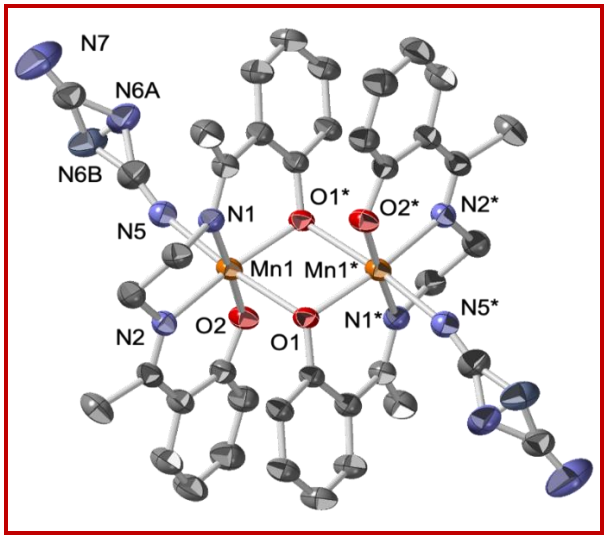

Figure 2. View of the structure of **1** with the labelling scheme around the Mn^{III} centres. H atoms have been omitted for clarity. Ellipsoids are drawn at 30 % probability.

Table 2. Selected coordination bond lengths (Å) and bond angles (°) for complex **1**.

Bond distances (Å)			
Atoms	**Distance (Å)**	**Atoms**	**Distance (Å)**
Mn1-O1	1.914(3)	Mn1-N2	2.002(4)
Mn1-O2	1.853(3)	Mn1-N5	2.199(5)
Mn1-N1	1.989(4)	Mn1-O1*	2.388(3)
Bond angles (º)			
Atoms	**Angle (º)**	**Atoms**	**Angle (º)**
O1-Mn1-O2	95.22(14)	O1*-Mn1-O2	92.48(13)
O1-Mn1-N1	87.98(19)	N1-Mn1-N2	84.88(16)
O1-Mn1-N2	166.02(15)	N1-Mn1-N5	88.50(16)
O1-Mn1-N5	96.53(15)	O1*-Mn1-N1	86.52(13)
O1-Mn1-O1*	78.88(12)	N2-Mn1-N5	95.29(16)
O2-Mn1-N1	176.41(13)	O1*-Mn1-N2	88.68(13)
O2-Mn1-N2	91.64(15)	O1*-Mn1-N5	173.33(13)
O2-Mn1-N5	92.75(16)	Mn1-O1-Mn1*	101.12(12)

* = 1-x, 1-y, 1-z

The doubly deprotonated Schiff base ligand, L^{2-} acts as a tetradentate N_2O_2 chelating ligand that occupies the four equatorial positions of the Mn^{III} ion. Additionally, the O1 atom also connects to the neighboring Mn^{III} ion, generating the Mn_2O_2 central unit with a double phenoxido bridge. The dicyanamide anions act as monodentate terminal ligands and extend on both sides of the dimer (Figure 2).

The dimer is further stabilized by two intradimer π···π interactions between the two Schiff base ligands (Figure 3). The dimers are connected by C-H···N hydrogen bonds involving the two non-coordinated N atoms of the dca^- ligands, to form a 2D supramolecular lattice plane parallel to the [*-1 2 2*] plane (Figure 4). Additionally, there are interdimer C-H···π interactions that generate

chains along the *b* axis (Figure 5). All the structural parameters of the hydrogen bonds and π-interactions are summarized in Tables 3-4. Interestingly, complex **1** can be considered as a fragment of a Mn^{III} chain reported by Ghosh et al., formulated as $[Mn_2(L)_2(dca)]ClO_4 \cdot CH_3CN$ (**2**, CCDC code = OHASIB) where double phenoxido bridged Mn^{III} dimers are connected by $\mu_{1,5}$-dca^- bridges (Figure 6) [29].

Table 3. Hydrogen bond dimensions of complex **1**.

D-H···A	D-H/(Å)	H···A (Å)	D···A/(Å)	< D-H···A (º)
C9-H9B···N6B	0.97	2.602	3.494	153
C37-H37C···N7	0.96	2.699	3.383	129

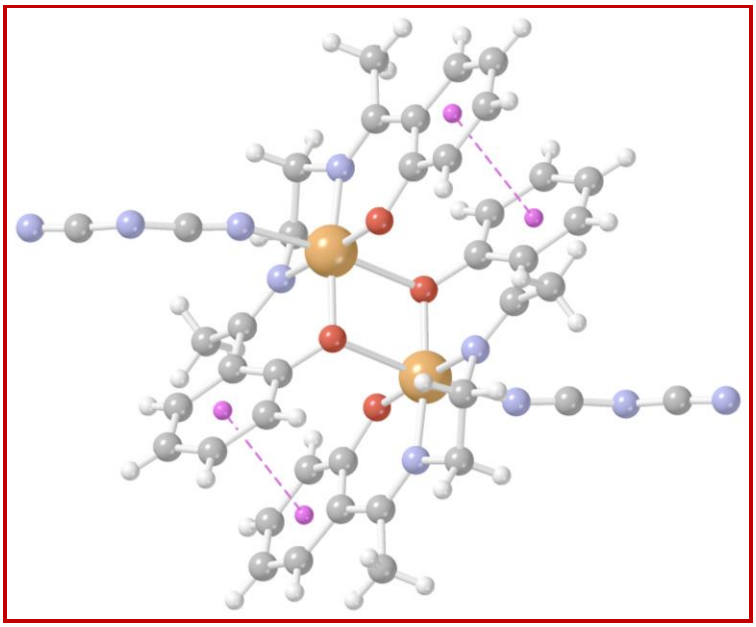

Figure 3. Dimer formation is also stabilized by intradimer π···π interactions (shown as pink dotted lines connecting the ring centroids, C_g). Colour code: C = grey, H = white, Mn = orange, N = blue, O = red, C_g = pink.

Table 4. π-interaction dimensions in complex **1**.

π···π interactions				
$R_i \cdots R_j$	Symmetry	Distance between ring centroids/(Å)	R_i-Perp (Perpendicular distance $R_i \cdots R_j$)/(Å)	α (Dihedral Angle between Planes (°)
$R_1 \cdots R_2$	1-x, 1-y, 1-z	4.031(10)	3.835(4)	21.8(4)
C-H···π interactions				
C-H···R_i	Symmetry	H···R_i (Å)	C-H···R_i (°)	C···R_i (Å)
C38-H38B···R_2	1-x, 1-y, 1-z	3.131(12)	129.6	3.82(2)

R_1: C1-C2-C3-C4-C5-C6; R_2: C11-C12-C13-C14-C15-C16.

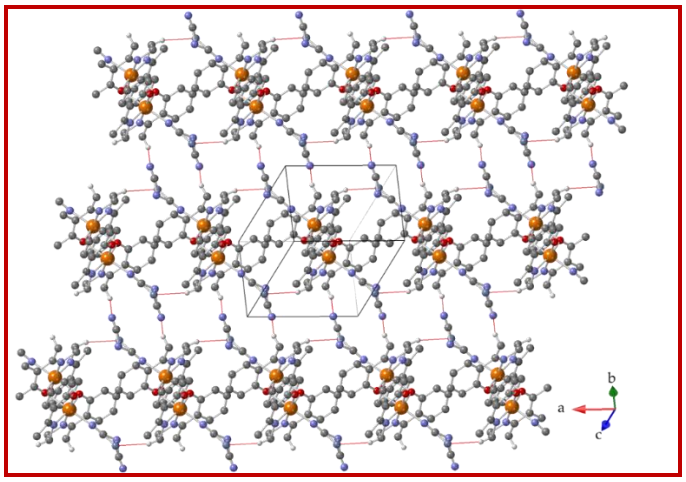

Figure 4. 2D supramolecular lattice formed by C-H···N hydrogen bonding interactions in **1** (shown as red thin lines). H atoms (except H9B and H37C) have been omitted for clarity.

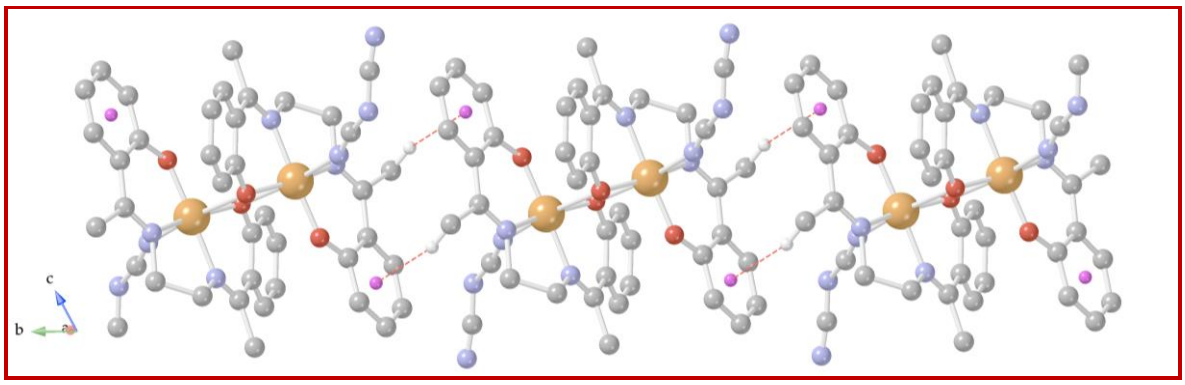

Figure 5. Formation of supramolecular chains through double C-H···π interactions along the *b* axis (showed as red dotted lines). Colour code: C = grey, H = white, Mn = orange, N = blue, O = red, C_g = pink. H atoms (except H12C) have been omitted for clarity.

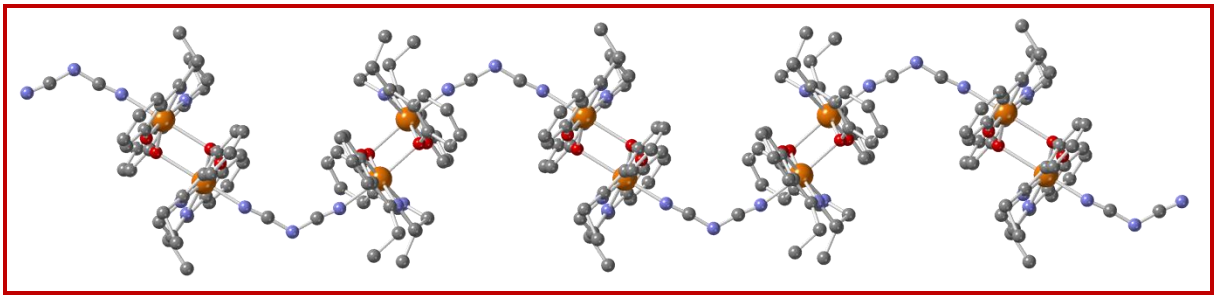

Figure 6. Structure of compound OHASIB showing the alternating chains with double phenoxido and $\mu_{1,5}$-dca$^-$ bridges connecting the Mn(III) ions. Colour code: C = grey, H = white, Mn = orange, N = blue, O = red.

7.3.3 Electronic absorption spectra

The electronic absorption spectrum of complex **1** has been recorded in acetonitrile (Figure 7). The spectrum shows a very low intensity single absorption band at 670 nm (inset in Figure 7) that can be attributed to a d-d transition in the complex which is consistent with a distorted octahedral geometry around the Mn^{III} ion. The LMCT ($PhO \rightarrow Mn^{III}$) band is observed at 454 nm ($\varepsilon = 2515\ M^{-1}cm^{-1}$). There are also two bands in the UV region at 240 nm ($\varepsilon = 21667\ M^{-1}cm^{-1}$) and 285 nm ($\varepsilon = 10205\ M^{-1}cm^{-1}$) appeared due to intra ligand π-π^* and n-π^* transitions.

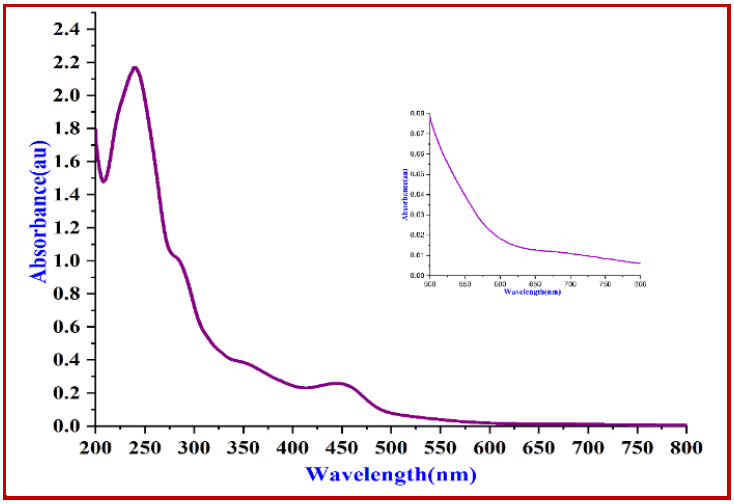

Figure 7. Absorption spectrum of the complex (10^{-4} M) in acetonitrile solution.

In the FT-IR spectrum of complex **1** (Figure 8), three sharp peaks at 2273, 2152 and 2216 cm^{-1} are obtained because of the asymmetric, symmetric and symmetric + asymmetric stretching of the C≡N bonds of the dicyanamide ligands, respectively. The band at ν = 1587 cm^{-1} has been observed due to the C=N stretching of immine bond of the Schiff's base ligand. A sharp peak at 1297 cm^{-1} can be attributed to the C-$O_{phenolic}$ stretching. The ν(Mn-O) and ν(Mn-N) are located at 601 and 451 cm^{-1}, respectively.

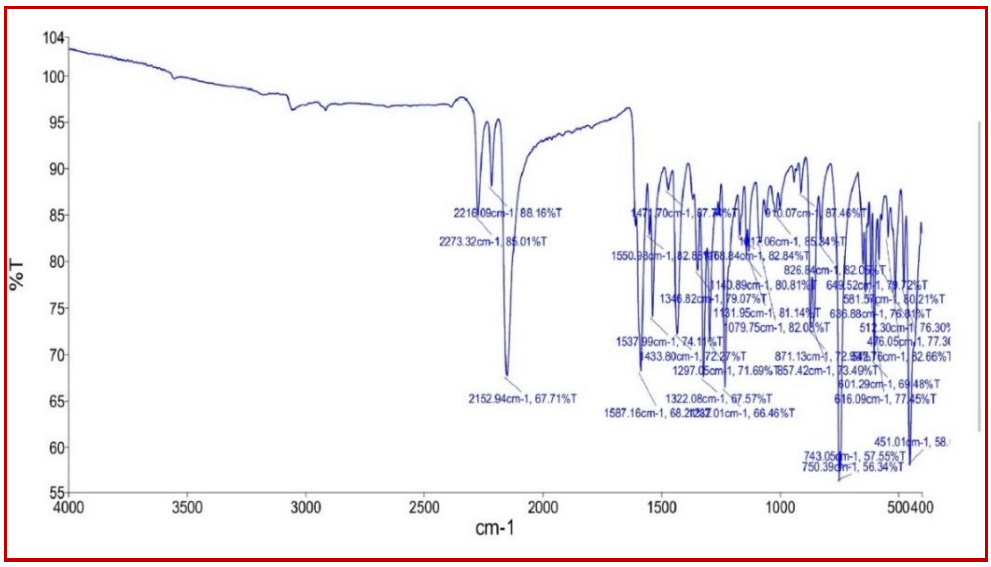

Figure 8. IR spectrum of the complex **1**

7.3.4 Cyclic voltametric study

The study of the electrochemical properties of a metal complex is important to assess its capability to mimic the functionality of metalloenzymes. The electrochemical behavior of the complex has been investigated by using cyclic voltammetry in acetontrile solution at a scan rate of 50 mV s^{-1} with respect to an Ag/AgCl electrode using tetrabutylammonium bromate as supporting electrolyte.

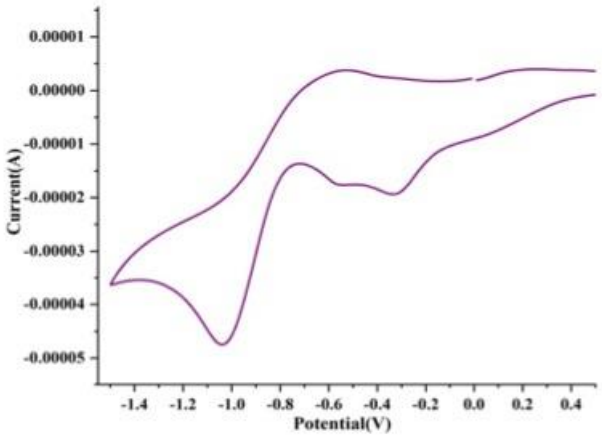

Figure 9. Cyclic voltammograms of the complex in acetontrile medium with respect to an Ag/AgCl electrode using tetrabutylammonium bromate as supporting electrolyte at a scan rate of 50 mV s^{-1}.

The cyclic voltammogram (CV) of the complex is irreversible and displays two redox processes with E_c^1 = -0.32 V, E_a^1 = 0.19 V, ΔE_{pc} = 0.51 V, $E^{1/2}$ = -65 mV and E_c^2 = -1.03 V, E_a^2 = -0.56 V, ΔE_{pc} = 0.47 V, $E^{1/2}$ = -0.795 V as can be seen in Figure 9. The cyclic voltammogram (CV) of the complex is irreversible and displays two redox processes with E_c^1 = -0.32 V, E_a^1 = 0.19 V, ΔE_{pc} = 0.51 V, $E^{1/2}$ = -65 mV and E_c^2 = -1.03 V, E_a^2 = -0.56 V, ΔE_{pc} = 0.47 V, $E^{1/2}$ = -0.795 V as can be seen in Fig. 9.

7.3.5 Magnetic properties

The thermal variation of the product of the molar magnetic susceptibility times the temperature ($\chi_m T$) for compound **1** shows a room temperature value of $\chi_m T$ *ca*. 6.0 cm^3 K mol^{-1}, which is the expected value for two independent Mn^{III} ions with a ground spin state S = 2 and a g value close to 2. When the sample is cooled, $\chi_m T$ remains constant down to *ca*. 20 K and exhibits a sharp decrease at lower temperatures to reach a value of *ca*. 3.0 cm^3 K mol^{-1} at 2 K (Fig. 10). This behaviour suggests the presence of an overall weak antiferromagnetic interaction in the metal complex and/or a zero-field splitting (ZFS) of the S = 2 ground spin state. Since the compound

contains a symmetric dimeric Mn^{III} complex with a double phenoxido bridge, we have fit the magnetic data of the compound using three different models: (i) a Mn^{III} dimer with ZFS in the Mn^{III} ions, (ii) two independent Mn^{III} monomers with a ZFS and (iii) a Mn^{III} dimer with no ZFS. For the two first models we have tried with either positive and negative initial values of the ZFS. Using these three models with the program PHI [58] we obtain reasonable fits in the whole temperature range with the five different possibilities: (i) dimer + ZFS (D > 0), (ii) dimer + ZFS (D < 0), (iii) dimer with no ZFS, (iv) two monomers + ZFS (D > 0) and (v) two monomers + ZFS (D < 0) (Fig. 11) with the parameters as displayed in Table 5. Nevertheless, in the low temperature region, the best fit is obtained with the second possibility (a Mn^{III} dimer with a negative value of D, solid line in Figure 10 and orange line in Figure 11) with the following parameters: g = 1.9946(5), J = -0.065(1) cm^{-1} and D = -1.80(2) cm^{-1} (the Hamiltonian is written as $H = -J(S_1S_2)$). These values indicate that the magnetic coupling through the double phenoxido bridge is almost negligible. As expected, the inclusion of a ZFS to the dimer model reduces the antiferromagnetic coupling along the double phenoxido bridge. The obtained D value is very close to those observed in other high spin Mn^{III} complexes [59].

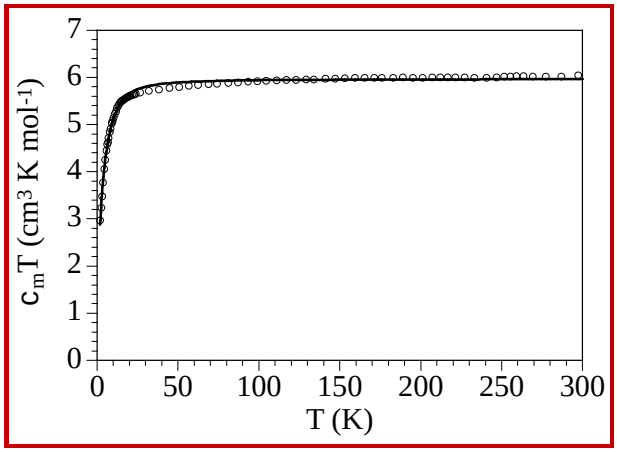

Figure 10. Thermal variation of $\chi_m T$ for compound **1**. Solid line is the best fit to a Mn^{III} dimer model with negative zero field splitting.

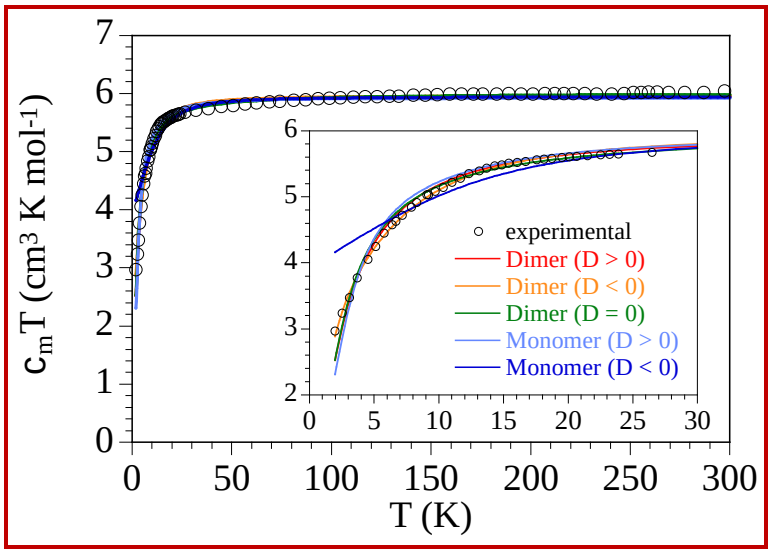

Figure 11. Thermal variation of $\chi_m T$ for complex **1** with the best fit obtained for different models: (i) a Mn(III) dimer with positive ZFS, (ii) a Mn(III) dimer with negative ZFS, (iii) a Mn(III) dimer with no ZFS, (iv) two Mn(III) monomers with positive ZFS and (v) two Mn(III) monomers with negative ZFS. Inset shows the low temperature region.

Table 5. Magnetic parameters obtained with the fit of the thermal variation of $\chi_m T$ for complex **1** to different models.

Model	g	J (cm^{-1})	|D| (cm^{-1})
Dimer + ZFS (D > 0)	1.9948(7)	-0.132(4)	+1.32(4)
Dimer + ZFS (D < 0)	**1.9948(7)**	**-0.065(1)**	**-1.80(2)**
Dimer	2.0019(7)	-0.244(1)	-
Monomers + ZFS (D > 0)	1.986(1)	-	+2.33(2)
Monomers + ZFS (D < 0)	1.989(2)	-	-2.71(7)

The best model is indicated in bold

The very weak antiferromagnetic coupling through the double phenoxido bridge is the expected one since the O atoms connect an axial position of one Mn^{III} ion with an equatorial position of the other Mn^{III} ion. This connectivity precludes the overlap of the magnetic orbitals and, therefore, reduces the magnetic coupling. Moreover, a complete experimental and theoretical

study performed by Ghosh *et al*. on Mn^{III} dimers with a double phenoxido bridge, shows that the coupling in all cases is very weak although it may be ferro or antiferromagnetic [29].

In case of Mn^{III} dimers, the Jahn-Teller distortion originates a short and a long Mn-O bond distances (in complex **1** these distances are 1.914(3) and 2.388(3) Å). It is well established that the main structural parameter determining the magnetic coupling is the long Mn-O bond distance [31, 38, 60]. When this long Mn-O bond distance is large (above *ca*. 2.4 Å) then the orbital overlap is reduced and the coupling is weak and ferromagnetic as a result of the orbital orthogonality of the d_z^2 and d_p orbitals (d_{xy}, d_{xz} and d_{yz}). For shorter Mn-O bond distances (as in complex **1**) the overlap increases, resulting in a weak antiferromagnetic interaction, as observed in complex **1** (J_{23} = -0.065(1) cm^{-1}). The negligible coupling observed in complex **1** agrees with a distance very close to the crossing point between ferro- and antiferromagnetic coupling. The second structural parameter that plays a role in the J value is the Mn-O-Mn bond angle (101.12(12)º in complex **1**). Both, experimental results and theoretical calculations, show that when the Mn-O distance is short (2.3 - 2.5 Å) there is a linear relationship between the Mn-O-Mn angle and J, with a negative slope that indicates that the larger the angle, the lower the J value [29]. Although the slope and the crossing angle from ferro- to antiferromagnetic interaction depends on the Mn-O bond distance, the larger the angle, the more antiferromagnetic the J value is. The Mn-O-Mn angle in complex **1** point to a weak antiferromagnetic interaction through the double phenoxido bridge, in agreement with the obtained J value in complex **1**.

Since Mn^{III} ions present a large magnetic anisotropy [1,14,51], we have performed AC measurements with different applied DC fields at low temperatures. These measurements show the presence of a frequency-dependent out of phase signal (χ''_m) at low temperatures only when a

DC field is applied (Figure 12). The analysis of the frequency dependence of out of phase signal at 2 K with the Debye model shows that the relaxation time increases as the DC field increases and reaches a maximum at around 2000 Oe (0.2 T, Figure 12). Accordingly, we have measured the frequency dependence of the AC signal with an applied DC field of 0.2 T in the temperature range of 2 - 4 K (Figure 13a). These measurements show an out-of phase signal with a maximum that shifts to higher frequencies as the temperature increases.

The field dependence of the relaxation time can be fitted to the following equation:

$$\tau^{-1} = ATH^{n} + \frac{B_1}{1+B_2H^2} + D \qquad (1)$$

with n = 2 for a non-Kramers ion, A = 7.6(8)x10^5 s^{-1} K^{-1} T^{-2}, B_1 = 1.10(9)x10^5 s^{-1}, B_2 = 55(9) T^{-2} and D = -2.7(1)x10^4 s^{-1} (solid line in Fig. 12 right).

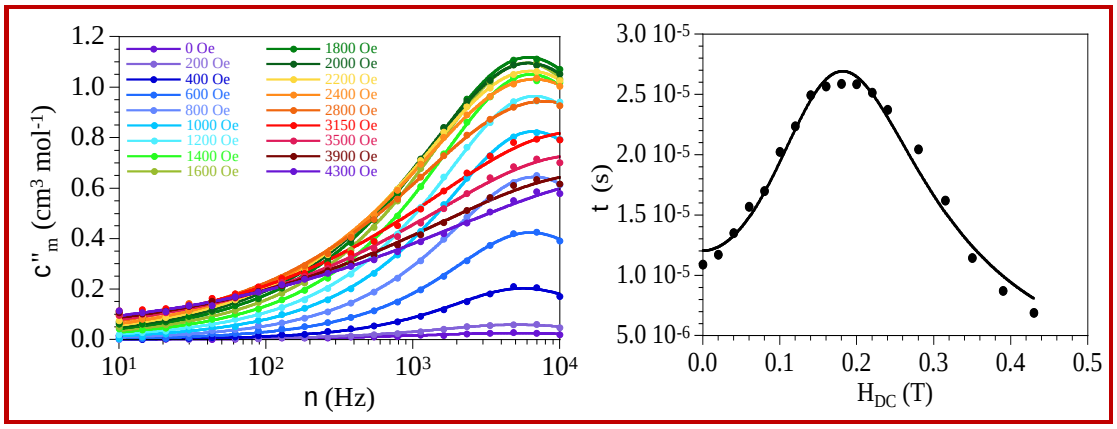

Figure 12. **(left)** Frequency dependence of the out of phase signal of complex **1** at 2.0 K with different DC fields. Solid lines are the fit to the Debye model. **(right)** Field dependence of the relaxation time (τ) of complex **1** at 2 K. Solid line is the fit to equation (1).

The fit of the frequency dependence of the χ''_m signal to the Debye model for complex **1** provides reliable relaxation times (τ) only in the temperature range 2.0 - 2.6 K (as at higher temperatures the maximum frequency is above the frequency limit of our equipment). The

Arrhenius plot of these relaxation times (Ln τ *vs.* 1/T, Figure 13b) shows a straight line in the 2.4 - 2.6 K range and a curvature in the 2.0 - 2.4 K range that can be very well reproduced with equation (2), including the Direct and Orbach mechanisms, respectively:

$$\tau^{-1} = AT + \tau_0^{-1}\exp\left(\frac{-U_{eff}}{k_B T}\right) \qquad (2)$$

with A = 206(9)×10^2 s^{-1}K^{-1}, τ_0 = 8(1)×10^{-19} s and U_{eff} = 73(4) K (solid line in Fig. 13b), indicating that the relaxation of the magnetization follows an activated process with a quite high energy barrier.

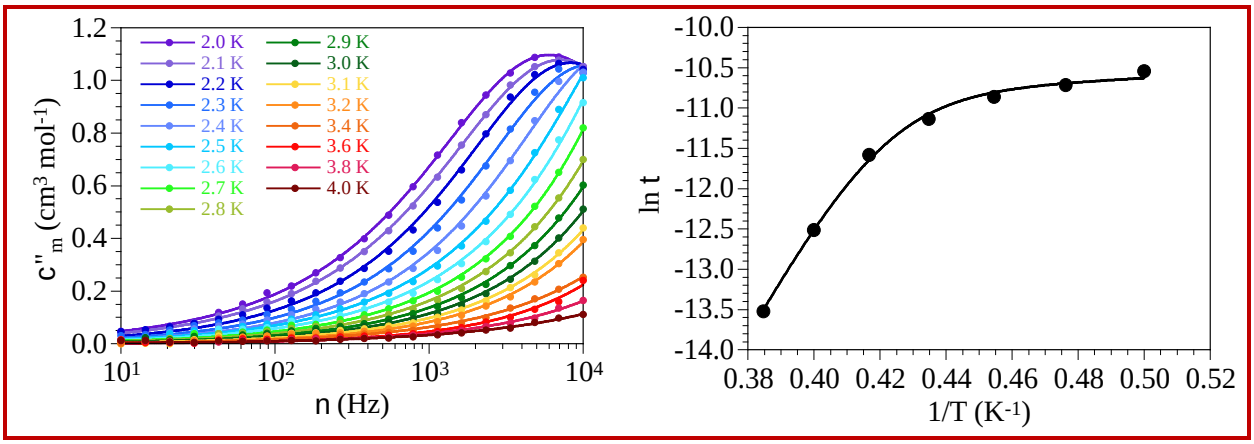

(a) **(b)**

Figure 13. **(a)** Frequency-dependence of the out of phase susceptibility (χ_m'') at low temperatures with an applied DC field of 0.2 T for complex **1**. Solid lines are the best fit to the Debye model. **(b)** Arrhenius plot of the relaxation time for compound **1** with a DC field of 0.2 T. Solid line is the best fit to equation (2).

7.3.6 Catechol oxidation activity

3,5-di-tert-butylcatechol (3,5-DTBC) is an extensively used substrate in the study of model complex catalysed catechol-oxidase-like reactions. This is because of its low redox potential, which makes it easily oxidisable and also the presence of bulky substituents prevents further

oxidations and ring-opening reaction [61]. The oxidation product, 3,5-di-tert-butylquinone (3,5-DTBQ) is also very stable and exhibits a characteristic absorption maximum at 402 nm in acetonitrile solution [46, 62]. In order to examine the catechol-oxidase-like activity of complex **1**, we dissolved the complex in acetonitrile by sonicating it few minutes to prepare a 10^{-4} (M) solution of the complex and treated this solution with 100 equivalents of 3,5-DTBC (10^{-2} (M)) in open air. In this catalytic reaction the aerial O_2 works as an oxidant. The course of the reaction was monitored by recording the UV-Vis spectra of the reaction mixture at intervals of 5 minutes. As can be seen in Figure 14, the formation of 3,5-DTBQ causes a blue shift in the absorption band of the complex from 454 nm to 401 nm with steady and gradual increase of the absorption intensity. These results confirm the catalytic oxidation of 3,5-DTBC to 3,5-DTBQ in solution. Interestingly, if we perform the same experiment in identical reaction conditions in methanol, no absorption band corresponding to 3,5-DTBQ was observed (Figure 15). This result indicates that methanol is not a suitable solvent for the oxidation of 3,5-DTBC catalysed by complex **1**. A control experiment was also performed in acetonitrile under the same conditions using Mn^{III} chloride instead of complex **1** but no characteristic absorption band of 3,5-DTBQ was observed even after 4 hours. A second control experiment performed under the same conditions, but without adding complex **1**, showed that the oxidation of 3,5-DTBC started only after 12 hours. Hence, both the control experiments unequivocally prove the effective catalytic activity of complex **1** towards catechol oxidation.

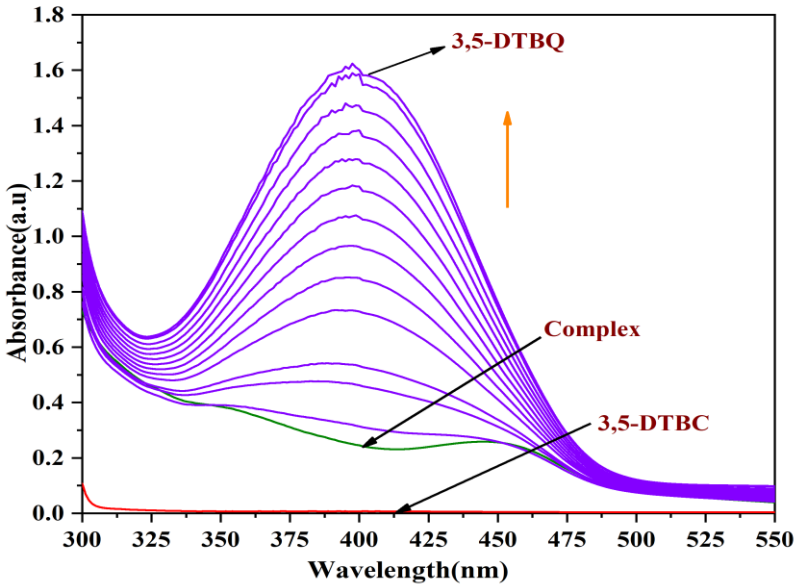

Figure 14. Absorption spectra after addition of 100 equivalents of 3,5-DTBC to a 10^{-4} (M) solution containing complex **1** in acetonitrile. The spectra were recorded at 5 minutes. intervals during ca. 1 hour.

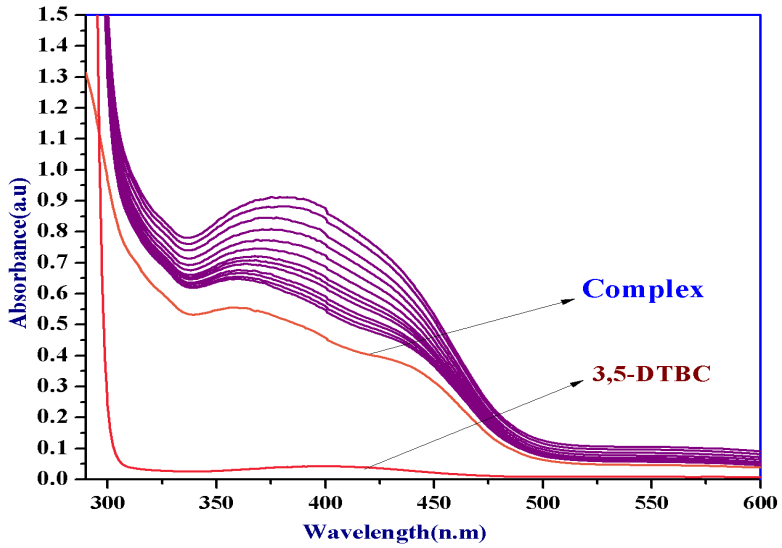

Figure 15. Electronic absorption spectra after addition of 100 equivalents of 3,5-DTBC to a solution containing compound **1** (10^{-4} M) in methanol. The spectra were recorded at 5 min intervals.

As the catalytic activity of the complex has been assessed using aerial O_2 as oxidant, it is therefore important to know the fate of the aerial O_2 during the oxidation of 3,5-DTBC and for this purpose a protocol experiment has been carried out following the procedure reported earlier [63]. Upon performing the catalytic oxidation of catechol for a duration of one hour, the pH of the solution was brought to 2 by dropwise addition of H_2SO_4. Thereafter, we have added 1 mL of 10 % KI solution and two drops of 3 % solution of ammonium molybdate in the solution obtained from the previous step and recorded the UV-Vis spectrum of the resultant mixture (Figure 16) to monitor the characteristic peak of I_3^-. In the UV-Vis spectrum the characteristic peak of I_3^- at 353 nm (ε = 26000 $Lmol^{-1}cm^{-1}$) has been detected. This experiment indicates that aerial O_2 is reduced to H_2O_2 during oxidation of catechol molecule to quinone (Scheme 3) [63].

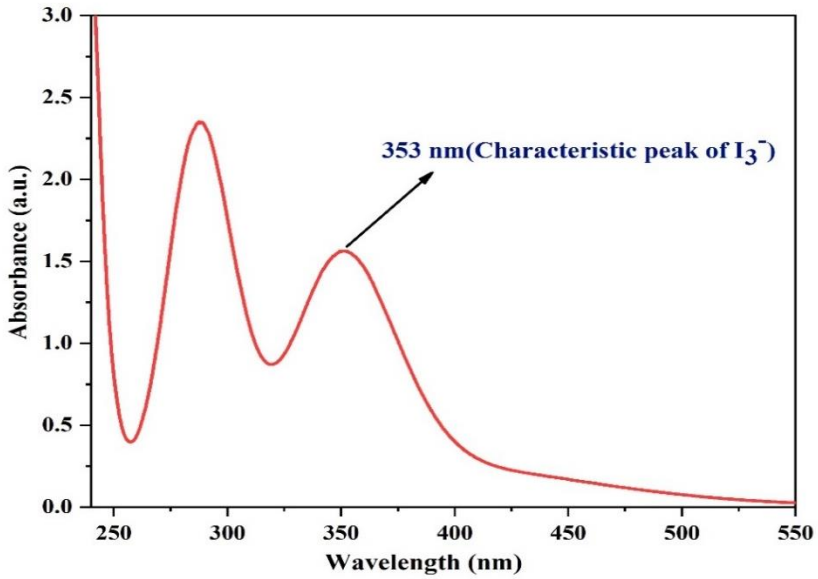

Figure 16. UV-Vis spectra of the reaction mixture of 3, 5-DTBC, complex **1** and KI

The detailed reaction procedure is as follows: The complex and 3,5-DTBC (100 equiv.) solutions were prepared in acetonitrile and mixed as needed for kinetic study. After one hour of reaction, an equal volume of water was added to the reaction mixture and the pH of the solution was brought to 2 by acidifying it with H_2SO_4 to restrain any further oxidation. The quinone (3,5-

DTBQ) formed as product was extracted thrice with dichloromethane. 1 mL of a 10% solution of KI and three drops of 3% solution of ammonium molybdate were then added to the aqueous layer. The formed H_2O_2 oxidizes I^- ions to I_2 which further reacts with excess I^- ion and form I_3^- ion. The formation of I_3^- was monitored spectrophotometrically by development of its characteristic absorption band at $\lambda = 353$ nm ($\varepsilon = 26000\ M^{-1}cm^{-1}$) in the UV-Vis spectrum.

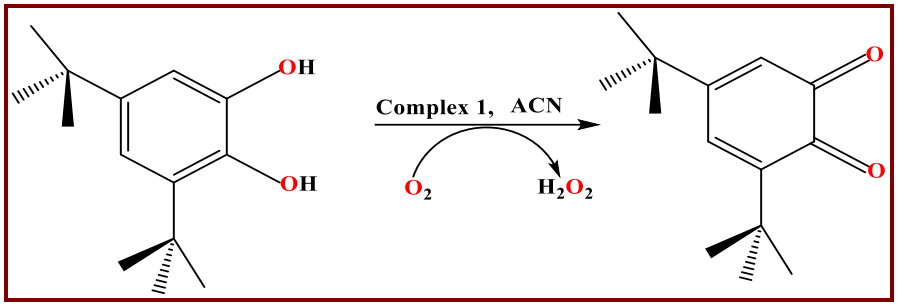

Scheme 3. Catalytic Oxidation of 3,5-DTBC to 3,5-DTBQ in acetonitrile (ACN).

7.3.7 Kinetic study for catechol oxidation

The kinetic study of the catalytic oxidation of 3,5-DTBC to 3,5-DTBQ by complex **1** was carried out following the initial rate method by measuring the increase of the absorbance of the quinone band at 401 nm. In order to determine the main kinetic parameters and the oxidation rate dependence on the substrate concentration (3,5-DTBC), a 10^{-4} (M) solution of complex **1** in acetonitrile has been reacted with increasing concentrations of 3,5-DTBC, from 10 to 100 equivalents, i.e., from 10^{-3} (M) to 10^{-2} (M), under aerobic condition. The initial rate is determined from the slope of the absorbance *vs.* time plot (Figure 17) recording the absorbance data for a duration of first 15 minutes, at an interval of 5 minutes and considering the molar extinction coefficient of quinone (3,5-DTBQ) as 1630 $M^{-1}cm^{-1}$.

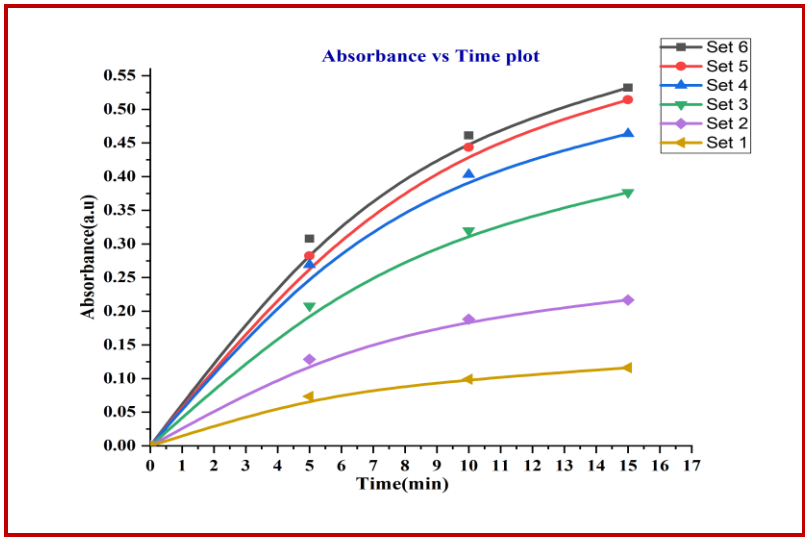

Figure 17. Absorbance vs Time plot

A first-order dependence is found at low concentrations of the substrate, whereas saturation kinetics has been noticed at higher substrate concentrations (Figure 18). The Michaelis-Menten model approach can be used to explain this type of saturation rate dependence as observed in the present case. Thus, a treatment on the basis of Michaelis-Menten equation for enzymatic kinetics is applied here and linearized by using Lineweaver-Burk plot (double reciprocal plot) to calculate the Michaelis-Menten constant (K_M) and the maximum rate (V_{max}) achieved by the system. The values of K_M and V_{max} are 8.473×10^{-3} M and 5.82×10^{-5} Mmin^{-1}, respectively. The value of turnover number (k_{cat}) as calculated by dividing the V_{max} value by the concentration of the complex. is 34.94 h^{-1}.

7.3.8 ESI-Mass Spectrometric Study

The mass spectrum (ESI-MS positive) of complex **1** and a 1:100 mixture of complex **1** with 3,5-DTBC after 10 minutes of mixing have been recorded separately in acetonitrile medium to get an insight into the structure of the complex in solution phase as well as to probe the presence of possible substrate-catalyst intermediates involved in the catechol oxidation reaction. The mass

spectrum of complex **1** (Figure 19) exhibits a base peak at *m/z* = 349.25 that indicates the presence of mononuclear species $[Mn(L)]^+$ ($C_{18}H_{18}MnN_2O_2$) in the solution phase. Additional peaks at *m/z* = 431.2 and 390.6 can be assigned to the solvent bound mononuclear species $[Mn(L)(CH_3CN)_2]^+$ ($C_{22}H_{24}MnN_4O_2$) and $[Mn(L)(CH_3CN)]^+$ ($C_{20}H_{21}MnN_3O_2$), respectively. It may be noted that very low intensity peaks are also found at higher *m/z* values (*m/z* = 612.08, 721.39 and 780.4) indicating the presence of complex **1** in the solution.

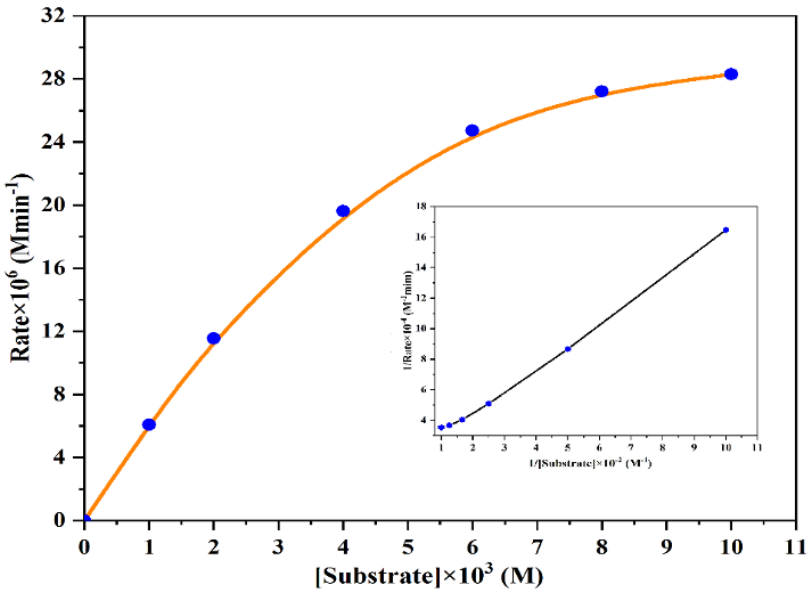

Figure 18. Plot of initial rates *vs*. substrate concentration for the oxidation of 3,5-DTBC to 3,5-DTBQ catalysed by complex **1**. The Inset shows the Lineweaver-Burk plots.

The mass spectrum of the 1:100 mixture (Fig. 20) shows a base peak at *m/z* = 243.13 that corresponds to the quinone-sodium aggregate $[(3,5\text{-DTBQ})Na]^+$ ($C_{14}H_{20}O_2Na$). The peak at *m/z* = 570.3 indicates the existence of 1:1 mononuclear species-substrate aggregate $[Mn(L)(3,5\text{-DTBQ})H]^+$ ($C_{32}H_{39}MnN_2O_4$) formed during the course of the catalytic oxidation. Hence, on the basis of the mass spectrometric evidence, it can be inferred that complex **1** predominantly exists as a mononuclear species $[Mn(L)]^+$ in acetonitrile solution after its dissociation.

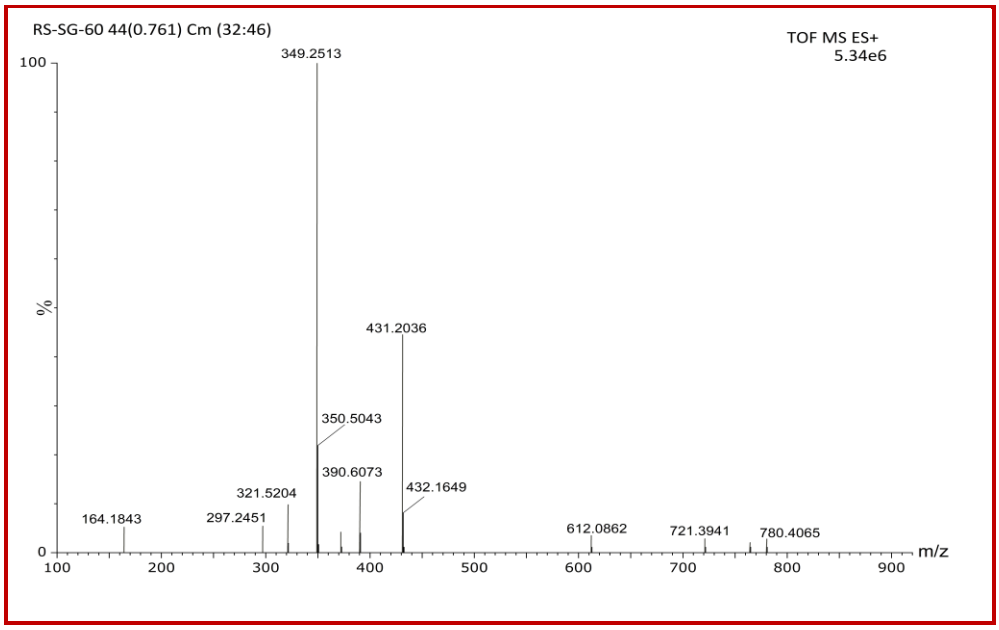

Figure 19. Electrospray mass spectrum (ESI-MS positive) of complex **1** in acetonitrile.

It is worthy to note that complex **1** did not exhibit catalytic activity in the oxidation of 3,5-DTBC in methanol under the same reaction condition as we have mentioned earlier. Very similar observation has been reported in the literature for a series of dinuclear Mn^{III}-Schiff base complexes, however, another series of mononuclear Mn^{III}-Schiff base complexes display good catalytic activity in both methanol and acetonitrile solvents [64]. Hence, from the outcome of the present catalytic study and previous findings, it will be reasonable to conclude that the good coordinating ability of MeOH molecule precludes the dissociation of the Mn^{III} dimer to form the mononuclear species, $[Mn(L)]^{+}$, which is actually the active form of catalyst, whereas this does not happen in acetonitrile solution.

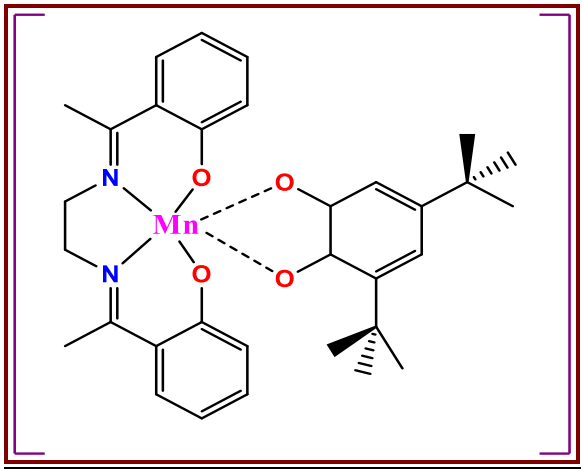

Scheme 4. The possible 1:1 substrate-catalyst intermediate formed by mononuclear manganese species with 3,5-DTBQ in acetonitrile [m/z = 570.3].

This mononuclear species $[Mn(L)]^{+}$ is actually the active form of catalyst that binds with the substrate 3,5-DTBC (1:1) in the course of the oxidation (Scheme 4).

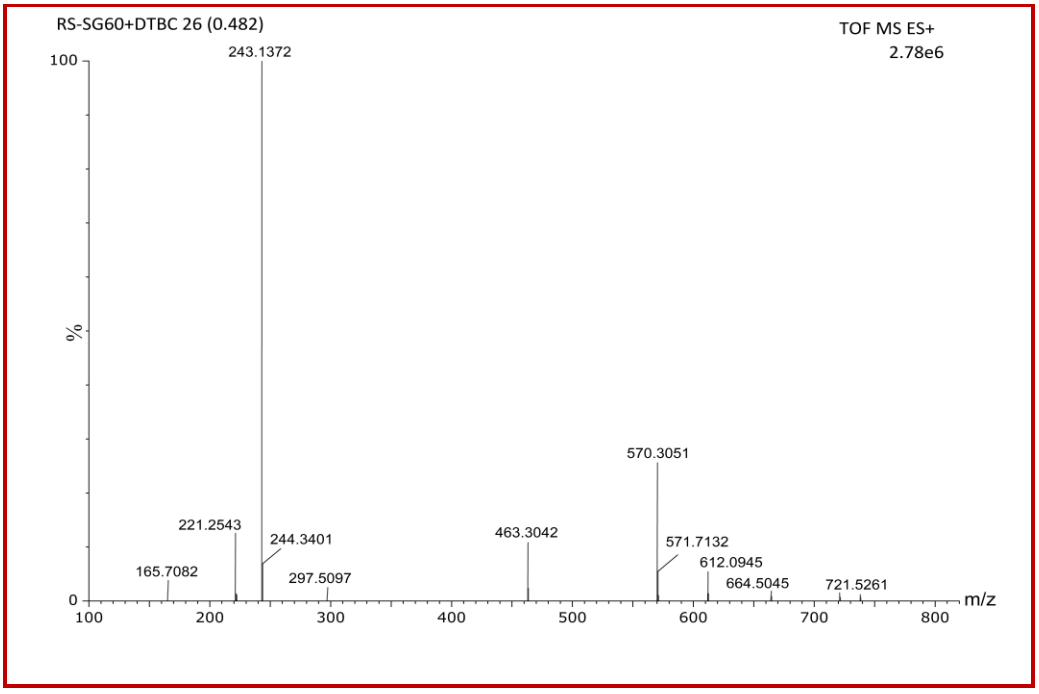

Figure 20. Electrospray mass spectrum (ESI-MS positive) of a 1:100 mixture of the complex and 3,5-DTBC in acetonitrile, recorded just after 10 min of mixing.

Metal complexes comprising higher valent metal centres such as Cu^{II}, Mn^{III} and Mn^{IV} usually exhibit significant catalytic activity in the catechol oxidation reaction because they can be easily reduced to their stable lower valencies [65-66]. In the UV–vis spectrum of the complex **1** in acetonitrile, a band appears at 454 nm due to the ligand to metal charge-transfer (PhO → Mn^{III}). This band completely disappears upon addition of 100 equivalent of the substrate 3,5-DTBC (Figure 21). This spectrophotometric study clearly suggests that in the present case, the catalytic oxidation of 3,5-DTBC to 3,5-DTBQ by aerial O_2 takes place with the concomitant reduction of Mn^{III} ions to Mn^{II} state. The Mn^{II} ions are further oxidised back into Mn^{III} by the molecular O_2 present in the reaction media. The catalytic activity of the complex in terms of the parameters such as K_M, V_{max} and k_{cat} has been compared with manganese and other metal-based complexes toward catalytic oxidation of catechol and presented in Table 6. This comparative study reveals that the present dimeric Mn^{III}-complex exhibits moderate catalytic activity in the oxidation of catechol substrate.

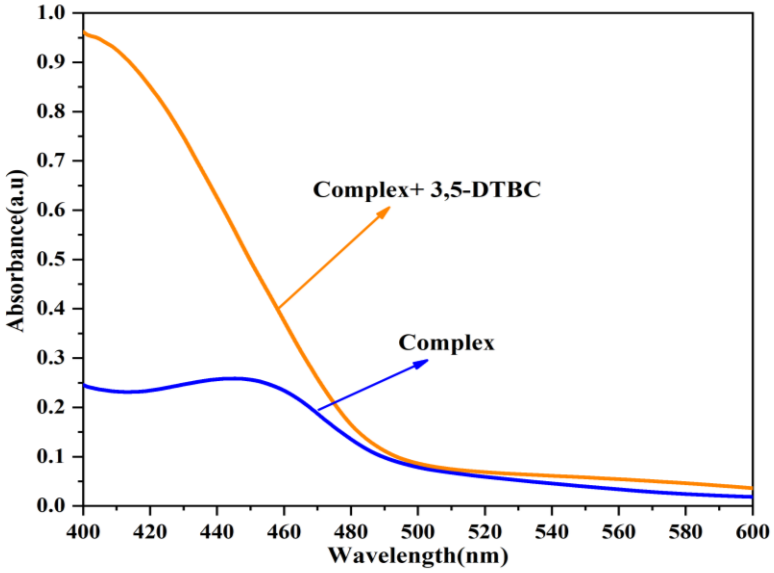

Fig. 21. UV-vis spectra of the complex **1** alone and after addition of 100 equivalents of 3,5-DTBC in acetonitrile.

Table 6. A comparison of catechol oxidase mimicking activity of some previously reported metal complexes.

Complexes	Solvent	V_{max} (Ms^{-1})	K_M (M)	k_{cat} (h^{-1})	Ref.
$[Mn^{III}(L)_2(OAc)(AcOH)]$	[a]	18.3×10^{-5}	–	1.32×10^{6}	[44]
$[Mn^{III}_2\ Mn^{II}(O_2CCH_2Cl)_4$-$(dmp)_2(H_2O)_2$	[c]	1.50×10^{-4}	7.49×10^{-5}	9.01×10^{3}	[45]
$[Mn^{II}(o\text{-}(NO_2)C_6H_4COO)_2(pyz)(H_2O)]_n$	[c]	8.67×10^{-6}	1.7×10^{-4}	177	[46]
$[Mn^{III}L^2(SCN)(H_2O)]$	[b]	2.1×10^{-3}	–	134	[67]
$[Mn^{III}L(N_3)(H_2O)]$	[d]	1.76×10^{-7}	0.001022	25.4	[68]
$[Mn^{III}L(OAc)(H_2O)]$	[d]	1.19×10^{-7}	0.0007731	17.2	[68]
$[Mn^{III}Mn^{II}L(\mu\text{-}O_2CPh)(MeOH)\ (ClO_4)]^+$	[c]	4.34×10^{-8}	0.0006265	15.6	[69]
$[Mn^{III}\ (L)Cl]$	[c]	1.00×10^{-4}	65×10^{-4}	3.60×10^{3}	[64]
$[Mn^{III}_2(L)Cl_4]\cdot4H_2O$	[c]	6.70×10^{-5}	2.40×10^{-3}	2.41×10^{3}	[64]
$[Mn^{II}_2(L)_2(NO_2)_2]$	[c]	3.98×10^{-6}	4.9×10^{-4}	1472.74	[56]
$[Mn^{II}_4Mn^{III}_4O_2(pyz)_2(C_6H_5CH_2COO)_{10}]$	[c]	1.18×10^{-5}	1.75×10^{-4}	2.55×10^{3}	[70]
$[Cu(L^1)_2(ClO_4)_2]_2$	[b]	5×10^{-7}	3.70×10^{-4}	34.32	[71]
$[Cu_2(L^2)_2(\mu\text{-}ClO_4)](ClO_4)$	[b]	7.3×10^{-7}	6.40×10^{-4}	26.52	[71]
$[Co_2(cpdp)(Hphth)]$	[b]	2.8×10^{-7}	2.175×10^{-3}	20.64	[72]
$[Co_2(cpdp)(Hisophth)]$	[b]	2.1×10^{-7}	2.719×10^{-3}	15.45	[72]
$[Co_4(cpdp)_2(terephth)]$	[b]	3.2×10^{-7}	2.599×10^{-3}	47.32	[72]
$[Cu_2(Hhdpa)_2].2CH_3OH.6H_2O$	[b]	2.3×10^{-7}	5.039×10^{-3}	17.05	[73]
$Na_4[Zn_2(hdpa)_2](OAc)_2$	[b]	1.3×10^{-7}	1.78×10^{-2}	9.13	[73]
$[Ni_4(L)_2(H_2O)_8(\mu_2\text{-}H_2O)_2](NO_3)_6(H_2O)_6$	[d]	3.514×10^{-7}	1.966×10^{-3}	12.65	[74]
$[Mn^{III}_2(L)_2(dca)_2]$	[c]	9.7×10^{-7}	8.473×10^{-3}	34.94	This work

Where, solvent: [a]= CH_3CN: DMF(9:1), [b]= CH_3OH, [c]= CH_3CN, [d]= DMF and 'L' denotes respective ligand system

7.4. Conclusions

In this work we have reported the structure, magnetic properties and bio-catalytic activity of a unique dimeric Mn^{III} complex containing Schiff's base and dca^- ligands. The complex **1** is a centrosymmetric Mn^{III} dimer showing a rare combination of double phenoxido bridges with terminal dca^- ligands. Complex **1** is the first reported dimeric Mn^{III} complex of a Schiff base ligand having two terminal dca^- ligands. We have shown that for the ratio1:2 of Mn and dca^-leads to formation of a dimeric Mn^{III} complex, in contrast to the discrete mononuclear complexes or 1D structures previously obtained for 1:1 ratio of Mn and dca^-. The complex **1** exhibits an almost negligible Mn^{III}-Mn^{III} coupling and a field-induced single-molecule magnet behaviour, with a high energy barrier of 73(4) K due to the large magnetic anisotropy of the Mn^{III} centres. Additionally,

the complex **1** exhibits significant solvent selective catechol-oxidase-like activity for the model substrate 3,5-DTBC in acetonitrile medium.

References

[1] D. Li, H. Wang, S. Wang, Y. Pan, C. Li, J. Dou and Y. Song, *Inorg. Chem*., **2010**, 49, 3688-3690.

[2] A. J. Tasiopoulos, W. Wernsdorfer, K. A. Abboud and G. Christou, *Angew. Chem. Int. Ed*., **2004**, 43, 6338-6342.

[3]L. A. Kushch, V. D. Sasnovskaya, A. I. Dmitriev, E. B. Yagubskii, O.V. Koplak, L.V.Zorina and D. W. Boukhvalov, *Dalton Trans*., **2012**, 41, 13747-13754.

[4] C. C. Stoumpos, R. Inglis, O. Roubeau, H. Sartzi, A. A. Kitos, C. J. Milios, G. Aromi, A. J. Tasiopoulos, V. Nastopoulos, E. K. Brechin, S. P. Perlepes and *Inorg. Chem*., **2010**, 49, 4388-4390.

[5] M. Carboni and J.-M. Latour, *Coord. Chem. Rev*., **2011**, 255, 186-202.

[6] G. Maayan and G. Christou, *Inorg. Chem*., **2011**, 50, 7015-7021.

[7] D. Lieb, A. Zahl, T. E. Shubina and I. Ivanovic-Burmazovic, *J. Am. Chem. Soc*. **2010**, 132, 7282-7284.

[8] D. Shen, C. Miao, S. Wang, C. Xia and W. Sun, *Eur. J. Inorg. Chem*., **2014**, 49, 5777.

[9] G. Maayan, N. Gluz and G. Christou, *Nature Catal*., **2018**, 1, 48-54.

[10] M. H. Cheaha, M. Zhangb, D. Shevelac, F. Mamedova, A. Zounib and J. Messinger, *Proc. Natl. Acad. Sci*. **2020**, 117, 141-145.

[11] P. A. Vigato, S. Tamburini and L. Bertolo, *Coord. Chem. Rev*. **2007**, 251, 1311-1492.

[12] C. N. R. Rao, S. Natarajan and R. Vaidhyanathan, *Angew. Chem., Int. Ed*. **2004**, 43,1466-1496.

[13] R. Bagai and G. Christou, *Inorg. Chem*. **2007**, 46, 10810-10818.

[14]. J. H. Song, K. S. Lim, D. W. Ryu, S. W. Yoon, B. J. Suh and C. S. Hong, *Inorg. Chem*. **2014**, 53, 7936-7940.

[15] T. Taguchi, W. Wernsdorfer, K. A. Abboud and G. Christou, *Inorg. Chem*. **2010**, 49, 10579-10589.

[16]. J. G.-Segura, J. Campo, I. Imaz, K. Wurst, J. Veciana, P. Gerbier and D. Ruiz-Molina, *Dalton Trans*. **2007**, 2450-2456.

[17] L. Bogani and W. Wernsdorfer, *Nature Mater*. **2008**, 7, 179-186.

[18] A.V. Palii, S. M. Ostrovsky, S. I. Klokishner, B. S. Tsukerblat, C. P. Berlinguette, K. R. Dunbar and J. R. Galán-Mascarós, *J. Am. Chem. Soc*. **2004**, 126, 16860-16867.

[19] E. Cremades, J. Cano, E. Ruiz, G. Rajaraman, C. J. Milios and E. K. Brechin, *Inorg. Chem*. **2009**, 48, 8012-8019.

[20] N. Lima, A. Caneschi, D. Gatteschi, M. Kritikos and L. G. Westin, *Inorg. Chem*. **2006**, 45, 2391-2393.

[21] S. Goswami, S. Singha, I. Saha, A. Chatterjee, S. K. Dey, C. J. Gómez García, A. Frontera, S. Kumar and R. Saha, *Inorg. Chem*. **2020**, 59, 8487-8497.

[22] I. Dasna, S. Golhen, L. Ouahab, N. Daro and J. P. Sutter, New J. Chem. **2001**, 25, 1572-1576.

[23] J. L. Manson, C. R. Kmety, F. Palacio, A. J. Epstein and J. S. Miller, *Chem. Mater*. **2001**, 13, 1068-1073.

[24] M. Maiti, D. Sadhukhan, S. Thakurta, S. Roy, G. Pilet, R. J. Butcher, A. Nonat, L. J. Charbonniere and S. Mitra, *Inorg. Chem*. **2012**, 51, 12176-12187.

[25] S. Dalai, P. S. Mukherjee, E. Zangrando and N. Ray Choudhuri, *New J. Chem*., **2002**, 26, 1185-1189.

[26] D. J. Price, S. R. Batten, B. Moubaraki and K. S. Murray, *Ind. J. Chem. A*. **2003**, 42, 2256-2266.

[27] Q. Shi, R. Cao, X. Li, J. Luo, M. Hong and Z. Chen, *New J. Chem*. **2002**, 26, 1397-1401.

[28] Y. Zhang, X. Wang, X. Zhang, T. Liu, W. Xu and S. Gao, *Inorg. Chem*. **2010**, 49, 5868-5875.

[29] P. Seth, S. Giri and A. Ghosh, *Dalton Trans*. **2015**, 44, 12863-12870.

[30] P. Pandey, S. Tripathi, M. Shanmugam, R. J. Butcher and S. S. Sunkari, *Inorg. Chim. Acta*. **2019**, 495, 118997.

[31] Z. Lu, M. Yuan, F. Pan, S. Gao, D. Zhang and D. Zhu. *Inorg. Chem*. **2006**, 45, 3538-3548.

[32] Q.Wu, Y-G. Li, Y-H. Wang, R. Clerac, Y. Lua and E. B. Wang, *Chem. Commun*., **2009**, 5743–5745.

[33] H. Miyasaka, R. Clerac, W. Wernsdorfer, L. Lecren, C. Bonhomme, K. Sugiura and M. Yamashita, *Angew. Chem. Int. Ed*., **2004**, 43, 2801–2805.

[34] C. K.Terajima, H. Miyasaka, K. Sugiura, R. Clerac and H. Nojiri, *Inorg. Chem*. **2006**, 45, 4381−4390.

[35] H. Hiraga, H. Miyasaka, R. Clerac, M. Fourmigue and M. Yamashita, *Inorg. Chem*. **2009**, 48, 2887-2898.

[36] Y. Sawada, W. Kosaka, Y. Hayashi and H. Miyasaka, *Inorg. Chem*. **2012**, 51, 4824-4832.

[37] T. Akitsu, Y. Takeuchi and Y. Einaga, *Acta Cryst*. **2005**, 61, 324–328.

[38] H. Miyasaka, R. Clérac, T. Ishii, H. Chang, S. Kitagawa and M. Yamashita, *J. Chem. Soc. Dalton Trans*. **2002**, 28, 1528-1534.

[39] K. S. Banu, T. Chattopadhyay, A. Banerjee, S. Bhattacharya, E. Suresh, M. Nethaji, E. Zangrando and D. Das, *Inorg. Chem*. **2008**, 47, 7083-7093.

[40] J. H. Whittaker, *Metal Ions in Biological Systems*, Ed. Marcel Dekker, New York, **2000**, vol 37. Chapter 18, pp. 587-611.

[41]. D. W. Yoder, J. Hwang and J. E. Penner-Hahn, *Metal Ions in Biological Systems*, Ed. Marcel Dekker, New York, **2000**, vol. 37. Chapter 16, pp. 527-557.

[42] M. H. Gold, H. L. Youngs and M. D. S. Gelpke, *Metal Ions in Biological Systems, Ed. Marcel Dekker*, New York, **2000**, vol. 37. Chapter 17, pp. 559-586.

[43]. K. N. Ferreira, T. M. Iverson, K. Maghlaoui, J. Barber and S. Iwata, *Science*, **2004**, 303, 1831-1838.

[44] S. K. Dey and A. Mukherjee, *Chem Cat Chem*. **2013**, 5, 3533-3537.

[45] M. Pait, M. Shatruk and D. Ray, *Dalton Trans*. **2015**, 44, 11741-11754.

[46] P. Kar, Y. Ida. T. Kanetomo, M.G.B. Drew, T, Ishida and A. Ghosh, *Dalton Trans*. **2015**, 44, 9795-9804.

[47] S. K. Dey and A. Mukherjee, *Coord. Chem. Rev.* **2016**, 310, 80-115.

[48] S. Ghosh, S. Giri and A. Ghosh, *Polyhedron*, **2015**, 102, 366–374.

[49] G. A. Bain and J. F Berry, *J. Chem. Educ*. **2008**, 85, 532-536.

[50] G. M. Sheldrick, *SHELXL 97*, Program for Crystal Structure Refinement, University of Göttingen, Göttingen, Germany, **1997**.

[51]. G. M. Sheldrick, Crystal structure refinement with SHELXL. *Acta Cryst*. **2015**, 71, 38.

[52] A. L. Spek, Single-crystal structure validation with the program PLATON, *J. Appl. Cryst*. **2003**, 36, 7-13.

[53] L. J. Farrugia, ORTEP-3 for Windows - a version of ORTEP-III with a Graphical User Interface (GUI) *J. Appl. Cryst*. **1997**, 30, 565.

[54] L. J. Farrugia, WinGX suite for small-molecule single-crystal crystallography *J. Appl. Cryst*. **1999**, 32, 837-838.

[55] G. Bhargavi, M. V. Rajasekharan and J. P. Tuchages, *Inorg. Chim. Acta*, **2009**, 362, 3247-3252

[56] P. Seth, M. G. B. Drew and A. Ghosh, *J. Mol. Catal. A: Chem*. **2012**, 365, 154-161.

[57] S. Saha, D. Mal, S. Koner, A. Bhattacherjee, P. Gütlich, S. Mondal, M. Mukherjee and K. Okamoto, *Polyhedron*, **2004**, 23, 1811-1817.

[58] N. F. Chilton, R. P. Anderson, L. D. Turner, A. Soncini and K. S. Murray, *J. Comput. Chem*. **2013**, 34, 1164-1175.

[59] C. Duboc, *Chem. Soc. Rev*. **2016**, 45, 5834-5847.

[60] S. Mandal, G. Rosair, J. Ribas and D. Bandyopadhyay, *Inorg. Chim. Acta.* **2009**, 362, 2200-2204.

[61] J. Mukherjee and R. Mukherjee, *Inorg. Chim. Acta*. **2002**, 337, 429-438.

[62] F. Zippel, F. Ahlers, R. Werner, W. Haase, H. F. Nolting and B. Krebs, *Inorg. Chem*. **1996**, 35, 3409-3419.

[63] A. Biswas, L. K. Das, M. G. B. Drew, C. Diaz and A. Ghosh, *Inorg. Chem*. **2012**, 51, 10111.

[64] S. Mukherjee, T. Weyhermüller, E. Bothe, K. Wieghardt and P. Chaudhuri, *Dalton Trans*. **2004**, 22, 3842-3853.

[65] I. A. Koval, P. Gamez, C. Belle, K. Selmeczi and J. Reedijk, *Chem. Soc. Rev*. **2006**, 35, 814-840.

[66] M. Maiti, D. Sadhukhan, S. Thakurta, E. Zangrando, G. Pilet, A. Bauza, A. Frontera, B. Dede and S. Mitra, *Polyhedron*, **2014**, 75, 40-49.

[67] P. Chakraborty, S. Majumder, A. Jana and S. Mohanta, *Inorg. Chim. Acta*. **2014**, 410.

[68] A. Jana, N. Aliaga-Alcalde, E. Ruiz and S. Mohanta, *Inorg. Chem*. **2013**, 52, 7732-7746.

[69] K. S. Banu, T. Chattopadhyay, A. Banerjee, M. Mukherjee, S. Bhattacharya, G. K. Patra, E. Zangrando and D. Das, *Dalton Trans*. **2009**, 40, 8755-8764.

[70] P. Kar, R. Haldar, C.J. Gomez-Garcia and A. Ghosh, *Inorg. Chem*. **2012**, 51, 4265–4273.

[71] M. Sheoran, K. Bhar, S. Jain, M. Rana, T. A. Khan and A. K. Sharma, *Polyhedron*. **2019**, 161, 169-178.

[72] A. Majumdera, N. Dutta, S. Haldara, A. Dasb, L. Carrellac and M. Bera, *Inorganica Chimica Acta*, **2020**, 510, 119752.

[73] A. Patra, G. C. Giri, T. K. Sen, L. Carrella, S. K. Mandal and M. Bera, *Polyhedron*, **2014**, 67, 495-504.

[74] T. Chakraborty, S. Mukherjee, S. Dasgupta, B. Biswas and D. Das, *Dalton Trans*, **2019**, 48, 2772-2784.

Chapter 8

Conclusions and future prospects of the Work

8.1 Conclusion

Finally, in this chapter, the major outcomes and future prospects of the work will be depicted. The thesis includes the design and detail structural characterisation of a number of novel transition and lanthanide metal ions-based functional materials: {[Ni(squarate)(2,2′-bipy)(H_2O)]·H_2O}$_n$ (compound **I**), [Pr(1,10 phen)$_2$ (H_2O)$_5$] Cl_3(H_2O) (CH_3OH), (compound **II**), [Cu_2 (oxalate)(1,10-phen)$_2Cl_2$], (compound **III**) [Mn(L)(H_2O)Cl], (compound **IV**) (H_3O)[Mn(L)(H_2O)$_2$]{[Mn(L)(H_2O)]$_2$Fe(CN)$_6$}·4H_2O (compound **V**), and [Mn_2(L)$_2$(dca)$_2$] (compound **VI**) [where, 2,2′-bipy = 2,2′-bipyridine, 1,10-phen = 1,10-phenanthroline and H_2L = Schiff's base ligand, dca= dicyanmide] synthesised by utilising the 'node and spacer' approach of crystal engineering. The judicious selection of ligands and metal ions/cluster with clear understanding of their preferred interactions is the backbone of the design of targeted materials having desired functionalities. Synthesis of the desired materials using preselected ligands and metal ions/cluster in solid crystalline form can be achieved by rational modification of reaction techniques and tuning of various factors like temperature, solvent polarity, solvent ratio, pH, reagent ratio and reaction time etc. These synthesised materials are valuable treasures in designing functional materials though CE as well as synthetic coordination chemistry and also have incredible application prospects. In depth study of functional properties of the synthesised materials to explore their potential applications in bio catalysis, product selective catalysis of epoxidation, magnetic properties and supramolecular host-guest chemistry have been done with outmost care. Theoretical investigation to find out the structure properties relationship of the materials is also performed for three representative samples. The conclusions of the thesis work are depicted below:

[**1**] A novel squarato-bridged 2D coordination polymer {[Ni(squarate)(2,20-bipy)(H2O)]H2O}n with the squarato di aninon exhibiting very rare $\mu_{1,2,3}$ bridging mode has been successfully synthesized. These 2D coordination sheets are packed via π···π interactions leading to the formation of 3D supramolecular structure with 1D supramolecular channels. These 1D channels are filled with guest water molecules which get stability through hydrogen bonding interactions. The structural study indicates the presence of unusual rare $\mu_{1,2,3}$ bridging mode of squarato-dianinon in the complex and the magnetic measurements have revealed that the complex is antiferromagnetic in nature. This is in agreement with the magnetic property of the sole previous example of $\mu_{1,2,3}$ -squarato-bridged compound. Due to the presence of p-electrons the complex becomes fluorescence active. By providing the second example of $\mu_{1,2,3}$ bridging pattern of squarato-dianion we have established that the squarate exhibits versatile bridging mode due to strong donor ability of its oxygen atoms. Taking into account the present and large number of previous works it may be concluded that the squarato-bridged metal complexes provide the unique opportunity to study the wide variety of bridging modes exhibited by the ligand and to investigate the influence of different bridging modes on magnetic property of such systems. In summary, we have presented a new 2D coordination polymer formed by utilizing unusual $\mu_{1,2,3}$ bridging pattern of squarato-dianion that exhibits multiple functionalities: (a) acts as metal–organic supramolecular host, (b) exhibits antiferromagnetic behavior and (c) photo-luminescent activity.

[**2**] It has been shown that hybrid water chloride system can be incorporated in a Pr (III)-based complex synthesized by using a neutral ligand 1,10-phenanthroline. The cationic complex $[Pr(phen)_2(H_2O)_5]^{3+}$ has been stabilized by the counter chloride anions. The 2D sheets are formed within the *ac*-plane by using the π···π interactions between 1D supramolecular chains formed by connecting the monomeric units. These 2D sheets are further packed by π···π interactions to form

the MOSH having hydrophobic pockets in which guest water, chloride and methanol are stabilized through weak interactions. The hydrogen bonding interactions among coordinated water along with the guests form a unique 2D supramolecular water-chloride-methanol sheet. The guest responsive hydrophobic pockets between 2D supramolecular sheets are flexible in nature. The MOSH can shrink and readjust itself with the retention of crystallinity upon the expulsion and introduction of guest species. It also regains its original shape upon reabsorption of guest species. The present system thus behaves like a dynamic supramolecular metal-organic host which can breathe upon heating and cooling with simultaneous aquation. This dynamic nature is due to the strong affinity of the host towards the guest molecules. The coordination tendency of the Pr(III) ion and the self-assembling tendency of water-chloride and methanol stabilize the system and these are responsible for the affinity of the host towards the guest molecules. The unique hydrogen bonded network of water-chloride and methanol molecules obtained in the present crystalline host will enhance our knowledge on the water-anion assembly and further work may help to understand how water-chloride and methanol may behave in biological processes like chloride ion transportation. In summary, the present crystal structure is a very interesting example of dynamic supramolecular metal-organic host and will act as a guide in the design of further metal-organic host systems where metal coordination tendency towards water molecules and anion-water self-assembling tendency can be utilized.

[**3**] A binuclear Cu(II) complex, $[Cu_2(oxalate)(1,10\text{-phen})_2Cl_2]$ (where 1,10-phen = 1,10-phenanthroline), has been designed and synthesised by using hydrophilic oxalate as bridging ligand and the hydrophobic 1,10-phen as the blocking ligand. The complex exhibits very good thermal stability and photoluminescence activity along with product selective catalytic activity for epoxidation of alkenes in presence of H_2O_2. Structural analysis has revealed that binuclear metallic

units of the complex are packed by supramolecular hydrogen bonding and π···π interactions and forms a 3D supramolecular architecture. The cyclic voltametric study suggests that both the copper centres are strongly coupled to each other through the oxalato-bridge**.** Owing to the presence of π-electrons in auxiliary ligand (1,10-phenenthroline), the complex shows strong fluorescence active behaviour. The presence of co-ordinately unsaturated Cu-centres makes the complex active catalyst in the high valued oxidation reaction of alkenes. By optimizing the oxidation reactions of alkenes using this binuclear Cu(II) complex, it has been established that in all cases the maximum catalytic efficiency can be achieved at 50 °C in presence of H_2O_2 as oxidant with acetonitrile solvent. Interestingly, the complex shows 100% selectivity for the oxidation of *cis*-cyclooctene to the corresponding epoxide in presence of H_2O_2 as oxidant at 50 ºC with 70% conversion in acetonitrile. The complex also exhibits product selectivity and percentage conversion of 89 % and 67 %, respectively, for styrene and 76 % and 82 % for cyclohexene under the same reaction condition.

[**4**] In this report, we have presented a unique example of an inorganic reaction where a selective metal-ligand bond undergoes dissociation assisted by the formation of intermolecular π-π and H-bonding interactions. DFT calculations at the PBE1PBE/def2-TZVP level confirm that the summation of the energies of all these intermolecular interactions overpasses the metal-ligand one. This fact has allowed us to prepare a trimeric molecular metamagnet from a monomeric metamagnetic precursor for the first time.

A novel Schiff base ligand (H_2L) has been successfully synthesised and it is used for the preparation of a Mn(III) monomer [Mn(L)(H_2O)Cl], (compound **IV**) that shows a very weak antiferromagnetic coupling through intermolecular π-π and H-bonding interactions. This weak antiferromagnetic interaction can be cancelled out by the application of an external magnetic field,

giving rise to a metamagnetic behaviour with a critical field of 2.0 T at 2 K. Combination of this Mn(III) monomer with $[Fe(CN)_6]^{4-}$ generates a Mn_2Fe trimer where the diamagnetic $[Fe(CN)_6]^{4-}$ complex acts as a linear connector between two monomeric Mn(III) complexes. These anionic trimers crystallize with a cationic Mn(III) monomer (closely related to the precursor monomer) in a 1:1 co-crystal to form $(H_3O)[Mn(L)(H_2O)_2]\{[Mn(L)(H_2O)]_2Fe(CN)_6\}\cdot 4H_2O$ (compound **V**). The trimers are further assembled by π-π and H-bonding interactions to build 1D supramolecular chains. Compound **2** also behaves as a metamagnet with a slightly higher critical field of 2.5 T at 2 K. The magnetic behaviour of both compounds has been reproduced with a simple model of a S = 2 monomer with a ZFS and a very weak intermolecular interaction (compound **IV**) and a S = 2 monomer with ZFS plus an antiferromagnetically coupled S = 2 dimer with a ZFS (compound **V**). [**5**] The design, synthesis, structure, magnetic properties and bio-catalytic activity of a unique dimer Mn^{III} complex containing Schiff's base and dca^- ligands synthetized by the reaction of $MnCl_2$ with dca^- at 1:2 ratio has been reported. The complex is a centrosymmetric Mn^{III} dimer showing a rare combination of double phenoxido bridges with terminal dca^- ligands. Complex is the first reported dimeric Mn^{III} complex of a Schiff base ligand having two terminal dca^- ligands. Complex shows that the use of a 1:2 Mn:dca^- ratio leads, for the first time, to a dimeric Mn^{III} complex, in contrast to the discrete mononuclear complexes or 1D structures previously obtained with a 1:1 Mn:dca^- ratio. Complex exhibits an almost negligible Mn^{III} - Mn^{III} coupling and a field-induced single-molecule magnet behaviour, with a high energy barrier of 73(4) K due to the large magnetic anisotropy of the Mn^{III} centers. Additionally, we have shown that the complex shows an appreciable solvent selective catechol-oxidase-like activity for the model substrate 3,5-DTBC in acetonitrile medium.

8.2 Future prospect of the work

Functional metal organic materials offer colossal opportunities for their applications in all most all modern scientific and technological arenas ranging from micro level laboratory synthesis to large scale industrial preparation. Current research trend in this field is to design multifunctional MOMs incorporating as many functionalities as possible in a single framework. The rational design of metal-organic frameworks may couple exciting application oriented functional properties such as magnetic, catalytic, electrical, optical, spintronic, sensor, luminescence, drug delivery etc. with the inherent porosity of the framework. As a consequence, a single framework becomes compatible for a number of applications. The transportation of ions, enzymes, hormones and drug molecules etc. in the living systems utilize weak supramolecular interactions to bind guest species with the carrier host. In this regard, dynamic metal–organic supramolecular hosts (MOSHs) having tunable porosity are tremendously used in various bio-related and other technological applications. Rational understanding about intermolecular forces and judicious use of building blocks are absolute requirements to develop of multi-functional metal organic materials. The present thesis deals with the design, synthesis, structural characterization, thermal, spectral and study of functional properties of a number of transition and lanthanide metal ions-based functional materials. Study of functional properties of the synthesised materials includes bio catalysis, product selective catalysis of epoxidation, magnetic properties and supramolecular host-guest chemistry etc. The outcomes of this thesis work originate the following future prospect.

[i] Design and synthesis of desired novel functional MOMs with judicious selection transition/ lanthanide metal ions, auxiliary and bridging ligands with the help of CE. This thesis offers ample scopes to manipulate bridging modes of ligands as well as modification and tuning of reaction controlling factors in order to have desired materials with good yield.

[ii] In supramolecular host-guest chemistry, the design of dynamic MOSHs is a daunting task because of difficulties in handling weak intermolecular forces. With the help of this thesis work, one can plan a design strategy for dynamic MOSHs incorporated with guest species. The breathing nature of dynamic MOSHs can be used a) as a vector for optimal uptake and delivery of drug molecules, b) in the guest dependent structural transformation etc. which will be addressed in our future research plan. In addition, the lanthanide based supramolecular metal organic materials will be very useful in sensing of hazardous species, photocatalysis, porous magnets, light-emitting devices, contrast agents for biological imaging etc.

[iii] Catalyst that prefers to generate the sole desire product, cut off the effort, time and cost of separation of the biproducts. The present thesis work presents design, synthesis and product selective catalysis of a metal organic material that trigger to design novel transition metal ions based functional materials having high product selective catalytic activity. Our future research goal is to design novel homogeneous and heterogeneous catalysts for industrial applications. As an extension of this thesis work, one can also develop new functional MOMs for catalysis of high-valued reactions like water dissociation, CO_2 reduction etc.

[iv] SMM, SCM and metamagnetic materials etc. are most useful classes of low dimensional molecular magnets due to their slow magnetic relaxation and high magnetic anisotropy. Nowadays, many research groups have focused on design multi-functional molecular magnets in conjugation with other functional properties like catalysis, electrical, sensing, porosity etc. There is an ample opportunity to identify the governing factors in modification and tuning of reaction techniques that will be helpful to achieve desired multi-functional magnetic materials. One can develop new magnetic materials that can act as a single chain magnet as well as electric conductor. As a future scope of the present thesis work, synthesising functional MOMs showing single

molecular magnetic behaviour with high blocking temperature as well as effective photocatalysts or sensors can be explored. Further, this thesis opens the scope to explore design multi-functional metamagnetic materials by controlling over weak supramolecular interactions.

[v] Findings of the present thesis will surely help to analyse several biological processes like oxygen transport by haemoglobin and myoglobin, different metallo-enzymatic catalysis, changes of physical properties with structural transformation etc. Finally, one can develop novel MOMs useful in proton conduction, solar cell, membrane for separation of toxic impurities from water, air, fuels, catalysis of H_2O dissociation etc.

List of publications

List of publications in international journals

Related to the thesis work:

[1] An unusual μ-$_{1,2,3}$-Squarato-Bridged two-dimensional coordination polymer: Crystal structure, thermal, photoluminescence and magnetic studies: **Somen Goswami**, Rajat Saha, Ian.M. Steele, Papri Dasgupta, Asok Poddar and Sanjay Kuma; Inorganica Chimica Acta. **2014**, 410, 111–117.

[2] A dynamic metal–organic supramolecular host based on weak p-stacking interactions incorporating 2D water-chloride-methanolic supramolecular sheet: Rajat Saha, **Somen Goswami**, Susobhan Biswas, Ian. M.Steele, Kamalendu Dey, Atish Dipankar Jana, and Sanjay Kumar; Inorganica Chimica Acta. **2014**, 423, 123–132.

[3] A bi-nuclear Cu (II)-complex for selective epoxidation of alkenes: Crystal structure, thermal, photoluminescence and cyclic voltammetry: **Somen Goswami,** Soumen Singha, Rajat Saha, Anupam Singha Roy, Manirul Islam and S. Kumar; Inorganica Chimica Acta. **2019**, 486, 352–360.

[4] Selective Metal−Ligand Bond-Breaking Driven by Weak Intermolecular Interactions: From Metamagnetic Mn(III)-Monomer to Hexacyanoferrate(II)-Bridged Metamagnetic Mn2Fe Trimer: **Somen Goswami**, Soumen Singha, Indrajit Saha, Abhishikta Chatterjee, Subrata K. Dey, Carlos J. Gomez Garc´ía, Antonio Frontera, Sanjay Kumar, and Rajat Saha; Inorg. Chem. **2020**, 59,12, 8487-8497.

[5] Double dicyanamide decorated double phenoxide bridged Mn (III) dimer with single-molecule magnetic behaviour and bio-catalytic activity: **Somen Goswami**, Soumen Singha, Bhaskar Khanra, Priyanka Chakraborty, Rajat Saha, Samia Benmansour, Subrata Kumar Dey, Carlos J. Gómez García and Sanjay Kumar; Inorganica Chimica Acta. **2023,** 550, 121370- 121379.

Not related to the thesis work:

[1] A Metal−Organic Framework to CuO Nanospheres of Uniform Morphology for the Synthesis of α-Aminonitriles under Solvent-Free Condition along with Crystal Structure of the Framework by S. Singha, A. Saha, **S. Goswami**, S. K. Dey, S. Payra, S. Banerjee, S. Kumar, and R. Saha, Cryst. Growth Des., **2018**, 18, 189−199.

[2] Synergistic Effect of Various Intermolecular Interactions on Self-assembly and Optoelectronic Behaviour in Co-crystals/Salts of Tetrabromoterephthalic Acid: A Report on Their Structure, Theoretical Study and Hirshfeld Surface Analysis, S. Singha, **S. Goswami**, S. K. Dey, R. Jana, P. P. Ray, I. Saha, C. Rizzoli, P. Pratim Bag, S. Kumar and R. Saha, CrystEngComm, **2020**, Accepted Manuscript, doi: 10.1039/D0CE01102A).

[3] Structural, optical, dielectric and electrical transport property of a [Mg(H2O)6]2+ -templated proton conducting, semiconducting and photoresponsive 3D Hydrogen bonded supramolecular framework, S. Singha, B. Khanra, **S. Goswami**, R. Mondal, R. Jana, A. Dey, S. Kumar Dey, P. P. Ray, C. Rizzoli, R. Saha, S. Kumar, New J. Chem., **2021**, 45, 20596-20611.

Seminar, Symposium and Conferences attended

SEMINAR, SYMPOSIUM, CONFERENCES ATTENDED

[1] 3rd International Conference on Global Trends in Pure and Applied Chemical Sciences (**ICGTCS**)- 2017 held at SRM University, Delhi-NCR Campus, Ghaziabad (U.P), India, during 8th - 9th December, 2017.

[2] International Conference on Emerging Trends in Chemical Sciences (**ETCS**) - 2018, held at Dibrughar University, Dibrughar, Assam, India, during 26th- 28th February, 2018.

[3] National Conference on Recent Developments in Nanoscience & Nanotechnology **(NCRDNN)-2019** held at Jadavpur University, Kolkata during January 29th-31st, 2019.

[4] International Seminar on International Year of the Periodic Table of Chemical Elements (**IYPT) - 2019** held at University of North Bengal, West Bengal, India, during November 22nd-23rd, 2019.

Appendix: Reprints of the published papers related to the thesis

Inorganica Chimica Acta 410 (2014) 111–117

Contents lists available at ScienceDirect

Inorganica Chimica Acta

journal homepage: www.elsevier.com/locate/ica

An unusual μ-$_{1,2,3}$-squarato-bridged two dimensional coordination polymer: Crystal structure, thermal, photoluminescence and magnetic studies

Somen Goswami [a], Rajat Saha [a], Ian M. Steele [b], Papri Dasgupta [c], Asok Poddar [c], Sanjay Kumar [a,*]

[a] Department of Physics, Jadavpur University, Jadavpur, Kolkata 700032, India
[b] Department of the Geophysical Sciences, The University of Chicago, USA
[c] Experimental Condensed Matter Physics Division, Saha Institute of Nuclear Physics, Kolkata 700064, India

ARTICLE INFO

Article history:
Received 31 July 2013
Received in revised form 23 October 2013
Accepted 31 October 2013
Available online 7 November 2013

Keywords:
2D coordination polymer
Squaric acid
Supramolecular interaction
Magnetic study
Photoluminescence study

ABSTRACT

A new 2D coordination polymer, {[Ni^{II}(squarate)(2,2′-bipy)(H_2O)]·H_2O}$_n$, [squarate = 3,4-dihydroxycyclobut-3-ene-1,2-dionate, 2,2′-bipy = 2,2′-bipyridine], has been synthesized by using multi-oxygen donor squaric acid ligand and characterized by single crystal X-ray crystallographic and various spectroscopic studies. The structural analysis has revealed that the complex crystallizes in orthorhombic P_{bca} space group and it has 3D supramolecular structure. Within the complex, the squarato-dianion exhibits unusual μ-$_{1,2,3}$ bridging mode with Ni(II) ions and 2D coordination sheets are formed through bridging the metal ions by squarato-anions. The 2D coordination sheets are packed along crystallographic ***b***-axis and the 2,2′-bipyridyl (blocking ligand) moieties are hanging in the interlamellar spaces between the 2D coordination sheets. These 2D coordination sheets are further bridged by supramolecular π···π interactions using 2,2′-bipyridyl ligands leading to the formation of 3D supramolecular framework which acts as a metal–organic supramolecular host (MOSH). During formation of 3D supramolecular structure, 1D supramolecular channels are formed along the crystallographic ***c***-axis. The guest water molecules get stability within such supramolecular channels through hydrogen bonding interactions with free oxygen atoms of bridging squarate ions. The thermal study indicates that the complex decomposes in three steps. The variable temperature magnetic measurements suggest that the complex is antiferromagnetic in nature. The complex exhibits solid-state photoluminescence spectra at room temperature due to π–π^*/n–π^* transition of the squarate and 2,2′-bipyridine ligands. The present study points to the squarato-bridged metal complexes as unique model system to carry out the study on different bridging modes exhibited by the ligand.

1. Introduction

In the recent past, the rational design and synthesis of coordination polymers have received paramount attention not only due to their aesthetical beautiful architectures and topologies but also for their several potential functional properties such as gas and solvent adsorption, catalysis, magnetism, ferroelectricity, nonlinear optical activity, optical sensing etc. [1–15]. The structural topology of coordination polymers can be tuned by judicious selection of parameters like stereo-electronic preferences of the metal ions, spatial disposition of binding sites within the ligands and reaction conditions. Moreover, several weak interactions such as directional hydrogen bonds, π···π interactions etc. may also play important role in determining the resultant architecture [16–18].

The ordered arrangement of paramagnetic metal centers within such coordination network allows us to design and synthesize novel magnetic materials such as ferromagnetic, ferrimagnetic, antiferromagnetic, canted-antiferromagnetic and spin glass systems [19–30]. It is well established that the propagation of magnetic exchange interaction within coordination polymers is greatly influenced by the nature of binding sites of ligands attached with metal centers and obviously on the coordination mode of the bridging ligands [31,32]. The oxygen donor based ligands such as carboxylates have widely used to design several types of magnetic materials. Besides, the multi oxygen donor ligands like rhodizonate, croconate and squarate are highly attractive for designing the metal clusters and coordination polymers [33–36]. These ligands have multi-oxygen donor sites around a planar-aromatic motif and thus they can exhibit different binding aptitudes with metal ions.

Here, we have used squaric acid as the bridging ligand. Due to its good donor ability offered by its four oxygen atoms, presence of extensive delocalized π-electrons, highly symmetrical, cyclic

* Corresponding author. Tel.: +91 9831115427; fax: +91 33 2414 6584.
E-mail address: kumars@phys.jdvu.ac.in (S. Kumar).

0020-1693/$ - see front matter © 2013 Elsevier B.V. All rights reserved.
http://dx.doi.org/10.1016/j.ica.2013.10.033

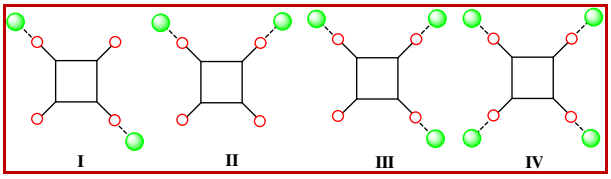

Scheme 1. Different bridging mode of squarate dianion.

shape and the stable aromatic character it has been attracted to several research groups. And, thus in last few years, a large number of discrete poly-nuclear and coordination polymers with diverse structural motifs have been synthesized using Squaric acid [37–46]. The different bridging modes exhibited by the squarate (Scheme 1) are: bridging *bis*- (μ-$_{1,2}$ and μ-$_{1,3}$), *tris*- (μ-$_{1,2,3}$) and *tetra-kis*-monodentate (μ-$_{1,2,3,4}$) that leads to the formation of bridged metal complexes with different extents of nuclearity and dimensionality. It is noteworthy that the binding modes of squarate dianion in the metal complexes are mainly governed by the structure and geometry of the blocking ligands coordinated to the central metal ions as well as the reaction conditions.

According to literature survey, the μ-$_{1,2}$ and μ-$_{1,3}$ bridging modes are most common [37–43], only in few cases μ-$_{1,2,3,4}$ bridging mode have been found [13,24,31,44,52]. The sole example of μ-$_{1,2,3}$ bridging pattern of squarate-dianion in a tri-nuclear Cu(II) complex has been reported by Vicente et al. [46]. In this endeavor, we are going to report a new 2D coordination polymer formed by using unusual μ-$_{1,2,3}$ bridging mode of squarate-dianion with Ni(II) and the blocking 2,2′-bipyridyl ligand. The structural analysis reveals that the blocking 2,2′-bipyridyl moiversuseties are hanging in the interlamellar space between 2D coordination sheets. The thermal and photoluminescence properties of the complex have been studied. The variable temperature magnetic measurements indicate that the complex is antiferromagnetic in nature.

2. Experimental

2.1. Materials and methods

Nickel(II) nitrate, hexahydrate; 2,2′-bipyridine; 3,4-dihydroxy-3-cyclobutene-1,2-dione (squaric acid) and sodium carbonate were purchased from Merck chemical company. All other chemicals were AR grade and used without further purification. The elemental analysis (C, H, N) was carried out using a Perkin-Elmer 240C elemental analyzer. The thermal analysis was carried out using a Mettler Toledo TGA-DTA 85 thermal analyzer under a flow of dinitrogen (30 ml min^{-1}). The sample was heated at a rate of 5 °C min^{-1} with inert alumina as a reference. The IR spectra of the sample were recorded on Nicolet Impact 410 spectrometer between 400 and 4000 cm^{-1}, using the KBr pellet method. The photoluminescence spectra were recorded by Shimadzu RF-5301PC spectrophotometer. The magnetization measurements were performed using a superconducting quantum interference device vibrating sample magnetometer (Quantum Design SVSM, USA) over a wide temperature range of 3–300 K. The experimental susceptibility data were corrected for underlying diamagnetism by use of tabulated Pascal's constants.

2.2. Synthesis of the complex

0.5 mmol squaric acid (0.05703 g) was dissolved in 10 ml distilled water and neutralized by aqueous solution of sodium carbonate to adjust the pH at 8.0. The nickel(II) nitrate, hexahydrate (0.2908 g, 1.0 mmol) was dissolved in 5 ml distilled water and added to the previous solution. The resultant mixture was stirred at room temperature for 15 min. Then, 10 ml methanolic solution of 2,2′-bipyridine (0.156 g, 1.0 mmol) was added to the previous solution and stirred for another 1 h. The whole mixture was then refluxed for 2 h at 90 °C. It was then allowed to cool to room temperature, the blue precipitate was filtered off and light blue colored filtrate was kept in undisturbed condition. After few days, the block shaped greenish blue colored crystals suitable for single crystal X-ray structural study were obtained and these were separated and dried. Yield 72%. *Anal.* Calc. for $C_{14}H_{11}N_2NiO_6$: C, 46.2; H, 2.5; N, 7.7. Found: C, 46.5; H, 2.4; and N, 7.5%. Selected IR bands (KBr pellet, cm^{-1}): ν (O–H) stretching 3445 (m); ν (CO) 1506 (m), 1524 (s), 1483 (s) and 1445 (w).

2.3. Crystallographic data collection and refinement

Suitable single crystal of the complex was mounted on a Bruker SMART diffractometer equipped with a graphite monochromator and Mo Kα (λ = 0.71073 Å) radiation. The structure was solved by Patterson method using SHELXS-97. The subsequent difference Fourier synthesis and least square refinement revealed the positions of the non-hydrogen atoms. The non-hydrogen atoms were refined with independent anisotropic displacement parameters. The hydrogen atoms were placed in idealized positions and their displacement parameters were fixed to be 1.2 times larger than those of the attached non-hydrogen atoms. The successful convergence was indicated by the maximum shift/error of 0.001 for the last cycle of the least squares refinement. All calculations have been carried out using SHELXS-97 [47], SHELXL-97 [48], PLATON-99 [49], ORTEP-32 [50] and WINGX system Ver-1.64 [51]. The data collection and structure refinement parameters and crystallographic data for the complex are given in Table 1. Some selected bond lengths, bond angles and non-covalent interaction parameters are presented in Table 2.

Table 1
Crystallographic data and refinement parameters of complex.

Crystal data	
Formula	$C_{14}H_9N_2NiO_5$, H_2O
Formula weight	362.97
Crystal system	orthorhombic
Space group	P_{bca} (No. 61)
a (Å)	12.774(5)
b (Å)	16.818(6)
c (Å)	12.140(5)
V (Å^3)	2608.1(17)
Z	8
D_{calc} (g/cm^3)	1.833
μ(Mo Kα) (mm)	1.525
F(000)	1464
Crystal size (mm)	0.08 × 0.08 × 0.40
Data collection	
T (K)	100
λ (Å)	Mo Kα 0.71073
θ min–max (°)	2.4–25.3
Dataset	−15:12; −19:20; −14:13
Total	12353
Unique data	2363
R_{int}	0.194
Observed data [$I > 2.0\sigma(I)$]	1088
Refinement	
Parameters refined	209
R	0.0726
wR_2	0.1516
S	0.80
Minmum and maximum resd. density [e/Å^3]	−0.75, 1.40

$w = 1/[s2(Fo2) + (0.0949P)2]$ where $P = (Fo2 + 2Fc2)/3$.

Table 2
Selected bond distances (Å) and bond angles (°) of the complex.

Ni1–O1	1.905(6)	Ni1–N2	1.968(7)
Ni1–O1W	1.925(5)	Ni1–O3*	2.460(6)
Ni1–N1	1.959(7	Ni1–O2**	2.555(6)
O1–Ni1–O1W	95.3(2)	O1W–Ni1–N1	175.1(3)
O1–Ni1–N1	89.4(3)	O1W–Ni1–N2	95.1(3)
O1–Ni1–N2	169.6(3)	O1W–Ni1–O3*	94.9(2)
O1–Ni1–O3*	94.7(2)	O1W–Ni1–O2**	79.8(2)
O1–Ni1–O2**	92.7(2)	O3*–Ni1–N1	86.1(2)
O2**–Ni1–N2	89.3(2)	O2**–Ni1–N1	98.6(2)
O2**–Ni–O3*	171.23(19)	O3**–Ni1–N2	84.2(2)
N1–Ni1–N2	80.2(3)		

* $3/2 - x, -y, 1/2 + z$;
** $1 - x, -y, -z$.

3. Result and discussion

3.1. Crystal structure description of the complex

The single crystal X-ray diffraction (SC-XRD) analysis reveals that the complex is a 2D coordination polymer and crystallizes in orthorhombic P_{bca} space group. The asymmetric unit contains one Ni^{2+} ion, one 2,2′-bipyridine, one squarate dianion, one coordinated water molecule and one guest water molecule, (Fig. 1). Ni(II) has a distorted octahedral coordination. N1 and N2 atoms of one 2,2′-bipyridine ligand, one oxygen atom (O1) of bridging squarate and O2W form the basal plane, and two oxygen atoms (O2 and O3) of two different squarate ions are at the *trans* axial coordination sites. Thus, the oxygen atoms of three symmetry related squarato-anions occupy facial positions in the coordination sphere. The distortion from perfect octahedral geometry is reflected in *cisoid* [79.8(2)–98.6(2)°] and *transoid* [169.6(3)–175.1(3)°] angles. Ni–N bond distances are within the range of 1.959(6)–1.968(7) Å and Ni–O bond distances are within the range of 1.905(6)–2.555(6) Å while Ni–O1W bond distance is 1.925(5) Å.

The squaric acid contains a four membered ring having one oxygen atom connected to each carbon atom. It can bind with metal ions by using these four oxygen atoms. It is a well established fact that the squarate dianion shows versatile bridging mode [31,37–46]. Here, the squarate dianion binds with three different metal ions in μ-$_{1,2,3}$ mode using its three oxygen donor centers O1, O2 and O3 while the other oxygen atom O4 remains inert towards coordination with metal ion (Fig. 2). The squarate dianion binds two metal centers Ni1 and Ni1* through O1 and O3 oxygen atoms in a *trans* bridging mode leading to formation of 1D coordination chain (Fig. 3) which are further connected by O2 oxygen atom of another squarate dianion which consequently binds with other two metal ions and this gives rise to a 2D coordination sheet structure within the crystallographic ***ac***-plane (Fig. 4). The 2D coordination sheets are packed in parallel way along crystallographic ***b***-axis. The coordinated 2,2′-bipyridyl units are pendant within the interlamellar spaces.

Such 2D sheets are packed along crystallographic ***b***-axis by recognizing each other to inter-digitated 2D + 2D structure *via* $\pi\cdots\pi$ stacking interactions. The pyridyl rings of pendant 2,2′-bipyridyl moieties of a 2D sheet interact with other pyridyl rings of neighboring 2D coordination sheets and by virtue of this the formation of 3D supramolecular structure takes place (Fig. 5). The distance between their centroids is 3.861(5) Å and the dihedral

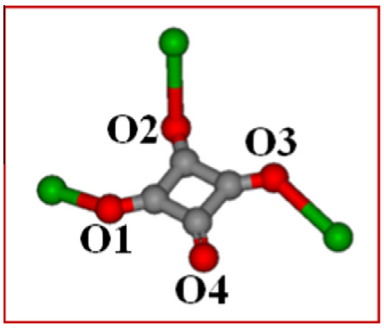

Fig. 2. $\mu_{1,2,3}$-Bridging pattern of squarate-dianion in the complex.

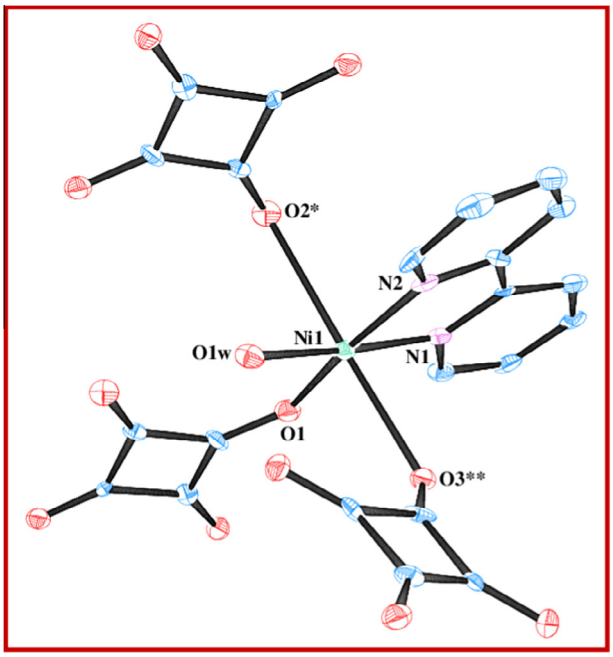

Fig. 1. ORTEP diagram of the complex.

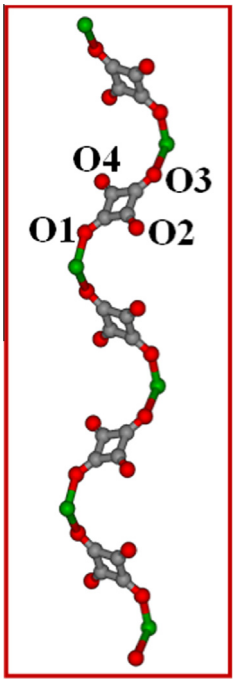

Fig. 3. *trans*-Binding mode of squarate-dianion ligand forms 1D coordination chain with metal centers.

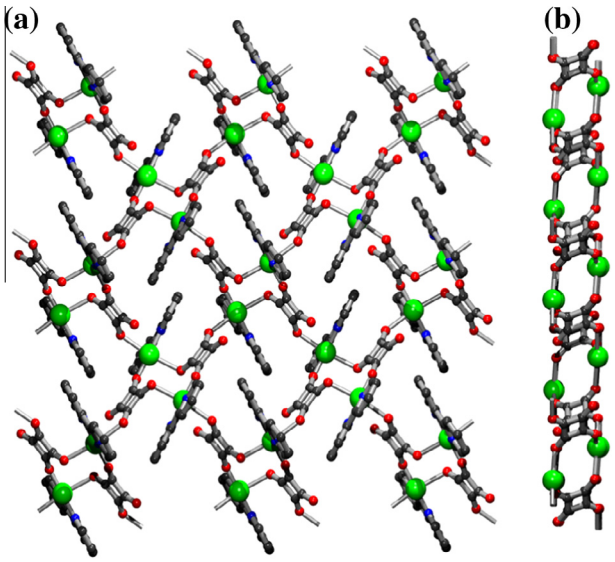

Fig. 4. (a) 2D coordination sheet of the complex within the ***ac***-plane; (b) view along ***b***-axis (coordinated 2,2′-bipyridyl moieties are omitted for clarity).

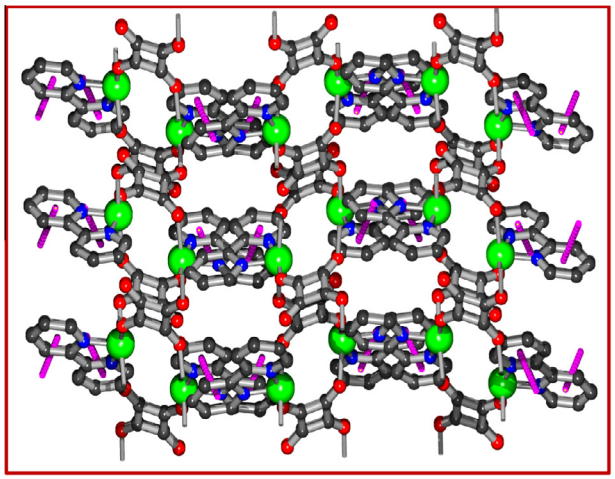

Fig. 5. 3D supramolecular structure formed by π···π interactions (magenta).

angle is 8.5(4)° (Symmetry: $x, 1/2 - y, -1/2 + z$). During formation of 3D supramolecular structure, 1D supramolecular channels are created along crystallographic ***c***-axis (Fig. 6). The guest water molecules persist within such supramolecular channels. The hanging π-rings from the 2D coordination sheets create hydrophobicity between the 2D sheets while in contrast the uncoordinated O4 oxygen atom of squarate dianion (directed toward the interlamellar spaces) creates hydrophilicity within such channels. The overall 3D structure behaves like as metal–organic supramolecular host (MOSH) and the uncoordinated water molecules act as guest. The guest water molecules also act as a bridge between the 2D coordination sheets through O2W–H1W2···O4 and O2W–H2W2···O3 hydrogen bonding interactions which give further stability to the three-dimensional (3D) supramolecular structure (Fig. 7). All hydrogen bonding interactions have been summarized in Table 3.

3.2. Thermal analysis

The thermal (TG–DTA) studies of coordination and supramolecular polymers are important to analyze their thermal stability

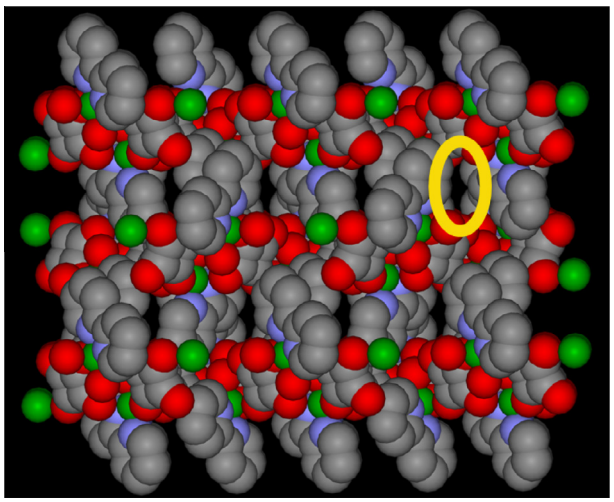

Fig. 6. During formation of 3D supramolecular structure 1D supramolecular channel is formed along crystallographic ***c***-axis.

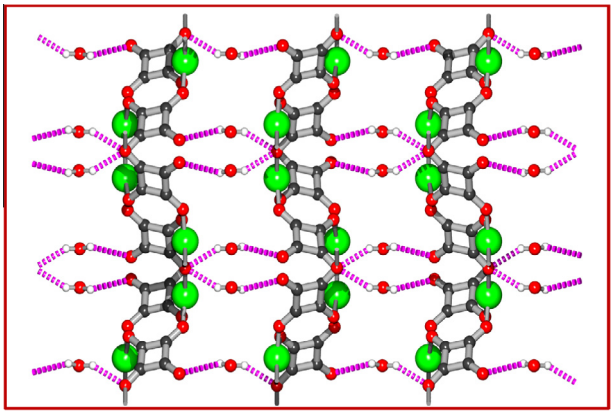

Fig. 7. 2D coordination sheets are connected by water mediated hydrogen bonding to form 3D supramolecular structure.

and to verify the stability of the guest species within the host. The thermal analysis reveals that the complex decomposes in three steps. The TG curve of the complex shows that mass loss starts at 50 °C (Fig. 8). A mass loss took place within the temperature range 50–85 °C that corresponds to the loss of guest water molecules. In the next step, the coordinated water molecules are released in the temperature range of 125–150 °C. The anhydrous compound is stable up to 275 °C and it decomposes at ~350 °C.

The DTA plot also supports the dehydration pattern of the complex (Fig. 8). Two small and broad endothermic peaks at 65 and 140 °C have been observed in the DTA curve of the complex. These endothermic peaks in the DTA curve correspond to the removal of the guest water and the coordinated water molecules, respectively. The endothermic peak (at 140 °C) indicates the conversion from crystalline to anhydrous state of the complex. The large exothermic peak at 350 °C corresponds to decomposition of the complex.

3.3. Magnetic study of the complex

The variable temperature magnetic studies have been performed in the temperature range 3–300 K. The χ_m *versus* T and $\chi_m T$ *versus* T plots of complex are shown in Fig. 9. The value of

Table 3
Hydrogen bond dimensions of the complex.

D–H···A	D–H/(Å)	H···A/(Å)	D···A/(Å)	<D–H···A /(Å)	Symmetry
O1W–H1W1···O4	0.87	2.04	2.553(8)	117	$3/2-x,-y,1/2+z$
O1W–H2W1···O2	0.90	1.78	2.657(8)	164	
O2W–H1W2···O4	0.85	2.50	2.892(7)	109	$-1/2+x,1/2-y,-z$
O2W–H2W2···O3	0.85	2.08	2.819(7	144	$1-x,-y,-z$
C1–H1···O1	0.95	2.30	2.818(10)	114	
C1–H1···O2W	0.95	2.36	3.146(11)	140	$1/2+x,1/2-y,-z$
C8–H8···O2W	0.95	2.25	3.203(11)	175	$x,1/2-y,1/2+z$
C10–H10···O1W	0.95	2.51	3.044(11)	116	

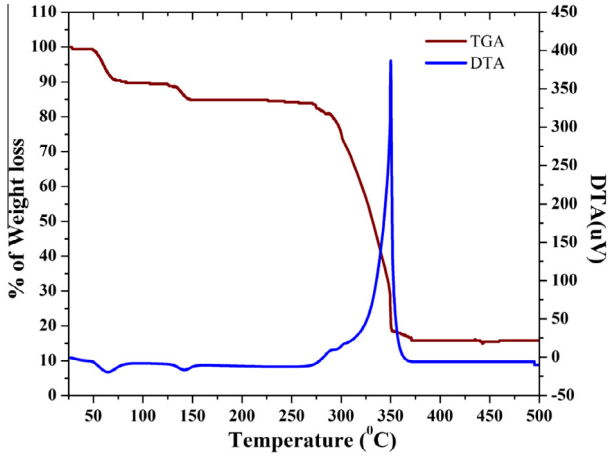

Fig. 8. TG-DTA plot of the complex.

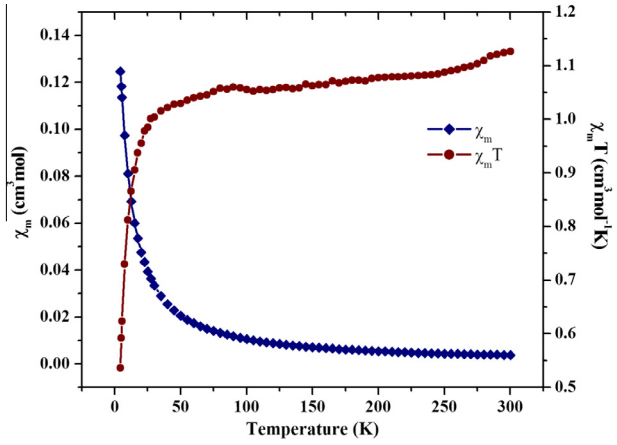

Fig. 9. Both χ_m *vs. T* and $\chi_m T$ *vs. T* plots of the complex.

χ_m at 300 K is 0.0037 $cm^3\ mol^{-1}$, and on cooling χ_m value increases very slowly and reaches to 0.025 $cm^3\ mol^{-1}$ at 40 K. Afterward, it increases sharply to the maximum value of 0.118 $cm^3\ mol^{-1}$ at 3 K. In order to determine the nature of magnetic interaction, the susceptibility data were fitted to the Curie–Weiss law. The Curie and Weiss constants are 1.11 $cm^3\ mol^{-1}$ K and $\theta = -5.496$ K, respectively (see Fig. 10). The negative value of the Weiss constant indicates the presence antiferromagnetic interaction between Ni(II) ions. The $\chi_m T$ value is 1.12 $cm^3\ mol^{-1}$ K at room-temperature which is slightly lower than that expected ($\chi_m T$ at 300 K = 1.32 $cm^3\ mol^{-1}$ K) for an isolated Ni(II) ion having two uncoupled spins, $S = 1$. The $\chi_m T$ value decreases monotonically with the decrease of temperature. Upon cooling $\chi_m T$ value decreases slowly up to 40 K and then it decreases very sharply

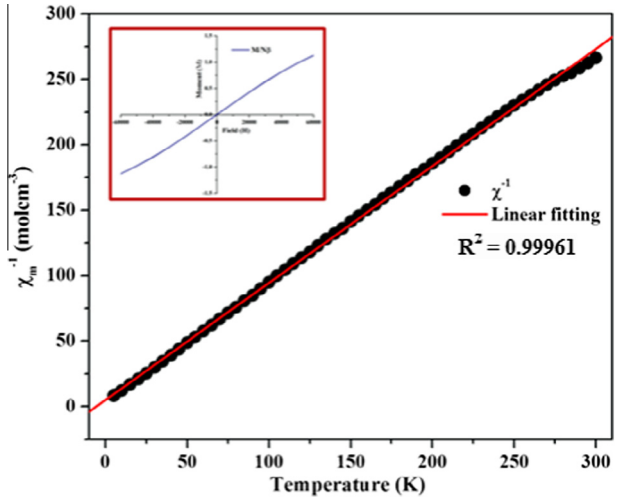

Fig. 10. The χ^{-1} *vs. T* plot for the complex (inset: *M vs. H* plot).

with further lowering temperature and attains a value of 0.59 $cm^3\ mol^{-1}$ K at 3 K. Such a behavior is typical of antiferromagnetic interaction. The isothermal magnetization (*M*) *versus* field (*H*) shows no hysteresis loop at 3 K (vide Inset of Fig. 10) indicating antiferromagnetic exchange interactions between Ni(II) centers. It may therefore be concluded that Ni(II) centers are coupled by antiferromagnetic interaction.

In order to correlate the magnetic behavior of the complex with the bridging mode of squarate dianion, we have taken into account the magnetic behavior of some previously reported squarato-bridged metal complexes. The detailed literature survey reveals that most of the squarato-bridged transition metal(II) complexes exhibit antiferromagnetic behavior irrespective of nature of binding mode of the squarate ligand, presence of other blocking ligand and dimensionality of the resultant complex. Massoud et al. have reported μ-$_{1,2}$-squarato-bridged complex $[Ni_2(TPA)_2(\mu\text{-}_{1,2}\text{-}C_4O_4)(H_2O)_2](ClO_4)_2${TPA = tris(2-pyridylmethyl)amine} that shows antiferromagnetic interaction between Ni(II) ions [37]. Xanthopoulos et al. have reported another μ-$_{1,2}$-squarato bridged complex $[Cu_2(SalNEt_2)_2(H_2O)(C_4O_4)]H_2O$ {$SalNEt_2$ = N-(2-(diethylamino)ethyl)-salicylideneaminate} and this complex also exhibits antiferromagnetic coupling between Cu(II) ions [41]. Massoud et al. have reported a series of dinuclear μ-$_{1,3}$-squarato-bridged Ni(II) and Cu(II) complexes $[Ni_2(2,3,2\text{-tet})_2(\mu\text{-}_{1,3}\text{-}C_4O_4)(H_2O)_2](ClO_4)_2$, $[Ni_2(aepn)_2(\mu\text{-}_{1,3}\text{-}C_4O_4)(H_2O)_2](ClO4)_2$, $[Cu_2(pmedien)_2(\mu\text{-}_{1,3}\text{-}C_4O_4)(H_2O)_2](ClO4)_2.4H_2O$ {where 2,3,2-tet = 1,4,8,11-tetraazaundecane, pmedien = *N*,*N*,*N*′,*N*″,*N*″-pentamethyldiethyl enetriamine [45]. All these complexes exhibit weak antiferromagnetic coupling between the metal ions. Recently, Escrivá et al. also has reported a squarato bridged complex $[Cu_2(HBIMAM)_2(C_4O_4)_3(H_2O)_2]_n.\ 2nH_2O$ {BIMAM = bis(imidazol-2-yl)methylamino methane} in which the suqarato-dianion bridge two Cu(II) ions through the μ-$_{1,3}$ fashion

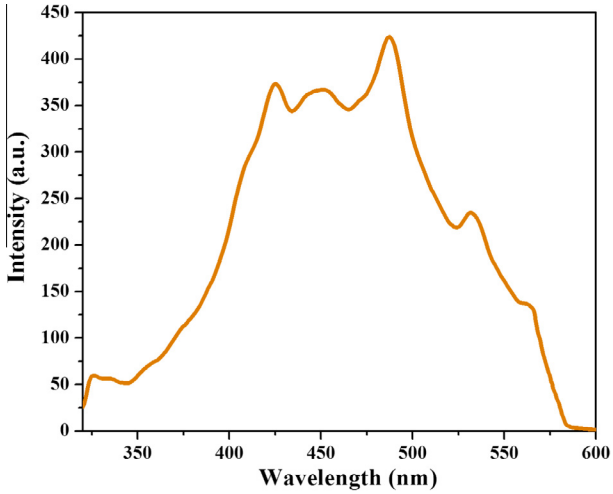

Fig. 11. Photoluminescence spectra of the complex.

[43] and the complex exhibits weak antiferromagnetic interaction between metal ions. Similar examples of μ-$_{1,2}$- and μ-$_{1,3}$-squarato bridged complexes have been reported by different groups [12,23,38–40]. The one and only reported μ-$_{1,2,3}$-squarato bridged complex $[Cu_3$-(pmap)3(μ-$_{1,2,3}$–$C_4O_4)]$ $(ClO_4)_4{\cdot}2H_2O]$ {pmap = bis-[2-(2-pyridyl)ethyl]-(2-pyridyl)methylamine} also exhibits antiferromagnetic coupling between its three Cu(II) centers [46]. Castro et al. have reported μ-$_{1,2,3,4}$-squarato bridged tetranuclear compound $[Cu_4(tren)_4(\mu$-$_{1,2,3,4}$-$C_4O_4)](ClO_4)_6$ that displays antiferromagnetic coupling between metal centers [31]. After literature survey, it can be said that the extent of antiferromagnetic interaction depends upon the bridging fashion of the squarate ligand and obviously the metal ions present in the complexes. In contrast, Cangussu et al. have reported a bi-nuclear squarato bridged $[Cu_2(bpcam)_2(\mu_{1,3}$-$C_4O_4)(H_2O)_4]{\cdot}10H_2O$ {where bpcam = bis(2-pyrimidylcarbonil)amidate} complex that shows weak ferromagnetic interaction due to accidental orthogonality in the complex [12]. Such weak to very weak ferromagnetic interaction has also been reported for some other squarato bridged metal complexes having μ-$_{1,2}$, μ-$_{1,3}$, μ-$_{1,2,3,4}$ types bridging fashions [13,24,44,52]. The present complex under investigation is a μ-$_{1,2,3}$-squarato bridged compound where a squarato-dianion simultaneously binds three different Ni(II) ions and also exhibits antiferromagnetic behavior following the general trend for squarato bridged metal complexes.

3.4. Photoluminescence study

The emission spectra of the complex have been carried out in solid state at room temperature. The luminescent behavior of the complex corresponds to a ligand-centered (LC) fluorescence. The complex has shown emission maxima at 424 nm and 487 nm upon excitation at 300 nm (Fig. 11). This can be attributed to the π–π^* transition in the squarate and 2,2′-bipyridine ligands. The small peak around 531 nm is possibly caused by extended π-conjugation within the ligand system.

4. Conclusion

In conclusion, we have successfully synthesized a novel squarato-bridged 2D coordination polymer $\{[Ni(squarate)(2,2'$-bipy$)(H_2O)]{\cdot}H_2O\}_n$ where the squarato di-aninon exhibits very rare μ-$_{1,2,3}$ bridging mode. These 2D coordination sheets are packed *via* $\pi\cdots\pi$ interactions leading to the formation of 3D supramolecular structure with 1D supramolecular channels. These 1D channels are filled with guest water molecules which get stability through hydrogen bonding interactions. The structural study indicates the presence of unusual rare μ-$_{1,2,3}$ bridging mode of squarato-dianinon in the complex and the magnetic measurements have revealed that the complex is antiferromagnetic in nature. This is in agreement with the magnetic property of the sole previous example of μ-$_{1,2,3}$-squarato-bridged compound. Due to presence of π-electrons the complex becomes fluorescence active. By providing the second example of μ-$_{1,2,3}$ bridging pattern of squarato-dianion we have established that the squarate exhibits versatile bridging mode due to strong donor ability of its oxygen atoms.

Taking into account the present and large number of previous works it may be concluded that the squarato-bridged metal complexes provide the unique opportunity to study the wide variety of bridging modes exhibited by the ligand and to investigate the influence of different bridging modes on magnetic property of such systems. Finally, we have presented a new 2D coordination polymer formed by utilizing unusual μ-$_{1,2,3}$ bridging pattern of squarato-dianion that exhibits multiple functionalities: (a) acts as metal–organic supramolecular host, (b) exhibits antiferromagnetic behavior and (c) photo-luminescent activity.

Acknowledgments

This article is dedicated to the memory of Late Dr. Golam Mostafa (1962-2011). R. S. acknowledges financial support from the Council of Scientific and Industrial Research (CSIR), New Delhi under the SRF Program (09/096(0565)2008-EMR-I).

Appendix A. Supplementary material

CCDC 951933 contains the supplementary crystallographic data for this paper. These data can be obtained free of charge from The Cambridge Crystallographic Data Centre via www.ccdc.cam.ac.uk/data_request/cif. Supplementary data associated with this article can be found, in the online version, at http://dx.doi.org/10.1016/j.ica.2013.10.033.

References

[1] K. Maruoka, N. Murase, H. Yamamoto, J. Org. Chem. 58 (1993) 2938.
[2] C. Chen, K.S. Suslick, Coord. Chem. Rev. 128 (1993) 293.
[3] D. Gatteschi, A. Caneschi, R. Sessoli, A. Cornia, Chem. Soc. Rev. 25 (1996) 101.
[4] D. Gatteschi, Adv. Mater. 6 (1994) 635.
[5] C. Cadiou, R.A. Coxell, A. Graham, A. Harrison, M. Helliwell, S. Parsons, R.E.P. Winpenny, Chem. Commun. 10 (2002) 1106 (and references therein).
[6] D.J. Price, S.R. Batten, B. Moubaraki, K.S. Murray, Chem. Commun. 7 (2002) 762.
[7] M. Eshel, A. Bino, I. Felner, D.C. Johnston, M. Luban, L.L. Miller, Inorg. Chem. 39 (2000) 1376 (and references therein).
[8] L.K. Thompson, Coord. Chem. Rev. 249 (2005) 2549.
[9] O. Kahn, Molecular Magnetism, VCH, New York, 1993.
[10] D. Gatteschi, R. Sessoli, Angew. Chem., Int. Ed. 42 (2003) 268.
[11] I. Castro, M.L. Calatayud, J. Sletten, F. Lloret, M. Julve, Inorg. Chim. Acta 287 (1999) 173.
[12] D.S. Cangussu, H.O. Tumpf, H. Adams, J.H. Thomas, F. Lloret, M. Julve, Inorg. Chim. Acta 358 (2005) 2292.
[13] Y. Akhriff, J. Server-Carrió, A. Sancho, J. Garcia-Lozano, E.J. Escrivá, L. Soto, Inorg. Chem. 40 (2001) 6832.
[14] S. Konar, P.S. Mukherjee, E. Zangrando, F. Lloret, N.R. Chaudhuri, Angew. Chem., Int. Ed. 41 (2002) 1561.
[15] S. Dalai, P.S. Mukherjee, E. Zangrando, F. Lloret, N.R. Chaudhuri, J. Chem. Soc., Dalton Trans. 25 (2002) 822.
[16] I.L. Karle, D. Ranganathan, V. Haridas, J. Am. Chem. Soc. 118 (1996) 7128.
[17] B.D. Alleyne, L.A. Hall, H.-A. Hosein, H. Jaggernauth, A.J.P. White, D.J.J. Williams, J. Chem. Soc., Dalton Trans. 22 (1998) 3845.
[18] S. Lopez, S.W. Keller, Inorg. Chem. 38 (1999) 1883.
[19] P.S. Mukherjee, S. Konar, E. Zangrando, T. Mallah, J. Ribas, N.R. Chaudhuri, Inorg. Chem. 42 (2003) 2695.
[20] J.-M. Rueff, J.-F. Nierengarten, P. Gilliot, A. Demessence, O. Cregut, M. Drillon, P. Rabu, Chem. Mater. 16 (2004) 2933.
[21] J.D. Martin, R.F. Hess, P.D. Boyle, Inorg. Chem. 43 (2004) 3242.

[22] P. Chaudhuri, K. Oder, K. Wieghardt, S. Gehring, W. Haase, B. Nuber, J. Weiss, J. Am. Chem. Soc. 110 (1988) 3657.
[23] X. Solans, M. Aguilló, A. Gleizes, J. Faus, M. Julve, M. Verdaguer, Inorg. Chem. 29 (1990) 775.
[24] H.-A. Hosein, H. Jaggernauth, B.D. Alleyne, L.A. Hall, A.J.P. White, D.J. Williams, Inorg. Chem. 38 (1999) 3716.
[25] H. Tamaki, Z.J. Zhong, N. Matsumoto, S. Kida, M. Koikawa, N. Achiwa, Y. Hashimoto, H. Okawa, J. Am. Chem. Soc. 114 (1992) 6974.
[26] E. Coronado, J.R. Galan-Mascaros, C. Martí-Gastaldo, J. Mater. Chem. 16 (2006) 2685.
[27] E. Coronado, J.R. Galan-Mascaros, C. Martí-Gastaldo, CrystEngComm 11 (2009) 2143.
[28] E. Coronado, J.R. Galan-Mascaros, C. Martí-Gastaldo, J. Am. Chem. Soc. 130 (2008) 14987.
[29] Y.-C. Ou, J. Wang, J.-D. Leng, Z.J. Lin, M.-L. Tong, Dalton Trans. 40 (2011) 3592.
[30] R. Saha, S. Kumar, CrystEngComm 14 (2012) 4980.
[31] I. Castro, J. Sletten, M.L. Calatayud, M. Julve, J. Cano, F. Lloret, A. Caneschi, Inorg. Chem. 34 (1995) 4903.
[32] M. Viertelhaus, H. Henke, C.E. Anson, A.K. Powell, Eur. J. Inorg. Chem. 12 (2003) 2283.
[33] D. Braga, G. Cojazzi, L. Maini, F. Grepioni, New J. Chem. 25 (2001) 1221.
[34] D. Deguenon, G. Bernardinelli, J.P. Tuchagues, P. Castan, Inorg. Chem. 29 (1990) 3031.
[35] C.-C. Wang, C.-H. Yang, G.-H. Lee, Inorg. Chem. 41 (2002) 1015.
[36] L. Soto, N. Ruiz, H. Núñez, J. Server-Carrió, E. Escrivà, A. Sancho, J. Gracía-Lozano, Inorg. Chim. Acta 359 (2006) 3221.
[37] S.S. Massoud, F.A. Mautner, R. Vicente, F.R. Louka, Eur. J. Inorg. Chem. 23 (2008) 3709.
[38] C.-C. Wang, C.-H. Yang, G.-H. Lee, H.-L. Tsai, Eur. J. Inorg. Chem. 7 (2005) 1334.
[39] R. Kirchmaier, E. Altin, A. Lentz, Z. Kristallogr, New Cryst. Struct. 218 (2003) 541.
[40] I. Castro, M.L. Calatayud, J. Sletten, F. Lloret, M. Julve, J. Chem. Soc., Dalton Trans. 5 (1997) 811.
[41] C.E. Xanthopoulos, M.P. Sigalas, G.A. Katsoulos, C.A. Tsipis, C.C. Hajikostas, A. Terzis, M. Mentzafos, Inorg. Chem. 32 (1993) 3743.
[42] J.A.C. van Ooijen, J. Reedijk, A.L. Spek, Inorg. Chem. 18 (1979) 1184.
[43] E. Escrivá, L. Soto, J. Server-Carrió, C.J. Gómez-García, G.M. Espallargas, N. Ruiz, A. Sancho, J. García-Lozano, C.R. de Arellano, Polyhedron 56 (2013) 90.
[44] F. Dumestre, B. Soula, A.M. Galibert, P.-L. Fabre, G. Bernardinelli, B. Donnadieu, P. Castan, J. Chem. Soc., Dalton Trans. 24 (1998) 4113.
[45] S.S. Massoud, F.A. Mautner, R. Vicente, J.S. Dickens, Inorg. Chim. Acta 361 (2008) 299.
[46] R. Vicente, E. Ruiz, J. Cano, S.S. Massoud, F.A. Mautner, Inorg. Chem. 47 (2008) 4648.
[47] G.M. Sheldrick, SHELXS 97, Program for Structure Solution, University of Gottingen, Germany, 1997.
[48] G.M. Sheldrick, SHELXL 97, University of Gottingen, Germany, Program for Crystal Structure Refinement, 1997.
[49] A.L. Spek, J. Appl. Crystallogr. 36 (2003) 7.
[50] L.J. Farrugia, J. Appl. Crystallogr. 30 (1997) 565.
[51] L.J. Farrugia, J. Appl. Crystallogr. 32 (1999) 837.
[52] P.S. Mukherjee, S. Konar, E. Zangrando, C. Diaz, J. Ribas, P.S. Chaudhuri, J. Chem. Soc., Dalton Trans. 18 (2002) 3471.

Inorganica Chimica Acta 423 (2014) 123–132

Contents lists available at ScienceDirect

Inorganica Chimica Acta

journal homepage: www.elsevier.com/locate/ica

A dynamic metal–organic supramolecular host based on weak π-stacking interactions incorporating 2D water-chloride-methanolic supramolecular sheet

Rajat Saha [a], Somen Goswami [a], Susobhan Biswas [a], Ian M. Steele [c], Kamalendu Dey [b,*], Atish Dipankar Jana [d,*], Sanjay Kumar [a,*]

[a] Department of Physics, Jadavpur University, Jadavpur, Kolkata 700032, India
[b] Department of Chemistry, University of Kalyani, Kalyani 741235, West Bengal, India
[c] Department of the Geophysical Sciences, The University of Chicago, Chicago, USA
[d] Department of Physics, Behala College, Parnasree, Kolkata 700060, India

ARTICLE INFO

Article history:
Received 8 June 2014
Received in revised form 20 July 2014
Accepted 27 July 2014
Available online 12 August 2014

Keywords:
Cationic metal–organic complex
π···π interaction
2D water-chloride-methanolic supramolecular sheet
Dynamic host
Photoluminescence

ABSTRACT

Herein, we report the formation of a unique water-chloride-methanol 2D supramolecular network within the hydrophobic interlayer cavities of a novel flexible metal–organic supramolecular host (MOSH) framework formed by π-induced self-assembly of the monomeric metal–organic complex $[Pr(1,10\text{-phen})_2(H_2O)_5]Cl_3(H_2O)(CH_3OH)$ (1,10-phen = 1,10-phenanthroline) (**complex 1**). Single crystal X-ray diffraction (SC-XRD), powder X-ray diffraction (PXRD) and spectroscopic techniques are used to characterize the complex. The structural analysis reveals that in this MOSH the discrete metal–organic moieties are connected by π···π interactions to form 2D metal–organic supramolecular sheet structures. The guest water and methanol molecules together with counter chloride anions stabilize in the MOSH framework through hydrogen bonding interactions between the 2D metal–organic supramolecular layers. The hydrogen bonding interactions among the coordinated water and guest species form a unique 2D supramolecular water-chloride-methanol sheet structure. Upon removal of guest water and methanol molecules by heat treatment the supramolecular framework gets shrunk but retains the crystallinity while upon re-absorption of water molecules it undergoes structural change with expansion of effective guest accessible void space. The flexibility of the supramolecular framework and the mechanism of thermally induced phase transformation in the MOSH are examined by PXRD study. The photoluminescence property of the **complex 1** and the crystalline complex obtained after rehydration has been thoroughly investigated. The theoretical analysis has been performed to resolve the issue of stability of the 2D supramolecular water-chloride-methanol sheet in the MOSH framework and it has been found that for **complex 1** the stabilization energy of the $[(H_2O)_6\text{-}(CH_3OH)\text{-}Cl_3]_n^{3-}$ is 1949.427Kcal mol^{-1}.

1. Introduction

The self-assembly of discrete molecular units via covalent or non-covalent interactions, such as, hydrogen-bonding, π-stacking interactions, etc. is a popular approach for design and synthesis of new compounds having wide range of application potential [1–6]. During self assembly the discrete metal–organic moieties connect themselves through cooperative non-covalent interactions and this leads to formation of metal–organic supramolecular host (MOSH) [7–12]. The guest molecules get stability in the MOSHs through supramolecular interactions. The MOSHs can very efficiently release and absorb guest molecules in a controlled manner [13–14]. Depending on the design strategy, the MOSHs are classified in two broad categories, viz., charged MOSH and uncharged MOSH. The uncharged MOSHs are capable of accommodating neutral guest species like simple water clusters [15–19], whereas the cationic MOSHs can easily accommodate anionic guest species like chloride-hydrates [20–24]. Since the ion transportation is a very important phenomenon in various chemical and biological processes in the living systems [25–29], several novel strategies have been adopted for recognition and transportation of ions in the self-assembled complexes [30–31]. The self-assembly is one of the unique approaches for construction of ion channels in cationic

* Corresponding authors. Tel.: +91 9831115427; fax: +91 33 2413 8917 (S. Kumar).
E-mail addresses: kdey_chem.@rediffmail.com (K. Dey), atishdipankarjana@yahoo.in (A.D. Jana), kumars@phys.jdvu.ac.in (S. Kumar).

http://dx.doi.org/10.1016/j.ica.2014.07.077
0020-1693/

MOFs. The cationic metal–organic complex formation can be realized without using any anionic donor ligands.

Studies on water clusters in metal–organic host complexes have attracted a great deal of attention during recent times [32–36]. On the other hand, hybrid clusters of water and other small organic molecules or ions formed by hydrogen bonding interaction have drawn relatively less attention. In particular, there are very few reports on experimental identification and analysis of discrete water-chloride clusters (the hydrogen-bonded assemblies of water on crystallization and chloride counter ions in crystalline materials) [19–24]. The hydration phenomenon of chloride ion has canonical importance in the field of biochemistry [37] and supramolecular chemistry. Moreover, drug molecules are generally organic molecules and they dissolve in organic solvents like methanol, ethanol, etc. For efficient delivery of the anionic drug molecules a better understanding of the mode of interaction of the anions with organic solvents and water is a prerequisite. More than 70% of enzymes, substrates and cofactors are anions. Thus, more theoretical and experimental investigations on hybrid water-chloride clusters with other organic molecules are very essential taste.

In this context, we have reported previously the formation of a 2D water sheet, a helical-water chain and water-chloride tape in chiral supramolecular complexes and supramolecular hosts [38,39]. As a continuing effort, in this report, we have shown that a water-chloride-methanol 2D supramolecular network can be created within the hydrophobic interlayer cavities of a dynamic MOSH. A simple strategy that can be adopted for possible isolation of a hybrid water-chloride system is to use a neutral ligand in synthesizing Pr(III)-based cationic complexes. In this effort, we have successfully synthesized a metal–organic complex [Pr(1,10-phen)$_2$(H_2O)$_5$] Cl_3(H_2O)(CH_3OH), which includes water, chloride and methanol as guest molecules using 1,10-phenanthroline ligand. It is expected that the chelating nature of 1,10-phenanthroline along with its inherent π-stacking capability would integrate the discrete metal moieties at least in one direction. The X-ray crystal structure analysis has revealed that the complex assembles into a 2D supramolecular architecture through π···π interactions. The complex behaves like a dynamic metal–organic supramolecular host (MOSH). Three chloride ions, one guest water molecule and one guest methanol molecule along with five coordinated water molecules form unique water-chloride-methanol hybrid 2D hydrogen bonded network and is stabilized within the hydrophobic interlayer cavities. The most important property of the present MOSH is its breathing nature – when the host is heated up it expels the guest molecules and during cooling the species absorbs the water molecules from the atmosphere. The dynamic breathing metal–organic frameworks (MOFs) are easy to design but a dynamic supramolecular host like the present one is rarely observed as it requires involvement of weak forces. The present work shows how weak π···π stacking forces can be employed in designing host–guest frameworks and may work as effective example in designing new dynamic MOSHs.

2. Experimental

2.1. General

The ingredients praseodymium (III) chloride, hepta-hydrate and 1,10-phenanthroline were purchased from Merck Chemical Company and all other chemicals used were AR grade. The elemental analysis (C, H and N) was carried out using a Perkin-Elmer 240C elemental analyzer. The IR spectrum was recorded between 400 and 4000 cm^{-1} using a Nicolet Impact 410 spectrometer employing the KBr pellet method. The thermal analysis was carried out using a Mettler Toledo TGA-DTA 85 thermal analyzer under a flow of N_2 (30 ml min^{-1}). The sample was heated at a rate of 10 °C min^{-1} with inert alumina as a reference. The photoluminescence spectra were collected on a Shimadzu RF-5301PC Spectrophotometer. The Powder X-ray diffraction (PXRD) patterns were recorded by using Cu-K_α radiation (Bruker D8; 40 kV, 40 mA).

2.2. Synthesis of **complex 1** {[Pr(1,10-phen)$_2$(H_2O)$_5$]Cl_3(H_2O)(CH_3OH)}

5 ml aqueous solution of $PrCl_3 \cdot 7H_2O$ (0.93 g, 0.0025 mol) was added drop-wise to a solution of 1,10-phenanthroline (0.90 g, 0.005 mol) in MeOH (5 ml). The resulting solution was then filtered off and was kept in open air. After 10 days, the light greenish yellow colored single crystals suitable for single crystal X-ray (SCXRD) study appeared and they were collected by filtration. Yield: 1.40 g (75% based on Pr). *Anal.* Calc. for $C_{25}H_{32}PrN_4O_7Cl_3$: C, 40.15; H, 4.31; N, 7.49. Found: C, 40.02; H, 4.39; N, 7.36%. IR (KBr, cm^{-1}): 3332br, 2298vw, 1627s, 1593s, 1574s, 1518s, 1421 m, 1343s, 1299m, 1102m, 1091w, 863m, 846s, 772s, 722w, 635w. λ_{max} (in MeOH) 260 nm, 324 nm (shoulder).

2.3. Crystallographic data collection and refinement

The suitable single crystal of the **complex** was mounted on a Bruker SMART diffractometer equipped with a graphite monochromator and Mo Kα (λ = 0.71073 Å) radiation and the data was collected at room temperature. The structure was solved by Patterson method using the SHELXS97 program. The hydrogen atoms were placed in idealized positions and their displacement parameters were fixed to be 1.2 times larger than those of the attached non-hydrogen atoms. The position of non-hydrogen atoms were refined with independent anisotropic displacement parameters. The subsequent difference Fourier synthesis and least-square refinement revealed the positions of the non-hydrogen atoms. The successful convergence was indicated by the maximum shift/error of 0.001 for the last cycle of the least square refinement. All calculations were carried out using SHELXS 97 [40], SHELXL 97 [41], PLATON 99 [42], ORTEP-32 [43] and WinGX system Ver-1.64 [44]. The data collection, structure refinement parameters and crystallographic data of **complex 1** are provided in Table 1.

3. Results and discussion

3.1. Crystal structure of **complex 1** {[Pr(1,10-phen)$_2$(H_2O)$_5$]Cl_3(H_2O)(CH_3OH)}

The analysis of SCXRD data have revealed that **complex 1** is a neutral mononuclear compound in which the Pr^{3+} ion is coordinated to two different 1,10-phen ligands and five water molecules as shown in Fig. 1. Each asymmetric unit contains one metal–organic moiety, three chloride anions, one guest methanol molecule and one guest water molecule. In the present case Pr(III) shows nine coordination mode. The four nitrogen atoms (N1, N2, N3 and N4) of two different 1,10-phen ligands and five water molecules (O1W, O2W, O3W, O4W and O5W) fulfill the nine coordination of Pr(III) through formation of a paddle-wheel shaped molecular structure. Some selected coordination bond lengths and bond angles are listed in Table 2 and 3, respectively. The two 1,10-phen moieties are nearly at the *trans* position to each other. The Pr–N bond lengths lie between 2.662(2) and 2.723(2) Å which are well within the range of other reported Pr(III)-phen complexes [45–48]. It is well known that the lanthanide ions have high affinity for hard donor atoms and ligands with oxygen or hybrid oxygen–nitrogen atoms [49]. The Pr–O_{water} distances are in the range between 2.448(2) and 2.487(2) Å (average 2.477 Å), which are comparable with those observed in other Pr^{3+} ion complexes with

Table 1
Crystallographic data and refinement parameters of **complex 1**.

Crystal data	
Formula	$C_{24}H_{26}N_4O_5Pr$, CH_4O, H_2O, 3Cl
Formula weight	747.81
Crystal system	triclinic
Space group	$P\bar{1}$ (No. 2)
a [Å]	8.872(3)
b [Å]	9.192(3)
c [Å]	18.920(6)
α [°]	88.790(5)
β [°]	84.689(5)
γ [°]	69.159(5)
V [Å^3]	1435.7(8)
Z	2
D_{calc} [g cm^{-3}]	1.730
μ (Mo Kα) [mm^{-1}]	2.027
F(000)	752
Data collection	
Temperature (K)	100
Radiation [Å]	Mo Kα 0.71073
Theta min–max [°]	1.1, 28.4
Dataset	−11: 11; −12: 12; −25: 24
Total	16947
Unique data	6698
R_{int}	0.015
Observed data [$I > 2\sigma(I)$]	6510
Refinement	
Nref, Npar	6698; 361
R	0.0276
wR_2	0.0717
S	1.06
Maximum and average shift/error	0.00, 0.00
Minimum and maximum residual density [e Å^{-3}]	−0.91, 1.51

Table 2
Selected bond lengths (Å) of **complex 1**.

Bonds	Bond distance	Bonds	Bond distance
Pr1–O1W	2.4826(19)	Pr1–O2W	2.484(2)
Pr1–O3W	2.487(2)	Pr1–O4W	2.448(2)
Pr1–O5W	2.481(3)	Pr1–N1	2.709(2)
Pr1–N2	2.662(2)	Pr1–N3	2.723(2)
Pr1–N4	2.677(2)		

analogous ligands [48]. It is noteworthy that the monomeric units are further connected by supramolecular hydrogen bonding and π···interactions with the guest molecules to form a 3D supramolecular structure.

3.2. Supramolecular structure

In the present system, the monomeric metal–organic units are connected by supramolecular π-interactions to from 2D supramolecular sheets and between two 2D supramolecular sheets one guest methanol molecule, one guest water molecule and three charge neutralized chloride ions are accumulated by self-assembly. The pyridyl ring [Cg1] of the 1,10-phen ligand in one metal–organic unit bridges the phenyl ring [Cg5] of a symmetry [2 − x, −y, 1 − z] related metal–organic unit. Again, the pyridyl ring [Cg4] of the same 1,10-phen unit interacts with another phenyl ring [Cg6] of the same symmetry [2 − x, −y, −z] related unit. In this way, the monomeric units are connected to form 1D supramolecular chains along the crystallographic c-axis as shown in Fig. 2. These 1D supramolecular chains are further connected by π···π interactions to form 2D supramolecular sheets within the ac-plane, (Fig. 3). The pyridyl ring [Cg2] of one 1,10-phen unit connects the self-complementary pyridyl ring [Cg2] of a symmetry related [1 − x, −y, 1 − z] nearby unit. All the π···π interaction parameters are summarized in Table 4. The 2D supramolecular sheets are packed along b-axis to form metal–organic supramolecular hosts (Fig. 4) bearing hydrophobic pockets lined up by the 1,10-phen ligands. These hydrophobic pockets are filled up by one water molecule, one methanol molecule and three counter chloride ions. All these guest molecules interact with the metal–organic moieties through hydrogen bonding interactions. Among the guest species, only Cl1 is connected with the framework by hydrogen bonding interactions as shown in Figure S1. Two chloride ions, one water molecule and one methanol molecule form a [$Cl_2(H_2O)$(MeOH)] cluster by hydrogen bonding interactions as shown in Figure S2.

The hydrogen bonding interactions between the coordinated water molecules and the guest species have formed a 2D supramolecular network in the crystallographic ab-plane (Figs. 5 & S3). Cl1 is bound to H2W2 of O2W water molecule and the other hydrogen atom H1W2 is connected with methanolic oxygen atom O1. O1 is also connected with H2W1 of O1W water molecule. Methanolic hydrogen atom H1O1 is attached with Cl3. The other hydrogen atom H1W1 is bound to atom Cl2 and Cl2 binds the H2W5 of O5W water molecule. Other hydrogen atom H1W5 is bound to Cl1. This Cl1 is also connected with the H1W4 of O4W water molecule. Second hydrogen atom H2W4 of O4W binds the Cl3 atom which is consequently bound to H1W6 of O6W. The other hydrogen atom H2W6 of O6W has formed bond with Cl2 while Cl2 is bound to H2W3 of O3W water molecule and H1W3 of O3W is connected with Cl1, which is bound to H2W2. All these together build

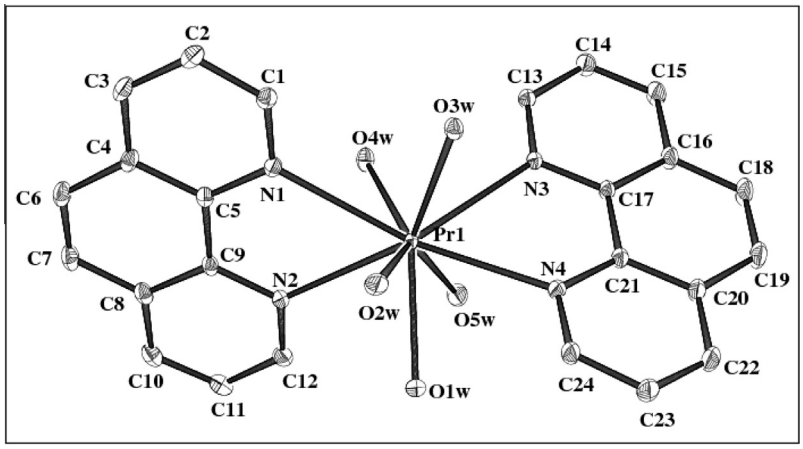

Fig. 1. The ORTEP diagram of **complex 1**.

Table 3
Selected bond angles (°) of **complex 1**.

O1W–Pr1–O2W	70.13(8)	O5W–Pr1–N3	69.76(6)
O1W–Pr1–O3W	132.85(7)	O5W–Pr1–N4	78.94(6)
O1W–Pr1–O4W	131.25(7)	N1–Pr1–N2	61.66(6)
O1W–Pr1–O5W	70.69(8)	N1–Pr1–N3	121.07(5)
O1W–Pr1–N1	117.99(6)	N1–Pr1–N4	148.66(6)
O1W–Pr1–N2	71.28(6)	N2–Pr1–N3	139.58(6)
O1W–Pr1–N3	120.93(6)	N2–Pr1–N4	139.99(5)
O1W–Pr1–N4	69.50(6)	N3–Pr1–N4	61.26(5)
O2W–Pr1–O3W	72.48(6)	O2W–Pr1–O4W	140.55(6)
O2W–Pr1–O5W	140.40(6)	O2W–Pr1–N1	73.26(6)
O2W–Pr1–N2	91.74(6)	O2W–Pr1–N3	128.55(6)
O2W–Pr1–N4	82.37(6)	O3W–Pr1–O4W	95.90(6)
O3W–Pr1–O5W	135.36(6)	O3W–Pr1–N1	76.02(6)
O3W–Pr1–N2	137.58(6)	O3W–Pr1–N3	65.66(6)
O3W–Pr1–N4	78.07(6)	O4W–Pr1–O5W	73.53(6)
O4W–Pr1–N1	67.32(6)	O4W–Pr1–N2	71.39(6)
O4W–Pr1–N3	73.85(6)	O4W–Pr1–N4	133.18(6)
O5W–Pr1–N1	132.31(6)	O5W–Pr1–N2	81.04(6)

up a supramolecular 2D sheet of $\{(H_2O)_6\text{-}(CH_3OH)\text{-}Cl_3\}_n$. The hydrogen bonding association of the guest with the host leads to the formation of a 3D supramolecular assembly of the host–guest framework (Figure S4). All the hydrogen bonding interactions are summarized in Table 5.

3.3. Thermal analysis

We have studied the thermal stability of the complex (Fig. 6). The thermogravimetric analysis shows a weight loss of 12.43% (calculated 13.91%) in the temperature range between 40 and 117 °C which corresponds to the loss of one lattice water molecule, one methanol molecule and three coordinated water molecules. A further weight loss of 3.96% occurs between 117 and 257 °C consistent with the loss of two coordinated water molecules (calculated 4.82%). The observed weight losses are a little bit lower than the theoretical values. The slight discrepancy is due to weight loss occurring even at lower than 40 °C, illustrating the dynamic nature of the water molecules in the solid state.

3.4. Study on dynamic nature of the host–guest binding-removal and reintroduction of guests

The rigid metal–organic coordination polymers have attracted considerable interest because of their potential applications in catalysis, adsorption and ion exchange [50–52]. However, the flexible metal–organic frameworks are more efficient for these applications [53–56], as flexible frameworks are very sensitive to the presence of guests and undergo structural changes depending upon the number and nature of the guest molecules [57–60]. The thermal study of **complex 1** has revealed that within 117 °C one guest water molecule, one methanol molecule and three coordinated water molecules escape from the complex. Therefore, to study the nature of the framework after evacuation of the guest water, guest methanol and coordinated water molecules we have heated **complex 1** at 117 °C for 3 h and subsequently recorded the PXRD data of the heat treated sample. The PXRD analysis indicates that this heat treated sample is crystalline in nature. So, even after the removal of the coordinated and guest water and methanol molecules the host retains its crystallinity. Due to heating, the peak at 9.37° (1st peak) disappears while a new peak appears at 13.56°. Moreover, the intensity of the peak at 10.27° decreases. As the 1st peak appears at a higher angle compared to that of the parent complex (**complex 1**) so it can be inferred that upon thermal treatment shrinking occurs i.e., the supramolecular sheets come closer to each other after heating. The PXRD pattern of this new complex matches well with the simulated XRD pattern of $[Pr(phen)_2Cl_3,H_2O]$ (Fig. 7) [61]. It may therefore be inferred that the structure of the sample obtained by heating **complex 1** at 117 °C is similar to that of $[Pr(phen)_2Cl_3,OH_2]$. Thus, upon removal of guest molecules and coordinated water molecules (partly) by heating, the supramolecular complex undergoes structural changes that leads to the formation of a new complex having the crystal structure similar to that of $[Pr(phen)_2Cl_3,H_2O]$.

The crystalline nature of the partially evacuated complex inspired us to study the flexibility of the complex upon heat treatment. So, this partially evacuated complex was kept in open air. After 14 days, a light green crystalline solid (**complex 1a**) was collected and PXRD pattern of **complex 1a** was recorded. The PXRD pattern shows that the peak at 9.37° reappears which indicates that the heated complex absorb water from air and water molecules enter between the 2D supramolecular metal–organic sheets and this in turn has expanded the channels between the sheets. There are some notable dissimilarity between the PXRD patterns of **complex 1**, **complex 1a** and the partially dehydrated complex. For **complex 1a** the intensity of the peak at 10.27° has diminished and highest peak has been found at 11.27°. Thus it can be concluded that due to soaking of water a new phase has been generated. All the PXRD patterns are presented in the Fig. 7. The results of PXRD study on **complex 1**, **complex 1a** and the partially dehydrated complex have clearly revealed that the MOSH under investigation exhibits *"shrinking and expanding ability"* upon evacuation and reintroduction of guest molecules.

We have examined the thermal behavior of **complex 1a** (Fig. 8). According to Figs. 6 and 8 thermal behavior of **complex 1** and **1a** is different up to 250 °C but it is nearly similar above 250 °C. This difference is due to the fact that **complex 1** contains methanol and water as guest along with the coordinated water molecules while **complex 1a** does not have any methanol molecule. The similarity of thermogravimetric curves of **complex 1** and **1a** indicates that the main structural pattern of the MOSH remains more or less same upon evacuation and reintroduction of guest molecules.

3.5. Temperature and heating time dependent PXRD studies

In order to investigate the mechanism of structural transformation, we have heated **complex 1** at different temperatures and for different time duration at a fixed temperature and we have

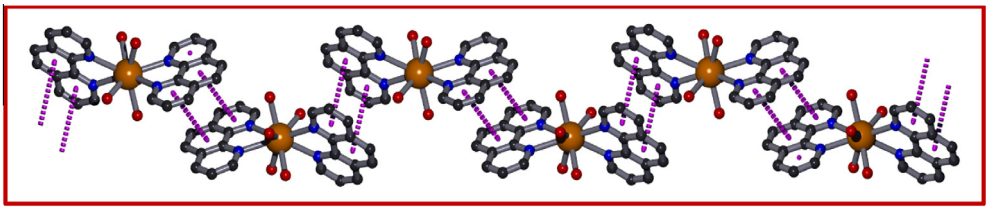

Fig. 2. 1D supramolecular chain is formed along crystallographic *c*-axis by $\pi\cdots\pi$ interactions (Pr = Orange, C = Grey, N = Blue, O = Red). (For interpretation of the references to colour in this figure legend, the reader is referred to the web version of this article.)

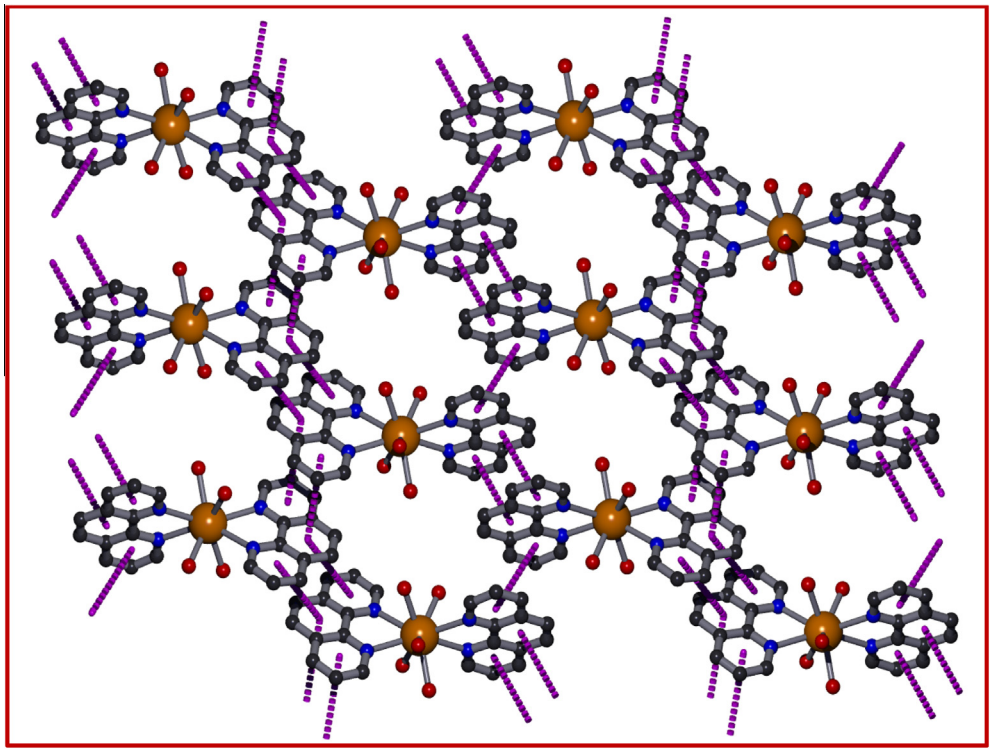

Fig. 3. 1D chains are further connected by π···π interactions to form 2D supramolecular sheets within *ac*-plane (Pr = Orange, C = Grey, N = Blue, O = Red). (For interpretation of the references to colour in this figure legend, the reader is referred to the web version of this article.)

Table 4
π··· interactions of **complex 1**.

$Cg_i\cdots Cg_j$	Cgi···Cgj distance/Å	α/(°)	Cgi perpendicular distance to Cgj	Symmetry
Cg1···Cg5	3.715(2)	1.07(13)	3.4051(11)	2 − *x*, −*y*, 1 − *z*
Cg2···Cg2	4.136(2)	0	3.5163(11)	1 − *x*, −*y*, 1 − *z*
Cg2···Cg5	3.919(2)	1.95(13)	3.5368(11)	1 − *x*, −*y*, 1 − *z*
Cg4···Cg4	3.703(2)	0	3.5580(11)	2 − *x*, −*y*, −*z*
Cg4···Cg6	3.883(2)	3.68(14)	3.5809(12)	2 − *x*, −*y*, −*z*
Cg5···Cg1	3.715(2)	1.07(13)	3.3901(11)	2 − *x*, −*y*, 1 − *z*
Cg5···Cg2	3.919(2)	1.95(13)	3.4800(11)	1 − *x*, −*y*, 1 − *z*
Cg5···Cg5	3.918(2)	0	3.3807(11)	2 − *x*, −*y*, 1 − *z*
Cg6···Cg4	3.883(2)	3.68(14)	3.4788(12)	2 − *x*, −*y*, −*z*
Cg6···Cg6	3.850(2)	0	3.4849(13)	1 − *x*, −*y*, −*z*

Cg1: N1–> C1–> C2–> C3–> C4–> C5–>; Cg2: N2–> C9–> C8–> C10–> C11–> C12–>; Cg4: N4–> C21–> C20–> C22–> C23––> C24–>; Cg5: C4–> C5–> C9–> C8–> C7–> C6–>; Cg6: C16–> C17–> C21–> C20–> C19–> C18–>.

recorded PXRD patterns of the samples obtained after heating (Figs. 9 and 10). We have heated the sample at 75, 100 and 120 °C for 1 h in each case and recorded the PXRD pattern of these heated products. The changes occurred in the PXRD patterns are shown in Fig. 9. The PXRD analysis reveals that upon heating at 75 °C the 1st peak shifts toward higher angle (at 9.67° from 9.43°) and a new sharp peak appears at 13.50° along with the changes in other peaks. The PXRD pattern obtained after heating **complex 1** at 120 °C is distinctly different from all previous phases. We have recorded the PXRD pattern of the sample after heating it at 120 °C for 40 min, 80 min and 120 min. No significant change has been observed in these PXRD patterns (Fig. 10). It may therefore be concluded that with the increase in heating temperature the structural transformation proceeds in stepwise manner through gradual removal of guest molecules. Moreover, upon heating at 120 °C for a certain time the guest water molecule, methanol molecule and three coordinated water molecules get released from the host framework and so a new phase has been produced and no further change occurs.

3.6. Photoluminescence study

For praseodymium (III), there are three possible emitting f-states, e.g., $^3P_0$, $^1D_2$ and $^1G_4$. However, in solution transitions takes place from two excited states ($^3P_0$ and $^1D_2$) [62], and from three excited states ($^3P_0$, $^1D_2$ and $^1G_4$) in solids [63–65]. Moreover, Pr^{3+} also emits efficient ultraviolet 5d-4f-luminescence [80–83] and this transition is used for the fluorometric determination of Pr^{3+} in solutions [65–67].

The emission spectrum of **complex 1** in solid state has been presented in Fig. 11. It is composed of four emission manifolds: the intense $^3P_0 \rightarrow {}^3H_4$ transition at 484 nm, the weak $^3P_0 \rightarrow {}^3H_5$ transition at around 505 nm, a complex band system in 558–670 nm range including the $^1D_2 \rightarrow {}^3H_4$ transition (572 nm), $^3P_0 \rightarrow {}^3H_6$ (592 nm) and $^3P_0 \rightarrow {}^3F_2$ (672 nm) transitions, and the weak $^3P_0 \rightarrow {}^3F_{3,4}$ emission at around 719 nm. The π-π* transition of 1,10-phen appears in the wavelength region of 340–420 nm with a broad band around 384 nm, which can be attributed to the phosphorescence of 1,10-phen [68]. The appearance of such phospho-

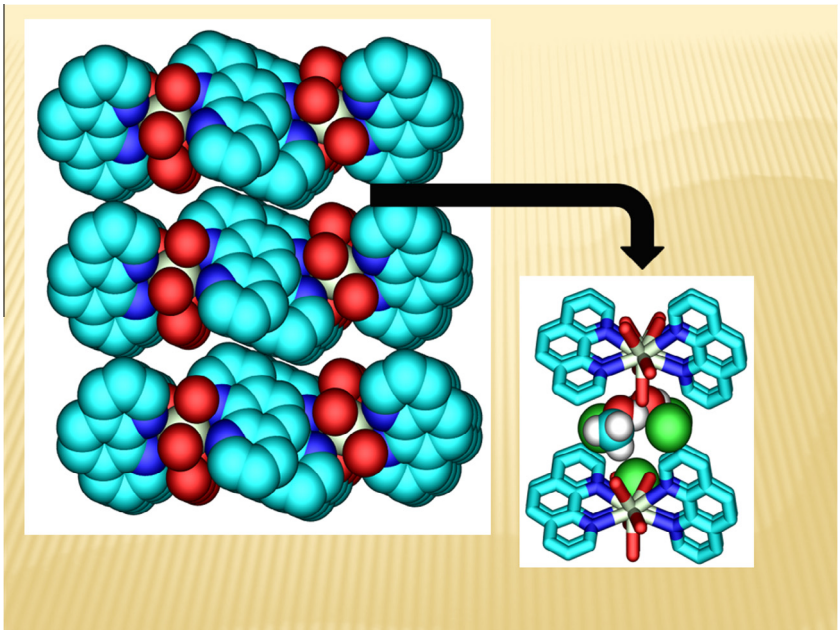

Fig. 4. Supramolecular hosts are filled up by guest molecules (Pr = Grey, C = Cyan, N = Blue, O = Red, Cl = Green). (For interpretation of the references to colour in this figure legend, the reader is referred to the web version of this article.)

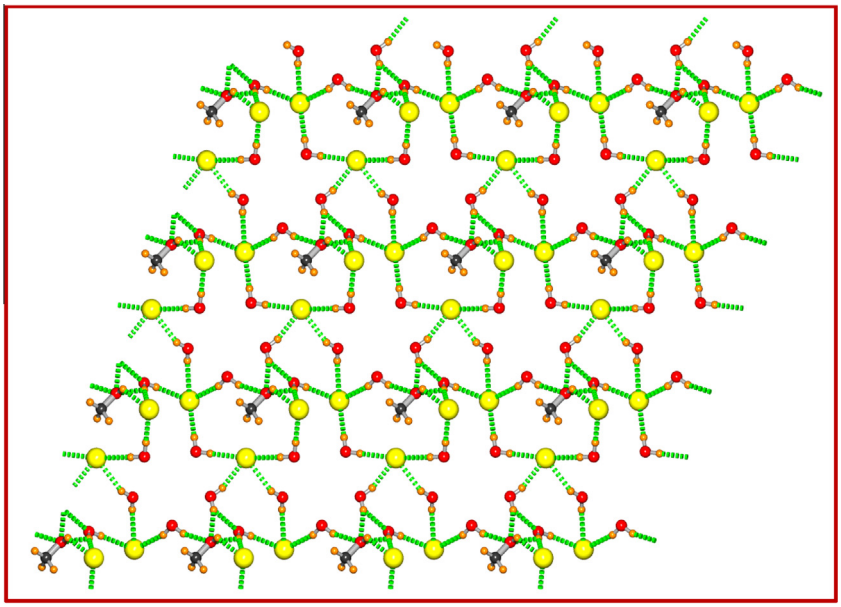

Fig. 5. 2D supramolecular sheet in crystallographic *ab*-plane formed by hydrogen bonding (green) interactions (C = Cyan, O = Red, H =White, Cl = Yellow). (For interpretation of the references to colour in this figure legend, the reader is referred to the web version of this article.)

rescence band at room temperature is a very rare case and it indicates the presence of stable triplet state in 1,10-phen.

The emission spectrum of **complex 1a** (Fig. 12) is nearly similar to that of **complex 1**. It shows an intense $^3P_0 \rightarrow {}^3H_4$ transition at 486 nm, a very weak peak at 500 nm for $^3P_0 \rightarrow {}^3H_5$ transition. A set of peaks with small intensity are also observed within the wavelengths range of 567–670 nm that includes the $^1D_2 \rightarrow {}^3H_4$ (567 nm), $^3P_0 \rightarrow {}^3H_6$ (594 nm) and $^3P_0 \rightarrow {}^3F_2$ (668 nm) transitions. The π-π^* transition of 1,10-phen appears in the wavelength region of 330–415 nm with a broad band around 385 nm, which can be assigned to the phosphorescence of 1,10-phenanthroline. Thus, the photoluminescence property of **complex 1** and **1a** is similar in nature.

3.7. Theoretical study

We performed an *ab initio* geometrical optimization of the H-atom positions at the MP2 level of DFT theory with the 6-31**G(d,p) basis set by freezing the positions of the heavy oxygen atoms for a quantitative understanding of the stability of the water-chloride-methanol cluster. All calculations have been implemented with the GAUSSIAN-03 package [69]. We have performed the calculation with one motif made of six water-one methanol-three chloride, $[(H_2O)_6\text{-}(CH_3OH)\text{-}Cl_3]_n^{3-}$ (**Figure S5**) as it is the basic repeating unit of the whole water-chloride-methanolic sheet. We consider the stabilization energy of the cluster association having n number of water molecules ($E_{n\text{-mer}}$) to be equal to

Table 5
Hydrogen bond dimensions of **complex 1**.

D–H···A	D–H/Å	H···A/Å	D···A/Å	<D–H···A/(°)	Symmetry
O1W–H1W1···Cl2	0.87	2.27	3.110(3)	163	$x, -1+y, z$
O1W–H2W1···O1	0.88	1.91	2.758(5)	163	$1+x, -1+y, z$
O2W–H1W2···O1	0.85	1.95	2.769(5)	162	$1+x, -1+y, z$
O2W–H1W2···O6W	0.85	2.17	2.711(4)	121	$1+x, -1+y, z$
O2W–H2W2···Cl1	0.86	2.24	3.077(2)	164	$1+x, y, z$
O3W–H1W3···Cl1	0.88	2.21	3.092(2)	180	$1+x, y, z$
O3W–H2W3···Cl2	0.87	2.25	3.122(2)	179	
O4W–H1W4···Cl1	0.89	2.21	3.098(2)	179	
O4W–H2W4···Cl3	0.88	2.07	2.949(2)	179	
O5W–H1W5···Cl1	0.82	2.43	3.156(3)	149	
O5W–H2W5···Cl2	0.82	2.46	3.276(2)	169	$x, -1+y, z$
O1–H1O1···Cl3	0.86	1.98	2.444(5)	113	
O6W–H1W6···Cl3	0.87	2.22	3.087(3)	172	
O6W–H1W6···O1	0.87	1.84	2.336(6)	114	
O6W–H2W6···Cl2	0.86	2.32	3.176(4)	173	
C1–H1···O3W	0.95	2.44	3.130(3)	129	
C11–H11···Cl3	0.95	2.74	3.524(3)	140	$x, -1+y, z$
C13–H13···O4W	0.95	2.50	3.087(3)	120	
C19–H19···Cl1	0.95	2.80	3.744(3)	176	$1-x, -y, -z$
C24–H24···O1W	0.95	2.56	2.955(3)	106	
C25–H25B···Cl3	1.00	2.48	2.934(6)	107	
C25–H25C···Cl1	0.96	2.42	3.237(4)	143	

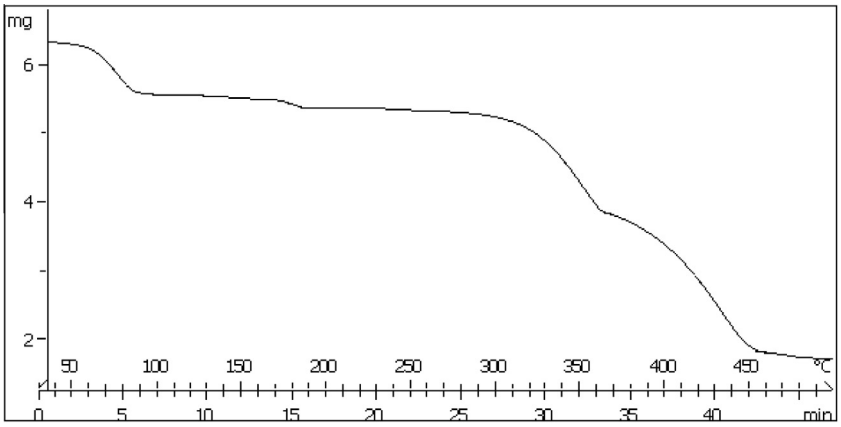

Fig. 6. The thermal plot of **complex 1**.

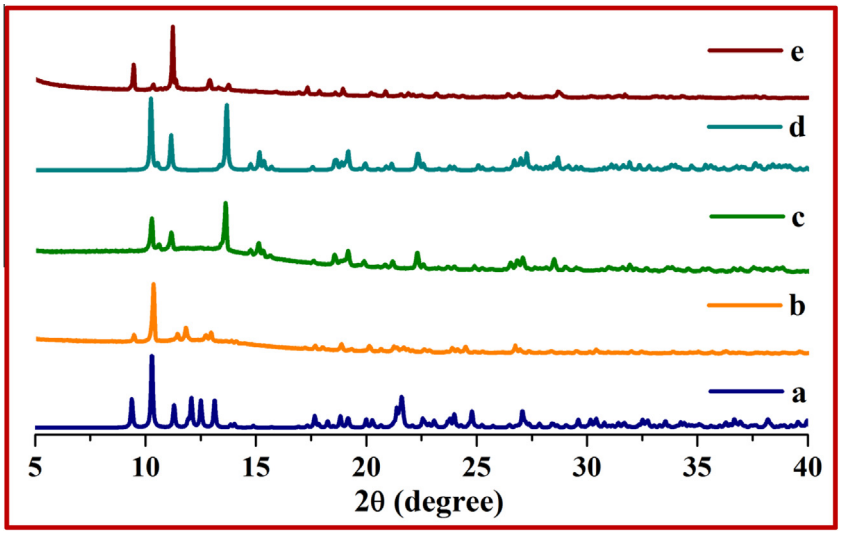

Fig. 7. PXRD patterns of the complexes: (a) simulated pattern of complex; (b) PXRD pattern of the as synthesized material; (c) PXRD pattern of the specimen obtained after removal of guest molecules; (d) simulated pattern of compound reported by M. Khorasani-Motlagh et.al.; (e) PXRD pattern of the compound after re-absorption of water.

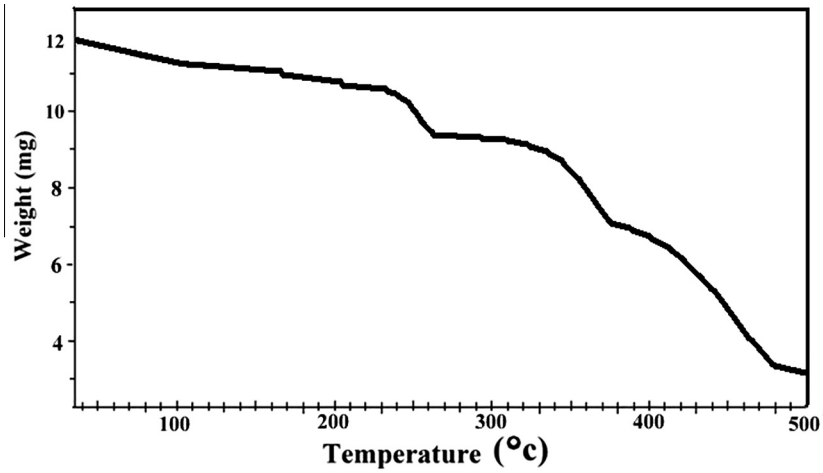

Fig. 8. Thermal plot of **complex 1a**.

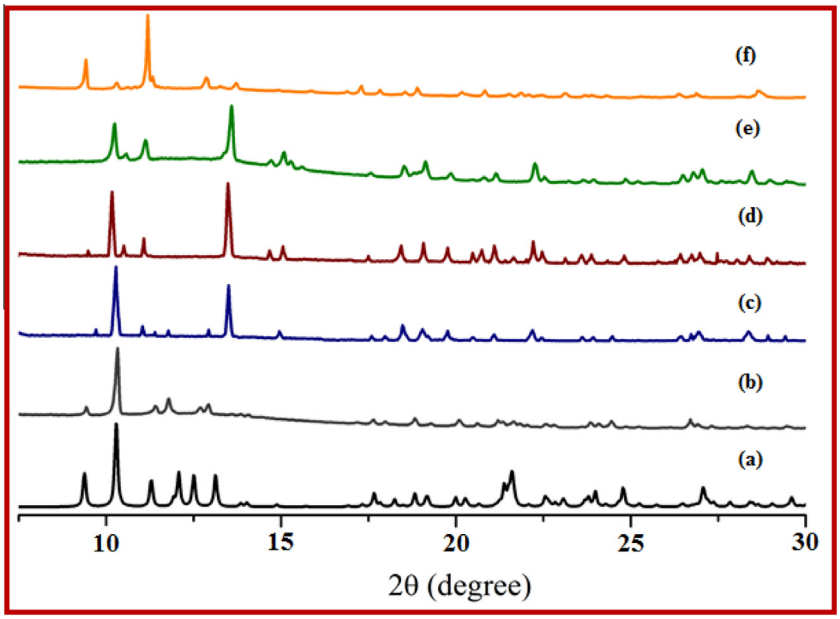

Fig. 9. PXRD patterns (a) black: simulated pattern, (b) deep gray: as synthesized pattern, (c) royal: after heating at 75 °C, (d) wine: after heating at 100 °C, (e) orchid: after heating at 120 °C, (f) orange: after rehydration. (For interpretation of the references to colour in this figure legend, the reader is referred to the web version of this article.)

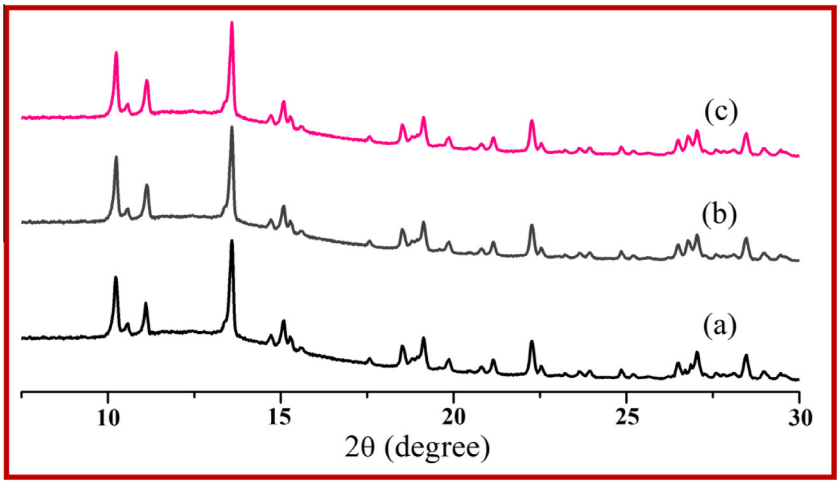

Fig. 10. PXRD patterns (a) black: after heating for 40 min, (b) deep gray: after heating for 80 min, (c) pink: after heating for 120 min at 120 °C. (For interpretation of the references to colour in this figure legend, the reader is referred to the web version of this article.)

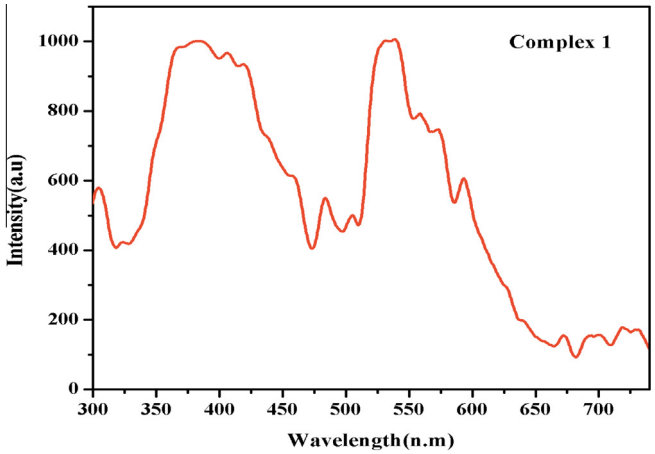

Fig. 11. Photoluminescence spectra of **complex 1**.

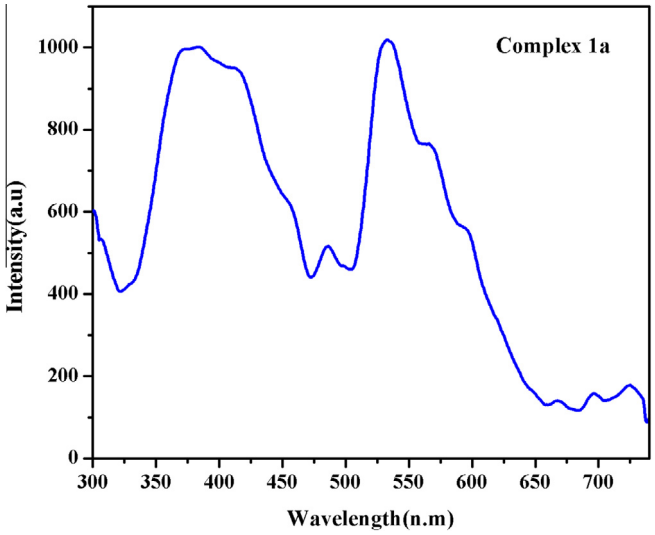

Fig. 12. Photoluminescence spectra of **complex 1a**.

$E_{n\text{-mer}} - (nE_{\text{monomer}})$ and similar approach has been adopted for chloride ion and methanol molecule. The monomeric energy was calculated by optimizing a single H_2O molecule, methanol molecule and chloride ion at the same level of the theory. The basis set superposition error (BSSE) was taken into account following the counterpoise method in the calculation of stabilization energy. The corrected stabilization energy of the $[(H_2O)_6\text{-}(CH_3OH)\text{-}Cl_3]_n^{3-}$ was found to be -1949.427 Kcal mol^{-1} for **complex 1**. The MP2 optimized coordinates of *water-chloride-methanol* cluster for **complex 1** is given in Table S1.

4. Conclusion

In this work, we have shown that hybrid water chloride system can be incorporated in a Pr(III)-based complex synthesized by using a neutral ligand 1,10-phenanthroline. The cationic complex $[Pr(phen)_2(H_2O)_5]^{3+}$ has been stabilized by the counter chloride anions. The 2D sheets are formed within the *ac*-plane by using the $\pi\cdots\pi$ interactions between 1D supramolecular chains formed by connecting the monomeric units. These 2D sheets are further packed by $\pi\cdots\pi$ interactions to form the MOSH having hydrophobic pockets in which guest water, chloride and methanol are stabilized through weak interactions. The hydrogen bonding interactions among coordinated water along with the guests form a unique 2D supramolecular water-chloride-methanol sheet. The guest responsive hydrophobic pockets between 2D supramolecular sheets are flexible in nature. The MOSH can shrink and readjust itself with the retention of crystallinity upon the expulsion and introduction of guest species. It also regains its original shape upon reabsorption of guest species. The present system thus behaves like a dynamic supramolecular metal–organic host which can breathe upon heating and cooling with simultaneous aquation. This dynamic nature is due to the strong affinity of the host towards the guest molecules. The coordination tendency of the Pr(III) ion and the self-assembling tendency of water-chloride and methanol stabilize the system and these are responsible for the affinity of the host towards the guest molecules. The unique hydrogen bonded network of water-chloride and methanol molecules obtained in the present crystalline host will enhance our knowledge on the water-anion assembly and further work may help to understand how water-chloride and methanol may behave in biological processes like chloride ion transportation. In summary, the present crystal structure is a very interesting example of dynamic supramolecular metal–organic host and will act as a guide in the design of further metal–organic host system – where metal coordination tendency towards water molecules and anion-water self-assembling tendency can be utilized.

Acknowledgments

We express our sincere gratitude to Late Dr. Golam Mostafa (1962-2011) for his encouragements and support. We acknowledges financial support from the Council of Scientific and Industrial Research (CSIR), Government of India (through grant number 09/096(0565)2008-EMR-I (for R. S.) and 60(1006)/13-EMR-II). We gratefully acknowledge Prof. R.N. Joardar, Professor (Retd.), Department of Physics, Jadavpur University for helpful discussion. We are grateful to Prof. A. Ghosh, Dept. of Chemistry, University of Calcutta for his kind assistance.

Appendix A. Supplementary material

CCDC contains the supplementary crystallographic data for 821326. These data can be obtained free of charge from The Cambridge Crystallographic Data Centre via www.ccdc.cam.ac.uk/data_request/cif. Supplementary data associated with this article can be found, in the online version, at http://dx.doi.org/10.1016/j.ica.2014.07.077.

References

[1] J.-M. Lehn, Supramolecular Chemistry, VCH, Weinheim, 1995.
[2] J.-M. Lehn, Angew. Chem., Int. Ed. Engl. 29 (1990) 1304.
[3] J.W. Ko, K.S. Min, M.P. Suh, Inorg. Chem. 41 (2002) 2151.
[4] T.K. Maji, P.S. Mukherjee, G. Mostafa, E. Zangrando, N. Ray Chaudhuri, Chem. Commun. (2001) 1368.
[5] L. Carlucci, G. Ciani, M. Moret, D.M. Proserpio, S. Rizzato, Angew. Chem., Int. Ed. 39 (2000) 1506.
[6] S. Biswas, G. Mostafa, I.M. Steele, S. Sarkar, K. Dey, Polyhedron 28 (2009) 1010.
[7] S. Kitagawa, R. Kitaura, S. Noro, Angew. Chem., Int. Ed. 43 (2004) 2334.
[8] G. Ferey, C. Mellot-Draznieks, C. Serre, F. Millange, J. Dutour, S. Surble, I. Margiolaki, Science 309 (2005) 2040.
[9] M. Dincă, J.R. Long, J. Am. Chem. Soc. 129 (2007) 11172.
[10] C.-D. Wu, A. Hu, L. Zhang, W. Lin, J. Am. Chem. Soc. 127 (2005) 8940.
[11] S. Horike, M. Dinc, K. Tamaki, J.R. Long, J. Am. Chem. Soc. 130 (2008) 5854.
[12] S. Hasegawa, S. Horike, R. Matsuda, S. Furukawa, K. Mochizuki, Y. Kinoshita, S. Kitagawa, J. Am. Chem. Soc. 129 (2007) 2607.
[13] H.-Q. Hao, W.-T. Liu, W. Tan, Z. Lin, M.-L. Tong, Cryst. Growth Des. 9 (1) (2009) 1459.
[14] K. Nagayoshi, M.K. Kabir, H. Tobita, K. Honda, M. Kawahara, M. Katada, K. Adachi, H. Nishikawa, I. Ikemoto, H. Kumagai, Y. Hosokoshi, K. Inoue, S. Kitagawa, S. Kawata, J. Am. Chem. Soc. 125 (2003) 221.
[15] M. Ding, J. Wu, Y. Liu, K. Lu, Inorg. Chem. 48 (2009) 7457.
[16] A.L. Gillon, N. Feeder, R.J. Davey, R. Storey, Cryst. Growth Des. 3 (2003) 663.

[17] C. Janiak, T.G. Scharmann, J. Am. Chem. Soc. 124 (2002) 14010.
[18] S. Pal, N.B. Sankaran, A. Samanta, Angew. Chem., Int. Ed. 42 (2003) 1741.
[19] M.T. Ng, T.C. Deivaraj, W.T. Klooster, G.J. McIntyre, J.J. Vittal, Chem. Euro. J 10 (2004) 5853.
[20] A.K. Ghosh, D. Ghoshal, J. Ribas, G. Mostafa, N.R. Chowdhury, Cryst. Growth Des. 6 (2006) 36.
[21] R.R. Fernandes, A.M. Kirillov, C.M. Fatima, G. da Silva, Z. Ma, J.A.L. da Silva, J.J.R.F. da Silva, A.J.L. Pombeiro, Cryst. Growth Des. 8 (2008) 782.
[22] P.S. Lakshminarayanan, E. Suresh, P. Ghosh, Angew. Chem., Int. Ed. 45 (23) (2006) 3807.
[23] R. Custelcean, M.G. Gorbunova, J. Am. Chem. Soc. 127 (2005) 16362.
[24] M.C. Das, S.K. Ghosh, S. Sen, P.K. Bharadwaj, CrystEngComm 12 (2010) 2967.
[25] M.C. Koch, K. Steinmeyer, C. Lorenz, K. Ricker, F. Wolf, M. Otto, B. Zoll, F. Lehmann-Horn, K.H. Grzeschik, T.J. Jentsch, Science 257 (1992) 797.
[26] K. Wichmann, B. Antonioli, T. Söhnel, M. Wenzel, K. Gloe, K. Gloe, J.R. Price, L.F. Lindoy, A.J. Blake, M. Schröder, Coord. Chem. Rev. 250 (2006) 2987.
[27] S. Chakrabarti, M.F.L. Parker, C.W. Morgan, C.E. Schafmeister, D.H. Waldeck, J. Am. Chem. Soc. 131 (2009) 2044.
[28] J.L. Sessler, P.A. Gale, W.-S. Cho, Anion Receptor Chemistry, The Royal Society of Chemistry, 2006.
[29] E.C. Constable, G. Zhang, C.E. Housecroft, M. Neuburger, S. Schaffner, CrystEngComm 11 (2009) 1014.
[30] P.D. Beer, A.P. Gale, Angew. Chem., Int. Ed. 40 (2001) 486.
[31] E.A. Meyer, R.K. Castellano, F. Diederich, Angew. Chem., Int. Ed. 42 (2003) 1210.
[32] L. Infantes, J. Chisholm, S. Motherwell, CrystEngComm 5 (2003) 480.
[33] I. Ravikumar, P.S. Lakshminarayanan, E. Suresh, P. Ghosh, Cryst. Growth Des. 6 (2006) 2630.
[34] P. Ren, B. Ding, W. Shi, Y. Wang, T.B. Lu, P. Cheng, Inorg. Chim. Acta. 359 (2006) 3824.
[35] Z.G. Li, J.W. Xu, H.Q. Via, N.H. Hu, Inorg. Chem. Commun. 9 (2006) 969.
[36] P.S. Lakshminarayanan, D.K. Kumar, P. Ghosh, Inorg. Chem. 44 (2005) 7540.
[37] J. M. Berg, J. L. Tymoczko, L. Stryer, Biochemistry, fifth ed.
[38] R. Saha, S. Biswas, G. Mostafa, CrystEngComm 13 (2011) 1018.
[39] R. Saha, S. Biswas, I.M. Steele, K. Dey, G. Mostafa, Dalton Trans. 40 (2011) 3166.
[40] G.M. Sheldrick, SHELXS 97, Program for Structure Solution, University of Göttingen, Germany, 1997.
[41] G.M. Sheldrick, SHELXL 97, Program for Crystal Structure Refinement, University of Göttingen, Germany, 1997.
[42] A.L. Spek, J. Appl. Crystallogr. 36 (2003) 7.
[43] L.J. Farrugia, J. Appl. Crystallogr. 30 (1997) 565.
[44] L.J. Farrugia, J. Appl. Crystallogr. 32 (1999) 837.
[45] Y.-H. Wana, L.-P. Zhanga, L.-P. Jina, J. Mol. Struct. 658 (2003) 253.
[46] L. Huang, L.-P. Zhang, J. Mol. Struct. 692 (2004) 249.
[47] L. Huanga, L.-P. Zhanga, L.-P. Jin, J. Mol. Struct. 692 (2004) 169.
[48] M. Khorasani-Motlagh, M. Noroozifar, S. Niromand, S. Khajeh, B.O. Patrick, Inorg. Chim. Acta. 362 (2009) 3785.
[49] Y. Li, F.-P. Liang, C.-F. Jiang, X.-L. Li, Z.-L. Chen, Inorg. Chim. Acta. 361 (2008) 219.
[50] O.M. Yaghi, M. O'Keeffe, N.W. Ockwig, H.K. Chae, M. Eddaoudi, J. Kim, Nature 423 (2003) 705.
[51] M.J. Rosseinsky, Microporous Mesoporous Mater. 73 (2004) 15.
[52] S. Kitagawa, R. Kitaura, S.I. Noro, Angew. Chem., Int. Ed. 43 (2004) 2334.
[53] S. Kitagawa, R. Kitaura, S.I. Noro, Angew. Chem. 116 (2004) 2388.
[54] S. Kitagawa, R. Matsuda, Coord. Chem. Rev. 251 (2007) 2490.
[55] G.S. Papaefstathiou, L.R. MacGillivray, Coord. Chem. Rev. 246 (2003) 169.
[56] D.N. Dybtsev, H. Chun, K. Kim, Angew. Chem. 116 (2004) 5143.
[57] R.J. Robson, Chem. Soc. Dalton Trans. (2000) 3735.
[58] B. Moulton, M.J. Zaworotko, Chem. Rev. 101 (2001) 1629.
[59] C.N.R. Rao, S. Natarajan, R. Vaidhyanaathan, Angew. Chem. 116 (2004) 1490.
[60] M. Dincă, A.F. Yu, J.R. Long, J. Am. Chem. Soc. 128 (2006) 8904.
[61] M. Khorasani-Motlagh, M. Noroozifar, S. Niromand, S. Khajeh, B.O. Patrick, Inorganica Chimica Acta. 362 (2009) 3785.
[62] E.B. Sveshnikova, N.T. Timofeev, Opt. Spektroskopiya. 48 (1980) 503.
[63] H. Dornauf, J. Heber, J. Lumin. 20 (1979) 271.
[64] V.P. Dotsenko, N.P. Efryushina, I.V. Berezovskaya, Opt. Spektrosk. 79 (1995) 105.
[65] W. Strek, J. Legendziewicz, E. Lukowiak, K. Maruszewski, J. Sokolnicki, A.A. Boiko, M. Borzechowska, Spectrochim. Acta A. 54 (1998) 2215.
[66] A.G. Svetashev, M.P. Tsvirko, Zh. Prikl, Spektrosk. 62 (1995) 249.
[67] V.T. Mishchenko, D.V. Demeshko, V.A. Perfilev, J. Anal. Chem. 48 (1993) 1268.
[68] M. Hasegawa, A. Ishii, S. Kishi, J. Photochem. Photobiol. A. 178 (2006) 220.
[69] M. J. Frisch, G. W. Trucks, H. B. Schlegel, G. E. Scuseria, M. A. Robb, J. R. Cheeseman, J. A. Jr. Montgomery, T. Vreven, K. N. Kudin, J. C. Burant, J. M. Millam, S. S. Iyengar, J. Tomasi, V. Barone, B. Mennucci, M. Cossi, G. Scalmani, N. Rega, G. A. Petersson, H. Nakatsuji, M. Hada, M. Ehara, K. Toyota, R. Fukuda, J. Hasegawa, M. Ishida, T. Nakajima, Y. Honda, O. Kitao, H. Nakai, M. Klene, X. Li, J. E. Knox, H. P. Hratchian, J. B. Cross, C. Adamo, J. Jaramillo, R. Gomperts, R. E. Stratmann, O. Yazyev, A. J. Austin, R. Cammi, C. Pomelli, J. W. Ochterski, P. Y. Ayala, K. Morokuma, G. A. Voth, P. Salvador, J. J. Dannenberg, V. G. Zakrzewski, S. Dapprich, A. D. Daniels, M. C. Strain, O. Farkas, D. K. Malick, A. D. Rabuck, K. Raghavachari, J. B. Foresman, J. V. Ortiz, Q. Cui, A. G. Baboul, S. Clifford, J. Cioslowski, B. B. Stefanov, G. Liu, A. Liashenko, P. Piskorz, I. Komaromi, R. L. Martin, D. J. Fox, T. Keith, M. A. Al-Laham, C. Y. Peng, A. Nanayakkara, M. Challacombe, P. M. W. Gill, B. Johnson, W. Chen, M. W. Wong, C. Gonzalez and J. A. Pople, Gaussian 03, Revision C.02, Gaussian Inc, Wallingford, CT, 2004.

Inorganica Chimica Acta 486 (2019) 352–360

Contents lists available at ScienceDirect

Inorganica Chimica Acta

journal homepage: www.elsevier.com/locate/ica

Research paper

A bi-nuclear Cu(II)-complex for selective epoxidation of alkenes: Crystal structure, thermal, photoluminescence and cyclic voltammetry

Somen Goswami[a], Soumen Singha[a], Rajat Saha[b], Anupam Singha Roy[c], Manirul Islam[c], S. Kumar[a,*]

[a] Department of Physics, Jadavpur University, Jadavpur, Kolkata 700032, India
[b] Department of Chemistry, Kazi Nazrul University, West Bengal 713340, India
[c] Department of Chemistry, University of Kalyani, West Bengal 741235, India

ARTICLE INFO

Keywords:
Binuclear Cu(II)-complex
Crystal structure
Spectral study
Catalysis
Selective epoxidation

ABSTRACT

Herein, we report the molecular and supramolecular structure, photoluminescence, redox behavior and product selective catalytic activity of $[Cu_2(oxalate)(1,10\text{-phen})_2Cl_2]$ (where 1,10-phen = 1,10-phenanthroline) synthesized by using hydrophilic oxalate as bridging ligand and the hydrophobic 1,10-phen as the blocker ligand. Structural analysis reveals that this binuclear Cu(II)-complex crystallizes in achiral monoclinic $P2_{1/n}$ space group and it has a 3D supramolecular structure. Each Cu-center displays five coordinated distorted square pyramidal geometry. Two such Cu centers are connected by oxalato-bridge to form the bi-nuclear-metal core and two 1,10-phen molecules block the outer periphery of the core and restrains further polymerization. These binuclear metallic units are connected by supramolecular hydrogen bonding and π···π interactions to form a 3D supramolecular architecture. The complex is stable up to 230 °C. A reversible redox couple centered at $(E_{1/2}) \sim -27$ mV with $\Delta E_p \sim 206$ mV corresponding to the $Cu^{II/I}$ couple was detected in the cyclic voltammogram of the complex in acetonitrile. The complex shows emission maxima at 451 and 480 nm upon excitation at 340 nm due to π-π* transition in the aromatic π-rings of 1,10-phenanthroline. Density functional analysis has been performed to explore the molecular structure and character of the orbitals within the complex. Due to the presence of five coordinated Cu-centers, the lewis acidic catalytic activity of the complex has been studied. It exhibits selective oxidation behavior for alkenes in presence of several oxidants. It shows 100% selectivity with 70% conversion for the oxidation of *cis*-cyclooctene to corresponding epoxide at 50 °C in presence of H_2O_2 as oxidant in acetonitrile.

1. Introduction

In the family of multinuclear metal complex, the di-, tri- and polynuclear Cu(II) complexes have drawn special attention for few decades due to their structural diversity, distorted coordination geometry, simple electronic configuration as well as their application in the field of magnetism, catalysis, biochemistry, medicine and sensing [1–17]. Plethora of examples of multinuclear metal complexes is available in the literature [1–25]. It is noteworthy that judicious selection of the metal ions, bridging and also terminal ligands is indispensable for rational design of multinuclear metal complexes with specific physicochemical properties [26–28]. Bridging ligands with potentially active oxygen or nitrogen donor atom such as phenoxo [1–4,10], azido [5], oxo/alkoxo [6,7,21,22], sulfato [11], dicyanamide [12], hydroxo [1,10,16,20], oxalato [14,23–25,29–38], carboxylate [4,39–44] etc., have been widely used to synthesize multinuclear homo- and heterometallic Cu(II) complexes. Again, oxalato dianion is a very attractive bridging ligand for synthesizing a diverse type of homo- and heterometallic Cu(II) complexes with interesting physical and chemical properties (magnetic, optical and catalytic) [23–25,36–38]. In this context, we have used the oxalate ligand in combination with 1,10-phenanthroline to synthesize a Cu(II) complex to explore the possible catalytic activity.

Synthesis of inorganic-organic hybrid catalysts for the selective production of organic compounds is of paramount importance in the field of synthetic and industrial chemistry [45]. In literature, numerous numbers of transition metal based complexes are reported with their several important catalytic activity based on several organic transformations and product selectivity. In this context, Cu(II) complexes have emerged as potential candidates for synthesis of organic molecules

* Corresponding author.
E-mail address: kumars@phys.jdvu.ac.in (S. Kumar).

https://doi.org/10.1016/j.ica.2018.10.066
Received 22 June 2018; Received in revised form 8 October 2018; Accepted 29 October 2018
Available online 31 October 2018
0020-1693/

because of their very good catalytic activity in catechol oxidation, sulfoxidation, alkene oxidation, epoxidation, condensation, atom transfer radical addition, olefin aziridination etc. under both homogeneous and heterogeneous conditions [45–48]. The catalytic efficiency and product selectivity of these complexes can also be tuned effectively by varying the ligand environment around the metal centre and reaction conditions [49–52].

Various oxygen containing value-added products like alcohols, aldehydes, ketones, and epoxides can be developed through oxidation of olefins, which is extremely important and useful reaction in both chemical and pharmaceutical industries [45,53–55]. Epoxide is considered as the most important product of olefin oxidation reaction because of their wide spread applications in the production of epoxy resins, paints, perfumes, surfactants, pharmaceutical products and polymers. Further, epoxides acts as a mediator in many organic syntheses and epoxidation of olefins is the key step in several organic synthesis and biological processes [56–65]. The traditional procedure for epoxidation of olefins using conventional oxidizing agent like H_2O_2, peracids, atmospheric O_2 suffers from very low conversion percentage and also lead to the formation of undesirable side products, which are sometimes very difficult to separate. Thus, finding the catalytic materials capable of producing epoxide by the oxidation of olefins with high selectivity is of immense importance from synthetic as well as industrial view points. In this context, transition metal based coordination complexes have emerged as a viable alternative to environmentally hazardous reagents abundantly used in both homogeneous and heterogeneous catalysis.

Under this background, herein we report the synthesis, characterization and selective catalytic activity of a binuclear Cu(II) complex $[Cu_2(oxalate)(1,10\text{-phen})_2Cl_2]$ synthesized by using hydrophilic oxalate ligand to bridge the metal centres and the hydrophobic 1,10-phen as the blocking ligand to prevent the formation of infinite architecture. This Cu-based binuclear complex shows selective catalytic behavior with very good yield for the oxidation of alkenes to their corresponding epoxides e.g., 100% selectivity with 70% conversion for epoxidation of *cis*-cyclooctene.

2. Experimental

2.1. Materials and methods

The copper (II) chloride dihydrate (99%), oxalic acid (99.9%) and 1,10-phenanthroline (99.9%) were purchased from Sigma Aldrich and used without further purification. Sodium carbonate (99%) and all other chemicals (AR grade) were purchased from Merck India and used as received. A Perkin- Elmer 240C elemental analyzer was employed to carry out Elemental analysis (C, H, N). The thermal analysis was performed using a Mettler Toledo TGA-DTA 85 thermal analyzer under a flow of N_2 ($30\,ml\,min^{-1}$). The sample was heated at a rate of $10\,^{\circ}C\,min^{-1}$ using inert alumina as a reference. IR study was done on Nicolet Impact 410 spectrometer between 400 and 4000 cm^{-1}, using KBr pellet method. A Perkin Elmer Lambda 365 UV-vis spectrophotometer was used to record the UV-vis absorption spectrum of the sample. Photoluminescence spectrum of the sample was recorded by Shimadzu RF-5301PC spectrophotometer. The cyclic voltametric measurement on the sample was carried out using Epsilon Basi-C3 Cell instrument at a scan rate of $100\,mV\,s^{-1}$ within potential range of 0–1.80 V with 1.0×10^{-3} M of complexes in acetonitrile solution deoxygenated by bubbling argon gas. Further, 0.1 M tetrabutylammonium perchlorate (TBAP) was taken as supporting electrolyte. The working electrode was a glassy-carbon disk ($0.32\,cm^2$) which was washed with absolute acetone and dichloromethane, polished with alumina solution and air-dried before each electrochemical run. The reference electrode was Ag/AgCl and platinum was used as the counter electrode. All experiments were performed in standard electrochemical cells at 25 °C. The EIS-MS was recorded with the help of Qtof Micro YA263 mass spectrometer. The powder X-ray diffraction (PXRD) pattern was collected at room temperature (22 °C) on Bruker D8 Advanced Diffractometer using CuKα radiation having wavelength 1.5418 Å. The generator voltage and current was set at 40 kV and 40 mA, respectively. The PXRD data was collected within the 2θ range of 5°–60° with a scan speed of 1 s/ step and step size of 0.02°.

2.2. Synthesis of the complex

At first, 0.5 mmol oxalic acid (0.04501 g) was dissolved in 10 ml distilled water and neutralized by aqueous solution of sodium carbonate to adjust the pH at 8.0 and 1.0 mmol of 1,10-phenanthroline (0.1802 g) was dissolved in 10 ml methanol separately. These two solutions were mixed together and stirred for 15 min at room temperature. Then the $CuCl_2{\cdot}2H_2O$ (0.1704 g, 1.0 mmol) was dissolved in 5 ml distilled water and added to the previous solution. The resultant mixture was stirred at room temperature for 30 min. The whole mixture was then refluxed for 1 h at 80 °C. It was then allowed to cool down to room temperature and kept in undisturbed condition for 2 h. A very small amount of precipitate formation was observed. Afterwards, the precipitate was filtered off and green colored filtrate was kept in undisturbed condition. After few (2–3) days, the block shaped green colored crystals suitable for single crystal x-ray structural study were obtained and these were separated and dried. Yield 79%.Anal. Calc. for $C_{26}H_{16}Cl_2Cu_2N_4O_4$: C, 48.2; H, 2.5; N, 8.6. Found: C, 48.5; H, 2.4; and N, 8.5%. Selected IR bands (KBr pellet, cm^{-1}): ν (O—H) stretching 3445 (m); ν (CO) 1506 (m), 1524 (s), 1483 (s), 1445 (w).

2.3. Crystallographic data collection and refinement

Suitable single crystal of the complex was mounted on a Bruker SMART diffractometer equipped with a graphite monochromator and Mo-Kα (λ = 0.71073 Å) radiation. The structure was solved by Patterson method using SHELXS-97 program. Subsequent difference Fourier synthesis and least square refinement revealed the positions of the non-hydrogen atoms. Non-hydrogen atoms were refined using independent anisotropic displacement parameters. Hydrogen atoms were placed in idealized positions and their displacement parameters were fixed to be 1.2 times larger than those of the attached non-hydrogen atoms. Successful convergence was indicated by the maximum shift/error of 0.001 for the last cycle of the least squares refinement. Analysis of single crystal X-ray data were carried out using SHELXS-97 [66], SHELXL-97 [67], PLATON-99 [68], ORTEP-32 [69] and WinGX system Ver-1.64 [70]. Data collection, structural refinement parameters and crystallographic data of the complex are provided in Table 1. Some selected bond lengths, bond angles and weak interaction parameters are summarized in Table 2.

2.4. Computational methodology

All theoretical calculations were performed with the Gaussian 09 W software package [71] employing the analytical gradient methods of DFT with Becke's three parameters (B3) exchange functional [72] and the Lee-Yang-Parr (LYP) nonlocal correlation functional (symbolized as B3LYP) [73]. For C, H, N, O and Cl atoms the 6-311 + + G (d,p) basis set was used while for the Cu atom LanL2DZ basis set was adopted. The ground state (S_0) geometries were fully optimized using the default criteria of the respective program in both the gaseous phase and solution phase with acetonitrile as solvent. Frequencies were calculated on the optimized geometries and the nature of the stationary point was confirmed by carrying out a normal mode analysis, where all vibrational frequencies were found to be positive, which confirms that the optimized structure is at one of the minima of the potential energy surface. Orbital analysis was carried out with the help of Gauss View and the MO composition analysis was done with GaussSum program [74].

Table 1
Crystallographic data and refinement parameters of the complex.

Formula	$C_{26}H_{16}Cl_2Cu_2N_4O_4$
Formula weight	646.43
Crystal System	Monoclinic
Space group	$P2_{1/n}$ (No. 14)
a (Å)	8.631(5)
b (Å)	11.927(7)
c (Å)	11.779(7)
β (°)	100.223(9)
V (Å^3)	1193.3(12)
Z	2
D(calc) (g/cm^3)	1.799
μ(Mo Kα)(mm)	2.050
F(0 0 0)	648
Crystal Size (mm)	0.12 × 0.12 × 0.48
T (K)	100
λ [Å]	Mo Kα 0.71073
Theta Min-Max [°]	2.4–25.3
Dataset	−10: 10; −14: 14; −14: 14
Total, Unique data	10723, 2140
R_{int}	0.093
Observed data	1392
Nref, Npar	2140, 172
R	0.0517
w*R*2	0.1092
S	0.94
Max. and Av. Shift/Error	0.00, 0.00
Min. and Max. Resd. Dens. [e/Å^3]	−0.52, 0.53

w = 1/[s2(Fo2) + (0.0949P)2] where P = (Fo2 + 2Fc2)/3.

Table 2
Some selected bond lengths (Å) and bond angles (°) of the complex.

Cu1-Cl1	2.287(2)	Cu1-O1	2.215(4)
Cu1-O2	1.999(4)	Cu1-N1	2.019(5)
Cu1-N2	2.050(5)	Cl1-Cu1-O1	110.69(10)
Cl1-Cu1-O2	94.40(11)	Cl1-Cu1-N1	96.36(14)
Cl1-Cu1-N2	142.72(14)	O1-Cu1-O2	80.75(14)
O1-Cu1-N1	90.42(16)	O1-Cu1-N2	106.56(16)
O2-Cu1-N1	167.98(17)	O2-Cu1-N2	92.78(17)
N1-Cu1-N2	81.87(19)		

2.5. Catalytic reaction methodology

The catalytic reactions were carried out in a glass batch reactor according to the following procedure. 5 mmol of substrate, 2 mg catalysts (i.e. 0.062% of mole of the substrate) and 5 ml solvent and were first mixed. The mixture was then equilibrated to the desired temperature in an oil bath. After addition of 30% hydrogen peroxide (10 mmol), the reaction mixture was stirred continuously. The reactions were performed in open air. The reaction products were quantified (GC data) by Varian 3400 gas chromatograph equipped with a 30 m CP-SIL8CB capillary column and a flame ionization detector and identified by Trace DSQ II GCMS equipped with a 60 m TR-50MS capillary column. The oxidation products were identified by comparing their retention times with those of authentic samples.

3. Results and discussion

3.1. Molecular and supramolecular structure of the complex

Single crystal X-ray diffraction (SCXRD) analysis revealed that the complex crystallizes in achiral $P2_1/n$ space group. The asymmetric unit contains one Cu^{2+} ion, one coordinated Cl^- ion, one phenanthroline ligand and half of oxalate moiety. The ORTEP diagram is presented in Fig. 1. The metal center exhibits five coordinated distorted square pyramidal geometry with τ value of 0.42 [75]. Two nitrogen atoms (N1 and N2) of phenanthroline ligand, one oxygen atom (O2) of the oxalate ligand and the chloride ion (Cl1) constitute the basal plane while the other oxygen atom (O1) of the oxalate occupies the axial positions. Here, the oxalate ligand acts as a bridge between two metal centers, on the other hand, the hydrophobic 1,10-phen acting as blocking ligand prevents the formation of infinite chain and in consequence the binuclear-complex formation takes place. The oxalate acts as both bridging ligand as well as chelating ligand. Using two oxygen atoms of two different carboxylato groups, oxalate binds one metal center in *syn-syn* fashion as a chelating ligand and using two oxygen atoms of the same carboxylato groups, it bridges between two metal centers in *anti-anti* binding mode. Wang et al., have reported a similar structure with $P2_1/c$ space group and distorted trigonal bipyramidal geometry while our complex crystallizes in $P2_1/n$ space group and its Cu(II) centers show square pyramidal coordination geometry [76]. Further, the structural parameters and packing behavior of the present complex is different from those of reported earlier. The molecular structure of this compound is similar to $[(bpy)_2Cu_2(C_2O_4)Cl_2]\cdot H_2O$ where the complex has a guest water molecule while the complex under investigation is devoid of any water molecule [77]. It has been reported that in $[(bpy)_2Cu_2(C_2O_4)Cl_2]\cdot H_2O$, Cu atom exhibits square pyramidal coordination where two nitrogen atoms of one 2,2́-bypyridyl and two syn oxygen atoms of oxalate moiety constitute the basal plane while chloride ion occupies the apical position. Here, the oxalate ion acts as bridging ligand and 2,2′-bypyridyl serves as blocking ligand. Although for both complexes, Cu atom exhibits square pyramidal coordination, there are distinct differences in constitution of the basal plane, apical position and bridging mode.

The Cu—N bond distances are in the range of 2.019–2.050 Å, Cu—O bond distances are in the range of 1.999–2.215 Å and Cu—Cl bond distance is ~2.287 Å. All other coordinated bond distances and bond angles are provided in Table 2. The supramolecular C—H···Cl (C1—H1···Cl1) and C—H···O (C8—H8···O1) hydrogen bonding interactions connect each molecular units to form 3D supramolecular structures (Figs. 2 and S1). π···π interactions among the aromatic rings of phenanthroline moieties also facilitate the 3D supramolecular structure formation, as shown in Figs. 2 and S1. All the hydrogen bonding and π···π interactions are summarized in Tables S1 and S2, respectively.

3.2. PXRD and thermal investigation

The phase purity of the bulk sample was examined by PXRD study. The PXRD pattern of the complex matches well with the X-ray diffraction pattern simulated from the SC-XRD data (Fig. S2). Thermogravimetric analysis (TGA) for coordination and supramolecular polymers are very important to analyze their thermal stability. The TGA curve of the sample (Fig. 3) reveals that it is stable up to 230 °C. A very few amount of weight loss (< 1%) below 100 °C can be attributed to the loss of absorbed moisture. The complex gradually decomposes in stepwise fashion within the temperature range of 230 and 900 °C due to the successive loss of coordinated moieties such as Cl^- ions, bridging oxalate ligand and phenanthroline (theo: 78%, exp: 91%). The final black residue after decomposition of the complex is probably the anhydrous copper oxide.

3.3. Cyclic voltammetric investigation

The cyclic voltammogram of the complex in acetonitrile is reversible in nature with $E_{1/2}$ ~ 27 mV and ΔE_p = 206 mV. The $E_{1/2}$ ~ 27 mV corresponds to one electron transfer process in the $Cu^{II/I}$ redox couple. It is already reported that, strongly electronically coupled systems can display surprisingly high ΔE_p value in cyclic voltammetric study [78]. Hence, the large ΔE_p value implies that, in the present complex two redox active copper centers are strongly electronically coupled to each other by the bridging oxalate dianion ligand. The reversibility of the redox process suggests that the basic geometry around the copper centre remains intact during the redox event (Fig. 4).

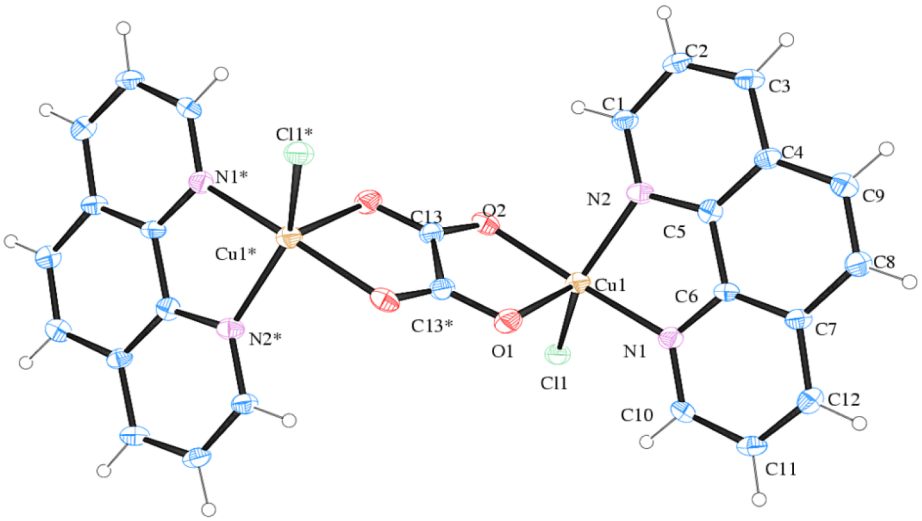

Fig. 1. ORTEP diagram of the complex.

3.4. Spectral studies

The electronic spectra of the complex were recorded at 300 K in acetonitrile medium. The UV-Vis spectra (Fig. S3) exhibit a peak at 270 nm (molar extinction coefficient (ε):39,800 $M^{-1}cm^{-1}$) that can be attributed to the π-π* transition within the 1,10-phenanthroline ligands. The absorption peak at 344 nm (ε: 7950 $M^{-1}cm^{-1}$) is due to the charge transfer from 1,10-phenanthroline ligand to Cu(II) metal ion. The absorption spectra also shows a broad band around 720 nm (ε: 3060 $M^{-1}cm^{-1}$) which can be assigned to the *d-d* transition.

The emission spectra of the complex have been studied in solid state at 300 K. The complex shows emission maxima at 451 and 480 nm upon excitation at 340 nm (Fig. 5) and this can be attributed to the π-π* transition in the aromatic π-rings of 1,10-phenanthroline ligands. The small peak around 522 nm is possibly caused by extended π-conjugation within the ligand system. The luminescent behavior of the complex corresponds to a ligand-centered (LC) fluorescence.

The emission spectra of the complex have been studied in acetonitrile medium. Upon exciting at 344 nm, the emission spectra show maxima at 405 nm and 430 nm (Fig. S4) due to the π-π* transition in the aromatic π-rings of 1,10-phenanthroline ligands. Hence, in solution phase a blue shift of the peaks is observed but the emission spectra of the complex are almost similar in nature in both solid state and solution phase. Thus, it may be inferred that the basic structure of the complex remains unchanged in solvent phase.

3.5. Study of ground state structure and molecular orbitals

We have optimized the molecular structures of the complex at electronic ground state (S_0) in both gaseous state and in acetonitrile solvent. The geometry optimized structures of the complex computed both in the gaseous and in solution phases are presented in Fig. 6. Some selected optimized geometrical parameters (bond lengths and bond angles) of the complex are summarized in Tables S3 and S4. In the

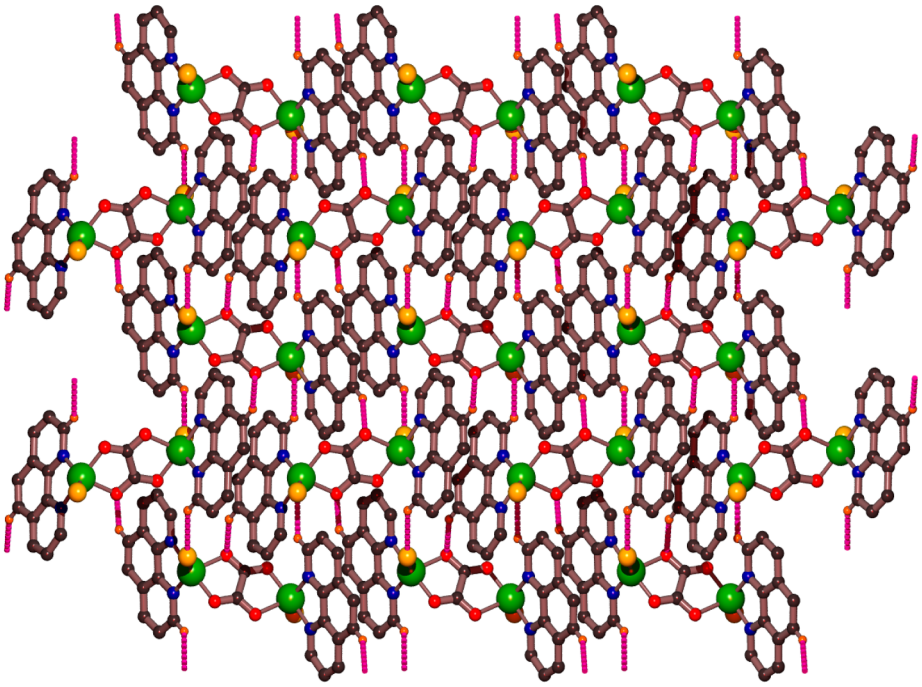

Fig. 2. 3D supramolecular structure of the complex formed by C—H···Cl and C—H···O hydrogen bonding interactions.

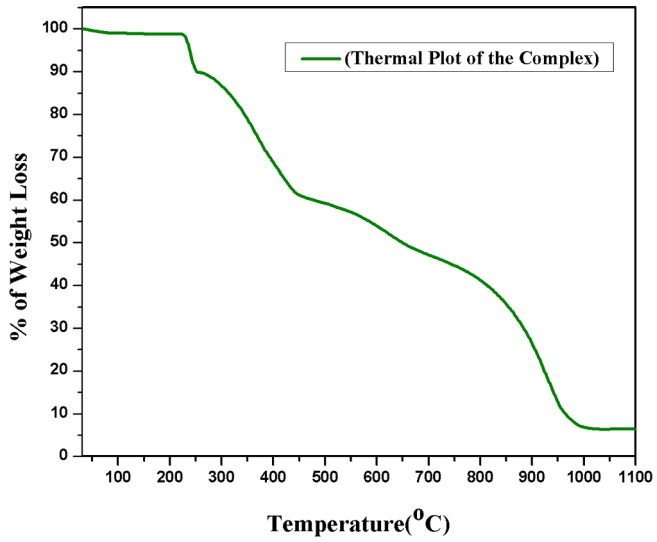

Fig. 3. Thermal plot of the complex.

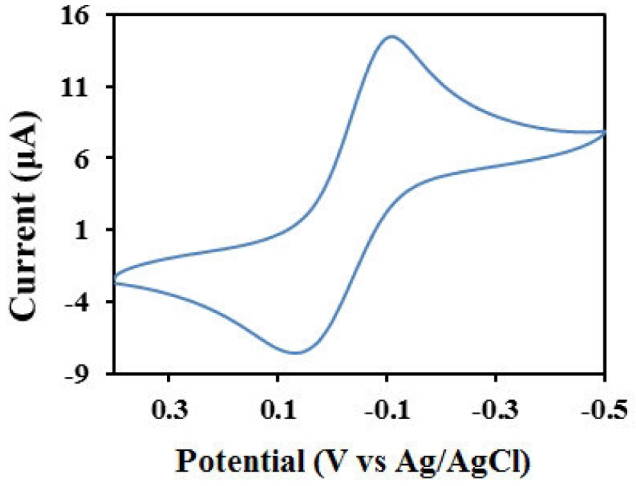

Fig. 4. CV plot of the complex.

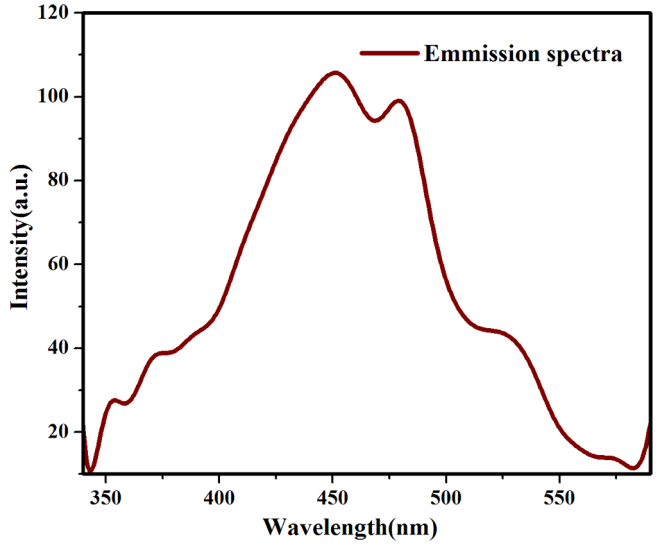

Fig. 5. Photoluminescence spectra of the complex in solid state.

optimized structures, both the Cu(II) centers of the complex show five coordinated distorted square pyramidal geometry. In the optimized structures, two oxygen atoms of two different carboxylate groups of oxalate ligand along with one Cl atom and one of the two N atoms of phenanthroline ligand constitute the basal plane whereas the remaining N atom of phenanthroline ligand occupies the axial position. On the other hand, in the crystalline molecular structure of the complex two N atoms of phenanthroline ligand, one oxygen atom of the oxalate ligand together with one Cl atom form the basal plane and another oxygen atom of a different carboxylate group of the oxalate ligand is in the apical position. Although the calculated structure and the crystal structure are geometrically same in nature (square pyramidal), the dissimilarity in position of atoms within the metallic coordination environment and different degree of distortion among them leads to apparent mismatch between the bond angles and bond lengths of these molecular structures.

Some selected frontier orbitals of the complex optimized in both the gaseous and solution phases are shown in Fig. 7. The HOMO–LUMO energy differences are 1.03 eV and 1.02 eV for the structures optimized in gaseous phase and in solution phase, respectively. For MO composition analysis the contributions from five fragments viz., Cu, phen1, phen2, Cl and oxalato have been considered. The orbital energies and the contribution from each fragment in terms of atomic orbital contribution to the frontier molecular orbital (MO) are listed in Table 3. For the HOMOs and LUMOs of the complex in both gaseous and solution phase, the degree of contribution coming from the p-orbitals of the C atoms in phenanthroline moieties, *d*-orbital of Cu atom, Cl and oxalato is significantly different.

3.6. Catalytic activity

The complex contains five coordinated - coordinatively unsaturated Cu-centers and thus the complex was been used for the Lewis acidic catalysis reaction under homogeneous conditions. Catalytic activity of the complex was assessed by studying the oxidation reaction of alkenes. In this study, *cis*-cyclooctene was selected as the model substrate to optimize the catalytic oxidation reaction conditions using H_2O_2 as oxidant. The catalytic oxidation of *cis*-cyclooctene produces the corresponding epoxide as the sole product in acetonitrile solvent with H_2O_2 at 50 °C (Scheme 1). The same experiment was performed without using H_2O_2 as oxidant keeping all the reaction parameters unchanged. The results of control experiments have revealed that presence of both the catalyst and oxidant are essential for the oxidation reaction. The oxidation of *cis*-cyclooctene in the absence of H_2O_2 does not occur and also in absence of the catalyst, trace amount of desired product was formed. Again, the same experiment was done in presence of $CuCl_2$ using H_2O_2 as oxidant in both methanol and acetonitrile medium. These experiments result very low conversion rate of *cis*-cyclooctene to the product suggesting very mild catalytic activity of $CuCl_2$ in the epoxidation reaction. Effects of solvent, oxidant, the ratio of oxidant/substrate and the temperature were also studied to find the most suitable reaction conditions to achieve the maximum conversion of *cis*-cyclooctene.

In order to study the solvent effect, catalytic oxidation reactions were carried out in methanol, ethanol, acetonitrile, chloroform and dichloromethane solvent and it was found that the highest conversion, 70% after 3 h, was obtained in acetonitrile at 50 °C. The catalytic activity of the complex decreased in the order: acetonitrile > methanol > ethanol > chloroform ~ dichloromethane (Fig. 8). In summary, the reactivity of the catalyst in other solvents was much lower than in acetonitrile. The efficiency of various oxidants, namely *tert*-BuOOH, H_2O_2, NaOCl and O_2 (1 atm) was studied in the same homogeneous catalytic oxidation reaction of *cis*-cyclooctene keeping all other conditions unchanged. The experimental outcomes revealed that H_2O_2 is the most efficient oxidant with complex as catalyst (Table 4).

The effect of temperature on the performance of the catalyst was also investigated. The same reaction has been carried out at three

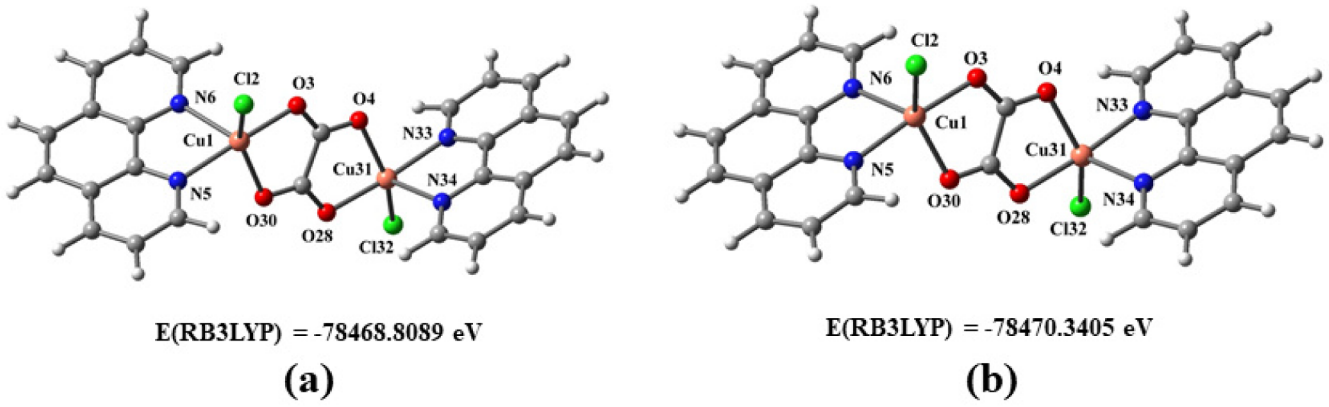

Fig. 6. Ground state optimized geometries and coordination environment of the complex in (a) gaseous phase and (b) solution state with acetonitrile as solvent.

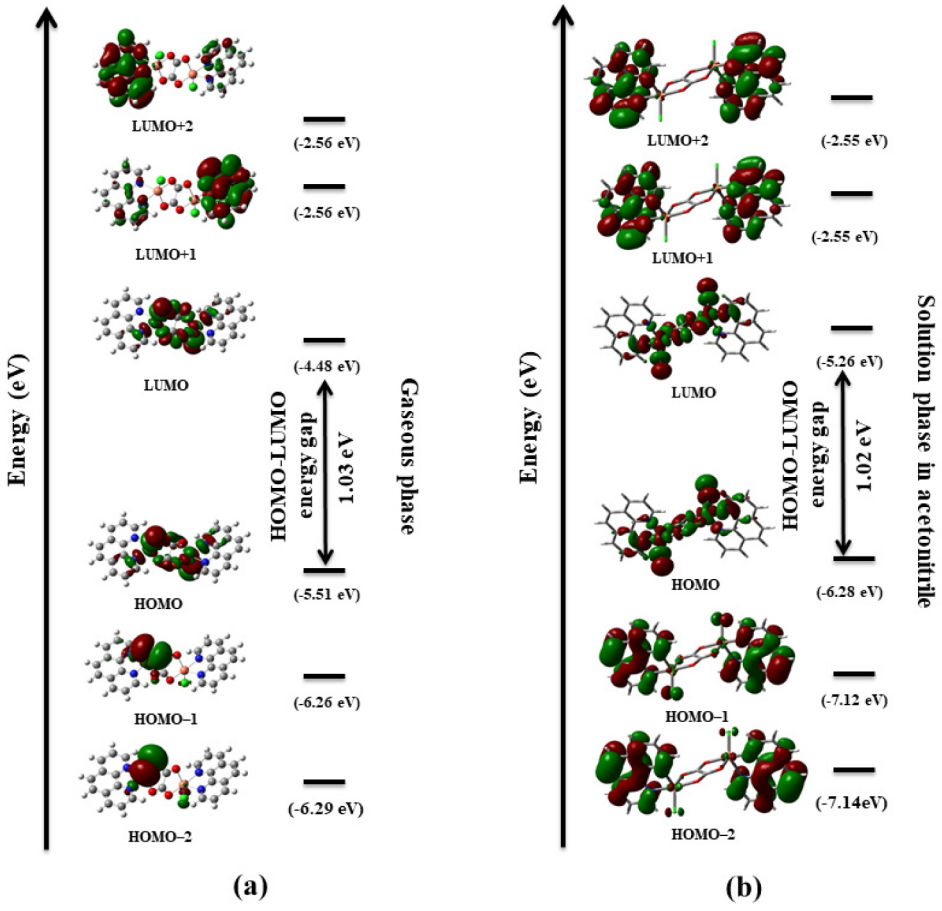

Fig. 7. Schematic diagram showing the selective frontier molecular orbitals for the complex in (a) gas phase and (b) solution state with acetonitrile as solvent.

different temperatures *viz.*, 40 °C, 50 °C and 60 °C with the fixed amount of *cis*-cyclooctene (5 mmol), H_2O_2 (10 mmol) and the complex (2 mg) in 5 ml acetonitrile (Table 4, entries: 3, 6 and 7) keeping the reaction conditions same as earlier. A maximum of 70% conversion was achieved at 50 °C while at 40 °C, the conversion was low. On the other hand, at 60 °C the initial conversion of *cis*-cyclooctene was higher than at 50 °C but when the reaction continues the conversion of *cis*-cyclooctene became almost same. Therefore, 50 °C is the optimum temperature and hence catalytic oxidation reactions of other alkenes were carried out at this temperature. The molar ratio of *cis*-cyclooctene to H_2O_2 was also varied (Table 4, entries: 3, 8 and 9) keeping all other experimental conditions same to examine the effect of molar ratio of the parent compound on the conversion process. The conversion of *cis*-cyclooctene was increased from 38% to 70% on increasing the *cis*-cyclooctene: H_2O_2 ratio from 1:1 to 1:2. On further increasing this ratio to 1:3, the conversion was hardly affected. Hence, it can be inferred that 1:2 ratio of *cis*-cyclooctene to H_2O_2 is sufficient for significant conversion of *cis*-cyclooctene. A blank experiment (Table 4, entry: 10) was also carried out in absence of the complex with H_2O_2 under the same experimental conditions which resulted in very low conversion of *cis*-cyclooctene that confirmed the high efficiency of the complex as a catalyst. All these optimized reaction conditions were applied to the complex-catalyzed oxidation reactions of other alkenes.

It is noteworthy that the complex-catalyzed oxidation reaction of *cis*-cyclooctene with H_2O_2 yields the corresponding epoxide with 100% product selectivity in acetonitrile medium (Table 5). The product was

Table 3
Selected MOs of the complex along with their energies and compositions.

MO	Energy (eV)		% Composition									
	Gas	Solution	Gas					Solution				
			Cu	Phen1	Phen2	Oxalato	Cl	Cu	Phen1	Phen2	Oxalato	Cl
HOMO-5	−6.90	−7.49	19	40	26	8	7	11	41	14	17	18
HOMO-4	−6.36	−7.30	4	2	60	14	19	10	37	38	0	14
HOMO-3	−6.32	−7.28	12	5	65	2	16	13	36	35	3	13
HOMO-2	−6.29	−7.14	4	55	3	16	21	3	47	47	1	1
HOMO-1	−6.26	−7.12	13	65	7	0	15	2	47	47	1	3
HOMO	−5.51	−6.28	34	27	25	6	8	35	27	27	5	7
LUMO	−4.48	−5.26	29	22	29	13	7	33	24	24	12	7
LUMO + 1	−2.56	−2.55	0	11	85	3	0	1	51	45	2	0
LUMO + 2	−2.55	−2.55	2	80	10	8	0	4	42	48	6	0
LUMO + 3	−2.45	−2.35	3	90	6	1	0	5	50	41	4	0
LUMO + 4	−2.44	−2.35	1	3	93	3	0	0	43	55	0	0
LUMO + 5	−1.37	−2.00	5	23	54	17	0	25	17	17	41	0

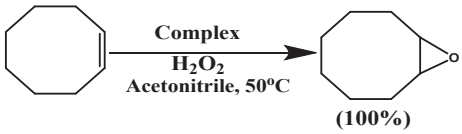

Scheme 1. Catalytic oxidation of *cis*-cyclooctene.

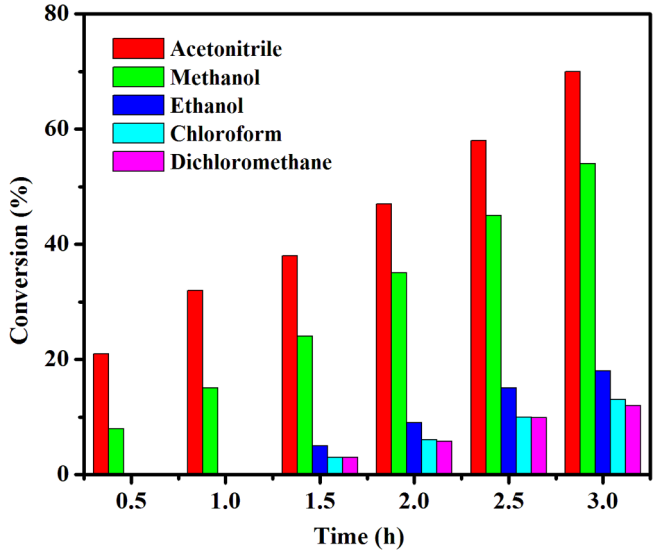

Fig. 8. Influence of solvent in the catalytic epoxidation of *cis*-cyclooctene by the complex. Reaction condition – catalyst: 2 mg, *cis*-cyclooctene: 5 mmol, H_2O_2:10 mmol, temperature: 50 °C, solvent (acetonitrile): 5 ml.

identified by GC spectroscopic study (Fig. S5). Under the same reaction condition, styrene gives styrene oxide with 89% product selectivity (67% conversion) along with a trace amount of benzaldehyde. In case of cyclohexene, product selectivity to the corresponding epoxide is about 76% with conversion % of 82. A little amount of allylic oxidation products (2-cyclohexene-1-ol and 2-cyclohexene-1-one) were also formed as side products in this case. All these experimental results are summarized in Table 5.

Definite identification of the active species involved in homogeneous catalysis is very difficult. In literature, it has been reported that in the reaction of a copper complex with H_2O_2, Cu(II) binds the peroxo-group and forms a Cu–hydroperoxo or Cu–peroxo pre-catalyst species that can act as a mediator to facilitate the oxo functionality to the

Table 4
Epoxidation of *cis*-cyclooctene using different oxidants with the complex as catalyst.

Entry	Oxidant	Temperature (°C)	Conversion (%)[a]
1	–	50	–
2	NaOCl	50	34
3	H_2O_2	50	70
4	*tert*-BuOOH	50	56
5	O_2 (1 atmosphere)	50	12
6	H_2O_2	50	45
7	H_2O_2	60	72
8[b]	H_2O_2	50	38
9[c]	H_2O_2	50	74
10[d]	H_2O_2	50	6

Reaction conditions: catalyst (2 mg), *cis*-cyclooctene (5 mmol), oxidant (10 mmol), acetonitrile (5 ml), time (3 h).
[a] Determined by GC.
[b] 5 mmol H_2O_2.
[c] 15 mmol H_2O_2.
[d] Without the complex.

organic substrates to give the corresponding oxidized products [79,80]. In order to identify the active species, we have recorded the UV-Vis spectra of the complex in presence of excess H_2O_2 in acetonitrile medium (Fig. 9). The UV-Vis spectra show an intense peak at around 430 nm with a shoulder in the range of 445–470 nm. This may be due to the existence of Cu–hydroperoxo or Cu–peroxo species [81,82]. In order to get an idea about the number of copper atom(s) present in the complex in solution state, we have recorded the ESI mass spectrum of the complex in acetonitrile medium. The mass spectrum of the complex shows *m/z* peaks at 611.5356, and 575.9754 (Fig. S6). These peaks are observed due to the fragments of the complex after expulsion of one and two Cl atom(s), respectively. The fragments consisting three peaks for isotopic distribution of two Cu atoms has been observed in the mass spectrum at lower *m/z* values. Hence, from the mass spectrum it can be inferred that two copper atoms bridged through oxalate ligand are present in the solution state and the complex exists as a binuclear species in acetonitrile medium. Further, from the photoluminescence study of the complex it has been found that the basic binuclear structure of the complex in solid state and solution phase is nearly identical. Thus, the result of mass spectroscopy study corroborates the outcome of the photoluminescence study. In case of homogeneous catalysis, recovery of catalyst for reuse is a very difficult task as the catalyst does not remain in its original form after the reaction. We have recovered the residue obtained after completion of the catalytic cycle. However, the FTIR spectra and PXRD pattern of this recovered material does not match with those of the original complex.

Table 5
Oxidation of various alkenes by the complex using H_2O_2 in acetonitrile[a].

Entry	Substrate	Conversion (%)[b]	Product	Selectivity (%)[b]	TOF[c]
1	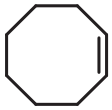	70	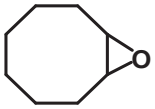	100	376.4
2		82	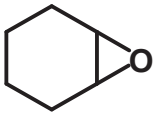	76	440.8
3	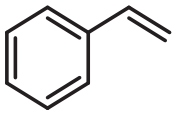	67	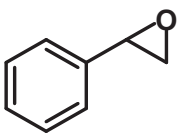	89	360.2

[a] Reaction conditions: catalyst (2 mg), alkenes (5 mmol), H_2O_2 (10 mmol), temperature (50 °C), acetonitrile (5 ml), time (3 h).
[b] Determined by GC.
[c] TOF: turnover frequency = moles of substrate converted per mole of metal complex per hour.

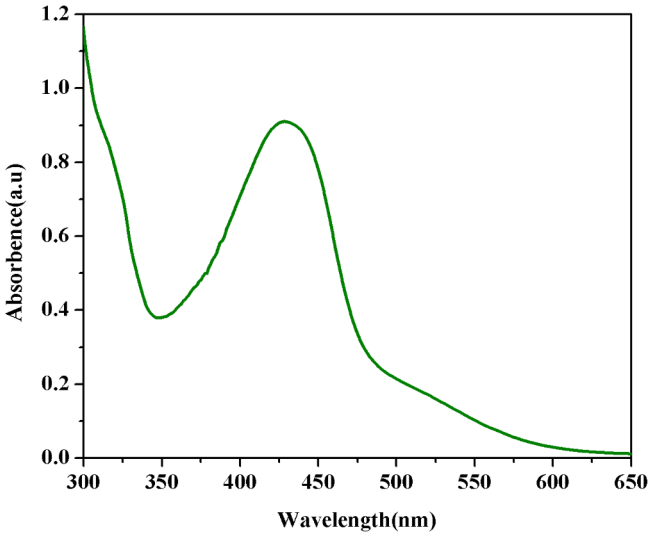

Fig. 9. UV-vis spectrum of the complex in presence of H_2O_2 in acetonitrile at room temperature.

4. Conclusion

In summary the binuclear Cu(II) complex, [Cu_2(oxalate)(1,10-phen)$_2Cl_2$] (where 1,10-phen = 1,10-phenanthroline), designed by using hydrophilic oxalate as bridging ligand and the hydrophobic 1,10-phen as the blocking ligand exhibits very good thermal stability and photoluminescence activity along with selective catalytic activity for epoxidation of alkenes in presence of H_2O_2. Structural analysis has revealed that binuclear metallic units of the complex are packed by supramolecular hydrogen bonding and π···π interactions and forms a 3D supramolecular architecture. The cyclic voltametric study suggests that both the copper centers are strongly coupled to each other through the oxalato-bridge. Owing to the presence of π-electrons in auxiliary ligand (1,10-phenenthroline), the complex shows strong fluorescence.

The presence of coordinately unsaturated Cu-centers inspired us to examine the catalytic activity of the complex toward oxidation of alkenes. By optimizing the oxidation reactions of alkenes using this binuclear Cu(II) complex, it has been established that in all the cases the maximum catalytic efficiency can be achieved at 50 °C in presence of H_2O_2 as oxidant with acetonitrile solvent. Interestingly, the complex shows 100% selectivity for the oxidation of *cis*-cyclooctene to the corresponding epoxide in presence of H_2O_2 as oxidant at 50 °C with 70% conversion in acetonitrile. The complex also exhibits product selectivity and percentage conversion of 89% and 67%, respectively, for styrene and 76% and 82% for cyclohexene under same reaction condition. Our future research goal is to design novel homogeneous and heterogeneous catalysts for industrial application.

Acknowledgments

One of the authors (SS) thanks DST, Government of India for providing fellowship under INSPIRE program. We acknowledge the financial assistance of DST, Government of India under PURSE and FIST program and UGC, Government of India for providing financial support under DSA and UPE program.

Appendix A. Supplementary data

Supplementary data to this article can be found online at https://doi.org/10.1016/j.ica.2018.10.066.

References

[1] F. Gennarini, R. David, I. López, Y. Le Mest, M. Réglier, C. Belle, A. Thibon-Pourret, H. Jamet, N. Le Poul, Inorg. Chem. 56 (2017) 7707.
[2] S.K. Barman, T. Mondal, D. Koley, F. Lloretc, R. Mukherjee, Dalton Trans. 46 (2017) 4038.
[3] D. Venegas-Yazigi, D. Aravenab, E. Spodine, E. Ruizd, S. Alvarez, Coord. Chem. Rev. 254 (2010) 2086.
[4] S. Sarkar, A. Mondal, D. Chopra, J. Ribas, K.K. Rajak, Eur. J. Inorg. Chem. (2006) 3510.
[5] M.G. Sommer, Y. Rechkemmer, L. Suntrup, S. Hohloch, M. van der Meer, J. van Slageren, B. Sarkar, Dalton Trans. 45 (2016) 17770.
[6] S. Sagar, S. Sengupta, A.J. Mota, S.K. Chattopadhyay, A.E. Ferao, E. Riviere, W. Lewisf, S. Naskar, Dalton Trans. 46 (2017) 1249.
[7] R. Golbedaghi, S. Azimi, A. Molaei, M. Hatami, B. Notash, J. Mol. Struct. 1146 (2017) 309.
[8] R. Vafazadeh, R. Esteghamat-Panah, A.C. Willis, A.F. Hill, Polyhedron 48 (2012) 51.
[9] A. Parween, S. Naskar, A.J. Mota, A.E. Ferao, S.K. Chattopadhyay, E. Rivière, W. Lewis, S. Naskar, New J. Chem. 41 (2017) 11750.
[10] R. Sanyal, P. Kundu, E. Rychagova, G. Zhigulin, S. Ketkov, B. Ghosh, S.K. Chattopadhyay, E. Zangrando, D. Das, New J. Chem. 40 (2016) 6623.
[11] R. Vafazadeh, B. Khaledi, A.C. Willis, M. Namazian, Polyhedron 30 (2011) 1815.
[12] B. Vangdal, J. Carranza, F. Lloret, M. Julve, J. Sletten, J. Chem. Soc., Dalton Trans. (2002) 566.
[13] A. Bhattacharjee, S. Halder, K. Ghosh, C. Rizzoli, P. Roy, New J. Chem. 41 (2017) 5696.
[14] M.J. Belousoff, B. Graham, B. Moubaraki, K.S. Murray, L. Spiccia, Eur. J. Inorg. Chem. (2006) 4872.
[15] K. Dhara, P. Roy, J. Ratha, M. Manassero, P. Banerjee, Polyhedron 26 (2007) 4509.
[16] P. Adak, B. Ghosh, A. Bauźa, A. Frontera, A.J. Blake, M. Corbella, C. Das

Mukhopadhyay, S.K. Chattopadhyay, RSC Adv. 6 (2016) 86851.
[17] K. Dhara, S. Karan, J. Ratha, P. Roy, G. Chandra, M. Manassero, B. Mallik, P. Banerjee, Chem. Asian J. 2 (2007) 1091.
[18] A. Ray, G.M. Rosair, R. Kadam, S. Mitra, Polyhedron 28 (2009) 796.
[19] J. Yuan, W.-B. Shi, H.-Z. Kou, Transit Metal. Chem. 40 (2015) 807.
[20] D. Sil, S. Bhowmik, F.S.T. Khan, S.P. Rath, Inorg. Chem. 55 (2016) 3239.
[21] F.S.T. Khan, T. Guchhait, S. Sasmal, S.P. Rath, Dalton Trans. 46 (2017) 1012.
[22] D. Mondal, M.C. Majee, Inorg. Chim. Acta. 465 (2017) 70.
[23] J. Martínez-Lillo, T.F. Mastropietro, G. De Munno, F. Lloret, M. Julve, J. Faus, Inorg. Chem. 50 (2011) 5731.
[24] I. Gryca, J. Palion-Gazda, B. Machura, M. Penkala, F. Lloret, M. Julve, Eur. J. Inorg. Chem. (2016) 5418.
[25] L.A. Dubraja, M. Jurić, F. Torić, D. Pajić, Dalton Trans. 46 (2017) 11748.
[26] B.J. Hollyday, C.A. Mirkin, Angew. Chem. Int. Ed. 40 (2001) 2022.
[27] C.N.R. Rao, S. Natarajan, R. Vaidhyanathan, Angew. Chem. Int. Ed. 43 (2004) 1466.
[28] S.-T. Zheng, G.-Y. Yang, Chem. Soc. Rev. 41 (2012) 7623.
[29] U. García-Couceiro, O. Castillo, A. Luque, J.P. García-Terán, G. Beobide, P. Román, Eur. J. Inorg. Chem. (2005) 4280.
[30] S. Anbu, M. Kandaswamy, Polyhedron 30 (2011) 123.
[31] I. Banerjee, J. Marek, R. Herchel, M. Ali, Polyhedron 29 (2010) 1201.
[32] J. Hagiwara, Y. Shimazaki, G. Saito, Inorg. Chim. Acta 363 (2010) 3178.
[33] P. Roy, M. Nandi, M. Manassero, M. Ricćo, M. Mazzani, A. Bhaumik, P. Banerjee, Dalton Trans. (2009) 9543.
[34] J.R. Zimmerman, A. Bettencourt-Dias, Inorg. Chem. Commun. 14 (2011) 753.
[35] R. Pedrido, M.J. Romero, M.R. Bermejo, M. Martinez-Calvo, A.M. Gonzalez- Noyab, G. Zaragoza, Dalton Trans. (2009) 8329.
[36] M. Verdaguer, Polyhedron 20 (2001) 1115–1128.
[37] E. Coronado, P. Day, Chem. Rev. 104 (2004) 5419.
[38] M.K. Saha, D.K. Dey, B. Samanta, A.J. Edwards, W. Clegg, S. Mitra, Dalton Trans. (2003) 488.
[39] R.N. Patel, D.K. Patel, K.K. Shukla, Y. Singh, J. Coord. Chem. 66 (2013) 4131.
[40] R. Baggio, M.T. Garland, J. Manzur, O. Peña, M. Perec, E. Spodine, A. Vega, Inorg. Chim. Acta 286 (1999) 74.
[41] E. Colacio, J.M. Domínguez-Vera, M. Ghazi, R. Kivekäs, M. Klinga, J.M. Moreno, Eur. J. Inorg. Chem. 1999 (1999) 441.
[42] E. Colacio, M. Ghazi, R. Kiveka, J.M. Moreno, Inorg. Chem. 39 (2000) 2882.
[43] V. Tangoulis, D. Panagoulis, C.P. Raptopoulou, C. Dendrinou-Samara, Dalton Trans. (2008) 1752.
[44] M.H. Sadhua, C. Mathoniereb, Y.P. Patilc, S.B. Kumar, Polyhedron 122 (2017) 210.
[45] J.-E. Backvall (Ed.), Modern Oxidation Methods, Germany, Wiley-VCH, Weinheim, 2004.
[46] S. Halder, A. Mukherjee, K. Ghosh, S. Dey, M. Nandi, P. Roy, J. Mol. Struct. 1101 (2015) 1.
[47] R. Saha, B. Joarder, A. Singha Roy, M. Sk Islam, S. Kumar, Chem. Eur. J. 19 (2013) 16607.
[48] K.C. Gupta, A.K. Sutar, Coord. Chem. Rev. 252 (2008) 1420.
[49] I.T. Horvath, Green Chem. 10 (2008) 1024.
[50] M.C. Pirrung, Chem. Eur. J. 12 (2006) 1312.
[51] N. Shapiro, A. Vigalok, Angew. Chem. Int. Ed. 47 (2008) 2849.
[52] M. Meunier, Chem. Rev. 92 (1992) 1411.
[53] B. Fredrich, W. Gerhartz, Ullmann's encyclopedia of industrial chemistry, Weinheim, New York, 2000, p. 470.
[54] Q.H. Xia, H.Q. Ge, C.P. Ye, Z.M. Liu, K.X. Su, Chem. Rev. 105 (2005) 1603.
[55] A.K. Yudin, Aziridines and Epoxides in Organic Synthesis, Wiley-VCH, Weinheim, 2006.
[56] A.J. Wu, J.E. Penner-Hahn, V.L. Pecoraro, Chem. Rev. 104 (2004) 903.
[57] B.S. Lane, K. Burgess, Chem. Rev. 103 (2003) 2457.
[58] R. Noyori, M. Aoki, K. Sato, Chem. Commun. (2003) 1977.
[59] T. Katsuki, Chem. Soc. Rev. 33 (2004) 437.
[60] T. Punniyamurthy, S. Velusamy, J. Iqbal, Chem. Rev. 105 (2005) 2329.
[61] H.C. Kolb, M.S. Van Nieuwenhze, K.B. Sharpless, Chem. Rev. 94 (1994) 2483.
[62] D.W. Nelson, A. Gypser, P.T. Ho, H.C. Kolb, T. Kondo, H.L. Kwong, D.V. McGrath, A.E. Rubin, P.O. Norrby, K.P. Gable, K.B. Sharpless, J. Am. Chem. Soc. 119 (1997) 1840.
[63] T. Katsuki, K.B. Sharpless, J. Am. Chem. Soc. 102 (1980) 5974.
[64] K. Sato, M. Aoki, M. Ogawa, T. Hashimoto, R. Noyori, J. Org. Chem. 61 (1996) 8310.
[65] W.A. Herrmann, R.W. Fischer, D.W. Marz, Angew. Chem., Int. Ed. Engl. 30 (1991) 1638.
[66] G.M. Sheldrick, SHELXS, 97Program for Structure Solution, University of Gottingen, Germany, 1997.
[67] G.M. Sheldrick, SHELXL 97, Program for Crystal Structure Refinement, University of Gottingen, Germany, 1997.
[68] A.L. Spek, J. Appl. Crystallogr. 36 (2003) 7.
[69] L.J. Farrugia, J. Appl. Crystallogr. 30 (1997) 565.
[70] L.J. Farrugia, J. Appl. Crystallogr. 32 (1999) 837.
[71] Gaussian 09, Revision A.02, M. J. Frisch, G. W. Trucks, H. B. Schlegel, G. E. Scuseria, M. A. Robb, J. R. Cheeseman, G. Scalmani, V. Barone, G. A. Petersson, H. Nakatsuji, X. Li, M. Caricato, A. V. Marenich, J. Bloino, B. G. Janesko, R. Gomperts, B. Mennucci, H. P. Hratchian, J. V. Ortiz, A. F. Izmaylov, J. L. Sonnenberg, D. Williams-Young, F. Ding, F. Lipparini, F. Egidi, J. Goings, B. Peng, A. Petrone, T. Henderson, D. Ranasinghe, V. G. Zakrzewski, J. Gao, N. Rega, G. Zheng, W. Liang, M. Hada, M. Ehara, K. Toyota, R. Fukuda, J. Hasegawa, M. Ishida, T. Nakajima, Y. Honda, O. Kitao, H. Nakai, T. Vreven, K. Throssell, J. A. Montgomery, Jr., J. E. Peralta, F. Ogliaro, M. J. Bearpark, J. J. Heyd, E. N. Brothers, K. N. Kudin, V. N. Staroverov, T. A. Keith, R. Kobayashi, J. Normand, K. Raghavachari, A. P. Rendell, J. C. Burant, S. S. Iyengar, J. Tomasi, M. Cossi, J. M. Millam, M. Klene, C. Adamo, R. Cammi, J. W. Ochterski, R. L. Martin, K. Morokuma, O. Farkas, J. B. Foresman, and D. J. Fox, Gaussian, Inc., Wallingford CT, 2016.
[72] A.D. Becke, J. Chem. Phys. 98 (1993) 5648.
[73] C.T. Lee, W.T. Yang, R.G. Parr, Phys. Rev. B 37 (1988) 785.
[74] M. O'Boyle, A.L. Tenderholt, K.M. Langner, J. Comp. Chem. 29 (2008) 839.
[75] A.W. Addison, T.N. Rao, J. Reedijk, J. van Rijn, G.C. Verschoor, J. Chem. Soc. Dalton Trans. (1984) 1349.
[76] M. Wang, B. Hu, X.T. Deng, C.G. Wang, Acta Cryst. E63 (2017) m710.
[77] S.K. Chattopadhyay, S. Seth, T.C.W. Mak, J. Coord. Chem. 55 (2002) 259.
[78] H. Dong, C.J. White, B. Zhang, C. Krebs, N.i. Lehnert, J. Am. Chem. Soc. (2018) ASAP 10.1021/jacs.8b08567.
[79] T. Osako, S. Nagatomo, Y. Tachi, T. Kitagawa, S. Itoh, Angew. Chem. Int., Ed. Eng. 41 (2002) 4325.
[80] S.T. Prigge, B.A. Eipper, R.E. Mains, L.M. Amzel, Science 304 (2004) 864.
[81] P. Roy, K. Dhara, M. Manassero, P. Banerjee, Inorg. Chem. Commun. 11 (2008) 265.
[82] J. Reim, R. Werner, W. Haase, B. Krebs, Chem. Eur. J. 4 (1998) 289.

Inorganic Chemistry

pubs.acs.org/IC

Article

Selective Metal−Ligand Bond-Breaking Driven by Weak Intermolecular Interactions: From Metamagnetic Mn(III)-Monomer to Hexacyanoferrate(II)-Bridged Metamagnetic Mn_2Fe Trimer

Somen Goswami, Soumen Singha, Indrajit Saha, Abhishikta Chatterjee, Subrata K. Dey,* Carlos J. Gómez García,* Antonio Frontera, Sanjay Kumar,* and Rajat Saha*

Cite This: https://dx.doi.org/10.1021/acs.inorgchem.0c00909

Read Online

ACCESS | Metrics & More | Article Recommendations | Supporting Information

ABSTRACT: Metal−ligand coordination interactions are usually much stronger than weak intermolecular interactions. Nevertheless, here, we show experimental evidence and theoretical confirmation of a very rare example where metal−ligand bonds dissociate in an irreversible way, helped by a large number of weak intermolecular interactions that surpass the energy of the metal−ligand bond. Thus, we describe the design and synthesis of trinuclear Mn_2Fe complex $\{[Mn(L)(H_2O)]_2Fe(CN)_6\}$,$^{2-}$ starting from a mononuclear Mn(III)-Schiff base complex: $[Mn(L)(H_2O)Cl]$ (**1**) and $[Fe(CN)_6]^{4-}$ anions. This reaction implies the dissociation of Mn(III)-Cl coordination bonds and the formation of Mn(III)-NC bonds with the help of several intermolecular interactions. Here, we present the synthesis, crystal structure, and magnetic characterization of the monomeric Mn(III) complex $[Mn(L)(H_2O)Cl]$ (**1**) and of compound $(H_3O)[Mn(L)(H_2O)_2]$-$\{[Mn(L)(H_2O)]_2Fe(CN)_6\}\cdot 4H_2O$ (**2**) (H_2L = 2,2′-((1*E*,1′*E*)-(ethane-1,2-diylbis-(azaneylylidene))bis(methaneylylidene))bis(4-methoxyphenol)). Complex **1** is a monomer where the Schiff base ligand (L) is coordinated to the four equatorial positions of the Mn(III) center with a H_2O molecule and a Cl^- ion at the axial sites and the monomeric units are assembled by $\pi-\pi$ and hydrogen-bonding interactions to build supramolecular dimers. The combination of $[Fe(CN)_6]^{4-}$ with complex **1** leads to the formation of linear Mn-NC-Fe-CN-Mn trimers where two *trans* cyano groups of the $[Fe(CN)_6]^{4-}$ anion replace the labile chloride from the coordination sphere of two $[Mn(L)(H_2O)Cl]$ complexes, giving rise to the linear anionic $\{[Mn(L)(H_2O)]_2Fe(CN)_6\}^{2-}$ trimer. This Mn_2Fe trimer crystallizes with an oxonium cation and a mononuclear $[Mn(L)(H_2O)_2]^+$ cation, closely related to the precursor neutral complex $[Mn(L)(H_2O)Cl]$. In compound **2**, the Mn_2Fe trimers are assembled by several hydrogen-bonding and $\pi-\pi$ interactions to frame an extended structure similar to that of complex **1**. Density functional theoretical (DFT) calculations at the PBE1PBE-D3/def2-TZVP level show that the bond dissociation energy (−29.3 kcal/mol) for the Mn(III)-Cl bond is smaller than the summation of all the weak intermolecular interactions (−30.1 kcal/mol). Variable-temperature magnetic studies imply the existence of weak intermolecular antiferromagnetic couplings in both compounds, which can be can cancelled with a critical field of ca. 2.0 and 2.5 T at 2 K for compounds **1** and **2**, respectively. The magnetic properties of compound **1** have been fit with a simple $S = 2$ monomer with $g = 1.959$, a weak zero-field splitting ($|D| = 1.23$ cm^{-1}), and a very weak intermolecular interaction ($zJ = -0.03$ cm^{-1}). For compound **2**, we have used a model with an $S = 2$ monomer with ZFS plus an $S = 2$ antiferromagnetically coupled dimer with $g = 2.009$, $|D| = 1.21$ cm^{-1}, and $J = -0.42$ cm^{-1}. The metamagnetic behavior of both compounds is attributed to the weak intermolecular $\pi-\pi$ and hydrogen-bonding interactions.

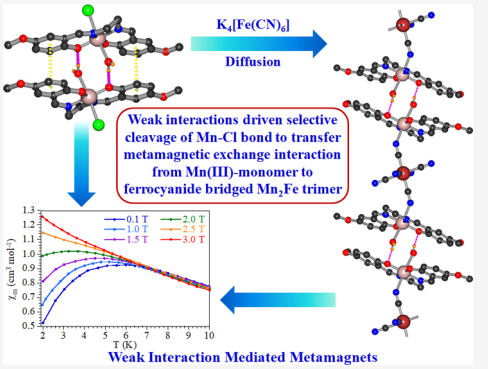

INTRODUCTION

Selective bond making−bond breaking is the finest art of chemistry and has tremendous significance in molecular and supramolecular chemistry.[1−4] After a prolonged research over centuries, chemists have gained mastery over covalent and metal−ligand coordination bond breaking−bond making processes, whereas control over the supramolecular interactions is still a daunting task. Several catalytic processes[5−9] are well-known for the selective bond activation, bond breaking, and bond making in organic chemistry. In coordination chemistry, the so-called *trans* effect,[10,11] the HSAB principle,[12,13] etc. can successfully explain the selective metal−ligand bond breaking−bond making process. In supramolecular chemistry, molecular recognition and aggregation constitute

Received: March 27, 2020

the base of selectivity and determine the final compound and strucutre.[14−18] Supramolecular interactions are much weaker than covalent/coordinate bonds and therefore a minor chemical or physical perturbation may cause a severe change in the weak interaction network of the system. Here, we present a case study where weak interactions drive a metal−ligand coordination bond dissociation during the formation of a hexacyanoferrate(II)-bridged Mn_2Fe trimer from a Mn(III)-monomeric precursor.

In molecular magnetism, metamagnets[19−22] are a special type of magnetic material in which two magnetic motifs (which may be a molecule, a one-dimensional (1D) chain, or a two-dimensional (2D) layer) interact antiferromagnetically (AF) through weak intermotif (molecule or chain or layer) interactions and the application of a DC field above a certain critical field (H_C) can alter this weak AF coupling into a ferromagnetic (FM) one at low temperatures (T_N).[23,24] Such coexistence of AF and FM in a material is difficult to predict and, consequently, highly challenging to design, but it may have significant applications in technologies associated with magnetic cooling[25] and the magnetocaloric effect.[26] This magnetic-field-induced first-order transition from AF to FM is critically dependent on the weak intermotif interactions. Mukherjee et al.[22] have reported that the metamagnetism arises due to weak C−H···N hydrogen-bonding interactions between azido-bridged 1D coordination chains of Ni^{II}−Schiff base complex. Chen et al.[27] have reported the metamagnetic behavior of 2-fold interpenetrated coordination layers, where weak hydrogen bonding and dipolar interactions between adjacent layers are responsible for such metamagnetic transition. Ghosh et al.[28] reported metamagnetism due to weak interchain C−H···N hydrogen bonding between neighboring coordination chains formed by Mn(III)-tridentate Schiff base units connected with azide ligands in its *end-on* (μ-1,1′) coordination mode. Therefore, to design a metamagnetic material, we must control the weak intermolecular interactions, although, due to the difficulty involved with this control, most of the reported molecular metamagnets are basically serendipitous. With this background, we have designed a strategy to prepare molecular metamagnets through controlled breaking of metal−ligand bonds helped by the cumulative functions of a large number of weak interactions.

In the past few years, high spin Mn(III)-Schiff base complexes have been used as structural building units to design several types of magnetic materials, such as single-chain magnets[29,30] (SCMs), single-molecule magnets[31,32] (SMMs), ferromagnets,[33,34] antiferromagnets,[35,36] etc., thanks to several unique properties of the Mn(III) ions: (i) stable oxidation state, (ii) high spin configuration (S = 2), (iii) easily substitutable axial sites, and (iv) unusual uniaxial anisotropy (D) arising from Jahn−Teller distortion in octahedral geometry.

In this context, we have synthesized a Mn(III) complex with a N_2O_2 donor-based Schiff base ligand and studied its structure and magnetic properties. X-ray structural study reveals Mn(III)-monomeric units with axial water and chloride ligands, that are further assembled by hydrogen bonds and $\pi-\pi$ interactions to form a supramolecular dimer with a very small intradimer antiferromagnetic coupling and a metamagnetic behavior with a critical field of ca. 2.0 T at 2 K. The hard acid−soft base interaction makes the coordinated chlorides highly labile and the reaction of complex **1** with $K_4[Fe(CN)_6]$ replaces the chlorides from the coordination sphere of two adjacent monomeric Mn(III) units to yield a *trans* cyanide-bridged Mn_2Fe trimer (complex **2**) that cocrystallizes in a 1:1 ratio with a Mn(III) monomer closely related to complex **1**. Structural analysis reveals the preservation of weak intermolecular hydrogen bonds and $\pi-\pi$ interactions during the transformation of the monomer into the trimer as well as the metamagnetic behavior. These Mn_2Fe trimers are assembled by hydrogen bonds and $\pi-\pi$ interactions, giving rise to supramolecular chains that also present a metamagnetic transition with a critical field of ca. 2.5 T at 2 K.

EXPERIMENTAL SECTION

Materials and Methods. $MnCl_2{\cdot}4H_2O$ (99%), 2-hydroxy-5-methoxybenzaldehyde (99.5%), ethylenediamine (99.5%), and $K_4[Fe(CN)_6]$ (99%) have been purchased from Sigma-Aldrich and used without further purification. Triethylamine and all other chemicals (AR grade) were purchased from Merck India and used as received. A PerkinElmer 240C elemental analyzer was employed to perform elemental analysis (C, H, N). The Fourier transform infrared (FT-IR) spectra have been recorded by a Nicolet Impact 410 spectrometer, using KBr pellets in the range of 400−4000 cm^{-1}.

Synthesis of the Ligand (H_2L). The Schiff's base ligand (H_2L = 2,2′-((1*E*,1′*E*)-(ethane-1,2-diylbis(azaneylylidene))bis-(methaneylylidene))bis(4-methoxyphenol)) was synthesized (see Scheme 1, presented later in this work) by refluxing 2-hydroxy-5-methoxybenzaldehyde (10 mmol, 1.525 g) with ethylenediamine (5 mmol, 300 mg) in a 2:1 ratio in methanol (20 mL) at 90 °C for 1 h. The reaction mixture was then cooled and filtered to separate out the yellow-colored crystalline solid product, washed with diethyl ether, and dried in air. Yield: ∼90%.

Synthesis of [(L)Mn(H_2O)Cl] (1). The Schiff base ligand H_2L (165 mg, 0.5 mmol) was dissolved in 20 mL of boiling methanol and the pH of the methanolic solution was adjusted to 9 by Et_3N. An aqueous solution (5 mL) of $MnCl_2{\cdot}4H_2O$ (100 mg, 0.5 mmol) was added to the previous solution and the resulting solution was refluxed for 2 h. The reaction mixture was cooled, filtered off, and the light yellowish brown filtrate was kept undisturbed for crystallization. Brown needlelike crystals suitable for single-crystal X-ray analyses were collected after 2 weeks. Yield: ∼86%. Anal. Calc. for $C_{18}H_{20}ClMnN_2O_5$: C, 49.7; H, 4.6; N, 6.4%. Found: C, 49.8; H, 4.5; N, 6.5%. Selected IR bands (KBr pellet, cm^{-1}): ν (C═N) 1605(s); ν (O−H) 3385(broad).

Synthesis of $(H_3O)[Mn(L)(H_2O)_2]\{[Mn(L)(H_2O)]_2Fe(CN)_6\}\cdot 4H_2O$ (2). The cocrystal of this hexacyanoferrate(II)-bridged trimeric complex was synthesized via a layering technique, using the monomeric complex **1** and a $K_4[Fe(CN)_6]$ solution in a 1:1 ratio with a water−methanol buffer solution. Complex **1** (110 mg, 0.25 mmol) was dissolved in 30 mL of a 9:1 methanol−water mixture. A second solution was prepared dissolving $K_4[Fe(CN)_6]$ (108 mg, 0.25 mmol) in 25 mL of distilled water. These two solutions were layered in eight different tubes using a 1:1 water−methanol buffer and kept undisturbed for crystallization. Deep-brown needle-shaped crystals suitable for X-ray diffraction (XRD) analysis were collected after one month, then washed with hexane and dried. Yield: 79%. Anal. Calc. for $C_{60}H_{73}FeMn_3N_{12}O_{21}$: C, 47.4; H, 4.8; N, 11.1%. Found: C, 47.5; H, 4.7; N, 11.1%. Selected IR bands (KBr pellet, cm^{-1}): ν(C≡N) stretching 2123, 2105(s); ν(C≡N) 1608(s); ν(O−H) 3410(broad).

Magnetic Measurements. Magnetic measurements on compound **1** and **2** (with masses of 33.446 and 4.406 mg, respectively) were performed using a Quantum Design MPMS-XL-7 SQUID magnetometer in the temperature range of 2−300 K in the presence of an external magnetic field of 0.1 T (and in the temperature range of 2−10 K with different applied fields in the range of 0.1−3.0 T). The isothermal magnetizations were measured at 2 K with magnetic fields of up to 7 T on the same samples. The susceptibility data were corrected for the sample holders previously measured using the same conditions and for the diamagnetic contributions of the compounds, as deduced by using Pascal's constant tables.[37]

https://dx.doi.org/10.1021/acs.inorgchem.0c00909
Inorg. Chem. XXXX, XXX, XXX−XXX

Theoretical Methods. All DFT calculations included in this manuscript have been performed using the Gaussian-16 program[38] at the PBE1PBE-D3/def2-TZVP level of theory and using the crystallographic coordinates. The formation energies of the assemblies have been evaluated by calculating the difference between the overall energy of the assembly and the sum of the monomers that constitute the assembly, which have been maintained frozen. The Atoms-in-Molecules (AIM)[39] analysis has been performed at the same level of theory. The calculation of AIM properties was done using the AIMAll program.[40]

Crystallographic Data Collection and Refinement. Suitable single crystals of complexes **1** and **2** were mounted on a Bruker SMART CCD diffractometer equipped with a graphite monochromator and Mo Kα (λ = 0.71073 Å) radiation, and then the structures were solved via the Patterson method, using several software programs.[41−45] The details of the process are given in the Supporting Information file. All the crystallographic data and refinement parameters of both complexes are presented in Table 1. Complex **2** contains disordered guest water molecules.

Table 1. Crystallographic Data Collection and Refinement Parameters of Compounds 1 and 2[a,b,c]

	Value/Comment	
parameter	1	2
formula	$C_{18}H_{20}ClMnN_2O_5$	$C_{60}H_{73}FeMn_3N_{12}O_{21}$
formula weight	434.75	1518.97
crystal system	orthorhombic	triclinic
space group	P_{bca}	$P\bar{1}$
a (Å)	11.826(6)	14.0832(14)
b (Å)	12.872(7)	15.0504(15)
c (Å)	22.919(12)	17.0031(18)
α (deg)	90	108.703(3)
β (deg)	90	101.649(3)
γ (deg)	90	90.023(4)
unit-cell volume, V (Å^3)	3489(3)	3335.1(6)
Z	8	2
ρ_{calc} (g/cm^3)	1.655	1.513
μ (Mo Kα) (mm)	0.945	0.850
F(000)	1792	1572
crystal size (mm^3)	0.08 × 0.12 × 0.16	0.12 × 0.16 × 0.20
temperature, T (K)	100	152
$\theta_{min-max}$ (deg)	1.8, 25.3	2.5, 27.2
total data	28731	34615
unique data	3156	14564
R_{int}	0.177	0.126
observed data [$I > 2.0\sigma(I)$]	1625	7216
N_{ref}	3156	14564
N_{par}	244	878
R	0.0581	0.0963
wR_2	0.1195	0.2874
S	0.80	1.01

[a] $R_1 = \sum||F_o| - |F_c||/\sum|F_o|$. [b] $wR_2(F_o^2) = [\sum[w(F_o^2 - F_c^2)^2/\sum wF_o^4]^{1/2}$. [c] GooF = $[\sum[w(F_o^2 - F_c^2)^2/(N_{obs} - N_{params})]^{1/2}$

RESULTS AND DISCUSSION

Synthesis. The tetradentate Schiff-base ligand (H_2L) was synthesized by the combination of ethylene diamine with 2-hydroxy-5-methoxybenzaldehyde in a 1:2 ratio (see Scheme 1). Combination of the synthesized ligand with $MnCl_2$ leads to the aerial oxidation of Mn(II) to Mn(III) with formation of the neutral complex **1**, that, besides the ligand L^{2-}, contains one Cl^- and one water molecule at the axial sites (Scheme 1). When complex **1** is reacted with $[Fe(CN)_6]^{4-}$, the cyanide groups replace the coordinated chloride ions of two neighboring Mn(III) monomers, connecting them through a Mn-NC-Fe-CN-Mn bridge (Scheme 1).

Structure of Complex [Mn(L)(H_2O)Cl] (1). The mononuclear complex **1** crystallizes in the orthorhombic centrosymmetric space group P_{bca}. The asymmetric unit contains one mononuclear unit, which contains one Mn(III) ion, one deprotonated ligand L^{2-}, one coordinated Cl^-, and one coordinated water molecule (Figure 1).

Selected coordination bond distances and angles are given in Table S1 in the Supporting Information. The metal center shows a distorted octahedral geometry. As observed in other N_2O_2 donor Schiff base-metal complexes, the four equatorial positions are occupied by the four donor atoms (N1, N2, O1, and O2) of the Schiff base while the *trans*-axial sites are occupied by one chloride ion (Cl1) and one water molecule (O1W). The Mn−O and Mn−N bond lengths of the Schiff-base donor atoms are in the normal range: Mn1−O1 = 1.881(4) Å, Mn1−O2 = 1.863(4) Å, Mn1−N1 = 1.979(4) Å, and Mn1−N2 = 1.973(4) Å, whereas the axial bond lengths are comparatively longer: Mn1−Cl1 = 2.554(2) Å and Mn1−O1W = 2.287(3) Å. These distances reflect the expected Jahn−Teller elongation along the axial bonds. The Mn center is displaced toward the Cl1 atom ∼0.073 Å from the mean plane formed by the donor atoms (O1−N1−N2−O2) of the Schiff-base ligand.

Supramolecular structural analysis reveals that two neighboring mononuclear units are connected in an antiparallel fashion by $\pi-\pi$ interactions to form a supramolecular dimer, which is further stabilized by a double O1W−H1W1···O1 hydrogen-bonding interaction (Figure 2). These dimers are bridged by O1W−H2W1···Cl1 hydrogen-bonding interactions to form supramolecular layers parallel to the crystallographic *ab*-plane (Figure S1 in the Supporting Information). These supramolecular layers are further bridged by C8−H8A···Cl1 and C15−H15···Cl1 hydrogen-bonding interactions to develop a 3D supramolecular structure (Figure S2). The hydrogen bonding and $\pi-\pi$ interaction parameters are summarized in Tables S2 and S3 in the Supporting Information.

Crystal Structure of $(H_3O)[Mn(L)(H_2O)_2]\{[Mn(L)(H_2O)]_2Fe(CN)_6\}\cdot 4H_2O$ (2). Single-crystal X-ray analysis reveals that this compound crystallizes in the centrosymmetric triclinic $P\bar{1}$ space group. It is a 1:1 cocrystal of a Mn_2Fe trimer and a Mn(III) monomer. The asymmetric unit contains one monomeric unit, two halves trimeric units, one oxonium cation, and four disordered guest water molecules (Figure 3). The trimeric unit is dianionic and its charge is balanced by the monocationic monomer and one oxonium ion. Note that the presence of the oxonium cation is not only established by charge balance requirements but also by the X-ray crystal data that shows three H atoms around the O5W atom with the expected trigonal pyramidal geometry with similar H−O−H bond angles of 104.4°, 104.6°, and 105.1°. The crystallographic data is presented in Table 1, and some selected coordination bond lengths and angles are summarized in Table S4 in the Supporting Information. The cocrystal contains two different trimeric units. Each trimeric unit is formed by two Mn(III)-Schiff base complexes connected through two *trans* cyanide groups of the hexacyanoferrate(II) unit that acts as a linear bridge, replacing the chloride groups in the original monomeric complex **1**. Interestingly, the water molecule remains coordinated with the Mn(III) ions, precluding the formation of an alternating cyanide-bridged Mn(III)−Fe(II)

https://dx.doi.org/10.1021/acs.inorgchem.0c00909
Inorg. Chem. XXXX, XXX, XXX−XXX

Scheme 1. Complete Synthetic Scheme of the Ligand (H_2L) and Complexes 1 and 2

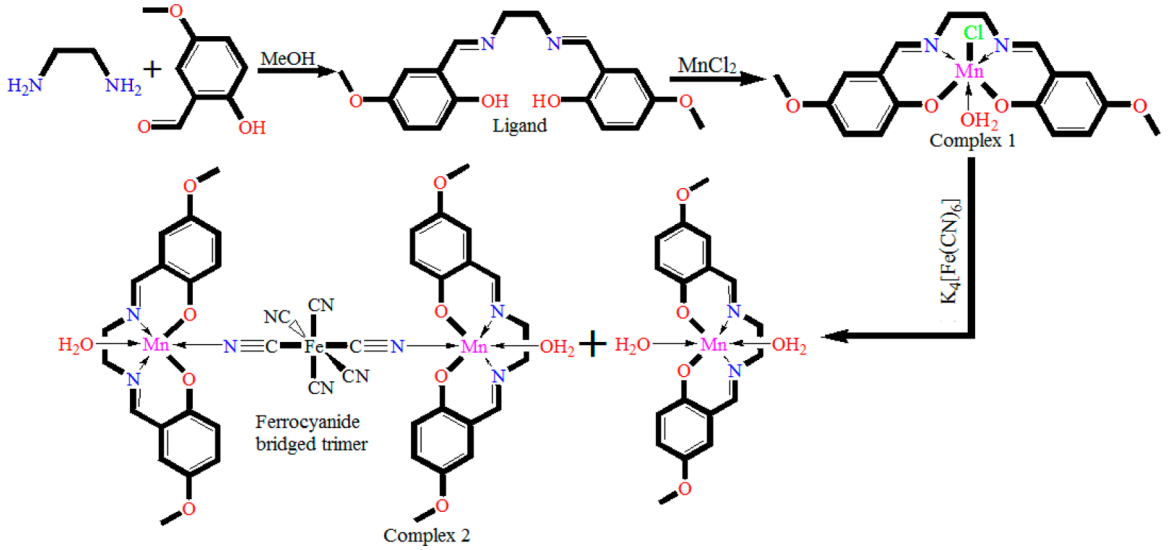

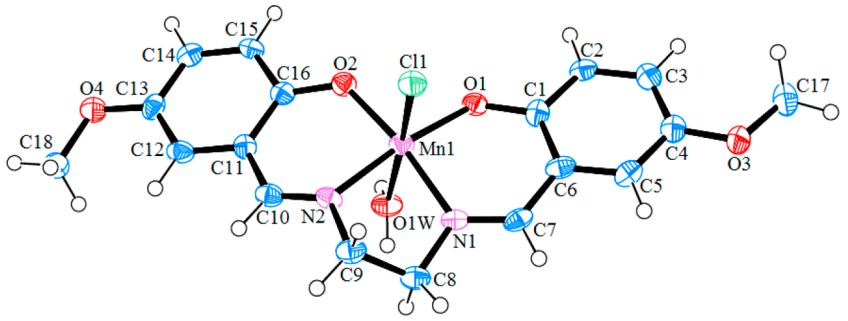

Figure 1. ORTEP diagram and labeling scheme of complex **1** with 30% ellipsoid probability.

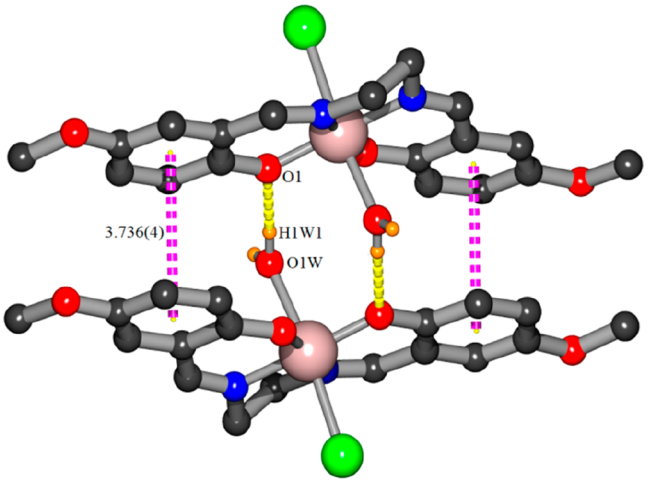

Figure 2. Supramolecular dimer formation with $\pi-\pi$ and O1W–H1W1···O1 hydrogen-bonding interactions in complex **1**.

chain. In each trimer, the asymmetric unit contains a full Mn(III)-Schiff base complex moiety and half $[Fe(CN)_6]^{4-}$ unit. In both trimers the Mn(III) ions show a distorted octahedral geometry where the four equatorial positions are occupied by the four donor sites of the Schiff base ligands and the axial positions are occupied by a water molecule and N atom of the CN group of the bridging $[Fe(CN)_6]^{4-}$ unit (Figure 3). In both trimers, the bond lengths from the N_2O_2 Schiff-base donor atoms to the metal centers are quite similar: Mn1–O1 = 1.862(5) Å, Mn1–O2 = 1.889(5) Å, Mn1–N1 = 1.981(6) Å, and Mn1–N2 = 1.985(6) Å for trimer **1** and Mn2–O5 = 1.872(5) Å, Mn2–O6 = 1.902(5) Å, Mn2–N6 = 1.977(6) Å, and Mn2–N7 = 1.997(6) Å for trimer **2**. In both trimers, the two axial bond lengths are longer than the equatorial ones: Mn1–O1W = 2.290(5) Å and Mn1–N3 = 2.316(6) Å in trimer **1** and Mn2–O2W = 2.294(5) Å and Mn2–N8 = 2.2478(6) Å in trimer **2**, indicating the presence of a Jahn–Teller elongation in both trimers, as observed in complex **1** (see above). The trimers are not linear, since the Mn–N≡C bond angles are 143.38° and 145.01° in trimers **1** and **2**, respectively.

In the monomeric unit, the metal ion (Mn3) also shows a distorted octahedral geometry, as in complex **1**. The Schiff base occupies the four equatorial coordination sites, using its four donor sites (O9, O10, N11, and N12). The corresponding bond lengths are similar to those observed in compound **1** and in both trimers in compound **2**: Mn3–O9 = 1.874(5) Å, Mn3–N12 = 1.984(6) Å, Mn3–O10 = 1.894(6) Å, and Mn3–N11 = 1.988(6) Å. In contrast to complex **1**, the two axial sites are occupied by two water molecules (O3W and O4W). As expected, the axial Mn–O bond lengths: Mn3–O3W = 2.299(6) Å and Mn3–O4W = 2.215(5) Å are longer than the equatorial ones, showing, once more, the existence of a Jahn–Teller elongation in the Mn(III)-monomeric unit. The Mn3 center is displaced toward the O4W molecule by ∼0.043 Å from the mean equatorial plane.

https://dx.doi.org/10.1021/acs.inorgchem.0c00909
Inorg. Chem. XXXX, XXX, XXX–XXX

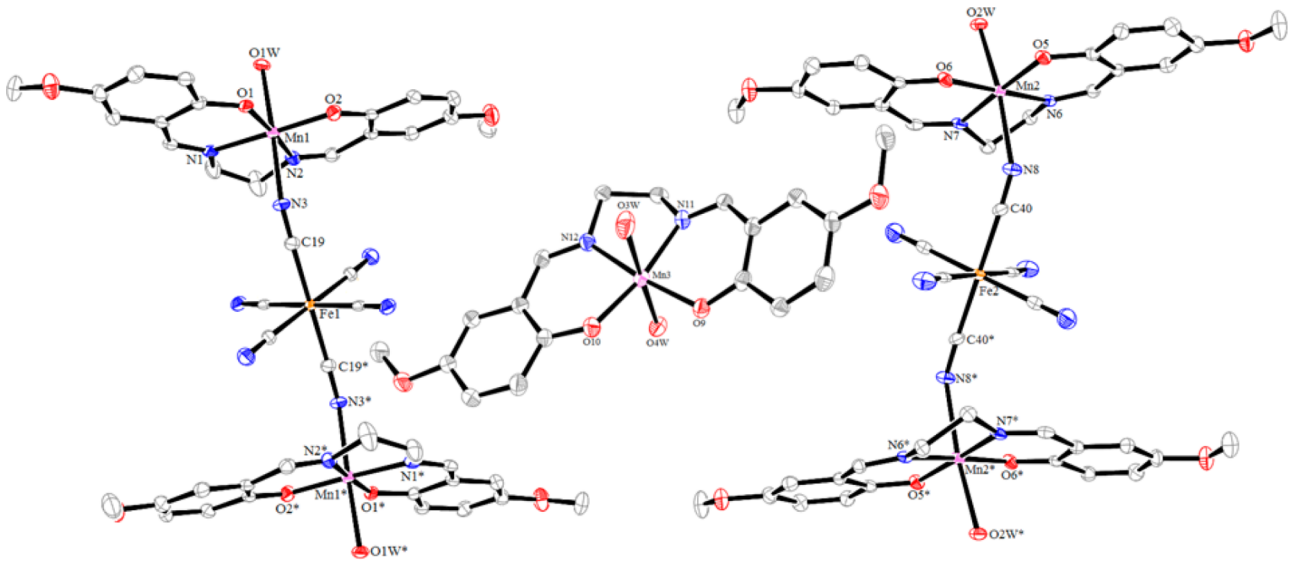

Figure 3. ORTEP diagram in **2** showing two complete trimers and a monomer with atom labeling. The solvent molecules, oxonium cation, and H atoms are omitted for clarity. Ellipsoids drawn at 15% probability.

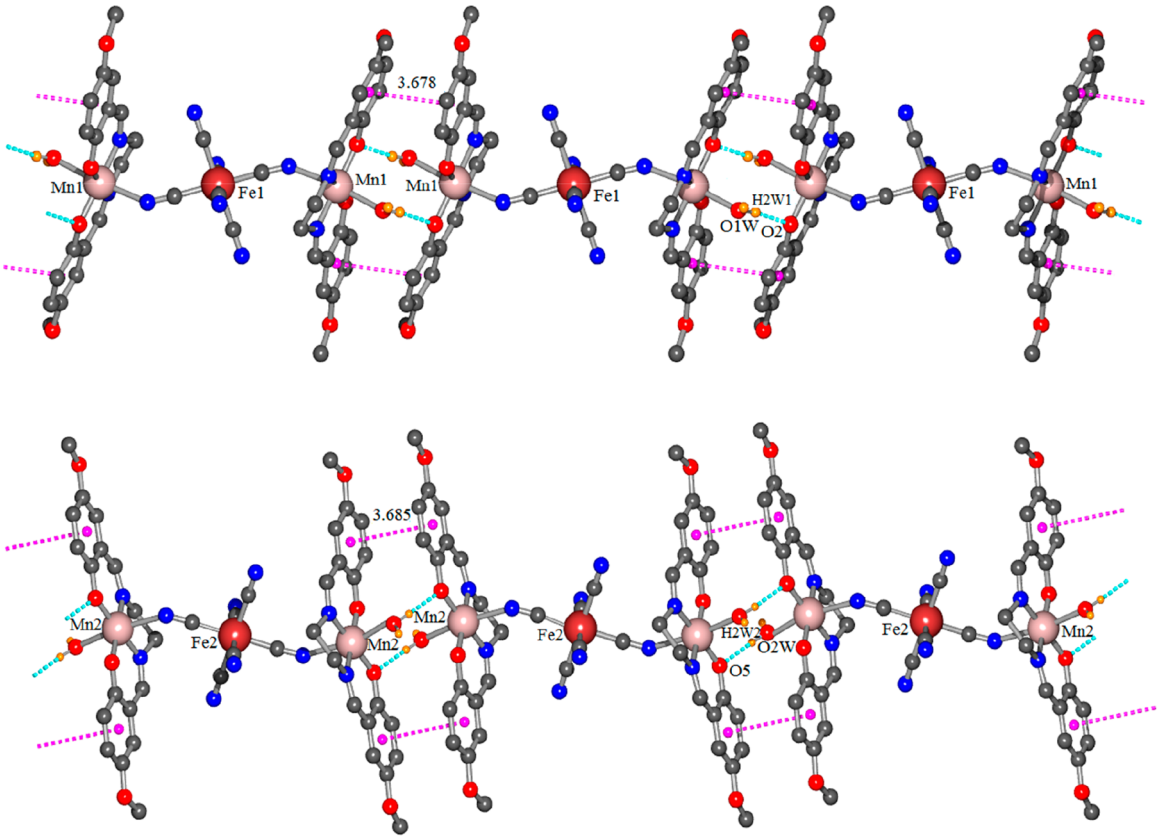

Figure 4. View of the chains of trimers Mn1−Fe1−Mn1 (top) and Mn2−Fe2−Mn2 (bottom), showing the centroids of the aromatic rings of the ligands (as pink spheres) and the shortest C_g−C_g distances (as pink dotted lines). Hydrogen bonds are indicated as light blue dotted lines.

Supramolecular structural analysis reveals that each trimeric unit is connected by hydrogen bonding interactions implying the coordinated water molecules and by π−π interactions to form supramolecular chains parallel to the crystallographic *b*-axis. Each independent trimer forms a different type of supramolecular chain (Figure 4). These two different chains are arranged parallel and are connected by O2W−H1W2···N4 and O1W−H1W1···N10 hydrogen-bonding interactions to form a supramolecular layer in the *ab*-plane.

The cations (the monomeric Mn(III) complex and the oxonium ions) and the disordered solvent molecules are located in the interlayer space. These molecules and ions are connected with the anionic supramolecular layers by means of hydrogen-bonding interactions. All these supramolecular

https://dx.doi.org/10.1021/acs.inorgchem.0c00909
Inorg. Chem. XXXX, XXX, XXX−XXX

interactions are summarized in Tables S5 and S6 in the Supporting Information.

Theoretical DFT Study of Noncovalent Interactions. To highlight the behavior of compounds **1** and **2** commented above and the easy replacement of the chloride ligand by the hexacyanoferrate(II) unit, we have performed DFT calculations at the PBE1PBE-D3/def2-TZVP level of theory (see the Theoretical Methods section for details). First, we have compared the hydrogen-bonded dimerization energy of the supramolecular dimer shown in Figure 2 to the dissociation energy of the Mn(III)-Cl coordination bond. The interaction energy of the dimer of compound **1**, along with the QTAIM distribution of bond critical points and bond paths, are given in Figure 5. It can be observed that the dimerization energy is

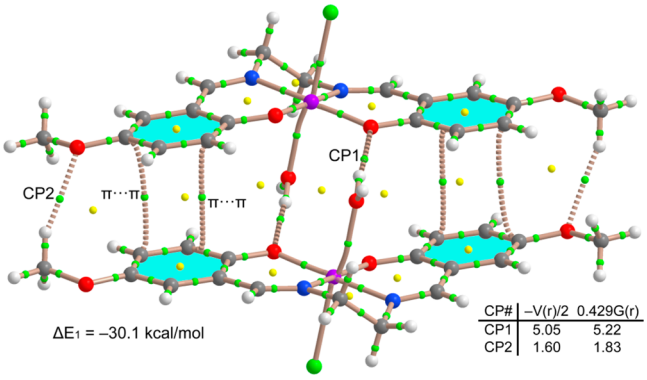

Figure 5. AIM distribution of bond and ring critical points (green and yellow spheres, respectively) and bond paths obtained for the self-assembled dimer of compound **1**. The dissociation energies of the hydrogen bonds using the $V(r)$ and $G(r)$ values at the bond CP are indicated in (kcal/mol) at the lower-right corner and the formation energy of the assembly (ΔE_1) is also given near the assembly.

very large (ΔE_1 = −30.1 kcal/mol), because of the cooperative formation of several O···H and C−H···O hydrogen bonds and $\pi-\pi$ interactions, which are characterized by the corresponding bond critical points (CPs) and bond paths interconnecting the interacting atoms. In order to measure the contribution of the hydrogen bonds, we have used the AIM energy densities at the bond CPs. This methodology has been effectively used by us and others to analyze several types of noncovalent interactions.[46−48] The dissociation energy of each hydrogen-bonding contact can be estimated according to the approach proposed by Espinosa et al.[49] and Vener et al.,[50] which developed energy descriptors specifically for hydrogen bonds. Figure 5 also shows the dissociation energy (in kcal/mol) obtained for each hydrogen bond using both indicators, i.e., the potential energy density $V(r)$ and the Lagrangian kinetic energy $G(r)$. The energies are indicated in Figure 5, and they evidence that the contribution of both O−H···O hydrogen bonds is ∼10.4 kcal/mol and that of the C−H···O bonds involving the methoxide groups is significantly smaller (i.e., 3.6 kcal/mol), using the $G(r)$ descriptor. Therefore, the contribution of the π-stacking and other long-range van der Waals interactions is very significant (∼16 kcal/mol). The dissociation energy of the Mn(III)−Cl coordination bond computed for **1** in MeOH at the same level of theory is −29.3 kcal/mol, which is slightly weaker that the dimerization energy.

We have also evaluated the reaction energy of the transformation depicted in Scheme 2 in order to rationalize the transformation of compound **1** to compound **2** upon the addition of hexacyanoferrate(II). Fortunately, the energy of formation of **2** from **1** is strongly favored (ΔE_r = −19.7 kcal/mol), using methanol as the solvent in the calculation. Note that this reaction energy does not compensate for the energy of the hydrogen-bonded dimer formation of **1** observed in the solid state (ΔE_1; see Figure 5). However, this matter is not important, because the same combination of interactions is also found in the solid state of compound **2**, as detailed in the supramolecular polymers shown in Figure 4. We have performed the QTAIM analysis of a dimeric model of the polymer that is shown in Figure 6, and exactly the same distribution of critical points and bond paths is obtained. It is also worthwhile to comment that the O−H···O hydrogen bonds in **2** are even stronger than those in compound **1**.

Taken together, the results from the theoretical DFT study of complexes **1** and **2** revealed that the ligand exchange of Cl^- by $[Fe(CN)_6]^{4-}$ is energetically favored and preferred over the water substitution since the Mn−Cl coordination bond is weaker than the strength of the weak interactions involved in the formation of the dimer/polymers (hydrogen bonds and $\pi-\pi$ interactions).

Magnetic Properties of Compound 1. At room temperature, the $\chi_m T$ value per Mn(III) ion for compound **1** is ca. 3.0 cm^3 K mol^{-1}, which is close to the expected value for an isolated Mn(III) ion with a ground spin state of S = 2 and a g-value close to 2. When the sample is cooled, $\chi_m T$ remains constant, down to ca. 20 K, and shows a sharp decrease at lower temperatures to reach a value of ca. 0.8 cm^3 K mol^{-1} at 2 K (Figure 7), which suggests the presence of a weak antiferromagnetic interaction in **1** and/or the presence of a zero field splitting in the Mn(III) ions. Since the structure of this compound indicates the presence of quasi-isolated Mn(III) monomers, we have fit the magnetic properties to a

Scheme 2. Transformation from 1 to 2 is Energetically Favorable in Methanol Medium

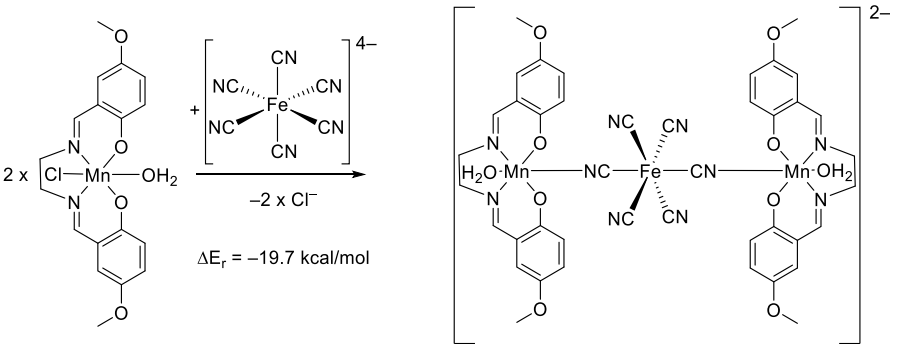

https://dx.doi.org/10.1021/acs.inorgchem.0c00909
Inorg. Chem. XXXX, XXX, XXX−XXX

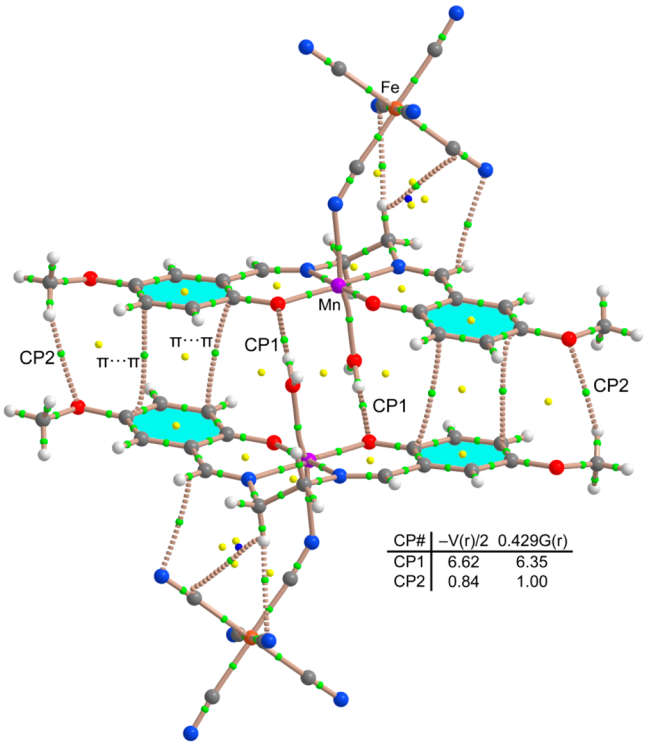

Figure 6. AIM distribution of bond and ring critical points (green and yellow spheres, respectively) and bond paths obtained for a model dimer of compound **2**. The dissociation energies of the hydrogen bonds using the $V(r)$ and $G(r)$ values at the bond CP are indicated in (kcal/mol) in the lower-right corner.

simple model considering an isolated $S = 2$ ion with a zero field splitting (ZFS) to account for the sharp decrease in $\chi_m T$ at low temperatures, using the program PHI.[51] This model reproduces very satisfactorily the magnetic properties of complex **1** in the entire temperature range with $g = 1.958$ and $|D| = 0.69$ cm^{-1} with a residual of 0.0679 (see the dotted line in Figure 7).

Although the magnetic fitting to a monomer with a ZFS produces very satisfactory results, and we have also considered the possible presence of a weak intermolecular interaction through the $\pi-\pi$ and hydrogen-bonding interactions. This weak intermolecular coupling is supported by the presence of a maximum at very low temperatures in the χ_m vs T plot (Figure 7b). Thus, if we include the presence of a weak intermolecular coupling with the mean field approximation (zJ), we can replicate even better the magnetic properties of compound **1** with $g = 1.959$, $zJ = -0.03$ cm^{-1}, and $|D| = 1.23$ cm^{-1} with a residual of 0.0158 (solid line in Figure 7). As expected, the interaction between the Mn(III) centers is weak and antiferromagnetic, since usually $\pi\cdots\pi$ interactions give rise to weak couplings.[52−57] On the other side, the D value found for the isolated Mn(III) center is quite low and is in the typical range observed (−3.8 cm^{-1} to +3.1 cm^{-1}) for mononuclear Mn(III) ions.[58]

Further confirmation of the presence of a very weak antiferromagnetic intermolecular interaction is provided by the isothermal magnetization at 2 K of compound **1** (Figure 8a). This measurement shows a sigmoidal shape with a maximum slope at ca. 2.0 T, as can be found in the derivative of the M vs H plot (Figure 8b), which suggests that **1** is a metamagnet with a critical field of ca. 2.0 T at 2 K (i.e., the weak antiferromagnetic coupling can be cancelled by applying a high magnetic field, above ca. 2.0 T, giving rise to a ferromagnetic coupling). Therefore, we can confirm that there is a very weak antiferromagnetic intermolecular interaction when the applied magnetic field is below ca. 2.0 T.

A further confirmation of this metamagnetic behavior is represented by the thermal variation of χ_m for different applied fields (Figure 9). As can be seen, χ_m shows a maximum at very low temperatures when the applied field in below ca. 2.0 T and the maximum disappears for fields above 2.0 T, in agreement with the isothermal magnetization measurements.

Magnetic Properties of Complex 2. The room-temperature value of $\chi_m T$ per formula unit (i.e., three Mn(III) ions and a Fe(II) ion) is ca. 9.0 cm^3 K mol^{-1} (Figure 10a). This value is close to the expected one for three $S = 2$ Mn(III) with $g = 2$ and indicates that the Fe(II) ion is a diamagnetic low spin Fe(II) ion (as expected for a Fe(II) coordinated to six strong-field CN ligands). When the temperature is reduced, $\chi_m T$ remains the same up to ca. 25 K, and below this temperature, it shows a progressive decrease to ca. 1.1 cm^3 K mol^{-1} at 2 K (see inset in Figure 10a). This behavior suggests the presence of a weak antiferromagnetic interaction in compound **2** and/or the presence of a zero field splitting in the Mn(III) ions. As observed in compound **1**, the thermal variation of χ_m shows a maximum at ca. 6 K (Figure 10b), suggesting that there is also a very weak antiferromagnetic coupling in compound **2**.

A detailed study of the structure of compound **2** indicates that the Mn(III) monomeric units are well-isolated but each Mn_2Fe trimer presents two short intertrimer $\pi\cdots\pi$ interactions and two hydrogen bonds with its two neighboring trimers to generate a regular chain of trimers (Figure 4). Nevertheless, since the Fe(II) ions are diamagnetic, the chains can be considered, from the magnetic point of view, as isolated Mn(III)−Mn(III) dimers. Note that since the two C_g-C_g distances and the hydrogen-bonding parameters are very similar in both chains (see Tables S5 and S6 in the Supporting

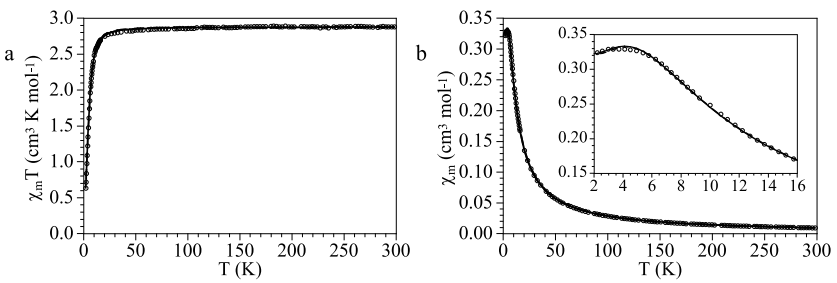

Figure 7. Thermal variation of (a) $\chi_m T$ and (b) χ_m for compound **1**. Solid and dotted lines represent the best fit to the models (see text).

https://dx.doi.org/10.1021/acs.inorgchem.0c00909
Inorg. Chem. XXXX, XXX, XXX−XXX

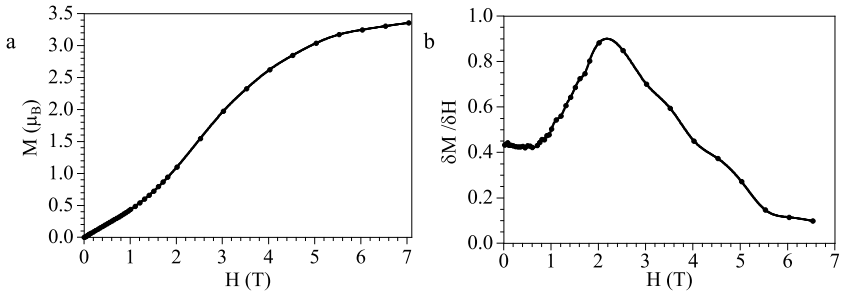

Figure 8. (a) Isothermal magnetization at 2 K for compound **1**. (b) Derivative of the magnetization, as a function of the magnetic field, showing a broad maximum at ca. 2.0 T.

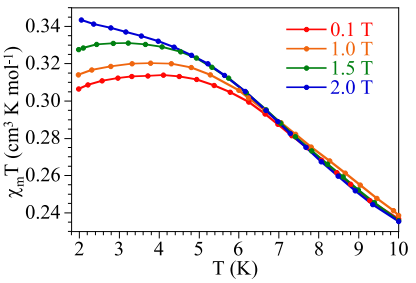

Figure 9. Thermal variation of χ_m for compound **1** in the low-temperature region with different applied fields.

Information), we can consider that the Mn(III)−Mn(III) coupling is the same in both chains.

Accordingly, we have fit the magnetic properties to a model of an isolated $S = 2$ ion with a ZFS plus a $S = 2$ dimer with a weak antiferromagnetic coupling (J) and a ZFS utilizing the program PHI.[43] In order to decrease the quantity of adjustable parameters, we have assumed that both Mn(III) dimers (Mn1−Mn1 and Mn2−Mn2) have the same coupling constant (J) and that all the Mn(III) ions have the same g- and D-values. This model reproduces very effectively the magnetic properties of compound **2** in the entire temperature range with $g = 2.009$, $|D| = 1.21$ cm^{-1}, and $J = -0.42$ cm^{-1}, with a residual of 0.1355 (solid lines in Figure 10; the exchange Hamiltonian is written as $H = -JS_1S_2$). As observed for compound **1**, the magnetic interaction between the Mn(III) centers is weak and antiferromagnetic, as expected for $\pi\cdots\pi$ interactions.[44−49] Again, the D value found is low and is within the typical range observed (−3.8 cm^{-1} to +3.1 cm^{-1}) for Mn(III) ions.[50]

An additional confirmation of the presence of an antiferromagnetic interaction in compound **2** is also given by the isothermal magnetization at 2 K (Figure 11a). This plot shows a sigmoidal shape with a maximum slope at ca. 2.5 T, as deduced from the maximum of the derivative (Figure 11b), suggesting that compound **2** also behaves as a metamagnet.

To confirm this metamagnetic behavior, we have also measured the magnetic susceptibility with different applied fields in the low-temperature region (see Figure 12). These measurements show the presence of a maximum in χ_m at low temperatures (∼6 K) that shifts to lower temperatures as the applied field increases and finally disappears for fields above 2.5 T, confirming that compound **2** is a metamagnet with a critical field of ca. 2.5 T.

CONCLUSIONS

In this work, we have presented a unique example of an inorganic reaction where a metal−ligand bond undergoes dissociation helped by the formation of intermolecular $\pi-\pi$ and hydrogen-bonding interactions. DFT calculations at the PBE1PBE-D3/def2-TZVP level confirm that the summation of the energies of all these intermolecular interactions surpasses the metal−ligand one. This fact has allowed us to prepare a trimeric molecular metamagnet from a monomeric metamagnetic precursor for the first time.

Thus, we present the formation of a novel Schiff-base ligand (H_2L) and the use of this ligand to prepare a Mn(III) monomer that exhibits very weak antiferromagnetic coupling through intermolecular $\pi-\pi$ and hydrogen-bonding interactions. This weak antiferromagnetic interaction can be cancelled out by the application of an external magnetic field, giving rise to a metamagnetic behavior with a critical field of ca. 2.0 T at 2 K. Combination of this Mn(III) monomer with $[Fe(CN)_6]^{4-}$ generates a Mn_2Fe trimer where the diamagnetic $[Fe(CN)_6]^{4-}$ complex acts as a linear connector between two monomeric Mn(III) complexes. These anionic trimers crystallize with a cationic Mn(III) monomer (closely related to the precursor monomer) in a 1:1 cocrystal to form compound **2**. The trimers are further assembled by $\pi-\pi$ and hydrogen-bonding

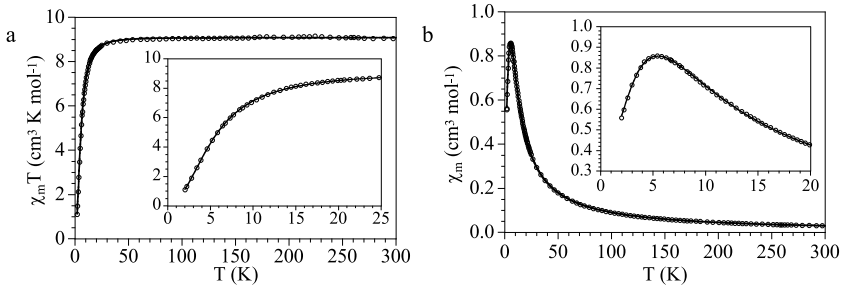

Figure 10. Thermal variation of (a) $\chi_m T$ and (b) χ_m for compound **2**. Insets show the low-temperature regions. Solid lines are the best fit to the model (see text).

https://dx.doi.org/10.1021/acs.inorgchem.0c00909
Inorg. Chem. XXXX, XXX, XXX−XXX

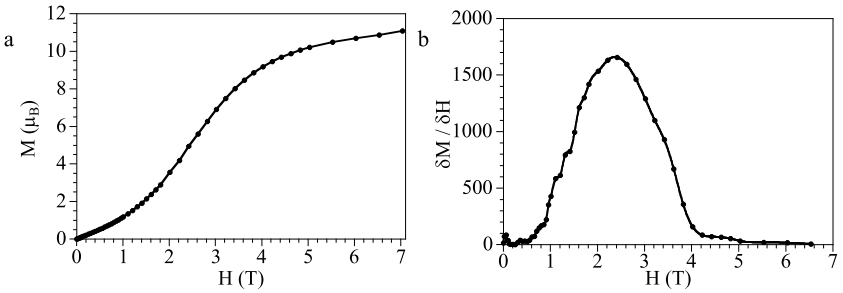

Figure 11. (a) Isothermal magnetization at 2 K for compound **2**. (b) Derivative of the magnetization *M*, as a function of *H*, showing a broad maximum at ca. 2.5 T.

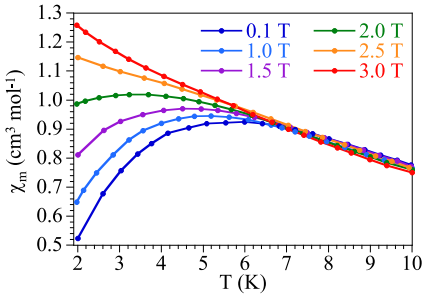

Figure 12. Thermal variation of χ_m for compound **2** in the low-temperature region with different applied fields.

interactions to build 1D supramolecular chains. Compound **2** also behaves as a metamagnet with a slightly higher critical field of ca. 2.5 T at 2 K. The magnetic behavior of both compounds has been reproduced with a simple model of a S = 2 monomer with a ZFS and a very weak intermolecular interaction (for **1**) and a S = 2 monomer with ZFS plus an antiferromagnetically coupled S = 2 dimer with a ZFS (for **2**). Finally, we hope that such study will help to analyze several biological processes, such as oxygen transport by hemoglobin and myoglobin, different metallo-enzymatic catalysis, etc.

■ ASSOCIATED CONTENT

Supporting Information

The Supporting Information is available free of charge at https://pubs.acs.org/doi/10.1021/acs.inorgchem.0c00909.

Figures showing the packing of compound, tables with bond distances, angles, and intermolecular interaction parameters for compounds **1** and **2** (PDF)

Accession Codes

CCDC 1994095 and 1991670 contain the crystallographic data of compounds **1** and **2**, respectively. This data can be obtained free of charge via http://www.ccdc.cam.ac.uk/conts/retrieving.html, or from the Cambridge Crystallographic Data Centre, 12 Union Road, Cambridge CB2 1EZ, UK; fax: (+44) 1223−336−033; or e-mail: deposit@ccdc.cam.ac.uk.

■ AUTHOR INFORMATION

Corresponding Authors

Rajat Saha − *Department of Physics, Jadavpur University, Kolkata 700032, India; Department of Chemistry, Kazi Nazrul University, Asansol 713340, WB, India;* orcid.org/0000-0003-1943-3650; Email: rajat.saha@knu.ac.in

Sanjay Kumar − *Department of Physics, Jadavpur University, Kolkata 700032, India;* orcid.org/0000-0002-0584-0901; Email: kumars@phys.jdvu.ac.in

Subrata K. Dey − *Department of Chemistry, Sidho-Kanho-Birsha University, Purulia 723104, WB, India;* Email: skdusask@yahoo.ca

Carlos J. Gómez García − *Departamento de Química Inorgánica, CMol. Universidad de Valencia, 46980 Paterna, Valencia, Spain;* orcid.org/0000-0002-0015-577X; Email: carlos.gomez@uv.es

Authors

Somen Goswami − *Department of Physics, Jadavpur University, Kolkata 700032, India*

Soumen Singha − *Department of Physics, Jadavpur University, Kolkata 700032, India*

Indrajit Saha − *Department of Chemistry, RKMRC, Narendrapur 700103, WB, India*

Abhishikta Chatterjee − *Department of Chemistry, Sidho-Kanho-Birsha University, Purulia 723104, WB, India*

Antonio Frontera − *Departament de Química, Universitat de les Illes Balears, 07122 Palma de Mallorca, Baleares, Spain;* orcid.org/0000-0001-7840-2139

Complete contact information is available at: https://pubs.acs.org/10.1021/acs.inorgchem.0c00909

Author Contributions

The manuscript was written through contribution of all authors. All authors have given approval to the final version of the manuscript.

Notes

The authors declare no competing financial interest.

■ ACKNOWLEDGMENTS

R. S. acknowledges SERB, Government of India for SERB-TARE project (File No: TAR/2018/000744). We thank the Spanish MINECO (ProjectNo. CTQ2017-87201-P AEI/FEDER, UE) and the Generalidad Valenciana (Prometeo/2019/076 project) for financial support.

■ REFERENCES

(1) Turro, N. J. Supramolecular organic photochemistry: Control of covalent bond formation through non-covalent supramolecular interactions and magnetic effects. *Proc. Natl. Acad. Sci. U. S. A.* **2002**, *99*, 4805−4809.

(2) Desiraju, G. R. Chemistry beyond the molecule. *Nature* **2001**, *412*, 397−400.

(3) Merlau, M. L.; del Pilar Mejia, M.; Nguyen, S. T.; Hupp, J. T. Artificial Enzymes Formed through Directed Assembly of Molecular Square Encapsulated Epoxidation Catalysts. *Angew. Chem., Int. Ed.* **2001**, *40*, 4239−4242.

https://dx.doi.org/10.1021/acs.inorgchem.0c00909
Inorg. Chem. XXXX, XXX, XXX−XXX

(4) Leung, D. H.; Fiedler, D.; Bergman, R. G.; Raymond, K. N. Selective C-H Bond Activation by A Supramolecular Host−Guest Assembly. *Angew. Chem., Int. Ed.* **2004**, *43*, 963−966.
(5) Jun, C.-H. Transition Metal-Catalyzed Carbon−Carbon Bond Activation. *Chem. Soc. Rev.* **2004**, *33*, 610−618.
(6) Annamalai, L.; Liu, Y.; Deshlahra, P. Selective C−H Bond Activation via NO_x-Mediated Generation of Strong H-Abstractors. *ACS Catal.* **2019**, *9*, 10324−10338.
(7) Della Ca', N.; Fontana, M.; Motti, E.; Catellani, M. Pd/Norbornene: A Winning Combination for Selective Aromatic Functionalization via C−H Bond Activation. *Acc. Chem. Res.* **2016**, *49*, 1389−1400.
(8) An, K.; Somorjai, G. A. Size and Shape Control of Metal Nanoparticles for Reaction Selectivity in Catalysis. *ChemCatChem* **2012**, *4*, 1512−1524.
(9) Lee, I.; Delbecq, F.; Morales, R.; Albiter, M. A.; Zaera, F. Tuning selectivity in catalysis by controlling particle shape. *Nat. Mater.* **2009**, *8*, 132−138.
(10) Pinter, B.; Van Speybroeck, V.; Waroquier, M.; Geerlings, P.; De Proft, F. Trans Effect and Trans Influence: Importance of Metal Mediated Ligand-Ligand Repulsion. *Phys. Chem. Chem. Phys.* **2013**, *15*, 17354−17365.
(11) Shaw, J. L.; Dockery, C. R.; Lewis, S. E.; Harris, L.; Bettis, R. The Trans Effect: A Guided-Inquiry Experiment for Upper-Division Inorganic Chemistry. *J. Chem. Educ.* **2009**, *86*, 1416−1418.
(12) Pearson, R. G. Hard and soft acids and bases, HSAB, part II, Underlying theories. *J. Chem. Educ.* **1968**, *45*, 643−648.
(13) Cárdenas, C.; Ayers, P. W. How Reliable is The Hard−Soft Acid−Base Principle? An Assessment from Numerical Simulations of Electron Transfer Energies. *Phys. Chem. Chem. Phys.* **2013**, *15*, 13959−13968.
(14) Yu, G.; Jie, K.; Huang, F. Supramolecular Amphiphiles Based on Host−Guest Molecular Recognition Motifs. *Chem. Rev.* **2015**, *115*, 7240−7303.
(15) Haino, T. Molecular-Recognition-Directed Formation of Supramolecular Polymers. *Polym. J.* **2013**, *45*, 363−383.
(16) Li, C. Pillararene-Based Supramolecular Polymers. From Molecular Recognition to Polymeric Aggregates. *Chem. Commun.* **2014**, *50*, 12420−12433.
(17) Roy, B.; Noguchi, T.; Tsuchiya, Y.; Yoshihara, D.; Yamamoto, T.; Shinkai, S. Molecular Recognition Directed Supramolecular Control Over Perylene-Bisimide Aggregation Resulting in Aggregation Induced Enhanced Emission (AIEE) and Induced Chiral Amplification. *J. Mater. Chem. C* **2015**, *3*, 2310−2318.
(18) Fiedler, D.; Leung, D. H.; Bergman, R. G.; Raymond, K. N. Selective Molecular Recognition, C-H Bond Activation, and Catalysis in Nanoscale Reaction Vessels. *Acc. Chem. Res.* **2005**, *38*, 349−358.
(19) Zhang, X.-M.; Wang, Y.-Q.; Wang, K.; Gao, E.-Q.; Liu, C.-M. Metamagnetism and Slow Magnetic Dynamics in An Antiferromagnet Composed of Cobalt(II) Chains with Mixed Azide−Carboxylate Bridges. *Chem. Commun.* **2011**, *47*, 1815−1817.
(20) Mukherjee, P. S.; Dalai, S.; Chaudhuri, N. R.; Zangrando, E.; Lloret, F. The First Metamagnetic One-Dimensional Molecular Material with Nickel(II) and End-to-End Azido Bridges. *Chem. Commun.* **2001**, 1444−1445.
(21) Zhou, Y. L.; Wu, M. C.; Zeng, M. H.; Liang, H. Magneto-Structural Correlation in A Metamagnetic Cobalt(II)-Based Pillared Trilayer Motif Constructed by Mixed Pyridyl-Type Carboxylate Ligands. *Inorg. Chem.* **2009**, *48*, 10146−10150.
(22) Boeckmann, J.; Wriedt, M.; Nather, C. Metamagnetism and Single-Chain Magnetic Behavior in a Homospin One-Dimensional Iron(II) Coordination Polymer. *Chem. - Eur. J.* **2012**, *18*, 5284−5289.
(23) Sun, W. W.; Tian, Y. C.; Jing, X. H.; Wang, Y. Q.; Gao, E. Q. Solvent-Modulated Metamagnetism in A Nickel(ii) Coordination Polymer with Mixed Azide and Carboxylate Bridges. *Chem. Commun.* **2009**, *31*, 4741−4743.
(24) Motokawa, N.; Matsunaga, S.; Takaishi, S.; Miyasaka, H.; Yamashita, M.; Dunbar, K. R. Reversible Magnetism Between an Antiferromagnet and A Ferromagnet Related to Solvation/Desolvation in A Robust Layered $[Ru_2]_2$TCNQ Charge-Transfer System. *J. Am. Chem. Soc.* **2010**, *132*, 11943−11951.
(25) Sandeman, K. G. Magnetocaloric Materials: The Search for New Systems. *Scr. Mater.* **2012**, *67*, 566−571.
(26) Annaorazov, M. P.; Asatryan, K. A.; Myalikgulyev, G.; Nikitin, S. A.; Tishin, A. M.; Tyurin, A. L. Alloys of The Fe-Rh System As a New Class of Working Material for Magnetic Refrigerators. *Cryogenics* **1992**, *32*, 867−872.
(27) Zeng, M.-H.; Zhang, W.-X.; Sun, X.-Z.; Chen, X.-M. Spin Canting and Metamagnetism in a 3D Homometallic Molecular Material Constructed by Interpenetration of Two Kinds of Cobalt(II) Coordination-Polymer Sheets. *Angew. Chem., Int. Ed.* **2005**, *44*, 3079−3082.
(28) Naiya, S.; Biswas, S.; Drew, M. G. B.; Gomez-García, C. J.; Ghosh, A. A Ferromagnetic Methoxido-Bridged Mn(III) Dimer and a Spin Canted Metamagnetic μ-1,3-Azido-Bridged Chain. *Inorg. Chem.* **2012**, *51*, 5332−5341.
(29) Miyasaka, H.; Clérac, R.; Mizushima, K.; Sugiura, K. I.; Yamashita, M.; Wernsdorfer, W.; Coulon, C. $[Mn_2(saltmen)_2Ni(pao)_2(L)_2](A)_2$ with L = Pyridine, 4-Picoline, 4-*tert*-Butylpyridine, *N*-Methylimidazole and A = ClO_4^-, BF_4^-, PF_6^-, ReO_4^-: A Family of Single-Chain Magnets. *Inorg. Chem.* **2003**, *42*, 8203−8213.
(30) Clérac, R.; Miyasaka, H.; Yamashita, M.; Coulon, C. Evidence for Single-Chain Magnet Behavior in a Mn^{III}−Ni^{II} Chain Designed with High Spin Magnetic Units: A Route to High Temperature Metastable Magnets. *J. Am. Chem. Soc.* **2002**, *124*, 12837−12844.
(31) Miyasaka, H.; Clerac, R.; Wernsdorfer, W.; Lecren, L.; Bonhomme, C.; Sugiura, K.; Yamashita, M. A Dimeric Manganese (III) Tetradentate Schiff Base Complex As a Single-Molecule Magnet. *Angew. Chem., Int. Ed.* **2004**, *43*, 2801−2805.
(32) Lü, Z.; Yuan, M.; Pan, F.; Gao, S.; Zhang, D.; Zhu, D. Syntheses, Crystal Structures, and Magnetic Characterization of Five New Dimeric Manganese(III) Tetradentate Schiff Base Complexes Exhibiting Single-Molecule-Magnet Behavior. *Inorg. Chem.* **2006**, *45*, 3538−3548.
(33) Tandon, S. S.; Thompson, L. K.; Manuel, M. E.; Bridson, J. N. Magnetostructural Correlations in.mu.2−1,1-N_3 Bridged, Dinuclear Copper(II) Complexes. 1. Ferromagnetic and Antiferromagnetic Coupling Associated with the Azide Bridge. *Inorg. Chem.* **1994**, *33*, 5555−5570.
(34) Naiya, S.; Drew, M. G. B.; Diaz, C.; Ribas, J.; Ghosh, A. Synthesis, Crystal Structure, and Magnetic Properties of a Very Rare Double μ-1,1-Azido- and a μ-1,1-(OMe)-Bridged Fe^{III} Dimer Containing a N,N,O-Donor Tridentate Schiff Base Ligand. *Eur. J. Inorg. Chem.* **2011**, *2011*, 4993−4999.
(35) Wang, T.-T.; Bao, S.-S.; Huang, J.; Li, Y.-Z.; Zheng, L.-M. Chiral One-Dimensional O−P−O Bridged $MnII^{I-S}$chiff Base Complexes. *Dalton Trans.* **2013**, *42*, 1842−1847.
(36) Yuan, M.; Gao, S.; Sun, H.-L.; Su, G. An Antiferromagnetic Mn(III) Chain Bridged by Hydrogencyanamide: $[MnIII^{(5\text{-}}$Brsalen)$(\mu 1,3_{\text{-NC}}NH)]n$. *Inorg. Chem.* **2004**, *43*, 8221−8223.
(37) Bain, G. A.; Berry, J. F. Diamagnetic corrections and Pascal's constants. *J. Chem. Educ.* **2008**, *85*, 532−536.
(38) Frisch, M. J.; Trucks, G. W.; Schlegel, H. B.; Scuseria, G. E.; Robb, M. A.; Cheeseman, J. R.; Scalmani, G.; Barone, V.; Petersson, G. A.; Nakatsuji, H.; Li, X.; Caricato, M.; Marenich, A. V.; Bloino, J.; Janesko, B. G.; Gomperts, R.; Mennucci, B.; Hratchian, H. P.; Ortiz, J. V.; Izmaylov, A. F.; Sonnenberg, J. L.; Williams-Young, D.; Ding, F.; Lipparini, F.; Egidi, F.; Goings, J.; Peng, B.; Petrone, A.; Henderson, T.; Ranasinghe, D.; Zakrzewski, V. G.; Gao, J.; Rega, N.; Zheng, G.; Liang, W.; Hada, M.; Ehara, M.; Toyota, K.; Fukuda, R.; Hasegawa, J.; Ishida, M.; Nakajima, T.; Honda, Y.; Kitao, O.; Nakai, H.; Vreven, T.; Throssell, K.; Montgomery, J. A., Jr.; Peralta, J. E.; Ogliaro, F.; Bearpark, M. J.; Heyd, J. J.; Brothers, E. N.; Kudin, K. N.; Staroverov, V. N.; Keith, T. A.; Kobayashi, R.; Normand, J.; Raghavachari, K.; Rendell, A. P.; Burant, J. C.; Iyengar, S. S.; Tomasi, J.; Cossi, M.; Millam, J. M.; Klene, M.; Adamo, C.; Cammi, R.; Ochterski, J. W.; Martin, R. L.; Morokuma, K.; Farkas, O.; Foresman, J. B.; Fox, D. J. *Gaussian 16, Revision A.01*; Gaussian, Inc.: Wallingford, CT, 2016.

https://dx.doi.org/10.1021/acs.inorgchem.0c00909
Inorg. Chem. XXXX, XXX, XXX−XXX

(39) Bader, R. F. W. A Bond Path: A Universal Indicator of Bonded Interactions. *J. Phys. Chem. A* **1998**, *102*, 7314−7323.
(40) Keith, T. A. *AIMAll (Version 13.05.06)*; TK Gristmill Software: Overland Park, KS, 2013.
(41) Sheldrick, G. M. *SHELXS 97, Program for Structure Solution*; University of Göttingen, Göttingen, Germany, 1997.
(42) Sheldrick, G. M. *SHELXL 97, Program for Crystal Structure Refinement*; University of Göttingen, Göttingen, Germany, 1997.
(43) Spek, A. L. Single-crystal structure validation with the program PLATON. *J. Appl. Crystallogr.* **2003**, *36*, 7−13.
(44) Farrugia, L. J. ORTEP-3 for Windows - a version of ORTEP-III with a Graphical User Interface (GUI). *J. Appl. Crystallogr.* **1997**, *30*, 565.
(45) Farrugia, L. J. WinGX suite for small-molecule single-crystal crystallography. *J. Appl. Crystallogr.* **1999**, *32*, 837−838.
(46) Białek, M. J.; Zaręba, J. K.; Janczak, J.; Zoń, J. Chains, Layers, Channels, and More: Supramolecular Chemistry of Potent Diphosphonic Tectons with Tuned Flexibility. The Generation of Pseudopolymorphs, Polymorphs, and Adducts. *Cryst. Growth Des.* **2013**, *13*, 4039−4050.
(47) Mahmoudi, G.; Zaręba, J. K.; Gurbanov, A. V.; Bauzá, A.; Zubkov, F. I.; Kubicki, M.; Stilinović, V.; Kinzhybalo, V.; Frontera, A. Benzyl Dihydrazone versus Thiosemicarbazone Schiff Base: Effects on the Supramolecular Arrangement of Cobalt Thiocyanate Complexes and the Generation of CoN_6 and CoN_4S_2 Coordination Spheres. *Eur. J. Inorg. Chem.* **2017**, *2017*, 4763−4772.
(48) García-Raso, A.; Terrón, A.; López-Zafra, A.; García-Viada, A.; Barta, A.; Frontera, A.; Lorenzo, J.; Rodríguez-Calado, S.; Vázquez-López, E. M.; Fiol, J. J. Crystal Structures of N6-Modified-Amino Acid Related Nucleobase Analogs (II): Hybrid Adenine-*β*-Alanine and Adenine-GABA Molecules. *New J. Chem.* **2019**, *43*, 9680−9688.
(49) Espinosa, E.; Molins, E.; Lecomte, C. Hydrogen Bond Strengths Revealed by Topological Analyses of Experimentally Observed Electron Densities. *Chem. Phys. Lett.* **1998**, *285*, 170−173.
(50) Vener, M. V.; Egorova, A. N.; Churakov, A. V.; Tsirelson, V. G. Intermolecular Hydrogen Bond Energies in Crystals Evaluated Using Electron Density Properties: DFT Computations with Periodic Boundary Conditions. *J. Comput. Chem.* **2012**, *33*, 2303−2309.
(51) Chilton, N. F.; Anderson, R. P.; Turner, L. D.; Soncini, A.; Murray, K. S. PHI. A Powerful New Program for The Analysis of Anisotropic Monomeric and Exchange-Coupled Polynuclear d- and f -block Complexes. *J. Comput. Chem.* **2013**, *34*, 1164−1175.
(52) Wojciechowska, A.; Janczak, J.; Zierkiewicz, W.; Rytlewski, P.; Rojek, T.; Duczmal, M. Copper(II) Complex with L-Arginine - Crystal Sructure, DFT Calculations, Spectroscopic, Thermal and Magnetic Properties. *Mater. Chem. Phys.* **2019**, *228*, 272−284.
(53) Chi, Y.; Shi, J.; Li, H.; Wei, W.; Cottrill, E.; Pan, N.; Chen, H.; Liang, Y.; Yu, L.; Zhang, Y.; Hou, C. pi-pi Stacking, Spin Density and Magnetic Coupling Strength. *Dalton Trans* **2013**, *42*, 15559−15569.
(54) Li, H.; Zhang, S.; Xie, L.; Yu, L.; Shi, J. pi-pi Stacking, Hydrogen Bonding and Anti-Ferromagnetic Coupling Mechanism on A Mononuclear Cu(II) Complex. *J. Coord. Chem.* **2011**, *64*, 1456−1468.
(55) Chi, Y.; Wei, W.; Shi, J.; Zhang, Y.; Liu, S. Intermolecular Interaction and Magnetic Coupling Mechanism Between Adjacent Mononuclear Ni(II) Complexes. *J. Coord. Chem.* **2012**, *65*, 2379−2390.
(56) Sutradhar, M.; Carrella, L. M.; Rentschler, E. Mononuclear Mn(III) and Dinuclear Mn(III,III) Schiff Base Complexes: Influence of *π*−*π* Stacking on Magnetic Properties. *Polyhedron* **2012**, *38*, 297−303.
(57) Chi, Y.; Yu, L.; Shi, J.; Zhang, Y.; Hu, T.; Zhang, G.; Shi, W.; Cheng, P. pi-pi Stacking and Ferromagnetic Coupling Mechanism on A Binuclear Cu(II) Complex. *Dalton Trans* **2011**, *40*, 1453−1462.
(58) Boca, R. Zero-Field Splitting in Metal Complexes. *Coord. Chem. Rev.* **2004**, *248*, 757−815.

https://dx.doi.org/10.1021/acs.inorgchem.0c00909
Inorg. Chem. XXXX, XXX, XXX−XXX

Inorganica Chimica Acta 550 (2023) 121370

Contents lists available at ScienceDirect

Inorganica Chimica Acta

journal homepage: www.elsevier.com/locate/ica

Double dicyanamide decorated double phenoxide bridged Mn^{III} dimer with single-molecule magnetic behaviour and bio-catalytic activity

Somen Goswami [a], Soumen Singha [a], Bhaskar Khanra [a], Priyanka Chakraborty [b], Rajat Saha [c], Samia Benmansour [c], Subrata Kumar Dey [b,*], Carlos J. Gómez García [c,*], Sanjay Kumar [a,*]

[a] Department of Physics, Jadavpur University, Jadavpur, Kolkata 700032, India
[b] Department of Chemistry, Sidho-Kanho-Birsha University, Purulia 723101, WB, India
[c] Departamento de Química Inorgánica. Universidad de Valencia, C/ Dr. Moliner, 50. 46100 Burjasot (Valencia), Spain

ARTICLE INFO

Keywords:
Dimeric Mn^{III} complex
Terminal dca^- ligand
Double phenoxido bridge
Single-molecule magnet
Catechol-oxidase activity

ABSTRACT

Herein, we report the magnetic properties and bio-catalytic activity of a flying bee-like double phenoxido bridged dinuclear Mn^{III}-Schiff base complex decorated with double dicyanamide (dca^-) ligands and formulated as: $[Mn_2(L)_2(dca)_2]$ (**1**) (where H_2L = 2,2′-((1E,1′E)-(ethane-1,2-diylbis(azanylylidene))-bis(ethan-1-yl-ylidene)) diphenol). The complex has been synthesised by one-pot stepwise reaction of the tetradentate Schiff's base ligand H_2L with $MnCl_2$ and dca^- at 1:1:2 ratio under aerobic conditions. It has been characterized by single crystal X-ray diffraction (SC-XRD) and spectroscopic techniques. Complex **1** contains two Mn^{III} ions connected by a double phenoxido bridge in an octahedral geometry and terminal dca^- ligands. The dimers are connected to other dimers through both hydrogen bonding and π-interactions to form an extended supramolecular network. The present study reveals that in presence of tetradentate Schiff base ligands, the use of a 1:2 Mn:dca^- ratio leads to formation of a dimeric Mn^{III} complex in contrast to the discrete mononuclear complexes or 1D structures previously obtained for the Mn:dca^- ratio of 1:1. The magnetic study indicates that the dimeric Mn^{III} complex shows a negligible Mn^{III}–Mn^{III} interaction and a large anisotropy. The AC susceptibility measurements indicate that complex **1** behaves as a field-induced single-molecule magnet (SMM), with a high energy barrier of 73(4) K. The study of model catechol oxidase-like enzyme activity of complex **1** indicates that the dimeric Mn^{III} complex acts as an active catalyst (k_{cat} = 34.94 h^{-1}) in the oxidation of 3,5-di-*tert*-butylcatechol (3,5-DTBC) in presence of aerial O_2 in acetonitrile medium.

1. Introduction

Among the transition metal ions, multinuclear manganese complexes have gained remarkable attention due to their potential applications in molecular magnetism [1–4] as well as their rich biochemistry [5–7] and versatile catalytic activities [8–10]. Large variety of ligands containing oxygen or nitrogen donor atoms like Schiff's bases, oxalato, carboxylato, azido, phenoxido/oxido, sulfato, dicyanamido, etc. are widely used to design and synthesize Mn-based complexes of different nuclearities and dimensionalities [11–17]. Moreover, high spin Mn^{III}-Schiff base complexes are extensively used as the basic building blocks for designing metal clusters due to their unique properties [18–21].

Due to its versatile coordination and bridging modes, quasi π-conjugated dicyanamide (dca^-) is one of the most widely employed bridging ligand in designing multinuclear and multidimensional metal complexes (Scheme S1). The nuclearity and architecture of dicyanamido bridged metal complexes exclusively depend upon the binding and bridging modes adopted by the dca^- ligand and metal:dca^- ratios [22–25]. From the literature survey, it is evident that, in presence of tetradentate Schiff base ligands, the use of dca^- at 1:1 Mn:dca^- ratio results in either different types of $\mu_{1,5}$–dca^- bridged 1D coordination polymers [26–29] or in discrete Mn^{III} complexes having terminal dca^- ligands [30]. In the present report, we have successfully synthesized a dimeric Mn^{III} complex $[Mn_2(L)_2(dca)_2]$ (**1**), having double terminal dca^- ligands, by using Mn and dca^- in 1:2 ratio for the first time.

Double phenoxido bridged Mn^{III}-Schiff base dimeric complexes show both ferro- or antiferromagnetic couplings with large uniaxial anisotropy that may lead to single-molecule magnet behaviour (with and without an applied DC field) [31–37]. Miyasaka et al. have performed a detailed investigation in order to find the origin of the magnetic

* Corresponding authors.
E-mail addresses: sanjay.kumar@jadavpuruniversity.in, kumar_dsa@yahoo.com (S. Kumar).

https://doi.org/10.1016/j.ica.2022.121370
Received 24 July 2022; Received in revised form 3 December 2022; Accepted 29 December 2022
Available online 30 December 2022

properties of such dimers [38]. They have shown that the magnetic coupling depends on the Mn-O (bridging) bond distance. In most cases, when the Mn-O bond distance is within the range 2.40–2.70 Å, the dimers show ferromagnetic interactions, whereas below this range they show antiferromagnetic couplings and above 2.80 Å the magnetic interaction is almost negligible.

Catechol-oxidase is an important plant enzyme that catalyses the oxidation of a range of *o*-diphenols (catechols) and produces corresponding quinones having significant role in disease resistance of higher plants [39]. Manganese ions are omnipresent in a large variety of naturally occurring redox enzymes because of their lower redox potentials [40–42]. In photosystem-II of plants and cyanobacteria a tetramanganese cluster acts as an active site in catalytic oxidation of water to O_2 [43]. Therefore, Mn-based complexes are widely used to mimic the catechol-oxidase activity in presence of model substrates in order to examine the mechanism and factors of the enzyme catalysed oxidation of catechols [44–47].

In this context, herein we report synthesis, crystal structure, spectral behaviour, magnetic properties and catalytic response of a dinuclear Mn^{III}-complex with a Schiff's base and dca^- ligands in 1:2 Mn:dca^- ratio. The dimeric Mn^{III} complex, with structural formula $[Mn_2(L)_2(dca)_2]$ (**1**) (H_2L = 2,2′-((1E,1′E) -(ethane-1,2-diylbis(azanylylidene))-bis(ethan-1-ylylidene)) diphenol) shows a rare assembly of double phenoxido bridges along with double terminal dca^- ligands. The magnetic properties of the complex reveal very weak antiferromagnetic interactions in it and, more interestingly, a field-induced single-molecule magnet behaviour thanks to the large magnetic anisotropy of the Mn^{III} ions. Complex **1** also exhibits solvent selective enzyme catechol oxidase-like activity for the oxidation of the model substrate 3,5-di-*tert*-butylcatechol (3,5-DTBC) in presence of aerial oxygen.

2. Experimental

2.1. Materials and methods

$MnCl_2{\cdot}4H_2O$ (99.9 %), 2-hydroxyacetophenone (98 %), sodium dicyanamide (96 %) and ethylenediamine (99.5 %) were obtained from Sigma Aldrich and used as received. Triethylamine and all other chemicals (AR grade) were obtained from Merck India and used as received. Elemental analysis (C, H, N) was performed by using a Perkin-Elmer 240C elemental analyser. A Nicolet Impact 410 spectrometer was used to record the FT-IR spectrum in the 400–4000 cm^{-1} range. Electronic absorption spectra were recorded in 10^{-4} M acetonitrile solutions using a Hitachi U-3501 spectrophotometer.

The cyclic voltametric measurement on complex **1** was carried out using Autolab/PGSTAT204 electrochemical workstation (Model Number: AUT204.S: 204 Potentiostat Galvanostat Module FRA32M. MAC204.S) at a scan rate of 50 mVs^{-1} within the potential range + 1.50 to −1.50 V on a 10^{-3} M solution of the complex in deoxygenated acetonitrile (by bubbling nitrogen gas). A 0.1 M tetrabutylammonium bromate (TBAB) solution was used as supporting electrolyte. The working electrode was a glassy-carbon disk (0.32 cm^2) which was washed with absolute acetone and dichloromethane, polished with alumina solution and air-dried before each electrochemical run. The Ag/AgCl and platinum wire were used as reference and counter electrode, respectively. The experiments were performed in standard electrochemical cells at 25 °C.

2.2. Synthesis of $[Mn_2(L)_2(dca)_2]$ (1)

The Schiff base ligand H_2L has been synthesised by following a standard procedure [48], detailed in the ESI file. The Schiff base ligand H_2L (297 mg, 1.0 mmol) was dissolved in 25 mL of a 1:1 methanol–acetonitrile mixture under boiling. The pH of the reaction mixture was adjusted to 9 by dropwise addition of Et_3N. $MnCl_2{\cdot}4H_2O$ (250 mg, 1.25 mmol) was dissolved in 5 mL of methanol by stirring and then added to the previous solution. The resulting solution was refluxed ~ 90 °C for 2 h. The reaction mixture was cooled to room temperature and sodium dicyanamide (224 mg, 2.5 mmol), dissolved in 2 mL of distilled water, was added to the previous reaction mixture and stirred for another 1.5 h. The resulting light brown precipitate was filtered off and the deep brown filtrate was kept undisturbed for crystallisation at room temperature. Brown block-shaped single crystals suitable for single crystal X-ray diffraction were obtained after two weeks. The crystals were filtered and air-dried. Yield: 1.323 g (74 %). Anal. Calc. (%) for $C_{40}H_{36}Mn_2N_{10}O_4$ (M = 830.67 g/mol): C, 57.78; H, 4.33 and N, 16.85 %. Found: C, 57.8; H, 4.3 and N, 16.9 %. Phase purity was confirmed by the X-ray powder diffractogram that shows a good agreement with the simulated one from the single crystal X-ray structure (Fig. S1, ESI file).

Table 1
Crystallographic data and refinement parameters of complex **1**.

Compound	**1**
CCDC	2,191,124
Formula	$C_{40}H_{36}Mn_2N_{10}O_4$
Formula weight	830.67
Crystal system	Triclinic
Space group	*P*-1 (#2)
a (Å)	8.6221(15)
b (Å)	10.8616(19)
c (Å)	11.741(2)
α (°)	64.798(5)
β (°)	73.308(6)
γ (°)	88.199(6)
V(Å^3)	947.7(3)
Z	1
ρ_{calc} (g/cm^3)	1.455
μ (Mo Kα) (mm)	0.723
F(0 0 0)	428
Crystal size (mm^3)	0.20 × 0.16 × 0.12
T (K)	293
$\theta_{min-max}$ (°)	2.0–27.2
Total data	27,641
Unique Data	4178
R_{int}	0.0667
Observed data [I > 2σ(I)]	3004
N_{par}	265
R	0.0790
wR_2^a	0.2167
G.O.F	1.052
Largest Peak/hole [e/Å^3]	0.710/-0.989

2.3. Magnetic measurements

Variable temperature magnetic susceptibility measurements were carried out in the temperature range 2–300 K with an applied magnetic field of 0.1 T (1000 Oe) on a polycrystalline sample with a mass of 13.598 mg using a Quantum Design MPMS-XL-7 SQUID magnetometer. The AC susceptibility measurements were performed on the same sample at 2.0 K with different applied dc fields (in the range 0–4300 Oe) with a field of 8 Oe oscillating in the range 10–10000 Hz using a Quantum Design PPMS-9 equipment. From the plot of the relaxation time *vs* the dc field (Fig. S6, ESI file), we determined an optimum dc field of 0.2 T (2000 Oe). Accordingly, we performed the frequency sweep from 10 to 10000 Hz at different temperatures in the range 2–4 K with an applied dc field of 0.2 T. The susceptibility data were corrected for the sample holder previously measured using the same conditions and for the diamagnetic contribution of the sample as deduced by using Pascaĺs constant tables [49].

2.4. Crystallographic data collection and refinement

Bruker SMART diffractometer equipped with a graphite monochromator and Mo-K_α (λ = 0.71073 Å) radiation were employed to collect the single crystal X-ray crystallographic data of compound **1**.

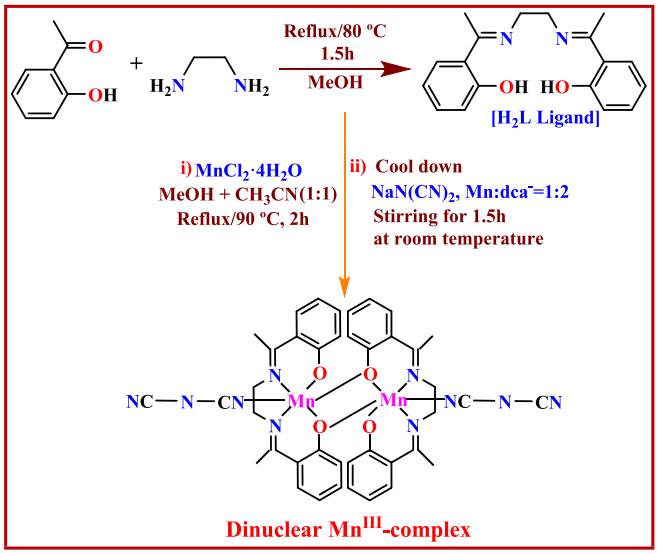

Scheme 1. Synthesis of the H_2L ligand and of the dimeric Mn^{III} complex **1**.

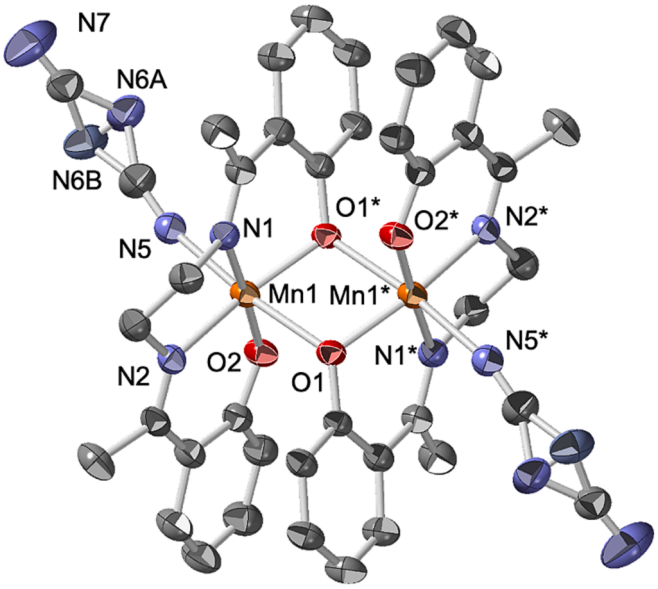

Fig. 1. View of the structure of **1** with the labelling scheme around the Mn^{III} centres. H atoms have been omitted for clarity. Ellipsoids are drawn at 30 % probability. * = 1 − x, 1 − y, 1 − z.

Unit cell parameters were determined by using the APEX2 [50] program. The SAINT [50] program was used for data reduction and correction or absorption was made using the SADABS [50] program. The structure was solved by Patterson method using the SHELXL-2014 [51] program embedded in WINGX software package [52]. Subsequent difference Fourier synthesis and least-square refinement revealed the positions of the non hydrogen atoms. Non-hydrogen atoms were refined with independent anisotropic displacement parameters. Hydrogen atoms were put in idealized positions and their displacement parameters were fixed to be 1.2 times larger than those of the attached non-hydrogen atoms. These results have been embedded in the CIF file. All Figures were drawn by using PLATON, ORTEP and Crystal Maker software [53,54]. Data collection and structure refinement parameters and crystallographic data for complex are given in Table 1.

3. Result and discussion

3.1. Synthesis

The N_2O_2-donor based tetradentate Schiff base ligand (H_2L) has been synthesized by the condensation under reflux of a mixture of 2-hydroxyacetophenone and ethylenediamine in a 2:1 ratio in methanol (Scheme 1). The synthesis of the dimeric Mn^{III} complex has been performed in a simple one-pot reaction by refluxing the ligand (H_2L) with $MnCl_2{\cdot}4H_2O$ at pH = 9 in a 1:1 mixture of methanol–acetonitrile, followed by the addition of an aqueous solution of sodium dicyanamide at room temperature (Scheme 1). It is noteworthy that this reaction is performed in open air at pH = 9, as a result the Mn^{II} ions are easily oxidized to Mn^{III} by atmospheric O_2 during the initial reaction with H_2L.

3.2. Molecular and supramolecular structure of complex *1*

The single crystal X-ray diffraction analysis reveals that complex **1** crystallizes in the triclinic *P*-1 space group and is a centrosymmetric dimeric neutral metal complex. The asymmetric unit contains one Mn^{III} ion, one L^{2-} ligand and one dca^- ligand (Fig. 1). Two such neighbouring asymmetric units are connected by double phenoxido bridges through O1 atoms to form the centrosymmetric dimer $[Mn_2(L)_2(dca)_2]$ (Fig. 1). The Mn ions present an elongated octahedral geometry with the four equatorial positions occupied by two imine N donor atoms (N1 and N2) of the Schiff base ligand and two oxygen atoms (O1 and O2) of the deprotonated hydroxide groups of the ligand. One of the axial coordination sites is occupied by a nitrogen atom (N5) of the dicyanamide ligand whereas the other is occupied by the O1 atom of the neighboring Mn-Schiff base moiety. The two equatorial Mn-O bonds (Mn1-O2 = 1.853(3) Å and Mn1–O1 = 1.914(3) Å) are shorter in length than the Mn–N ones (Mn1-N1 = 1.989(4) Å and Mn1-N2 = 2.002(4) Å). All these equatorial bond distances are shorter than the axial ones: Mn1-O1* = 2.388(3) Å and Mn1-N5 = 2.199(5) Å, as expected for a Mn^{III} ion with Jahn-Teller distortion. All the *cisoid* and *transoid* angles are in the range of 78.88(12) − 96.53(15)° and 166.02(15) − 176.41(13)°, respectively. All the bond lengths and angles around the Mn center are listed in Table S1 and are similar to those found in other similar Mn^{III} dimers with phenoxido bridges and Schiff base ligands [55–57].

The doubly deprotonated Schiff base ligand, L^{2-} acts as a tetradentate N_2O_2 chelating ligand that occupies the four equatorial positions of the Mn^{III} ion. Additionally, the O1 atom also connects to the neighboring Mn^{III} ion, generating the Mn_2O_2 central unit with a double phenoxido bridge. The dicyanamide anions act as monodentate terminal ligands and extend on both sides of the dimer (Fig. 1).

The dimer is further stabilized by two intradimer π···π interactions between the two Schiff base ligands (Fig. S2, ESI file). The dimers are connected by C—H···N hydrogen bonds involving the two non-coordinated N atoms of the dca^- ligands, to form a 2D supramolecular lattice plane parallel to the [−122] plane (Fig. 2). Additionally, there are interdimer C—H···π interactions that generate chains along the *b* axis (Fig. S3, ESI file). All the structural parameters of the hydrogen bonds and π-interactions are summarized in Tables S2–S3 (ESI file). Interestingly, complex **1** can be considered as a fragment of a Mn^{III} chain reported by Ghosh et al., formulated as $[Mn_2(L)_2(dca)]ClO_4{\cdot}CH_3CN$ (**2**, CCDC code = OHASIB) where double phenoxido bridged Mn^{III} dimers are connected by $\mu_{1,5}$-dca^- bridges (Fig. S4, ESI file) [29].

3.3. Electronic absorption spectra

The electronic absorption spectrum of complex **1** has been recorded in acetonitrile (Fig. S5, ESI file). The spectrum shows a very low intensity single absorption band at 670 nm (inset in Fig. S5, ESI file) that can be attributed to a d-d transition in the complex which is consistent with a distorted octahedral geometry around the Mn^{III} ion. The LMCT (PhO → Mn^{III}) band is observed at 454 nm ($\varepsilon = 2515\ M^{-1}\ cm^{-1}$). There

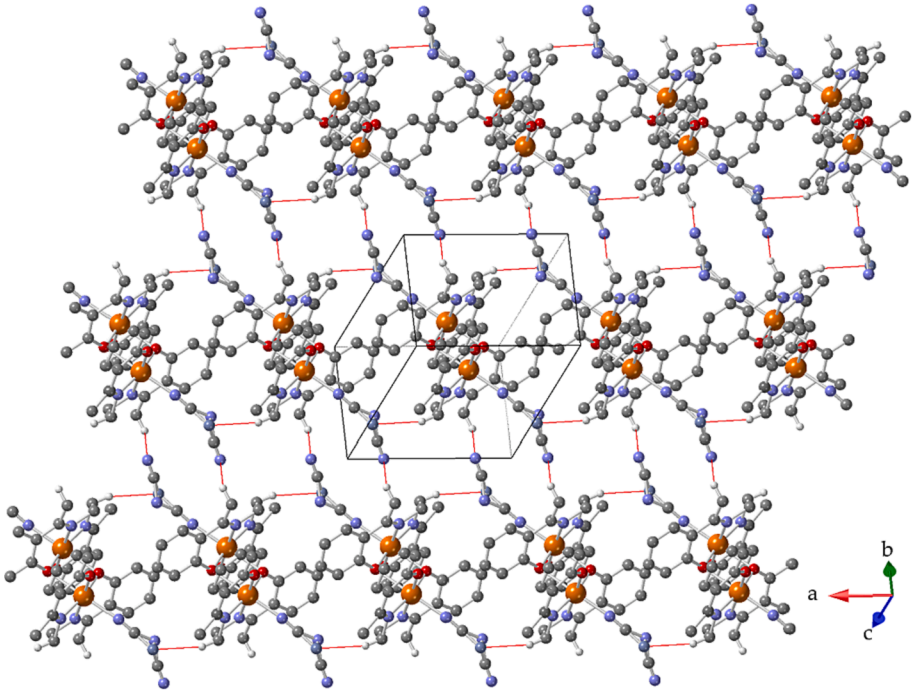

Fig. 2. 2D supramolecular lattice formed by C—H···N hydrogen bonding interactions in **1** (shown as red thin lines). H atoms (except H9B and H37C) have been omitted for clarity. (For interpretation of the references to colour in this figure legend, the reader is referred to the web version of this article.)

are also two bands in the UV region at 240 nm ($\varepsilon = 21667\ M^{-1}\ cm^{-1}$) and 285 nm ($\varepsilon = 10205\ M^{-1}\ cm^{-1}$) that appear due to intra ligand π-π* and n-π* transitions.

In the FT-IR spectrum of complex **1** (Fig. S6, ESI file), three sharp peaks at 2273, 2152 and 2216 cm^{-1} are observed due to the asymmetric, symmetric and symmetric + asymmetric stretching of the C≡N bonds of the dicyanamide ligands, respectively. The band at $\nu = 1587\ cm^{-1}$ is attributed to the C=N stretching of the immine bond of the Schiff's base ligand. A sharp peak at 1297 cm^{-1} can be attributed to the $C–O_{phenolic}$ stretching. The ν(Mn-O) and ν(Mn-N) vibrations are located at 601 and 451 cm^{-1}, respectively.

3.4. Cyclic voltametric study

The study of the electrochemical properties of a metal complex is important to assess its capability to mimic the functionality of metalloenzymes. The electrochemical behavior of the complex has been investigated by using cyclic voltammetry in acetontrile solution at a scan rate of 50 mV s^{-1} with respect to an Ag/AgCl electrode using tetrabutylammonium bromate as supporting electrolyte. The cyclic voltammogram (CV) of the complex is irreversible and displays two redox processes with E_c^1 = -0.32 V, E_a^1 = 0.19 V, ΔE_{pc} = 0.51 V, $E^{1/2}$ = -65 mV and E_c^2 = -1.03 V, E_a^2 = -0.56 V, ΔE_{pc} = 0.47 V, $E^{1/2}$ = -0.795 V as can be seen in Fig. 3. These peaks can be assigned to the Mn^{III}/Mn^{IV} and Mn^{II}/Mn^{III} redox couple, respectively. We may, therefore, infer that the complex can act as an active catalyst in the oxidation catechol substrate like catechol oxidase enzyme.

3.5. Magnetic properties

The thermal variation of the product of the molar magnetic susceptibility times the temperature (χ_mT) for compound **1** shows a room temperature value of χ_mT *ca.* 6.0 $cm^3\ K\ mol^{-1}$, which is the expected value for two independent Mn^{III} ions with a ground spin state S = 2 and a g value close to 2. When the sample is cooled, χ_mT remains constant down to *ca.* 20 K and exhibits a sharp decrease at lower temperatures to reach a value of *ca.* 3.0 $cm^3\ K\ mol^{-1}$ at 2 K (Fig. 4). This behaviour suggests the presence of an overall weak antiferromagnetic interaction in the metal complex and/or a zero-field splitting (ZFS) of the S = 2 ground spin state. Since the compound contains a symmetric dimeric Mn^{III} complex with a double phenoxido bridge, we have fit the magnetic data of the compound using three different models: (i) a Mn^{III} dimer with ZFS in the Mn^{III} ions, (ii) two independent Mn^{III} monomers with a ZFS and (iii) a Mn^{III} dimer with no ZFS. For the two first models we have tried with either positive and negative initial values of the ZFS. Using these three models with the program PHI [58] we obtain reasonable fits in the whole temperature range with the five different possibilities: (i) dimer + ZFS (D > 0), (ii) dimer + ZFS (D < 0), (iii) dimer with no ZFS, (iv) two monomers + ZFS (D > 0) and (v) two monomers + ZFS (D < 0) (Fig. S7, ESI file) with the parameters as displayed in Table S4 (ESI file). Nevertheless, in the low temperature region, the best fit is obtained with the second possibility (a Mn^{III} dimer with a negative value of D, solid line in Fig. 4 and orange line in Fig. S7, ESI file) with the following parameters: g = 1.9946(5), J = -0.065(1) cm^{-1} and D = −1.80(2) cm^{-1} (the Hamiltonian is written as $H = -JS_1S_2$). These values indicate that the magnetic coupling through the double phenoxido bridge is almost negligible. As expected, the inclusion of a ZFS to the dimer model reduces the antiferromagnetic coupling along the double phenoxido bridge. The obtained D value is very close to those observed in other high spin Mn^{III} complexes [59].

The very weak antiferromagnetic coupling through the double phenoxido bridge is the expected one since the O atoms connect an axial position of one Mn^{III} ion with an equatorial position of the other Mn^{III} ion. This connectivity precludes the overlap of the magnetic orbitals and, therefore, reduces the magnetic coupling. Moreover, a complete experimental and theoretical study performed by Ghosh *et al.* on Mn^{III} dimers with a double phenoxido bridge, shows that the coupling in all cases is very weak although it may be ferro or antiferromagnetic [29].

In case of Mn^{III} dimers, the Jahn-Teller distortion originates a short and a long Mn-O bond distances (in complex **1** these distances are 1.914 (3) and 2.388(3) Å). It is well established that the main structural parameter determining the magnetic coupling is the long Mn-O bond distance [31,38,60]. When this long Mn-O bond distance is large (above *ca.* 2.4 Å) then the orbital overlap is reduced and the coupling is weak

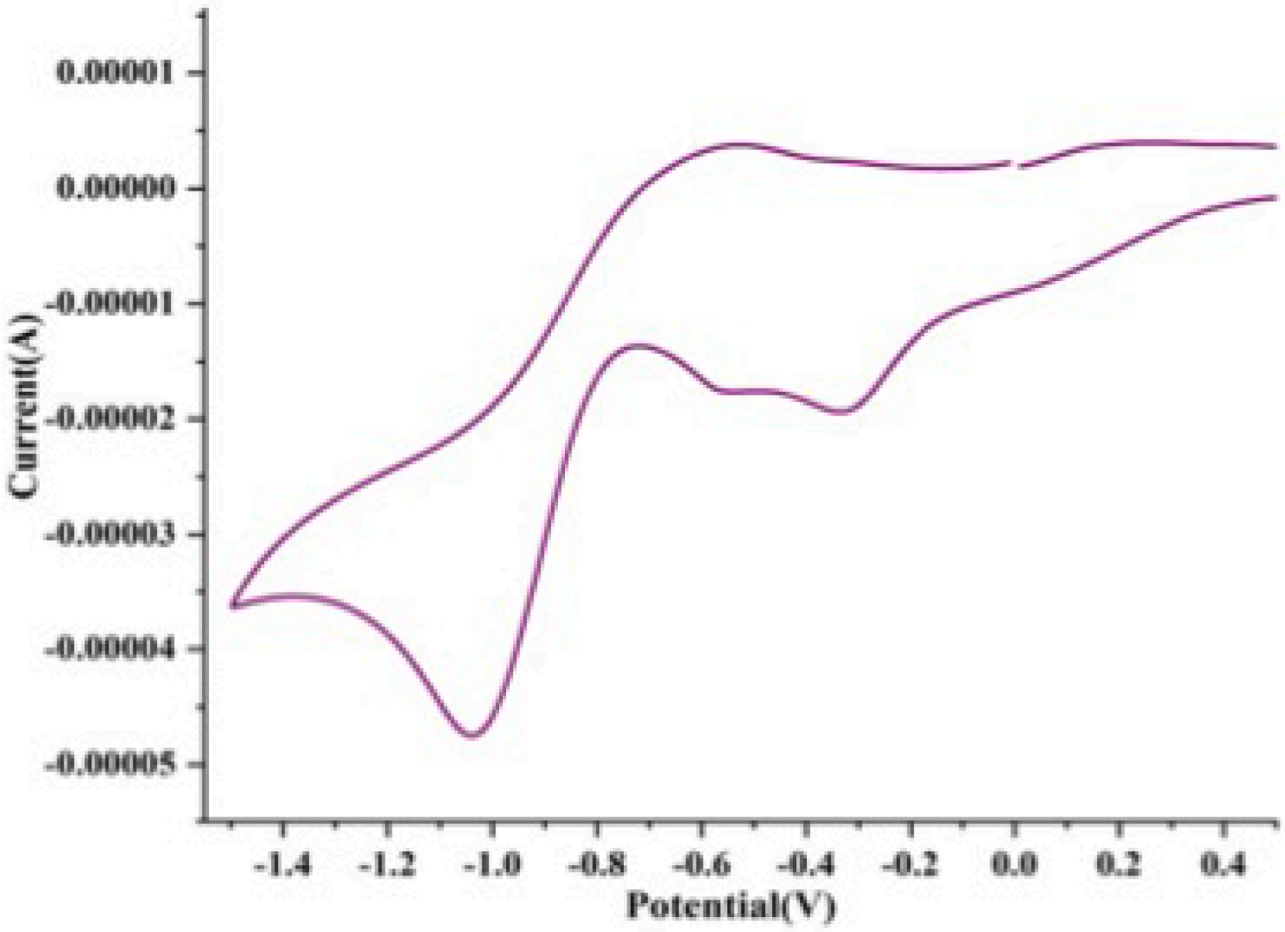

Fig. 3. Cyclic voltammogram of the complex in acetontrile medium with respect to an Ag/AgCl electrode using tetrabutylammonium bromate as supporting electrolyte at a scan rate of 50 mV s^{-1}.

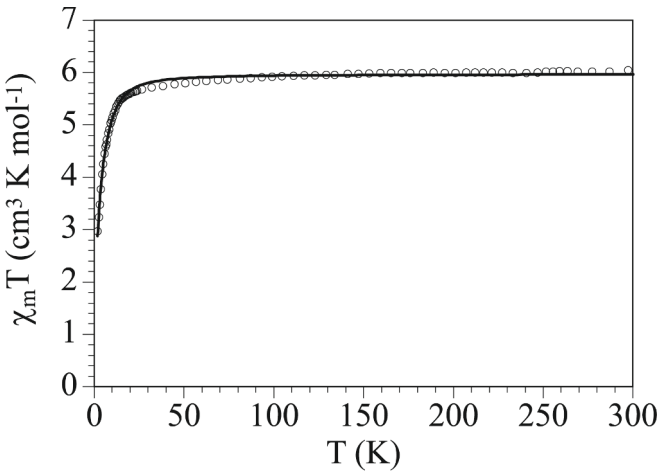

Fig. 4. Thermal variation of $\chi_m T$ for compound **1**. Solid line is the best fit to a Mn^{III} dimer model with negative zero field splitting.

and ferromagnetic as a result of the orbital orthogonality of the d_z^2 and d_p orbitals (d_{xy}, d_{xz} and d_{yz}). For shorter Mn-O bond distances (as in complex **1**) the overlap increases, resulting in a weak antiferromagnetic interaction, as observed in complex **1** ($J_{23} = -0.065(1)$ cm^{-1}). The negligible coupling observed in complex **1** agrees with a distance very close to the crossing point between ferro- and antiferromagnetic coupling. The second structural parameter that plays a role in the J value is the Mn–O–Mn bond angle (101.12(12)° in complex **1**). Both, experimental results and theoretical calculations, show that when the Mn–O distance is short (2.3–2.5 Å) there is a linear relationship between the Mn-O-Mn angle and J, with a negative slope that indicates that the larger the angle, the lower the J value [29]. Although the slope and the crossing angle from ferro- to antiferromagnetic interaction depends on the Mn-O bond distance, the larger the angle, the more antiferromagnetic the J value is. The Mn-O-Mn angle in complex **1** points to a weak antiferromagnetic interaction through the double phenoxido bridge, in agreement with the obtained J value in complex **1**.

Since Mn^{III} ions present a large magnetic anisotropy [1,14,51], we have performed AC measurements with different applied DC fields at low temperatures. These measurements show the presence of a frequency-dependent out of phase signal (χ''_m) at low temperatures only when a DC field is applied (Fig. S8, ESI file). The analysis of the frequency dependence of out of phase signal at 2 K with the Debye model shows that the relaxation time increases as the DC field increases and reaches a maximum at around 2000 Oe (0.2 T, Fig. S8, ESI file). Accordingly, we have measured the frequency dependence of the AC signal with an applied DC field of 0.2 T in the temperature range of 2–4 K (Fig. 5a). These measurements show an out of phase signal with a maximum that shifts to higher frequencies as the temperature increases.

The fit of the frequency dependence of the χ''_m signal to the Debye model for complex **1** provides reliable relaxation times (τ) only in the

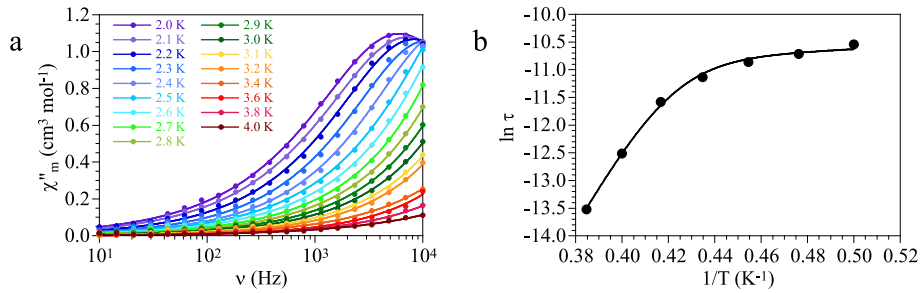

Fig. 5. (a) Frequency-dependence of the out of phase susceptibility (χ''_m) at low temperatures with an applied DC field of 0.2 T for complex **1**. Solid lines are the best fit to the Debye model. (b) Arrhenius plot of the relaxation time for compound **1** with a DC field of 0.2 T. Solid line is the best fit to Eq. (2).

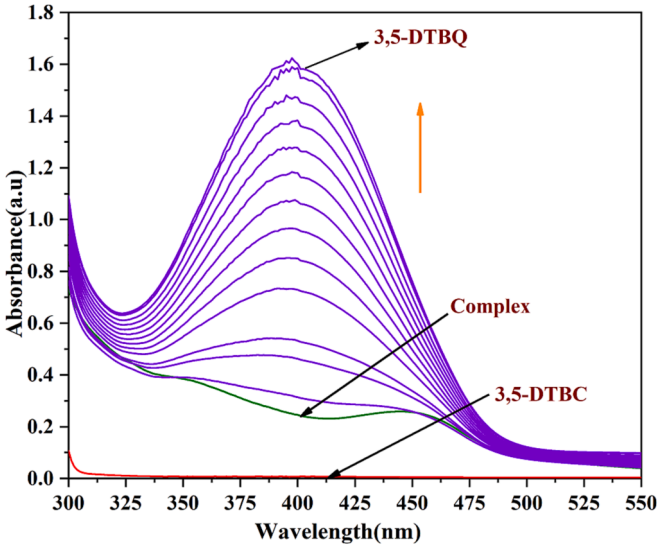

Fig. 6. Absorption spectra after addition of 100 equivalents of 3,5-DTBC to a 10^{-4} M solution containing complex **1** in acetonitrile. The spectra were recorded at 5 min. intervals during ca. 1 h.

temperature range 2.0–2.6 K (as at higher temperatures the maximum frequency is above the frequency limit of our equipment). The Arrhenius plot of these relaxation times (Ln τ *vs* 1/T, Fig. 5b) shows a straight line in the 2.4–2.6 K range and a curvature in the 2.0–2.4 K range that can be very well reproduced with equation (2), including the Direct and Orbach mechanisms, respectively:

$$\tau^{-1} = AT + \tau_0^{-1}\exp\left(\frac{-U_{eff}}{k_B T}\right) \quad (2)$$

with $A = 206(9) \times 10^2\ s^{-1}\ K^{-1}$, $\tau_0 = 8(1) \times 10^{-19}$ s and $U_{eff} = 73(4)$ K (solid line in Fig. 5b), indicating that the relaxation of the magnetization follows an activated process with a quite high energy barrier.

3.6. Catechol oxidation activity

3,5-di-*tert*-butylcatechol (3,5-DTBC) is an extensively used substrate in the study of model complex catalysed catechol-oxidase-like reactions. This is because of its low redox potential, which makes it easily oxidisable and also the presence of bulky substituents prevents further oxidations and ring-opening reaction [61]. The oxidation product, 3,5-di-*tert*-butylquinone (3,5-DTBQ) is also very stable and exhibits a characteristic absorption maximum at 402 nm in acetonitrile solution [46,62]. In order to examine the catechol-oxidase-like activity of complex **1**, we dissolved the complex in acetonitrile by sonicating it few minutes to prepare a 10^{-4} M solution of the complex and treated this solution with 100 equivalents of 3,5-DTBC (10^{-2} M) in open air. In this

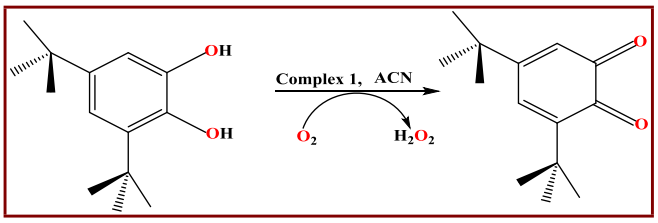

Scheme 2. Catalytic Oxidation of 3,5-DTBC to 3,5-DTBQ in acetonitrile (ACN).

catalytic reaction the aerial O_2 works as oxidant. The course of the reaction was monitored by recording the UV–vis spectra of the reaction mixture at intervals of 5 min. As can be seen in Fig. 6, the formation of 3,5-DTBQ causes a blue shift in the absorption band of the complex from 454 nm to 401 nm with steady and gradual increase of the absorption intensity. These results confirm the catalytic oxidation of 3,5-DTBC to 3,5-DTBQ in solution. Interestingly, if we perform the same experiment in identical reaction conditions in methanol, no absorption band corresponding to 3,5-DTBQ was observed (Fig. S9, ESI file). This result indicates that methanol is not a suitable solvent for the oxidation of 3,5-DTBC catalysed by complex **1**. A control experiment was also performed in acetonitrile under the same conditions using Mn^{III} chloride instead of complex **1** but no characteristics absorption band of 3,5-DTBQ was observed even after 4 h. A second control experiment performed under the same conditions, but without adding complex **1**, showed that the oxidation of 3,5-DTBC started only after 12 h. Hence, both the control experiments unequivocally prove the effective catalytic activity of complex **1** towards catechol oxidation.

As the catalytic activity of the complex has been assessed using aerial O_2 as oxidant, it is therefore, important to know the fate of the aerial O_2 during the oxidation of 3,5-DTBC and for this purpose a protocol experiment has been carried out following the procedure reported earlier [63]. Upon performing the catalytic oxidation of catechol for a duration of one hour, the pH of the solution was brought to 2 by dropwise addition of H_2SO_4. Thereafter, we have added 1 mL of 10 % KI solution and two drops of 3 % solution of ammonium molybdate in the solution obtained from the previous step and recorded the UV–vis spectrum of the resultant mixture (Fig. S10, ESI file) to monitor the characteristic peak of I_3^-. In the UV–vis spectrum the characteristic peak of I_3^- at 353 nm ($\varepsilon = 26000\ M^{-1}\ cm^{-1}$) has been detected. The detail of this experiment has been provided in the ESI file. This experiment indicates that aerial O_2 is reduced to H_2O_2 during oxidation of catechol molecule to quinone (scheme 2) [63].

3.7. Kinetic study for catechol oxidation

The kinetic study of the catalytic oxidation of 3,5-DTBC to 3,5-DTBQ by complex **1** was carried out following the initial rate method by measuring the increase of the absorbance of the quinone band at 401 nm. In order to determine the main kinetic parameters and the oxidation

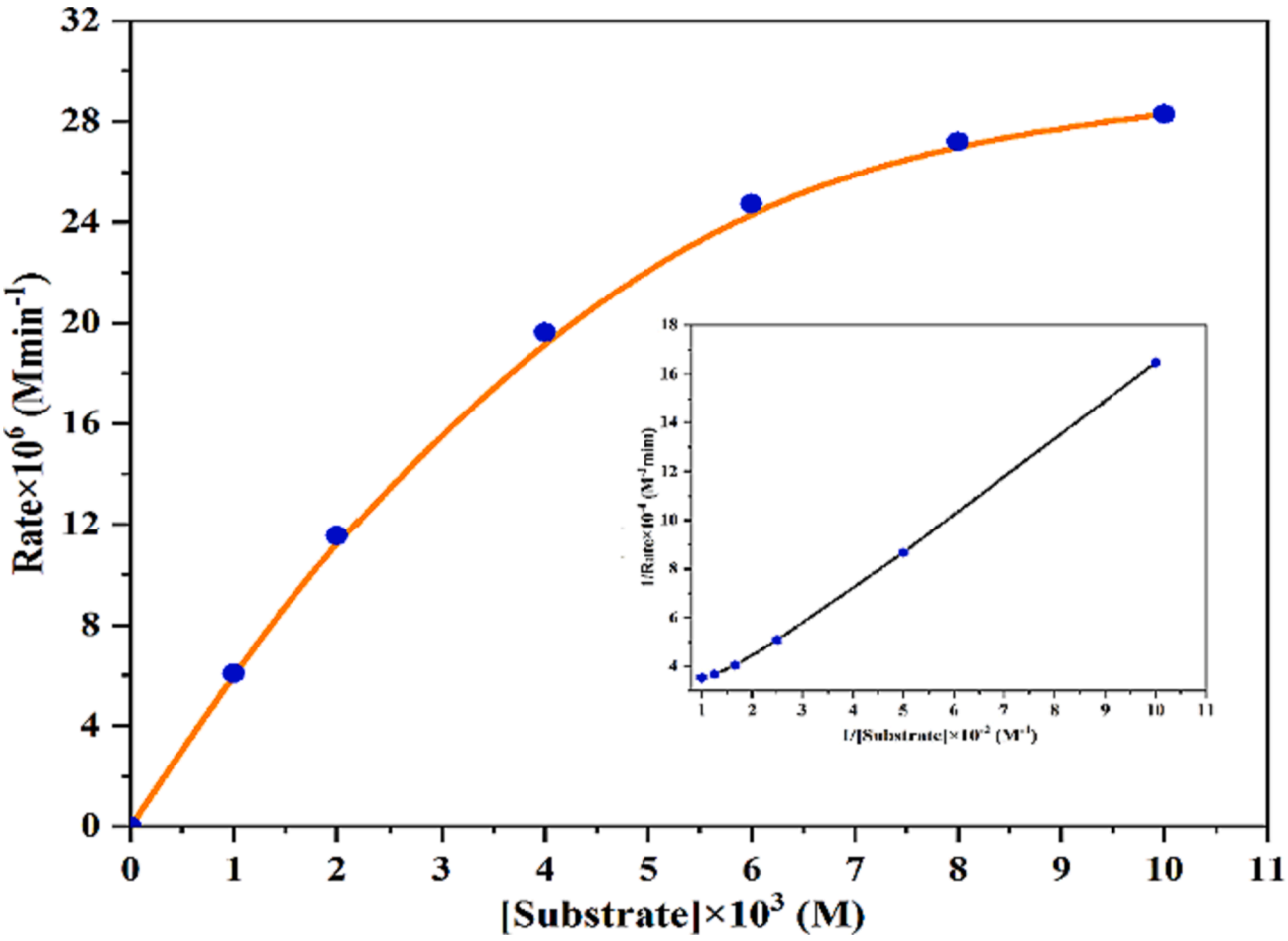

Fig. 7. Plot of initial rates *vs* substrate concentration for the oxidation of 3,5-DTBC to 3,5-DTBQ catalysed by complex **1**. The Inset shows the Lineweaver-Burk plots.

rate dependence on the substrate concentration (3,5-DTBC), a 10^{-4} M solution of complex **1** in acetonitrile has been reacted with increasing concentrations of 3,5-DTBC, from 10 to 100 equivalents, i.e., from 10^{-3} M to 10^{-2} M, under aerobic condition. The initial rate is determined from the slope of the absorbance *vs* time plot (Fig. S11, ESI file) recording the absorbance data for a duration of first 15 min, at an interval of 5 min and considering the molar extinction coefficient of quinone (3,5-DTBQ) as 1630 M^{-1} cm^{-1}. A first-order dependence is found at low concentrations of the substrate, whereas saturation kinetics has been noticed at higher substrate concentrations (Fig. 7). The Michaelis–Menten model approach can be used to explain this type of saturation rate dependence as observed in the present case. Thus, a treatment on the basis of Michaelis-Menten equation for enzymatic kinetics is applied here and linearized by using Lineweaver-Burk plot (double reciprocal plot) to calculate the Michaelis-Menten constant (K_M) and the maximum rate (V_{max}) achieved by the system. The values of K_M and V_{max} are 8.473 × 10^{-3} M and 5.82 × 10^{-5} M min^{-1}, respectively. The value of turnover number (k_{cat}) as calculated by dividing the V_{max} value by the concentration of the complex, is 34.94 h^{-1}.

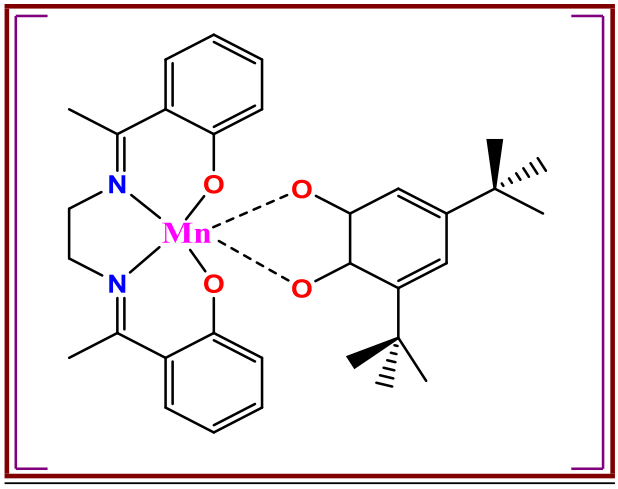

Scheme 3. The possible 1:1 substrate-catalyst intermediate formed by mononuclear manganese species with 3,5-DTBQ in acetonitrile [m/z = 570.3].

3.8. ESI-Mass spectrometric study

The mass spectrum (ESI-MS positive) of complex **1** and a 1:100 mixture of complex **1** with 3,5-DTBC (after 10 min of mixing) have been recorded separately in acetonitrile medium to get an insight into the structure of the complex in solution phase as well as to probe the presence of possible substrate-catalyst intermediates involved in the catechol oxidation reaction. The mass spectrum of complex **1** (Fig. S12, ESI file) exhibits a base peak at m/z = 349.25 that indicates the presence of mononuclear species $[Mn(L)]^+$ ($C_{18}H_{18}MnN_2O_2$) in the solution phase. Additional peaks at m/z = 431.2 and 390.6 can be assigned to the solvent bound mononuclear species $[Mn(L)(CH_3CN)_2]^+$ ($C_{22}H_{24}MnN_4O_2$) and $[Mn(L)(CH_3CN)]^+$ ($C_{20}H_{21}MnN_3O_2$), respectively. It may be noted that very low intensity peaks are also found at higher m/z values (m/z = 612.08, 721.39 and 780.4) indicating the presence of complex **1** in the solution. The mass spectrum of the 1:100 mixture (Fig. S13, ESI file)

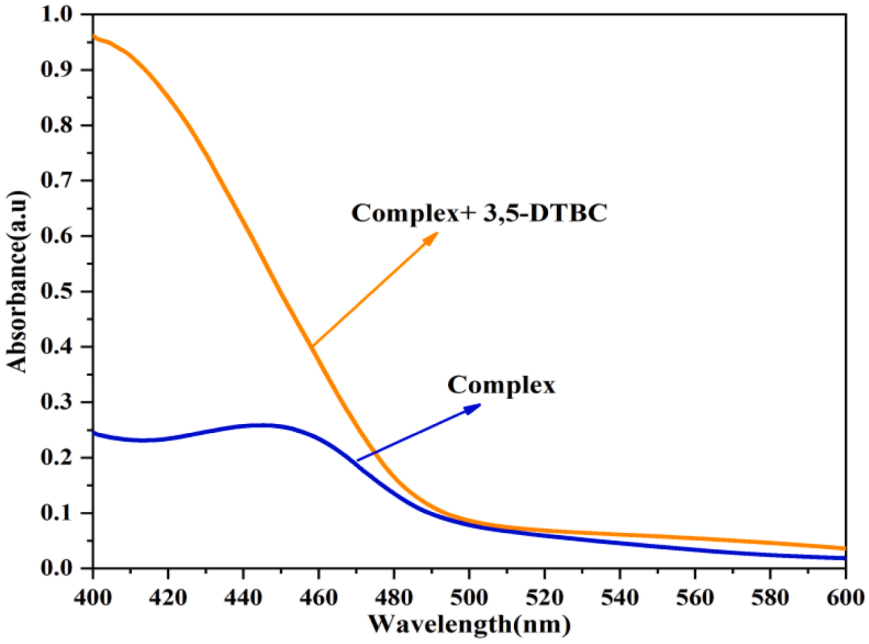

Fig. 8. UV–vis spectra of the complex **1** alone and after addition of 100 equivalents of 3,5-DTBC in acetonitrile.

Table 2
A comparison of catechol oxidase mimicking activity of some previously reported metal complexes.

Complexes	Solvent	V_{max}(Ms^{-1})	K_M(M)	k_{cat}(h^{-1})	Ref.
[Mn^{III}(L)$_2$(OAc)(AcOH)]	[a]	18.3×10^{-5}	–	1.32×10^{6}	[44]
[Mn^{III}_2 Mn^{II}(O_2CCH_2Cl)$_4$-(dmp)$_2$(H_2O)$_2$	[c]	1.50×10^{-4}	7.49×10^{-5}	9.01×10^{3}	[45]
[Mn^{II}(o-(NO_2)C_6H_4COO)$_2$(pyz)(H_2O)]$_n$	[c]	8.67×10^{-6}	1.7×10^{-4}	177	[46]
[$Mn^{III}L^2$(SCN)(H_2O)]	[b]	2.1×10^{-3}	–	134	[67]
[Mn^{III}L(N_3)(H_2O)]	[d]	1.76×10^{-7}	0.001022	25.4	[68]
[Mn^{III}L(OAc)(H_2O)]	[d]	1.19×10^{-7}	0.0007731	17.2	[68]
[$Mn^{III}Mn^{II}$L(μ-O_2CPh)(MeOH) (ClO_4)]$^+$	[c]	4.34×10^{-8}	0.0006265	15.6	[69]
[Mn^{III} (L)Cl]	[c]	1.00×10^{-4}	65×10^{-4}	3.60×10^{3}	[64]
[Mn^{III}_2(L)Cl_4]·4H_2O	[c]	6.70×10^{-5}	2.40×10^{-3}	2.41×10^{3}	[64]
[Mn^{II}_2(L)$_2$(NO_2)$_2$]	[c]	3.98×10^{-6}	4.9×10^{-4}	1472.74	[56]
[$Mn^{II}_4Mn^{III}_4O_2$(pyz)$_2$($C_6H_5CH_2COO$)$_{10}$]	[c]	1.18×10^{-5}	1.75×10^{-4}	2.55×10^{3}	[70]
[Cu(L^1)$_2$(ClO_4)$_2$]$_2$	[b]	5×10^{-7}	3.70×10^{-4}	34.32	[71]
[Cu_2(L^2)$_2$(μ-ClO_4)](ClO_4)	[b]	7.3×10^{-7}	6.40×10^{-4}	26.52	[71]
[Co_2(cpdp)(Hphth)]	[b]	2.8×10^{-7}	2.175×10^{-3}	20.64	[72]
[Co_2(cpdp)(Hisophth)]	[b]	2.1×10^{-7}	2.719×10^{-3}	15.45	[72]
[Co_4(cpdp)$_2$(terephth)]	[b]	3.2×10^{-7}	2.599×10^{-3}	47.32	[72]
[Cu_2(Hhdpa)$_2$].2CH_3OH·6H_2O	[b]	2.3×10^{-7}	5.039×10^{-3}	17.05	[73]
Na_4[Zn_2(hdpa)$_2$](OAc)$_2$	[b]	1.3×10^{-7} 1.78×10^{-2}	1.78×10^{-2}	9.13	[73]
[Ni_4(L)$_2$(H_2O)$_8$(μ_2-H_2O)$_2$](NO_3)$_6$(H_2O)$_6$	[d]	3.514×10^{-7}	1.966×10^{-3}	12.65	[74]
[Mn^{II}_2(L)$_2$(dca)$_2$]	[c]	9.7×10^{-7}	8.473×10^{-3}	34.94	This work

Where, solvent: [a] = CH_3CN: DMF(9:1), [b] = CH_3OH, [c] = CH_3CN, [d] = DMF and 'L' denotes respective ligand system.

shows a base peak at m/z = 243.13 that corresponds to the quinone-sodium aggregate [(3,5-DTBQ)Na]$^+$ ($C_{14}H_{20}O_2Na$). The peak at m/z = 570.3 indicates the existence of 1:1 mononuclear species-substrate aggregate [Mn(L)(3,5-DTBQ)H]$^+$ ($C_{32}H_{39}MnN_2O_4$) formed during the course of the catalytic oxidation. Hence, on the basis of the mass spectrometric evidence, it can be inferred that complex **1** predominantly exists as a mononuclear species [Mn(L)]$^+$ in acetonitrile solution after its dissociation. This mononuclear species [Mn(L)]$^+$ is actually the active form of the catalyst that binds with the substrate 3,5-DTBC (1:1) in the course of the oxidation (Scheme 3).

It is worthy to note that, complex **1** did not exhibit catalytic activity in the oxidation of 3,5-DTBC in methanol under the same reaction condition as we have mentioned earlier. Very similar observation has been reported in the literature for a series of dinuclear Mn^{III}-Schiff base complexes, however, another series of mononuclear Mn^{III}-Schiff base complexes display good catalytic activity in both methanol and acetonitrile solvents [64]. Hence, from the outcome of the present catalytic study and previous findings, it will be reasonable to conclude that the good coordinating ability of MeOH molecule precludes the dissociation of the Mn^{III} dimer to form the mononuclear species, [Mn(L)]$^+$, which is actually the active form of catalyst, whereas this does not happen in acetonitrile solution.

Metal complexes comprising higher valent metal centres such as Cu^{II}, Mn^{III} and Mn^{IV} usually exhibit significant catalytic activity in the catechol oxidation reaction because they can be easily reduced to their stable lower valencies [65–66]. In the UV–vis spectrum of the complex **1** in acetonitrile, a band appears at 454 nm due to the ligand to metal charge-transfer (PhO → Mn^{III}). This band completely disappears upon

addition of 100 equivalent of the substrate 3,5-DTBC (Fig. 8). This spectrophotometric study clearly suggests that in the present case, the catalytic oxidation of 3,5-DTBC to 3,5-DTBQ by aerial O_2 takes place with the concomitant reduction of Mn^{III} ions to Mn^{II} state. The Mn^{II} ions are further oxidised back into Mn^{III} by the molecular O_2 present in the reaction media. The catalytic activity of the complex in terms of the parameters such as K_M, V_{max} and k_{cat} has been compared with manganese and other metal-based complexes toward catalytic oxidation of catechol and presented in Table 2. This comparative study reveals that the present dimeric Mn^{III}-complex exhibits moderate catalytic activity in the oxidation of catechol substrate.

4. Conclusions

In this work we have reported the structure, magnetic properties and bio-catalytic activity of a unique dimeric Mn^{III} complex containing Schiff's base and dca^- ligands. The complex **1** is a centrosymmetric Mn^{III} dimer showing a rare combination of double phenoxido bridges with terminal dca^- ligands. Complex **1** is the first reported dimeric Mn^{III} complex of a Schiff base ligand having two terminal dca^- ligands. We have shown that the ratio 1:2 of Mn and dca^-leads to the formation of a dimeric Mn^{III} complex, in contrast to the discrete mononuclear complexes or 1D structures previously obtained for 1:1 ratio of Mn and dca^-. Complex **1** exhibits an almost negligible Mn^{III}–Mn^{III} coupling and a field-induced single-molecule magnet behaviour, with a high energy barrier of 73(4) K due to the large magnetic anisotropy of the Mn^{III} centres. Additionally, complex **1** exhibits significant solvent selective catechol-oxidase-like activity for the model substrate 3,5-DTBC in acetonitrile medium.

Declaration of Competing Interest

The authors declare that they have no known competing financial interests or personal relationships that could have appeared to influence the work reported in this paper.

Data availability

Data will be made available on request.

Acknowledgements

We acknowledge the financial support of DST-SERB under FIST program of Department of Physics, Jadavpur University, Department of Chemistry, Jadavpur University for procurement of equipments. BK acknowledges fellowship received under State Govt. Departmental Fellowship, Scheme of Jadavpur University. RS acknowledges DST-SERB for the financial support (SERB-TAR/2018/000744). We also thank the Generalidad Valenciana (project Prometeo/2019/076) and the Spanish MINECO (project PID-2021-125907NB-I00, AEI/FEDER, EU) for financial support. This study forms part of the Advanced Materials programme and was supported by MCIN with funding from European Union NextGenerationEU (PRTR-C17.I1) and by Generalitat Valenciana.

Appendix A. Supplementary data

Supplementary data to this article can be found online at https://doi.org/10.1016/j.ica.2022.121370.

References

[1] D. Li, H. Wang, S. Wang, Y. Pan, C. Li, J. Dou, Y. Song, Inorg. Chem. 49 (2010) 3688–3690.
[2] A.J. Tasiopoulos, W. Wernsdorfer, K.A. Abboud, G. Christou, Angew. Chem. Int. Ed. 43 (2004) 6338–6342.
[3] L.A. Kushch, V.D. Sasnovskaya, A.I. Dmitriev, E.B. Yagubskii, O.V. Koplak, L. V. Zorina, D.W. Boukhvalov, Dalton Trans. 41 (2012) 13747–13754.
[4] C.C. Stoumpos, R. Inglis, O. Roubeau, H. Sartzi, A.A. Kitos, C.J. Milios, G. Aromi, A. J. Tasiopoulos, V. Nastopoulos, E.K. Brechin, S.P. Perlepes, Inorg. Chem. 49 (2010) 4388–4390.
[5] M. Carboni, J.-M. Latour, Coord. Chem. Rev. 255 (2011) 186–202.
[6] G. Maayan, G. Christou, Inorg. Chem. 50 (2011) 7015–7021.
[7] D. Lieb, A. Zahl, T.E. Shubina, I. Ivanovic-Burmazovic, J. Am. Chem. Soc. 132 (2010) 7282–7284.
[8] D. Shen, C. Miao, S. Wang, C. Xia, W. Sun, Eur. J. Inorg. Chem. 49 (2014) 5777–5782.
[9] G. Maayan, N. Gluz, G. Christou, Nature Catal. 1 (2018) 48–54.
[10] M.H. Cheaha, M. Zhangb, D. Shevelac, F. Mamedova, A. Zounib, J. Messinger, Proc. Natl. Acad. Sci. 117 (2020) 141–145.
[11] P.A. Vigato, S. Tamburini, L. Bertolo, Coord. Chem. Rev. 251 (2007) 1311–1492.
[12] C.N.R. Rao, S. Natarajan, R. Vaidhyanathan, Angew. Chem. Int. Ed. 43 (2004) 1466–1496.
[13] R. Bagai, G. Christou, Inorg. Chem. 46 (2007) 10810–10818.
[14] J.H. Song, K.S. Lim, D.W. Ryu, S.W. Yoon, B.J. Suh, C.S. Hong, Inorg. Chem. 53 (2014) 7936–7940.
[15] T. Taguchi, W. Wernsdorfer, K.A. Abboud, G. Christou, Inorg. Chem. 49 (2010) 10579–10589.
[16] J.G. Segura, J. Campo, I. Imaz, K. Wurst, J. Veciana, P. Gerbier, D. Ruiz-Molina, Dalton Trans. (2007) 2450–2456.
[17] L. Bogani, W. Wernsdorfer, Nature Mater. 7 (2008) 179–186.
[18] A.V. Palii, S.M. Ostrovsky, S.I. Klokishner, B.S. Tsukerblat, C.P. Berlinguette, K. R. Dunbar, J.R. Galán-Mascarós, J. Am. Chem. Soc. 126 (2004) 16860–16867.
[19] E. Cremades, J. Cano, E. Ruiz, G. Rajaraman, C.J. Milios, E.K. Brechin, Inorg. Chem. 48 (2009) 8012–8019.
[20] N. Lima, A. Caneschi, D. Gatteschi, M. Kritikos, L.G. Westin, Inorg. Chem. 45 (2006) 2391–2393.
[21] S. Goswami, S. Singha, I. Saha, A. Chatterjee, S.K. Dey, C.J. Gómez García, A. Frontera, S. Kumar, R. Saha, Inorg. Chem. 59 (2020) 8487–8497.
[22] I. Dasna, S. Golhen, L. Ouahab, N. Daro, J.P. Sutter, New J. Chem. 25 (2001) 1572–1576.
[23] J.L. Manson, C.R. Kmety, F. Palacio, A.J. Epstein, J.S. Miller, Chem. Mater. 13 (2001) 1068–1073.
[24] M. Maiti, D. Sadhukhan, S. Thakurta, S. Roy, G. Pilet, R.J. Butcher, A. Nonat, L. J. Charbonniere, S. Mitra, Inorg. Chem. 51 (2012) 12176–12187.
[25] S. Dalai, P.S. Mukherjee, E. Zangrando, N. Ray Choudhuri, New J. Chem. 26 (2002) 1185–1189.
[26] D.J. Price, S.R. Batten, B. Moubaraki, K.S. Murray, Ind. J. Chem. A. 42 (2003) 2256–2266.
[27] Q. Shi, R. Cao, X. Li, J. Luo, M. Hong, Z. Chen, New J. Chem. 26 (2002) 1397–1401.
[28] Y. Zhang, X. Wang, X. Zhang, T. Liu, W. Xu, S. Gao, Inorg. Chem. 49 (2010) 5868–5875.
[29] P. Seth, S. Giri, A. Ghosh, Dalton Trans. 44 (2015) 12863–12870.
[30] P. Pandey, S. Tripathi, M. Shanmugam, R.J. Butcher, S.S. Sunkari, Inorg. Chim. Acta 495 (2019), 118997.
[31] Z. Lu, M. Yuan, F. Pan, S. Gao, D. Zhang, D. Zhu, Inorg. Chem. 45 (2006) 3538–3548.
[32] Q. Wu, Y.-G. Li, Y.-H. Wang, R. Clerac, Y. Lua, E-Bo. Wang, Chem. Commun. (2009) 5743–5745.
[33] H. Miyasaka, R. Clerac, W. Wernsdorfer, L. Lecren, C. Bonhomme, K. Sugiura, M. Yamashita, Angew. Chem. Int. Ed. 43 (2004) 2801–2805.
[34] C.K. Terajima, H. Miyasaka, K. Sugiura, R. Clerac, H. Nojiri, Inorg. Chem. 45 (2006) 4381–4390.
[35] H. Hiraga, H. Miyasaka, R. Clerac, M. Fourmigue, M. Yamashita, Inorg. Chem. 48 (2009) 2887–2898.
[36] Y. Sawada, W. Kosaka, Y. Hayashi, H. Miyasaka, Inorg. Chem. 51 (2012) 4824–4832.
[37] T. Akitsu, Y. Takeuchi, Y. Einaga, Acta Cryst 61 (2005) 324–328.
[38] H. Miyasaka, R. Clérac, T. Ishii, H. Chang, S. Kitagawa, M. Yamashita, J. Chem. Soc. Dalton Trans. 28 (2002) 1528–1534.
[39] K.S. Banu, T. Chattopadhyay, A. Banerjee, S. Bhattacharya, E. Suresh, M. Nethaji, E. Zangrando, D. Das, Inorg. Chem. 47 (2008) 7083–7093.
[40] J.H. Whittaker, in Metal Ions in Biological Systems, Ed. Marcel Dekker, New York, 2000, vol 37. Chapter 18, pp. 587-611.
[41] D. W. Yoder, J. Hwang and J. E. Penner-Hahn, in Metal Ions in Biological Systems, Ed. Marcel Dekker, New York, 2000, vol. 37. Chapter 16, pp. 527-557.
[42] M. H. Gold, H. L. Youngs and M. D. SollewijnGelpke, in Metal Ions in Biological Systems, Ed. Marcel Dekker, New York, 2000, vol. 37. Chapter 17, pp. 559-586.
[43] K.N. Ferreira, T.M. Iverson, K. Maghlaoui, J. Barber, S. Iwata, Science 303 (2004) 1831–1838.
[44] S.K. Dey, A. Mukherjee, Chem Cat Chem. 5 (2013) 3533–3537.
[45] M. Pait, M. Shatruk, D. Ray, Dalton Trans. 44 (2015) 11741–11754.
[46] P. Kar, Y. Ida, T. Kanetomo, M.G.B. Drew, T. Ishida, A. Ghosh, Dalton Trans. 44 (2015) 9795–9804.
[47] S.K. Dey, A. Mukherjee, Coord. Chem. Rev. 310 (2016) 80–115, and references therein.
[48] S. Ghosh, S. Giri, A. Ghosh, Polyhedron 102 (2015) 366–374.
[49] G.A. Bain, J.F. Berry, J. Chem. Educ. 85 (2008) 532–536.
[50] G. M. Sheldrick, SHELXL 97, Program for Crystal Structure Refinement, University of Göttingen, Göttingen, Germany, 1997.

[51] G.M. Sheldrick, Crystal structure refinement with SHELXL, Acta Cryst 71 (2015) 38.
[52] A.L. Spek, Single-crystal structure validation with the program PLATON, J. Appl. Cryst. 36 (1) (2003) 7–13.
[53] L.J. Farrugia, ORTEP-3 for Windows – a version of ORTEP-III with a Graphical User Interface (GUI), J. Appl. Cryst. 30 (1997) 565.
[54] L.J. Farrugia, WinGX suite for small-molecule single-crystal crystallography, J. Appl. Cryst. 32 (1999) 837–838.
[55] G. Bhargavi, M.V. Rajasekharan, J.P. Tuchages, Inorg. Chim. Acta 362 (2009) 3247–3252.
[56] P. Seth, M.G.B. Drew, A. Ghosh, J. Mol. Catal. A Chem. 365 (2012) 154–161.
[57] S. Saha, D. Mal, S. Koner, A. Bhattacherjee, P. Gütlich, S. Mondal, M. Mukherjee, K. Okamoto, Polyhedron 23 (2004) 1811–1817.
[58] N.F. Chilton, R.P. Anderson, L.D. Turner, A. Soncini, K.S. Murray, J. Comput. Chem. 34 (2013) 1164–1175.
[59] C. Duboc, Chem. Soc. Rev. 45 (2016) 5834–5847.
[60] S. Mandal, G. Rosair, J. Ribas, D. Bandyopadhyay, Inorg. Chim. Acta 362 (2009) 2200–2204.
[61] J. Mukherjee, R. Mukherjee, Inorg. Chim. Acta 337 (2002) 429–438.
[62] F. Zippel, F. Ahlers, R. Werner, W. Haase, H.F. Nolting, B. Krebs, Inorg. Chem. 35 (1996) 3409–3419.
[63] A. Biswas, L.K. Das, M.G.B. Drew, C. Diaz, A. Ghosh, Inorg. Chem. 51 (2012) 10111.
[64] S. Mukherjee, T. Weyhermüller, E. Bothe, K. Wieghardt, P. Chaudhuri, Dalton Trans. 22 (2004) 3842–3853.
[65] I.A. Koval, P. Gamez, C. Belle, K. Selmeczi, J. Reedijk, Chem. Soc. Rev. 35 (2006) 814–840.
[66] M. Maiti, D. Sadhukhan, S. Thakurta, E. Zangrando, G. Pilet, A. Bauza, A. Fron-tera, B. Dede, S. Mitra, Polyhedron 75 (2014) 40–49.
[67] P. Chakraborty, S. Majumder, A. Jana, S. Mohanta, Inorg. Chim. Acta 410 (2014) 65–75.
[68] A. Jana, N. Aliaga-Alcalde, E. Ruiz, S. Mohanta, Inorg. Chem. 52 (2013) 7732–7746.
[69] K.S. Banu, T. Chattopadhyay, A. Banerjee, M. Mukherjee, S. Bhattacharya, G. K. Patra, E. Zangrando, D. Das, Dalton Trans. 40 (2009) 8755–8764.
[70] P. Kar, R. Haldar, C.J. Gomez-Garcia, A. Ghosh, Inorg. Chem. 51 (2012) 4265–4273.
[71] M. Sheoran, K. Bhar, S. Jain, M. Rana, T.A. Khan, A.K. Sharma, Polyhedron 161 (2019) 169–178.
[72] A. Majumdera, N. Dutta, S. Haldara, A. Dasb, L. Carrellac, M. Bera, Inorg. Chim. Acta 510 (2020), 119752.
[73] A. Patra, G.C. Giri, T.K. Sen, L. Carrella, S.K. Mandal, M. Bera, Polyhedron 67 (2014) 495–504.
[74] T. Chakraborty, S. Mukherjee, S. Dasgupta, B. Biswas, D. Das, Dalton Trans. 48 (2019) 2772–2784.

Thesis: Somen Goswami

ORIGINALITY REPORT

6%
SIMILARITY INDEX

PRIMARY SOURCES

1	Binkadem, Mona Saad. "Supramolecular Interaction of Transition Metal Schiff Base Complexes", The University of Manchester (United Kingdom), 2021 ProQuest	93 words — < 1%
2	Maxcimilan Patra, Soumen Kumar Dubey, Sudipta Saha, Corrado Rizzoli, Subham Bhattacharjee, Rajat Saha. "Simultaneous presence of mono- and bi-cationic bipyridyls within a metal-organic supramolecular host: crystal structure, spectral and Hirshfeld surface analysis", Journal of Coordination Chemistry, 2022 Crossref	93 words — < 1%
3	repository.library.georgetown.edu Internet	92 words — < 1%
4	ir.library.illinoisstate.edu Internet	78 words — < 1%
5	Renata E. H. M. B. Osório, Rosely A. Peralta, Adailton J. Bortoluzzi, Vicente R. de Almeida et al. "Synthesis, Magnetostructural Correlation, and Catalytic Promiscuity of Unsymmetric Dinuclear Copper(II) Complexes: Models for Catechol Oxidases and Hydrolases", Inorganic Chemistry, 2012 Crossref	74 words — < 1%

6	Debasis Karmakar, Michel Fleck, Rajat Saha, Manas Layek, Sanjay Kumar, Debasis Bandyopadhyay. "Synthesis and crystal structure of a group of phenoxo-bridged heterodinuclear [NiIIHgII] Schiff base complexes", Polyhedron, 2013 Crossref	71 words — < 1%
7	ycm.uni-mysore.ac.in Internet	68 words — < 1%
8	Matteo Atzori, Luciano Marchiò, Rodolphe Clérac, Angela Serpe, Paola Deplano, Narcis Avarvari, Maria Laura Mercuri. "Hydrogen-Bonded Supramolecular Architectures Based on Tris(Hydranilato)Metallate(III) (M = Fe, Cr) Metallotectons", Crystal Growth & Design, 2014 Crossref	65 words — < 1%
9	pstorage-acs-6854636.s3.amazonaws.com Internet	61 words — < 1%
10	darwin.bth.rwth-aachen.de Internet	58 words — < 1%
11	www.mdpi.com Internet	52 words — < 1%
12	uilis.unsyiah.ac.id Internet	46 words — < 1%
13	Sayantani Mukherjee Chatterjee, Chetan Kumar Jain, Soumen Singha, Piyal Das et al. " Activity of Co –Quinalizarin: A Novel Analogue of Anthracycline-Based Anticancer Agents Targets Human DNA Topoisomerase, Whereas Quinalizarin Itself Acts via Formation of Semiquinone on Acute Lymphoblastic Leukemia MOLT-4 and HCT 116 Cells ", ACS Omega, 2018 Crossref	44 words — < 1%

14	Sk Amanullah, Paramita Saha, Rajat Saha, Abhishek Dey. " Synthetic Iron Porphyrins for Probing the Differences in the Electronic Structures of Heme , Heme , and Heme ", Inorganic Chemistry, 2018 Crossref	43 words — < 1%
15	Soumavo Ghosh, Yumi Ida, Takayuki Ishida, Ashutosh Ghosh. " Linker Stoichiometry-Controlled Stepwise Supramolecular Growth of a Flexible Cu Tb Single Molecule Magnet from Monomer to Dimer to One-Dimensional Chain ", Crystal Growth & Design, 2014 Crossref	43 words — < 1%
16	diposit.ub.edu Internet	43 words — < 1%
17	ri.conicet.gov.ar Internet	42 words — < 1%
18	www.science.gov Internet	42 words — < 1%
19	Jens Ackermann. "Tuning the Activity of Catechol Oxidase Model Complexes by Geometric Changes of the Dicopper Core", Chemistry - A European Journal, 01/04/2002 Crossref	39 words — < 1%
20	Kargal L. Gurunatha. "Structural Flexibility and Selective Guest Accommodation in Two Cu^{II} Metal-Organic Coordination Frameworks", European Journal of Inorganic Chemistry, 03/20/2009 Crossref	37 words — < 1%
21	Hazra, Arpan, K. L. Gurunatha, and Tapas Kumar Maji. "Charge-Assisted Soft Supramolecular	35 words — < 1%

Porous Frameworks: Effect of External Stimuli on Structural Transformation and Adsorption Properties", Crystal Growth & Design, 2013.
Crossref

22 Mal, D.. "Synthesis, X-ray crystal structure and magnetic study of the 1D {[Cu"2(N,N,N',N'-tetramethyl-ethylenediamine)"2(@m-1,5-dca)"2(dca)"2]}"n complex", Inorganica Chimica Acta, 20061001 — 33 words — < 1%
Crossref

23 Narayan Ch. Jana, Moumita Patra, Paula Brandão, Anangamohan Panja. "Synthesis, structure and diverse coordination chemistry of cobalt(III) complexes derived from a Schiff base ligand and their biomimetic catalytic oxidation of o-aminophenols", Polyhedron, 2019 — 33 words — < 1%
Crossref

24 Biswas, S.. "A novel 1D chain of azido bridged copper(II) with a salen-type di-Schiff base ligand", Journal of Molecular Structure, 20120718 — 32 words — < 1%
Crossref

25 Tanmoy Saha, Soumen Singha, Sanjay Kumar, Saurabh Das. "Spectroscopy driven DFT computation for a structure of the monomeric Cu2+-Curcumin complex and thermodynamics driven evaluation of its binding to DNA: Pseudo-binding of Curcumin to DNA", Journal of Molecular Structure, 2020 — 32 words — < 1%
Crossref

26 Swastik Mondal, Monika Mukherjee, Santu Chakraborty, Alok K. Mukherjee. "A Novel Three-Dimensional Network Containing Pr(III) Ions and Tartrate: Synthesis, Spectroscopic, Thermal, Ab Initio X-ray Powder Structure Analyses, and Photoluminescence Properties", Crystal Growth & Design, 2006 — 31 words — < 1%
Crossref

27	docksci.com Internet	31 words — < 1%
28	Qi-Feng Liang. "An 18-Membered Hexanuclear Manganese (MnN2)6 Metalladiazamacrocycle", Zeitschrift für Naturforschung B, 2009 Crossref	30 words — < 1%
29	mafiadoc.com Internet	30 words — < 1%
30	Sudipto Dey, Sayan Sarkar, Dinesh Maity, Partha Roy. "Rhodamine based chemosensor for trivalent cations: Synthesis, spectral properties, secondary complex as sensor for arsenate and molecular logic gates", Sensors and Actuators B: Chemical, 2017 Crossref	29 words — < 1%
31	Bhattacharya, A.. "Crystal structure and electronic properties of two nimesulide derivatives: A combined X-ray powder diffraction and quantum mechanical study", Chemical Physics Letters, 20100617 Crossref	27 words — < 1%
32	Javier Cepeda, Rolindes Balda, Garikoitz Beobide, Oscar Castillo et al. "Lanthanide(III)/Pyrimidine-4,6-dicarboxylate/Oxalate Extended Frameworks: A Detailed Study Based on the Lanthanide Contraction and Temperature Effects", Inorganic Chemistry, 2011 Crossref	27 words — < 1%
33	www.ijcm.ir Internet	27 words — < 1%
34	Rajeev Kumar. "Synthesis, structural, photophysical and thermal properties of some	26 words — < 1%

praseodymium(III) complexes", Journal of Coordination Chemistry, 2008
Crossref

35 scholarsmine.mst.edu
Internet
25 words — < 1%

36 Das, Shyamal, Debasish Saha, Srikanta Karmakar, and Sujoy Baitalik. "Effect of pH on the Photophysical and Redox Properties of a Ruthenium(II) Mixed Chelate Derived from Imidazole-4,5-dicarboxylic Acid and 2,2'-Bipyridine: An Experimental and Theoretical Investigation", The Journal of Physical Chemistry A, 2012.
Crossref
24 words — < 1%

37 Thorge Brünig, Kristijan Krekić, Clemens Bruhn, Rudolf Pietschnig. "Calorimetric Studies and Structural Aspects of Ionic Liquids in Designing Sorption Materials for Thermal Energy Storage", Chemistry - A European Journal, 2016
Crossref
24 words — < 1%

38 Samartzis, Alexandros. "Magnetic Investigation of Effective Spin-1/2 Magnetic Insulators Based on 3d and 4f Magnetic Ions.", Technische Universitaet Berlin (Germany), 2021
ProQuest
23 words — < 1%

39 Srinivasulu Parshamoni, Suresh Sanda, Himanshu Sekhar Jena, Kapil Tomar, Sanjit Konar. "Exploration of Structural Topologies in Metal–Organic Frameworks Based on 3-(4-Carboxyphenyl)propionic Acid, Their Synthesis, Sorption, and Luminescent Property Studies", Crystal Growth & Design, 2014
Crossref
23 words — < 1%

40 en.wikipedia.org
Internet

23 words — < 1%

41 "Advanced Structural Chemistry", Wiley, 2021 — 22 words — < 1%
Crossref

42 Miao, Xiao-He, and Long-Guan Zhu. "Supramolecular assembly under the control of the chelating ligand for the MnII/bridging ligands/3-sulfobenzoate system and catalytic properties for the disproportionation of hydrogen peroxide", New Journal of Chemistry, 2010. — 22 words — < 1%
Crossref

43 Abourahma, Heba. "Structural diversity in metal-organic nanoscale supramolecular architectures", Proquest, 20111108 — 21 words — < 1%
ProQuest

44 Maryam Lashanizadegan, Roya Karimi Alavijeh, Maryam Anafcheh. "Facile synthesis of Co(II) and Cu(II) complexes of 2-hydroxybenzophenone: An efficient catalyst for oxidation of olefins and DFT study", Journal of Molecular Structure, 2017 — 21 words — < 1%
Crossref

45 www.theses.fr — 21 words — < 1%
Internet

46 Sanjay Kumar, Soumen Singha, Rajkumar Jana, RITUPARNA MONDAL et al. "Photo-responsive Schottky Diode Behavior of a Donor-Acceptor Co-crystal with Violet Blue Light Emission", CrystEngComm, 2021 — 20 words — < 1%
Crossref

47 worldwidescience.org — 20 words — < 1%
Internet

48 Jan Boeckmann. "Metamagnetism and Single-Chain Magnetic Behavior in a Homospin One-Dimensional Iron(II) Coordination Polymer", Chemistry - A European Journal, 04/23/2012
Crossref
18 words — < 1%

49 Mouli Saha, Soumen Singha, Mousumi Chakraborty, Swagata Mazumdar, Sanjay Kumar, Parimal Karmakar, Saurabh Das. "Characterization of a MnII complex of Alizarin suggests attributes explaining a superior anticancer activity: A comparison with anthracycline drugs", Polyhedron, 2019
Crossref
17 words — < 1%

50 hdl.handle.net
Internet
17 words — < 1%

51 pubs.rsc.org
Internet
15 words — < 1%

52 tel.archives-ouvertes.fr
Internet
15 words — < 1%

53 Baldwin, Michael J., Neil A. Law, Timothy L. Stemmler, Jeff W. Kampf, James E. Penner-Hahn, and Vincent L. Pecoraro. "Reactivity of [{Mn^{IV}(salpn)}₂(μ-O,μ-OCH₃)]⁺ and [{Mn^{IV}(salpn)}₂(μ-O,μ-OH)]⁺: Effects of Proton Lability and Hydrogen Bonding", Inorganic Chemistry, 1999.
Crossref
14 words — < 1%

54 Jayanta K. Nath, Abhishake Mondal, Annie K. Powell, Jubaraj B. Baruah. " Structures, Magnetic Properties, and Photoluminescence of Dicarboxylate Coordination Polymers of Mn, Co, Ni, Cu Having -(4-
14 words — < 1%

Pyridylmethyl)-1,8-naphthalimide ", Crystal Growth & Design, 2014
Crossref

55 Li Wang, Wen Gu, Xiu-Jun Deng, Ling-Fei Zeng, Sheng-Yun Liao, Ming Zhang, Lin-Yan Yang, Xin Liu. "A Series of 2D and 3D Novel Lanthanide Complexes Constructed from Squarate C4O42−: Syntheses, Structures, Magnetic Properties, and Near-infrared Emission Properties", Australian Journal of Chemistry, 2011
Crossref
14 words — < 1%

56 Partha Mahata. "Magnetic behaviour in metal-organic frameworks—Some recent examples", Journal of Chemical Sciences, 01/2010
Crossref
13 words — < 1%

57 Chowdhury, Additi Roy, Pritam Ghosh, Biswajit Gopal Roy, Subhra Kanti Mukhopadhyay, Naresh Chandra Murmu, and Priyabrata Banerjee. "Cell permeable fluorescent colorimetric Schiff base chemoreceptor for detecting F− in aqueous solvent", Sensors and Actuators B Chemical, 2015.
Crossref
12 words — < 1%

58 Jones, L.F.. "Tuning magnetic properties using targeted structural distortion: New additions to a family of Mn"6 single-molecule magnets", Inorganica Chimica Acta, 20080901
Crossref
12 words — < 1%

59 MARÍA COMES NAVARRO. "Hybrid inorganic-organic materials for the optical recognition of neutral and anionic species", Universitat Politecnica de Valencia, 2016
Crossref Posted Content
12 words — < 1%

60 Ming-Hua Zeng, Wei-Xiong Zhang, Xian-Zhong Sun, Xiao-Ming Chen. "Spin Canting and Metamagnetism in a 3D Homometallic Molecular Material Constructed by Interpenetration of Two Kinds of Cobalt(II)-Coordination-Polymer Sheets", Angewandte Chemie, 2005
Crossref
12 words — < 1%

61 Zhang, Nan. "Influence of citrate ligands on ferric hydroxide nucleation at low molar ratios: Application for arsenic removal", Proquest, 20111004
ProQuest
12 words — < 1%

62 epdf.tips
Internet
12 words — < 1%

63 www.chem.tamu.edu
Internet
12 words — < 1%

64 Craven, Michael James. "Development of Phosphazene-Polyoxometalate Catalyst Systems for Multiphase Oxidations with Hydrogen Peroxide", The University of Liverpool (United Kingdom), 2020
ProQuest
11 words — < 1%

65 Liang Zhao, Virginie Niel, Laurence K. Thompson, Zhiqiang Xu et al. "Self-assembled polynuclear clusters derived from some flexible polydentate dihydrazide ligands", Dalton Transactions, 2004
Crossref
11 words — < 1%

66 Michio Sorai, Yasuhiro Nakazawa, Motohiro Nakano, Yuji Miyazaki. "Update 1 of: Calorimetric Investigation of Phase Transitions Occurring in Molecule-Based Magnets", Chemical Reviews, 2013
Crossref
11 words — < 1%

67	Nandi, S.. "Cobalt-thioalkylazoimidazole complexes: Structures, spectra and redox properties", Polyhedron, 20091103 Crossref	11 words — < 1%
68	Zilu Chen. "Construction of Planar Clusters Using Planar Aromatic Polyoxime Ligands: Synthesis, Structure, and Magnetic Properties", Crystal Growth & Design, 11/03/2010 Crossref	11 words — < 1%
69	aip.scitation.org Internet	11 words — < 1%
70	purehost.bath.ac.uk Internet	11 words — < 1%
71	Gargi Mukherjee, Kumar Biradha. " Coordination Polymers Containing M L and M L Metallacylces of Bis(pyridylcarboxamido)alkanes with an Odd Number of −(CH)– Groups as Spacers: Guest Inclusion and Networks Recognition via α Sheet ", Crystal Growth & Design, 2013 Crossref	10 words — < 1%
72	Jiang, M.X.. "Syntheses, crystal structures, and luminescence properties of lanthanide complexes with 5-carboxy-1-carboxymethyl-2-oxidopyridinium", Inorganica Chimica Acta, 20090601 Crossref	10 words — < 1%
73	Rituparna Biswas, Carmen Diaz, Ashutosh Ghosh. "Three nickel(II) complexes derived from a tridentate NNO donor Schiff base ligand: Syntheses, crystal structures and magnetic properties", Polyhedron, 2013 Crossref	10 words — < 1%

EXCLUDE QUOTES	ON	EXCLUDE SOURCES	OFF
EXCLUDE BIBLIOGRAPHY	ON	EXCLUDE MATCHES	< 10 WORDS